

Durham E-Theses

Cretaceous alkaline igneous rocks from the Águas Emendadas region, Goiás, central Brazil

Brod, Tereza Cristina Junqueira

How to cite:

Brod, Tereza Cristina Junqueira (1998) *Cretaceous alkaline igneous rocks from the Águas Emendadas region, Goiás, central Brazil*, Durham theses, Durham University. Available at Durham E-Theses Online: <http://etheses.dur.ac.uk/4909/>

Use policy

The full-text may be used and/or reproduced, and given to third parties in any format or medium, without prior permission or charge, for personal research or study, educational, or not-for-profit purposes provided that:

- a full bibliographic reference is made to the original source
- a [link](#) is made to the metadata record in Durham E-Theses
- the full-text is not changed in any way

The full-text must not be sold in any format or medium without the formal permission of the copyright holders.

Please consult the [full Durham E-Theses policy](#) for further details.

*Cretaceous Alkaline Igneous Rocks from
the Águas Emendadas Region,
Goiás, Central Brazil*

by

Tereza Cristina Junqueira Brod

**A Thesis submitted for the degree of
Master of Science.**

The copyright of this thesis rests with the author. No quotation from it should be published without the written consent of the author and information derived from it should be acknowledged.

**Department of Geological Sciences,
University of Durham.**



1998

11 MAY 1999

DECLARATION

I declare that this thesis, which I submit for the degree of Master of Science at the University of Durham, is my own work and no part of this has previously been submitted for a degree at this or any other university.

Tereza Cristina Junqueira Brod

University of Durham

September 1998

Copyright © 1998 Tereza Cristina Junqueira Brod

The copyright of this thesis rests with the author. No quotation or data from it should be published without T. C. J. Brod's prior written consent, and any other information derived from it should be acknowledged.

ABSTRACT

Cretaceous Alkaline Igneous Rocks from the Águas Emendadas Region, Goiás, Central Brazil.

Tereza Cristina Junqueira Brod, University of Durham.

Master of Science, 1998

The area of study is located in central Brazil, in the southern portion of Goiás state. The alkaline igneous rocks from Águas Emendadas Region comprise volcanic and pyroclastic varieties, emplaced in Phanerozoic sediments of the Paraná Basin and in Precambrian basement rocks. They were formed during a magmatic event which took place during Upper Cretaceous and belong to the Rio Verde - Iporá Igneous Province.

The pyroclastic rocks were formed by processes involving fluidization and phreatomagmatic events. Exsolution of volatiles and magma mixing are also involved in their genesis. The most common pyroclastic products are breccias with fragmental, lapilli-size "matrices" and fragments of various origins (e.g. accessory, cognate, juvenile) reaching up to metric dimensions. Armoured lapilli, "spinning droplets" and "frozen droplets" of magma occur in the breccia matrix and represent different stages of explosiveness.

? metre

Lavas, erupted in non-explosive intervals, are ultramafic to mafic (melaleucitites, melanephelinites, leucitites, basalts and basanites). They are usually porphyritic, with phenocrysts characteristically of olivine and/or clinopyroxene. Other common mineral phases include leucite (pseudo-leucite), nepheline, kalsilite, perovskite, phlogopite, Fe-Ti oxides and, in basalts and basanites only, plagioclase.

The rocks were variably altered by a combination of hydrothermal processes and weathering. Minerals resulting from these alterations include carbonate, zeolites, serpentine and hydroxides.

The chemical composition of several mineral phases is reported and discussed in terms of its effect on the magmatic processes. Fractionation of olivine, clinopyroxene, spinel-group minerals and perovskite controlled the chemical composition of magmas during evolution.

The whole-rock chemical data show that these rocks are divided into two groups one Mg-rich and the other Mg-poor. The Mg-rich rocks are SiO₂-poor, with high contents of CaO, TiO₂ and incompatible elements, and have chemical affinity with kamafugites (Ti-rich diopside phenocrysts and groundmass kalsilite are consistent with this). The occurrence of magma mixing is supported by the chemical data.

Acknowledgements

I would like to thank all those who contributed to the realisation of this work, in England and Brazil. To name them all would make a very long list and I don't want to risk forgetting anyone by mistake. So, thanks a lot for being so helpful and friendly!!!!

However, without some people it would not have happened at all and I owe them this thesis. They gave me their emotional support, funding and most of all, they believed in me: Pai, Mãe, Déi e Affonso MUITO OBRIGADA!

I also would like to mention those who were most closely involved giving their time and support:

First of all, my supervisors Prof. R.N. Thompson, at University of Durham and Dr. S.A. Gibson, at University of Cambridge, who both read and commented on several drafts of this thesis. They taught me a lot and I am deeply grateful for all that they have done for me while I was here.

Thanks to all members of the staff of the Department of Geological Sciences, at the University of Durham, who on so many occasions went beyond their obligations to help me.

I would also like to express my gratitude to Dr. C.H. Emeleus for his kind help with the petrography of the lavas.

In Cambridge, would like to thank Dr. S.J.B. Reed and Joanne Greenwood.

My friends, who put up with my mood swings and helped me to make my time a bit bigger, making photocopies, baby sitting and listening: The Dunnill's, Rees's, Neves's, Richardson's and the swimming club; in the future, you can all count on me!!!

Many thanks to Dr. Mike Richardson and Ana Maria for their encouragement and friendship.

In Brazil: I would like to express my appreciation to the Instituto de Geociências of the Universidade de Brasília for their loan of vehicles and equipment for the field work and logistic support. For their motivation and support I would like to thank: Prof. R.A. Fuck, Dr. G.R. Boaventura, Dr. M.M. Pimentel, Dr. P.R. Meneses, Dr. N.F. Botelho, Prof. J.R. Hirson, Dr. R. Moraes, Dr. F.O Silva, G.V. Pereira, L.R.C. Freitas Junior, L. A. B. Junqueira and M.C.B. Junqueira.

Finally, the field work would not have happened without the help, inspiration, expertise, friendship and patience (a lot of) from Prof. Othon Henry Leonardos and Maria das Graças Viana.

Contents

Chapter I - INTRODUCTION	1
Chapter II - GEOLOGICAL SETTING	6
II.1 INTRODUCTION	6
II.2 PRE-CAMBRIAN	8
II.3 PHANEROZOIC	10
Chapter III - RIO VERDE-IPORÁ IGNEOUS PROVINCE	15
Chapter IV - FIELD GEOLOGY AND PETROGRAPHY OF ÁGUAS EMENDADAS REGION	21
IV.1 FIELD RELATIONSHIPS	21
IV.1.1 Introduction	21
IV.1.2 Breccias	24
IV.1.3 Dykes	33
IV.1.4 Lavas	36
IV.2 PETROGRAPHY	39
IV.2.1 Introduction	39
IV.2.2 Volcanic Breccias and associated Dykes	41
Breccia Matrix	41
Homogeneous Mafic Igneous Rocks	48
Dykes	50
IV.2.3 Lavas	53
Melaleucitites	55
Melanephelinites (?)	58
Leucitites	62
Basalts and basanites	62

IV.3 INTERPRETATION	64
Chapter V - MINERAL CHEMISTRY	74
V.1 INTRODUCTION	74
V.2 OLIVINE	74
V.3 CLINOPYROXENE	75
V.4 FELDSPATHOIDS	77
V.5 FELDSPARS	78
V.6 PEROVSKITE	79
V.7 OPAQUES	79
V.8 CARBONATE	80
Chapter VI - GEOCHEMISTRY	82
VI.1 INTRODUCTION	82
VI.2 MAJOR ELEMENTS	86
VI.3 TRACE-ELEMENTS	97
VI.3.1 Complatible trace-elements	97
VI.3.2 Incompatible trace-elements	97
VI.4 MELALEUCITITES AND MELANEPHELINITES (?)	108
VI.5 INTERPRETATION	110
Chapter VII - CONCLUSIONS AND SUGGESTIONS FOR FURTHER STUDY	112
References cited	115
Appendix 1 - SAMPLE DESCRIPTIONS	124
Appendix 2 - SAMPLE PREPARATION AND ANALYTICAL TECHNIQUES	129
A2.1 INTRODUCTION	129
A2.2 LOSS ON IGNITION (LOI)	130
A2.3 FUSION DISC PREPARATION	130
A2.4 POWDER PELLET PREPARATION	131
A2.5 X-RAY FLUORESCENCE (XRF) ANALYSIS	131

A2.6 INDUCTIVELY COUPLED PLASMA MASS SPECTROMETRY (ICP-MS)	132
A2.7 ELECTRON PROBE MICROANALYSIS	135
Appendix 3 - WHOLE-ROCK CHEMICAL DATA	136
Table A3.1 - XRF data	137
Table A3.2 - ICP-MS data	140
Table A3.3 - CIPW norm	143
Table A3.4 - Normative composition of selected samples (Le Bas, 1973)	144
Appendix 4 - ELECTRON MICROPROBE DATA	145
Table A4.1 - Olivines	146
Table A4.2 - Clinopyroxenes	150
Table A4.3 - Feldspathoids	156
Table A4.4 - Feldspars	157
Table A4.5 - Perovskites	158
Table A4.6 - Opaques	159

The area of study is located in southern Goiás State (central Brazil), about 450 km Southwest of Brasília, between the towns of Amarinópolis and Montividiu (Fig. I.1). The main road access to the area is off the GO-174 road through small unpaved tracks. The region has a tropical climate and is covered by savannah-type vegetation. It has two main seasons, one dry and other rainy.

The main regional geomorphologic feature of the area is the Caiapó Graben (Fig. I.2), which defines the western limit of the “Planalto Setentrional da Bacia do Paraná” (Mamede *et al.*, 1983). In the study area, this structure comprises a number of subparallel normal faults, separating half-graben blocks oriented N-NW. The lower surface (to the west of the Caiapó Graben) is part of the Alcantilados Plateau. Pena and Figueiredo (1972) identified three planation surfaces, associated with the South-American (Palaeogene), Velhas (Neogene) and Paraguaçu (current) erosion cycles. The River Caiapó is part of the Amazon hydrographic Basin and the main river of the area.

Two stages of field work were carried out in July 1996, using the town of Iporá as the logistics base. The University of Brasília provided the field vehicles used in both stages, as well as a GPS receiver for the first stage.



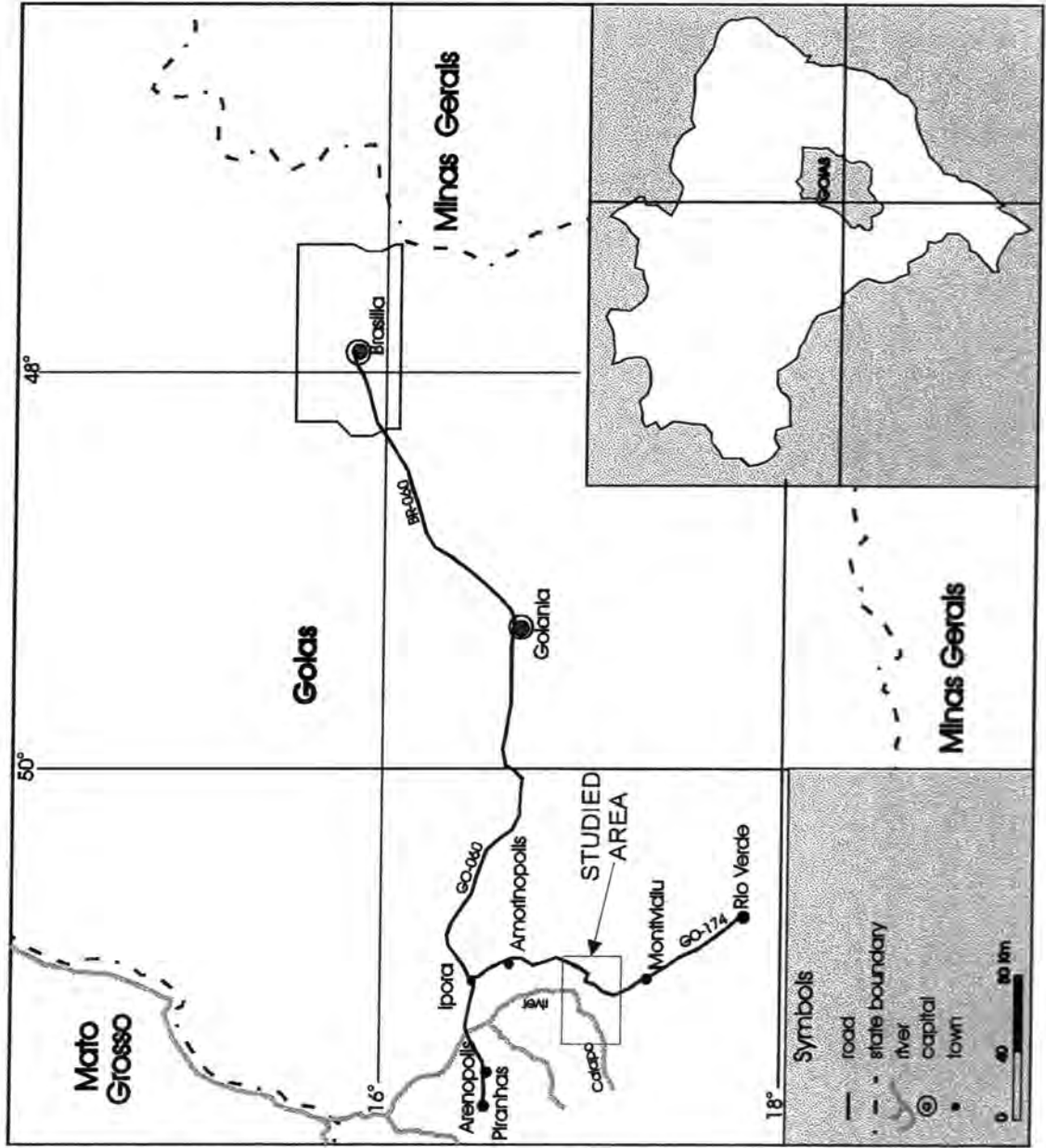


Figure 1.1 - Location map and road access to the studied area.



Figure 1.2 - Top: view of the Caiapó Graben from Neuzinha occurrence. Bottom: River Caiapó cutting Aquidauana sandstones.

Professor Othon H. Leonardos assisted in the first stage and the geologist Maria das Graças Viana in the second. A total of 70 samples were collected, including both rocks and minerals. The samples are labelled in numeric order, after the identification prefix 96AE. In addition to these, four other samples were supplied by Prof. R.N. Thompson and Dr S.A. Gibson, from their previous field work. These are labelled with the identifier prefix 92SOB. Sample descriptions and locations are listed in Appendix 1. Appendix 2 gives a detailed description of methods employed for sample preparation and analysis.

The aim of this work is to characterise petrologically the volcanic rocks from the Águas Emendadas Region. Due to time and financial constraints for field work in Brazil, the author did not undertake detailed geological mapping of the sampled occurrences. However, information on regional geology is provided in Chapters II and III, based on published maps. Previous mapping work by the author in the Iporá Region was also important in establishing background knowledge of the regional geology.

Five localities in the Águas Emendadas Region were sampled during the current research and alkaline rocks from the Amarinópolis Region were collected for comparison with the former. The studied rocks are part of the Cretaceous Rio Verde-Iporá Igneous Province. They intrude both the Pre-Cambrian basement and the Phanerozoic sediments in the Northeast margin of the Paraná Basin.

The main difficulties found during field work concern the access, distance and the scarcity of fresh rock-outcrops. The geological setting of many of the sampled localities favours the occurrence of vent-related hydrothermal

alteration. Further, the alkaline rocks are particularly susceptible to the strong tropical weathering regime prevalent in central Brazil.

The sampled occurrences in the Águas Emendadas Region comprise the Águas Emendadas Complex, Neuzinha, Marimbondo, Cacimba and Montividiu. In the northernmost, Amarinópolis Region, the visited localities include the Amarinópolis Complex, six other small dykes or plugs and a dyke from Morro do Macaco. The field descriptions and petrography of the Águas Emendadas Region can be found in Chapter IV. The mineral chemistry is discussed in Chapter V and electron microprobe analyses are found in Appendix 4. Chapter VI contains the interpretation of geochemical data for rocks of both regions. The results of chemical analyses are given in Appendix 3.

II.1 INTRODUCTION

The various geological units present in the Southwest part of Goiás State will be described below, in a chronological order (Fig. II.1).

The pre-Silurian units comprise localised, alloctonous fragments of Archean to Paleoproterozoic gneisses, orthogneisses, granites, metamorphosed volcanic-sedimentary sequences and molasses. They are all associated with the Brasiliano-Pan African Orogeny. After the amalgamation of the Gondwana supercontinent different intracratonic basins were formed including the Paraná Basin, whose the Northeast portion occupies a large portion of the studied region. During the Wealdenian reactivation there was an extrusive magmatic event, represented by the continental flood basalts of the Serra Geral Formation (a.k.a. Paraná Basalts) and by the alkaline rocks of the Iporá Province. Following this magmatism, sediments of the Bauru Group were deposited. During the Tertiary and Quaternary laterites, soils and alluvial deposits were formed.

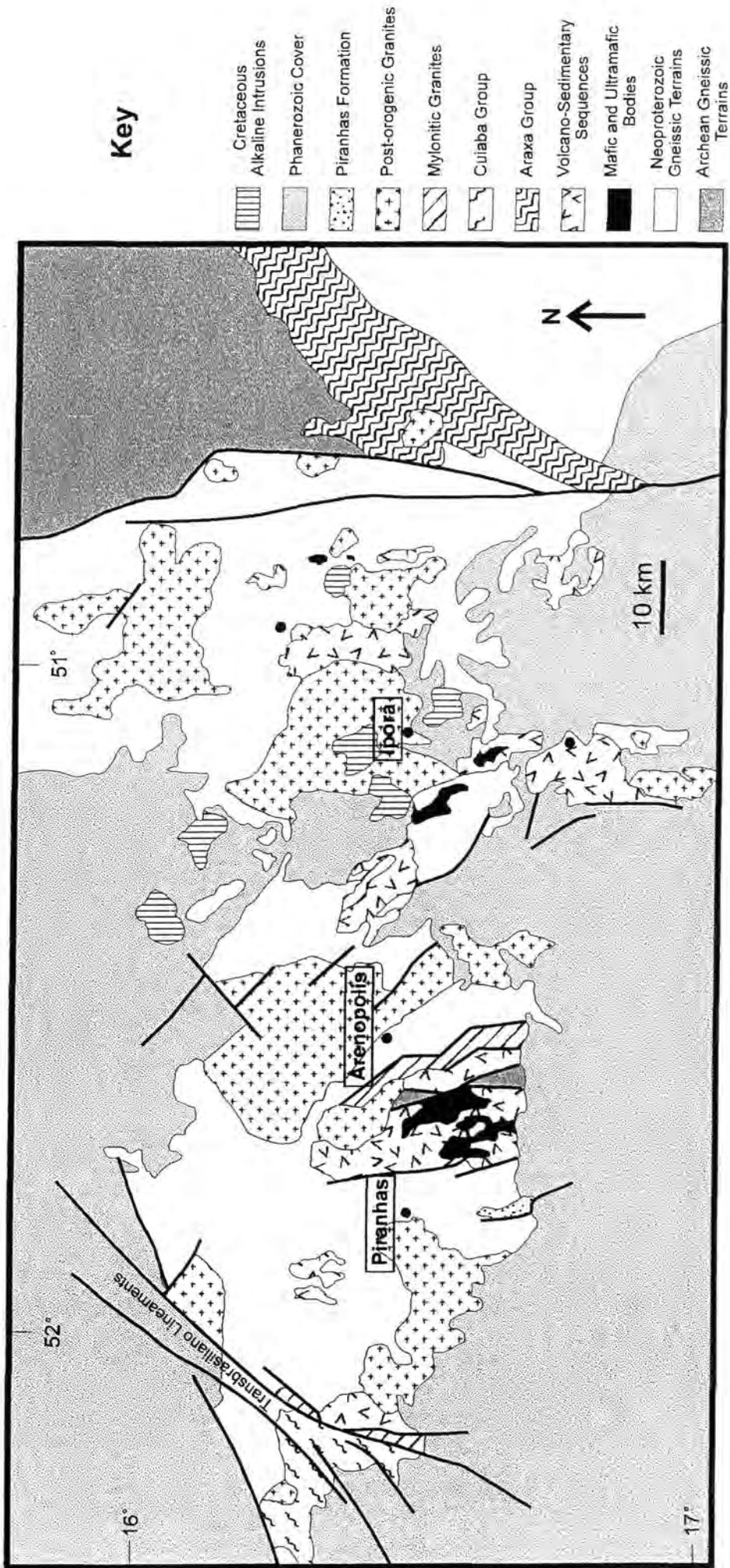


Figure II.1 - Geological Map of the Ipora Region (after Pimintel *et al.*, 1996).

II.2 PRE-CAMBRIAN

Between the towns of Arenópolis and Piranhas, gneisses are found tectonically emplaced in Neoproterozoic rocks of the Arenópolis Sequence. They occur as narrow and discontinuous strips (approximately 2km apparent thickness) limited by faults with a general N-S trend. The fault zones are occupied by biotite gneisses of Archean to Paleoproterozoic age, granitic to granodioritic in composition, metamorphosed to the amphibolite facies. These rocks are called Ribeirão Gneisses and are interpreted as crustal fragments tectonically emplaced into younger rocks (Pimentel, 1992; Pimentel and Fuck, 1992).

Hornblende-biotite plutonic orthogneisses of Neoproterozoic age crop out over large areas near the towns of Arenópolis, Israelândia and Sanclerlândia (the Arenópolis, Matrinxã and Sanclerlândia gneisses, respectively). They are grey-coloured, medium-grained, homogeneous and calcic to calc-alkaline in composition. The protoliths of these rocks are mostly gabbro-diorites to granites. Geochemical and geochronological data indicate that these gneisses are associated with the Brasiliano Orogeny (Pimentel, 1985; Pimentel and Fuck, 1987; Amaro, 1989; Pimentel, 1992).

Four volcanic-sedimentary sequences are known in the Southwest of the Goiás state: Bom Jardim, Arenópolis, Jaupaci and Iporá-Amorinópolis (Seer, 1985; Pimentel and Fuck, 1986; Amaro, 1989). These sequences comprise metavolcanic and metasedimentary rocks metamorphosed in greenschist to amphibolite facies. Tectonically emplaced mafic and

ultramafic bodies are often found associated with the volcanic-sedimentary sequences.

The metabasalts from these sequences are geochemically similar to low-K tholeiites of island arcs (Seer, 1985; Pimentel and Fuck, 1987; Amaro, 1989). Field and petrographic characteristics also indicate that the sequences are associated with island arcs (Seer, 1985).

The tectonically emplaced mafic and ultramafic bodies are interpreted by Pimentel and Fuck (1986,1987) as part of dismembered ophiolitic complexes, which have been strongly deformed, metamorphosed and are N-NW linearly oriented. These authors suggest the existence of at least two suture zones, resulting from the closure of small oceanic plates between the island arcs.

Intrusive bodies gabbroic to granitic composition are emplaced in the volcano-sedimentary sequences. They have cataclastic textures and show variable degrees of deformation. Angular xenoliths of amphibolitic composition, are locally found. Such xenoliths are interpreted as metabasalts from the volcanic-sedimentary sequences (Pimentel and Fuck, 1987b).

Elongated and mylonitized granitic bodies are also found. These are limited by faults, and usually show a vertical (N20W) mylonitic foliation, more noticeable at the limits of the bodies. Pimentel and Fuck (1992) obtained a Rb-Sr age of 698 +/- 10 M.y. for one of these granites.

The volcano-sedimentary sequences and associated rocks are interpreted as part of island arcs which started to evolve about 900 M.y. ago. This magmatic, metamorphic and deformational activity occurred throughout the Neoproterozoic, having its peak at approximately 600 M.y. About this time a

continental collision happened, after which the area started to stabilise and turned into a craton (Pimentel and Fuck, 1992b).

All the above mentioned units follow a general NNW to NNE trend, belonging to a major structure named the Transbrasiliano Lineament System. Mylonites from these units give ages varying from 630 to 594 M.y. and are associated with the end of the ocean closure and continental collision marking the end of the Brasiliano Orogeny (Pimentel *et al.*, 1991). During this tectonic cycle a progressive thickening of the crust took place (Pimentel and Fuck, 1992).

Late to postorogenic granitoid bodies, with dimensions up to batholithic, intruded the area. They consist of variable petrographic types, e.g. gabbro, quartz diorite, quartz monzonite, granodiorite, monzogranite and granite. They are divided into two age groups, one varying from 588 to 560 M.y. and the other between 508 and 485 M.y. (Pimentel *et al.*, 1996). The granites are metaluminous, K-rich and were emplaced in an extensional regime.

II.3 PHANEROZOIC

The Piranhas Formation comprises a poorly-sorted conglomerate which grades towards the top to a arkosic arenite with interbedded lenses of argillite (Rosito *et al.*, 1971). Clasts in the conglomerate include pyroclastic rocks, glassy basic lavas, trachytes, andesites, amphibolites, gneisses and granites (Faria *et al.*, 1975). The bedding has a NW strike and dip, varying

between 35° and 60° NE. The Piranhas formation is approximately 600m thick. These rocks were deposited over Pre-Cambrian rocks in a molassic environment with no associated volcanism. The top contact, with the Vila Maria Formation, is erosive (Faria *et al.*, 1975). The age limits for this formation are Cambrian and Pre-Devonian.

The Paraná Basin sedimentary rocks can be divided into five main sequences, limited by basin-wide unconformities: Silurian, Devonian, Permo-Carboniferous, Triassic and Jurassic-Cretaceous (Zalán *et al.*, 1990). These sequences developed during three different subsidence phases: Siluro-Devonian, Late-Carboniferous and Late-Jurassic to Early-Cretaceous (Fig. II.2).

The Rio Ivaí, Vila Maria, Furnas and Ponta Grossa formations are associated with the first subsidence phase. The last three formations are present in the study region. During the second phase of subsidence the Itararé Group and the Aquidauana, Rio Bonito, Irati, Terezinha and Rio do Rastro formations were deposited. Among these, only the Aquidauana Formation is known to occur in the area. The third subsidence phase is represented by the Rosário do Sul Group, Pirambóia, Botucatu and Serra Geral formations and the Bauru Group; the last three units occurring in the studied area. These three phases indicate nearly complete transgression-regression cycles (Zalán *et al.*, 1990).

The Vila Maria Formation marks the beginning of sedimentation in the NE portion Paraná Basin. Its type section is 14m thick (Faria, 1982) and comprises siliclastic rocks, starting with a polymitic diamictite at the bottom and grading to the sandstones of the Furnas Formation on the top. The Vila Maria Formation was deposited in a shallow marine environment, subjected to tide

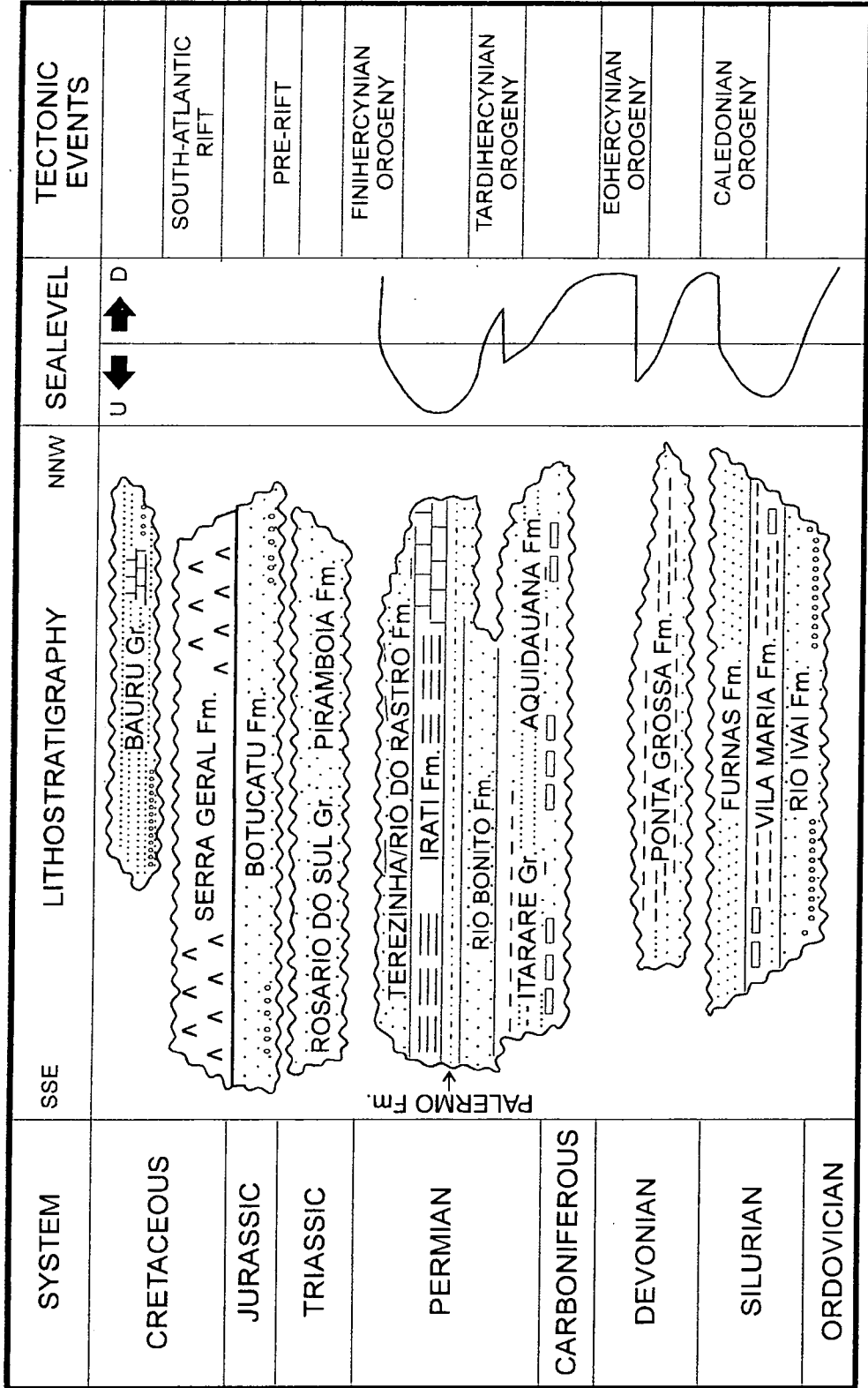


Figure II.2 - "Chronolithostratigraphic column in Parana Basin showing temporal and spatial distribution of main lithological units in a hypothetical SSE-NNW section. Also shown are tectonic events that have affected the basin evolution, as well as a tentative curve involving sealevel variation associated with Paleozoic sequences" (Zalan et al., 1990).

influence and periodical air exposure (Faria, 1982), during the Llandovery (Burjack and Popp, 1981).

The Furnas Formation is composed of a basal, polymitic conglomerate and poorly sorted sandstones (Andrade and Camarço, 1982), deposited in a fluvial continental environment and representing a regression phase (Zalán *et al.*, 1987). At the margins of the Paraná Basin the rocks of this Formation are found directly above the basement rocks. The upper contact with the Ponta Grossa Formation was considered to be discordant at the borders of the Basin and concordant at the centre (Andrade and Camarço, 1980). However, Burjack and Popp (1981) give a Llandovery age for the Furnas Formation and Upper-Devonian age for the Ponta Grossa Formation, which implies that they are discordant.

The Ponta Grossa Formation is the only part of the Devonian sequence present in the NE portion of the Paraná Basin. It covers the Silurian sequence in a transgressional event and was locally deposited directly over the Pre-Cambrian basement (Andrade e Camarço, 1980). Its main rock-types are siliclastic, including conglomerates and sandstones. The Ponta Grossa Formation has a discordant contact with the Aquidauana Formation, on the top.

The Aquidauana Formation is up to 300m thick and is sub-divided into three members. The Lower Member comprises diamictites and, locally, siltstone and shale, the Middle Member is represented by poorly-sorted sandstones, and the Upper is composed of siltstones and, rarely, phosphates (Camarço e Souza Jr., 1986).

From the Upper-Jurassic, the geological evolution of the southwestern Goiás was marked by intense magmatism. The first event is

represented by the extensive continental flood basalts of the Serra Geral Formation, with ages between 147 and 119 M.y. (Almeida, 1986). In the region this Formation comprises basalt lava flows and diabase dykes and sills (Bez *et al.*, 1971; Gaspar and Danni, 1981; Almeida, 1986).

The second phase of Post-Palaeozoic magmatism in the region comprises plutonic and volcanic alkaline rocks generated during the Upper Cretaceous. These rocks are collectively grouped by Almeida (1983) under the designation of Rio Verde-Iporá Igneous Province. The aim of this thesis is study some of the rocks associated with this magmatism. The Rio Verde-Iporá Igneous Province will be described in more detail in Chapter III.

After the alkaline magmatism, the Bauru Group was deposited (Gaspar and Danni, 1981; Danni *et al.*, 1990), starting with a basal polymictic conglomerate and grading towards the top into sandstones. Bands of flint occur throughout. The maximum thickness of the Bauru Group in the region is 150m (Camarço and Souza Jr., 1986). The same authors give an Upper Cretaceous age and favour a mixed fluvial-lacustrine depositional environment for this Group. This completes the evolution of the Paraná Basin in the area.

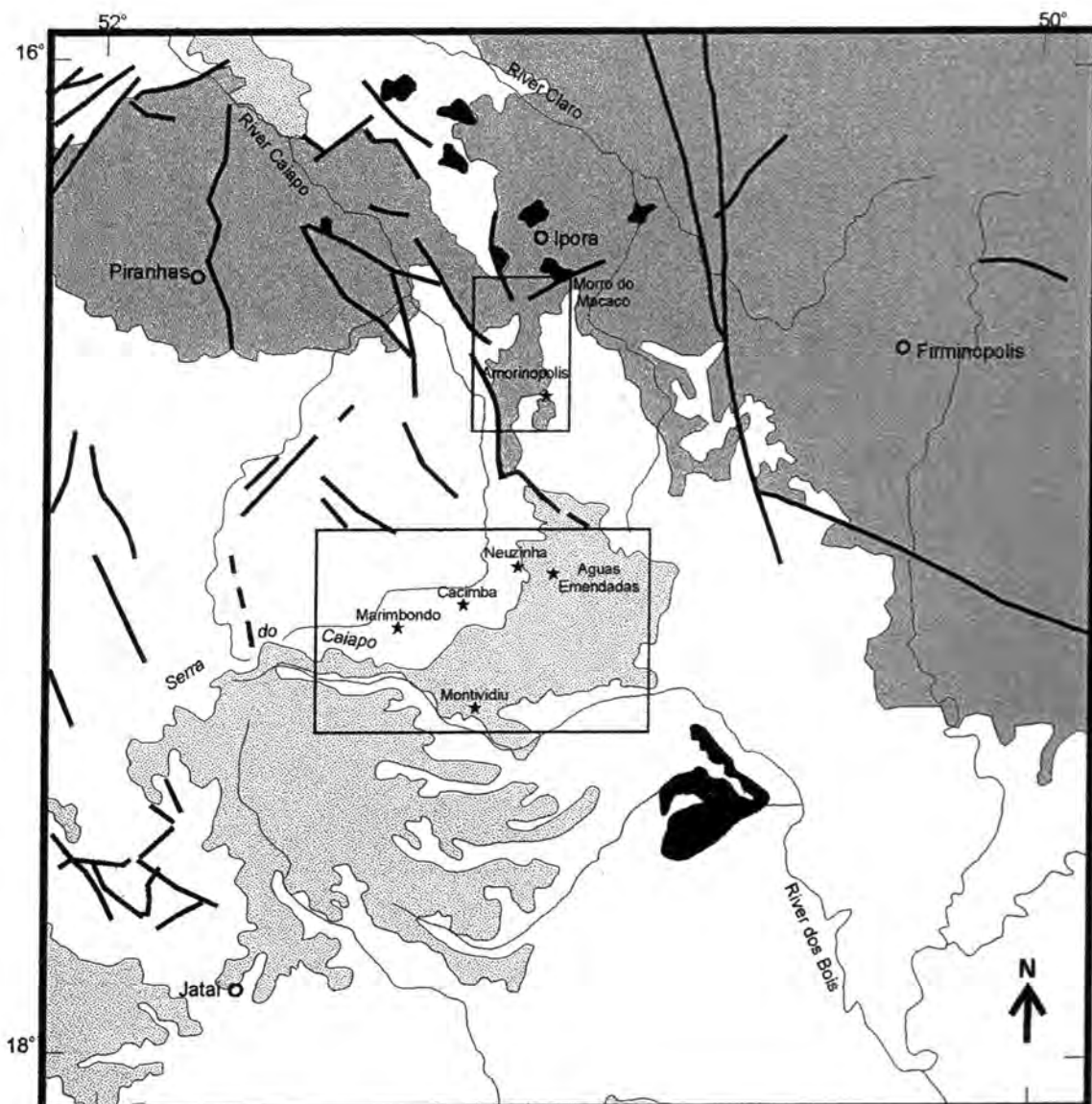
The Cenozoic is represented by detrital layers and laterites, which cover older rocks indiscriminately (Ilanhez *et al.*, 1983).

Chapter III - RIO VERDE-IPORÁ IGNEOUS PROVINCE

During the Late Cretaceous a series of alkaline provinces was formed around the margins of the Paraná Basin, among them the Rio Verde-Iporá Igneous Province (RVIIP) (Fig. III.1). Almeida (1967) associated these rocks with an extensional tectonic event (Wealdenian reactivation) leading to the emplacement, in a first stage, of alkaline rocks contemporaneous with the basalts of the Serra Geral Fm. and, in a second stage, to the Late Cretaceous alkaline rocks. Such event would have reactivated ancient fault zones of the basement, through which the magmas ascended. This event is considered to be an inland expression of the opening of the South-Atlantic Ocean (Almeida, 1983 and 1986).

Gibson *et al.* (1997) suggest that the main cause for the RVIIP magmatism is the impact of Trindade Mantle Plume close to the region of Iporá. However, VanDecar *et al.* (1995), based on seismic data, relate the Late Cretaceous magmatism to the Tristan da Cunha Mantle Plume, considering it an extension of the earlier Paraná Basin magmatism. The discussion of the causes of the magmatism is beyond the scope of this work, therefore it will not be taken any further.

The RVIIP occupies an area approximately 250km long by 70km wide, with N30W elongation. This coincides with a trend of faults in the



Key

- | | | | |
|---|-----------------------------|---|--------|
|  | Cenozoic Rocks |  | |
|  | * Cretaceous Alkaline Rocks |  | Faults |
|  | Parana Basin Rocks |  | Rivers |
|  | Pre-Cambrian Rocks |  | Towns |

Figure III.1 - Simplified geological map of the Ipora Province (After Schobbenhaus Filho *et al.*, 1984).

basement. The major old structures related with the ascent of alkaline magma are the Bom Jardim de Goiás Arch and the Transbrasiliano Lineament. The Bom Jardim de Goiás Arch is a regional anticline structure with the axis plunging S80W (Pena *et al.*, 1975). The Transbrasiliano Lineament follows a general Northeast orientation (Schobbenhaus Filho *et al.*, 1975). Rift tectonics affected the central-north portion of the RVIIP during the Upper Cretaceous (Almeida, 1983). The formation of the Caiapó Graben is associated with this event.

A wide variety of petrographic types is associated with the RVIIP magmatism, comprising intrusive, sub-volcanic and volcanic products. Volcanic rocks dominate in the South and intrusive bodies are more commonly found in the centre-north (Bez *et al.*, 1971; Danni, 1978; Barbour *et al.*, 1979; Gaspar and Danni, 1981; Danni and Gaspar, 1992; Danni *et al.*, 1992).

The mafic-ultramafic Alkaline Complex of Santa Fé, located in the North of the Province, is a ellipse-shaped body, measuring approximately 9.5km along its N-S axis and 6.5km across. It comprises dunites in the centre and clinopyroxenites, peridotites alkaline gabbros and syenites around the borders. K-Ar dating of biotite gives an age of 82.6 to 88.4 M.y. for these rocks. Lamprophyre and phonolite dykes also occur (Barbour *et al.*, 1979).

Near the town of Iporá, two Upper Cretaceous, concentrically zoned intrusions are described by Danni (1978). The Córrego dos Bois Complex is composed of two domes, covering an area of approximate 33km². The domes are formed mostly by dunites in the centre, surrounded by wehrlites, olivine pyroxenites and websterites. To the North and to the South rings of alkaline olivine gabbro, theralites and essexites are found. The whole

structure is surrounded by a narrow and discontinuous intrusion of nepheline syenite. Dykes of syenite intrude both the complex and the country rocks. The other intrusion is called the Morro do Macaco Complex. It is formed by four domes composed, from the core to the margin, of dunite, wehrlite, olivine pyroxenite and clinopyroxenite. Syenites are found to the West of the domes.

The Fazenda do Buriti Complex is located about 15km Northwest of Iporá, occupying an approximate area of 35km². The intrusive facies are represented by olivine clinopyroxenites, melagabbros, essexites, syenogabbros and syenites. Associated to these rocks, a trachytic sill and quartz microsyenites are found (Cerqueira and Danni, 1994).

Subvolcanic intrusions of picritic nature are commonly found in the region. They occur as dykes, plugs and sills. The dykes are often only a few metres wide and tens of metres long, filling fractures in the Pre-Cambrian basement, with N30W and N50E directions. The sills are normally emplaced in Paraná Basin strata. Their thickness is usually <5m but they can extend laterally for more than 500m. They have homogeneous aspect, with no visible indication of differentiation. The plugs are cylindrical in shape and can be up to 200m in diameter (Danni, 1994). The magma parental to the concentrically zoned intrusions in the region (e.g. Morro do Macaco) is believed to be of alkaline picritic composition, based in xenoliths found in these rocks (Danni *et al.*, 1992; Danni, 1994).

Near to the Bebedouro farm, 10km South of Amarinópolis (Fig. III.1), a sub-volcanic association occurs. This is the result of ultrabasic alkaline magmatism of perpotassic to sodic-potassic composition (Danni, 1985). The occurrence is about 1200m in diameter. It is occupied in the centre by a

cylinder-shaped intrusion of basanitic to tephritic composition. Ring and radial dykes of olivine leucite melanephelinites, melanalcitites and olivine nepheline melaleucitites preceded the main intrusion (Danni, 1985). The last event in the complex was degassing of the sub-volcanic reservoir, forming breccia pipes (Danni, 1985). At the Southwest of the main intrusion a katungite pipe is found. This is the only occurrence of this type of rock described in the region so far (Danni, 1985, Danni and Gaspar, 1992; Danni and Gaspar 1994). An important characteristic noticed by Danni and Gaspar (1994) is the high content of TiO_2 in the whole-rock analyses of this occurrence. Upper Cretaceous, high-Ti alkaline rocks are coincident geographically with high-Ti continental flood basalts of the Paraná Basin, and this feature has been related to the source of the magmatism (Gibson *et al.*, 1995b).

The Alkaline-Carbonatite Province of Santo Antônio da Barra (Gaspar and Danni, 1981) is located in the southern part of the RVIP. The volcanic rocks of Santo Antônio da Barra comprise alternated lavas and pyroclastic deposits. The rock types include analcimites, olivine analcimites, analcimitic breccias and carbonatitic pyroclastic rocks. Late dykes and plugs occur associated with these rocks, including fourchites, melamonchiquites, phonolites and trachytes. The magma parental to these rocks had a nephelinitic composition (Gaspar and Danni, 1981). It ascended through the Santo Antônio da Barra-Iporá tectonic-magmatic lineament, which is oriented N40-50W. A volcanoclastic conglomerate was deposited on top of the volcanic rocks (Rio Verdinho Formation; Gaspar and Danni, 1981). Sgarbi *et al.* (1998) suggest that the rocks from Santo Antônio da Barra have a chemical affinity

with kamafugites. K-Ar data give an 85 M.y. age for the volcanic rocks (Hasui *et al.*, 1971).

Other important volcanic association present in the RVIIP occurs in the Águas Emendadas Region, located between the towns of Amarinópolis and Montividiu. It comprises dykes, plugs, and volcanic vents and pyroclastic deposits, usually emplaced in the Aquidauana Formation and covered by the Bauru Group. The rock types present include olivine melanephelinites, olivine-analcite melanephelinites, olivine analcimites, nephelinites, micro-ijolites, basanites and tephrites. These rocks were considered an extension of the Alkaline-Carbonatitic Santo Antônio da Barra Province (Danni *et al.*, 1990). These authors also suggested that the leucititic and nephelinitic rocks originated from different magmas and that the leucititic rocks might be related to the sources of diamonds found in alluvial deposits nearby.

Based on aeromagnetic data, associated with microprobe analyses of stream sediment heavy mineral concentrate, Tompkins (1987) describes the occurrence of a probable kimberlite, South of Amarinópolis. However, she also considered that the lithosphere thickness is likely to be <150km in the region, not deep enough for the kimberlite to be diamondiferous. She therefore interpreted the source of diamonds in the region to be older (Pre-Cambrian).

Chapter IV - FIELD GEOLOGY AND PETROGRAPHY OF ÁGUAS EMENDADAS REGION

IV.1 FIELD RELATIONSHIPS

IV.1.1 Introduction

Breccias composed largely of volcanic rocks and crystal fragments are exposed in three different localities: Águas Emendadas (17°02'S 51°07'W), Neuzinha (17°01'S 51°08'W) and Marimbondo (17°09'S 51°22'W). They all occur as a central breccia, surrounded by lavas, which intrudes sedimentary rocks from the Paraná Basin (Fig. IV.1.1).

The Neuzinha breccia consists of a continuous outcrop of approximately 500m in diameter, cut by a track where the rocks are best exposed. It is mostly surrounded by lava, although it is not possible to see the contact relationships. The contact with the Aquidauana Formation is well exposed as a hornfelsed sandstone to the Southwest of the breccia. Neuzinha is the best preserved breccia among the localities sampled, even though it is still hydrothermally altered and weathered (Fig. IV.1.2).

Marimbondo is the southernmost locality visited. The access is limited by the thick vegetation cover. No relationship between the breccia and

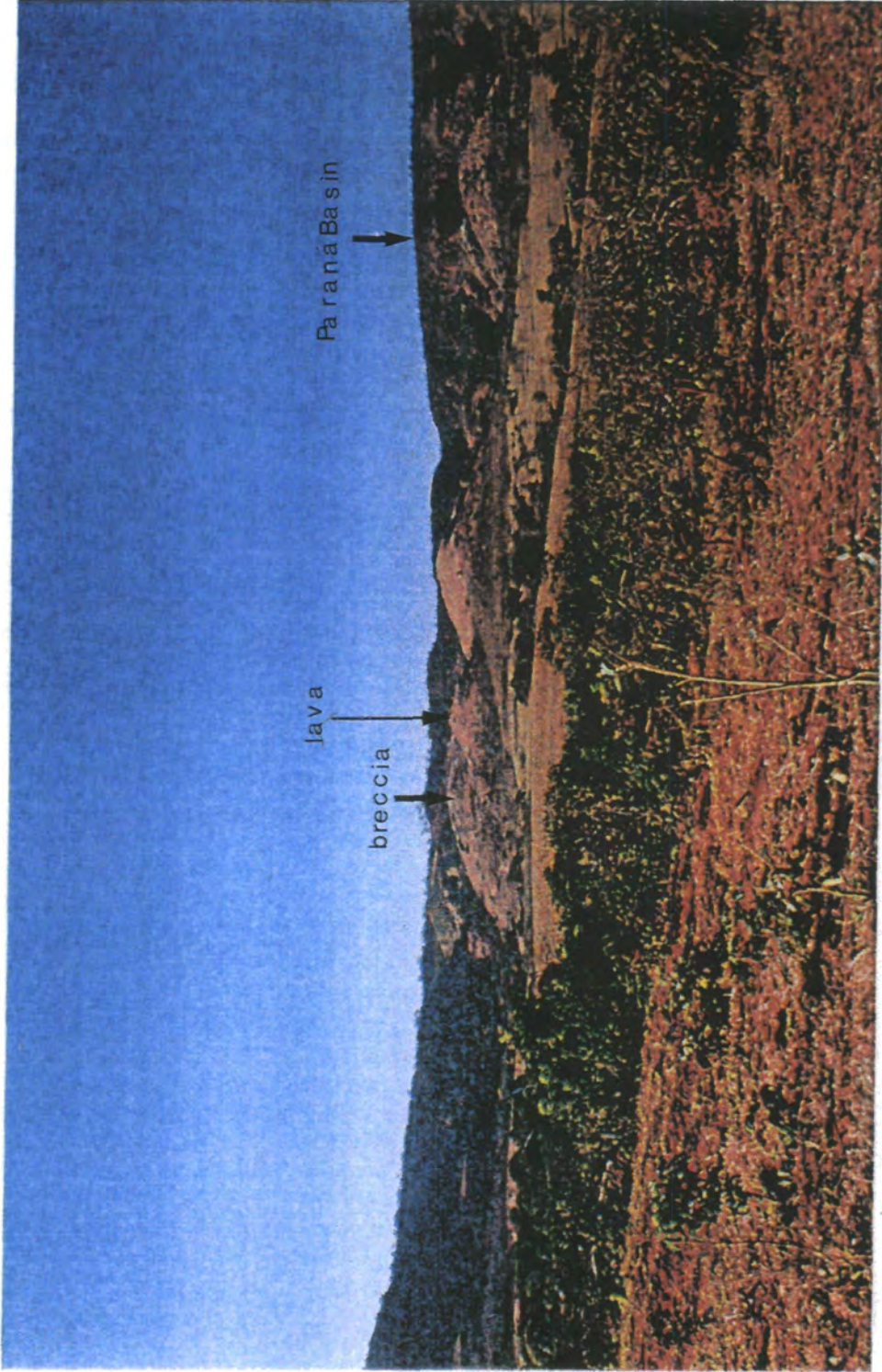


Figure IV.1.1 - View of the Neuzinha Occurrence, due east, showing an example of field relationships between breccia, lava (melaleucitite and melanephehinite (?) and sedimentary rocks of the Paraná Basin.

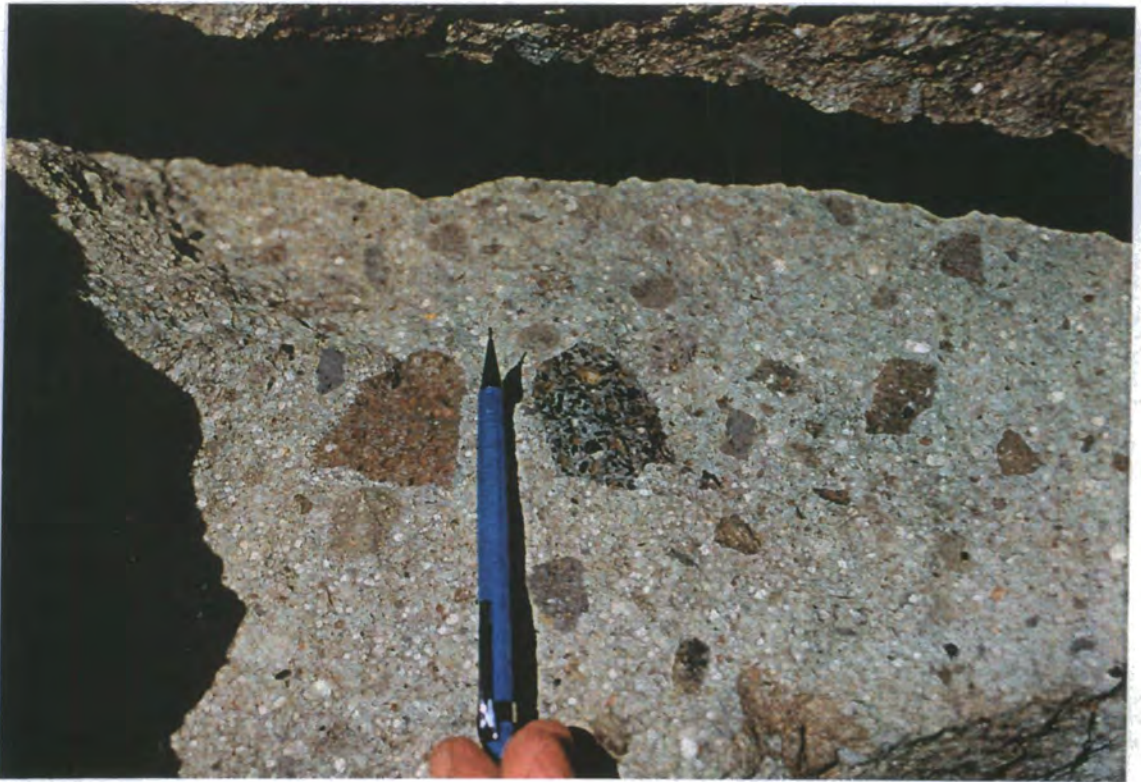


Figure IV.1.2 - Breccia outcrop at Neuzinha. Matrix-supported breccia with angular to rounded fragments. (a) accessory fragment; (b) cognate fragment; (c) phlogopite megacryst; (d) K-feldspar xenocryst. Pencil size for scale = 14.4 cm.

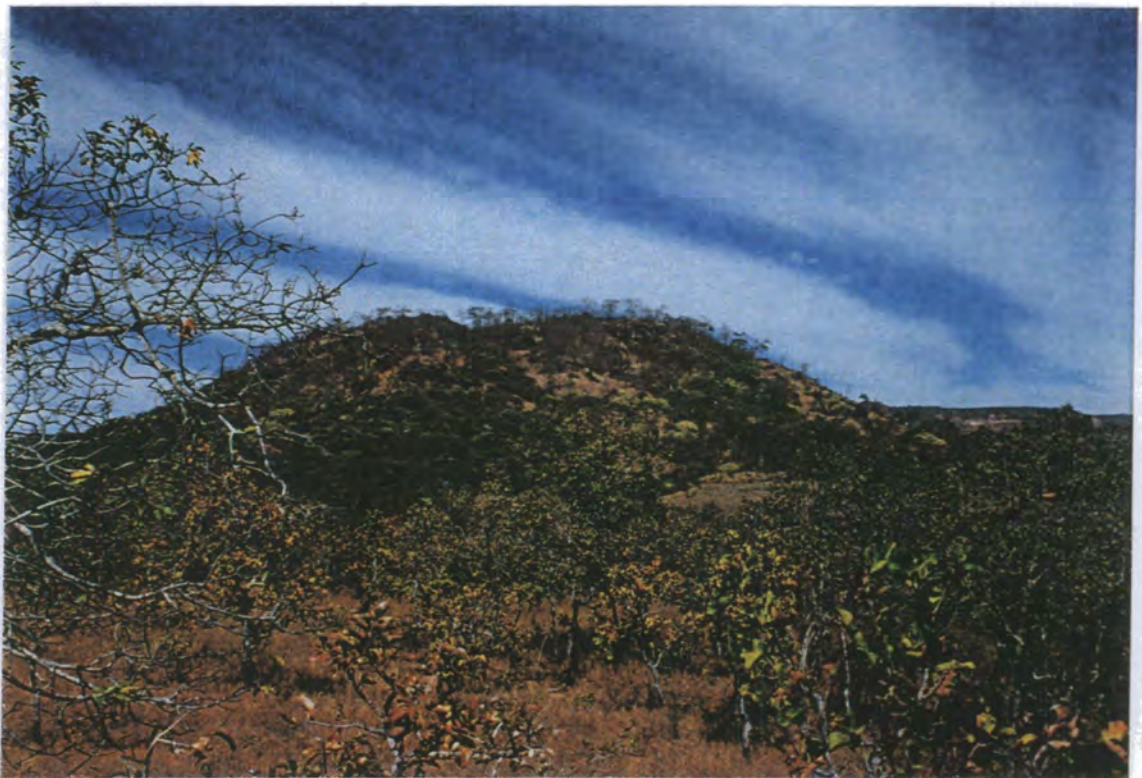


Figure IV.1.3 - View of Marimbondo Occurrence; facing Southeast. The nearest, left-hand side mound is a lava outcrop (melaleucitite). The breccia is located in the broader mound behind. Paraná Basin sediments form the plateau in the background.

lavas or country rocks could be observed. However, they are presumably the same as in Neuzinha and Águas Emendadas, since a similar pattern of a central breccia and a semicircle of lavas emplaced in rocks of the Paraná Basin is observed (Fig. IV.1.3). Sampling is very difficult as this breccia is the most weathered of the three.

Águas Emendadas is located in a valley cut in sandstones (Fig. IV.1.4). The outcrop is continuous for at least 1km, with an average width of 100m. This breccia has been strongly hydrothermally altered, and a pervasive carbonate/zeolite assemblage is observed throughout (Fig. IV.1.5). The contact with the Aquidauana Formation is very clear and can be observed in different places where development of hornfels and columnar jointing in the host sandstone occurs (Fig. IV.1.6).

The description and classification of volcanoclastic rocks follows the parameters used by Cas and Wright (1987). The division of fragments into size groups is listed in Fig. IV.1.7; while Fig. IV.1.8 presents a summary of fragment classification according to provenience.

IV.1.2 Breccias

The following description of the breccias and their field relations will be focused on Águas Emendadas because of the better exposure, but aspects of the other two will be also considered.

The breccias have an extreme range of grain size, with subangular blocks up to ~3m in diameter (Fig. IV.1.9) scattered in a breccia matrix that has an average grain size of ~5mm (1-50mm) (Fig. IV.1.10). The percentage of fine-



Figure IV.1.4 - View of Águas Emendadas outcrop. The breccia is well exposed along the stream bed. Lavas crop out in the hill on the left hand side and on the right bank. Paraná Basin sediments occur in the hills on the far side.



Figure IV.1.5 - Águas Emendadas. Carbonate/zeolite veinlets (white) crosscutting both the matrix and fragments of the breccia. This assemblage also occurs as interstitial white patches within the matrix.



Figure IV.1.6 - Águas Emendadas. Columnar jointing developed in sandstone of the Paraná Basin, as a result of thermal metamorphism at the contact with the breccia. The sandstone is recrystallised and shows hornfels texture.

FRAGMENT	SIZE RANGE	PYROCLASTIC ROCK
ash	<2mm	ash tuff
lapilli	2-64mm	lapillistone*
block/bomb	>64mm	pyroclastic breccia/ agglomerate

Figure IV.1.7 - Classification of fragments and associated pyroclastic rocks according to Cas and Wright (1987). * For rocks where mixed ash and lapilli are the constituent material, the term lapilli tuff is used in the text (Cas and Wright, 1987, p. 360).

Type of Fragment		Description	
Juvenile		"represents samples of the erupting magma."	
Lithic	cognate	"non-vesiculated juvenile magmatic fragments." "fragments that have solidified from the erupting magma."	
	xenolith	accessory	"country rock that has been explosively ejected during eruption."
		accidental	"clasts picked up locally by pyroclastic flows and surges."
Crystals	juvenile	"free crystals and angular fragments of crystals released during explosive disruption and breakage of porphyritic magmas and juvenile fragments."	
	xenocryst	"non-juvenile crystals derived by fragmentation of accessory and accidental lithics."	

Figure IV.1.8 - Terms and definitions used for classification of fragments according to their origin (Cas and Wright, 1987).

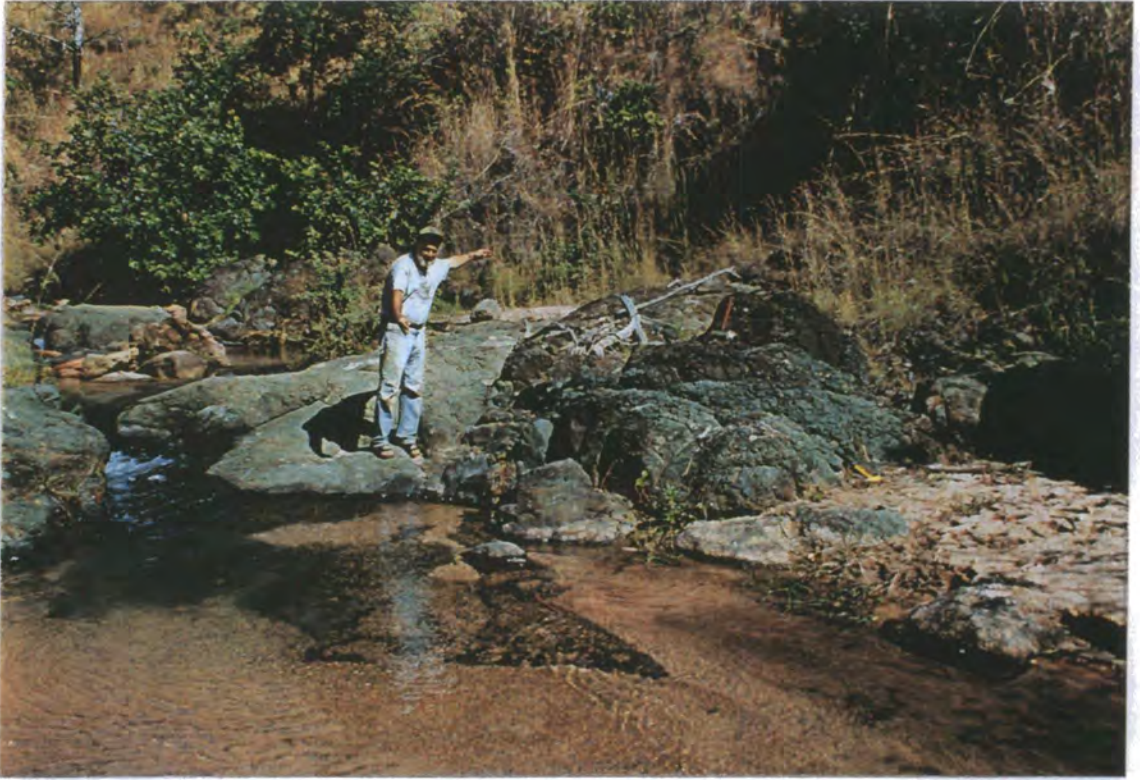


Figure IV.1.9 - Águas Emendadas. Large, dark-coloured block. The block is a cognate fragment of melaleucitite standing out in the more weathered breccia matrix. Its largest dimension reaches 3 m.

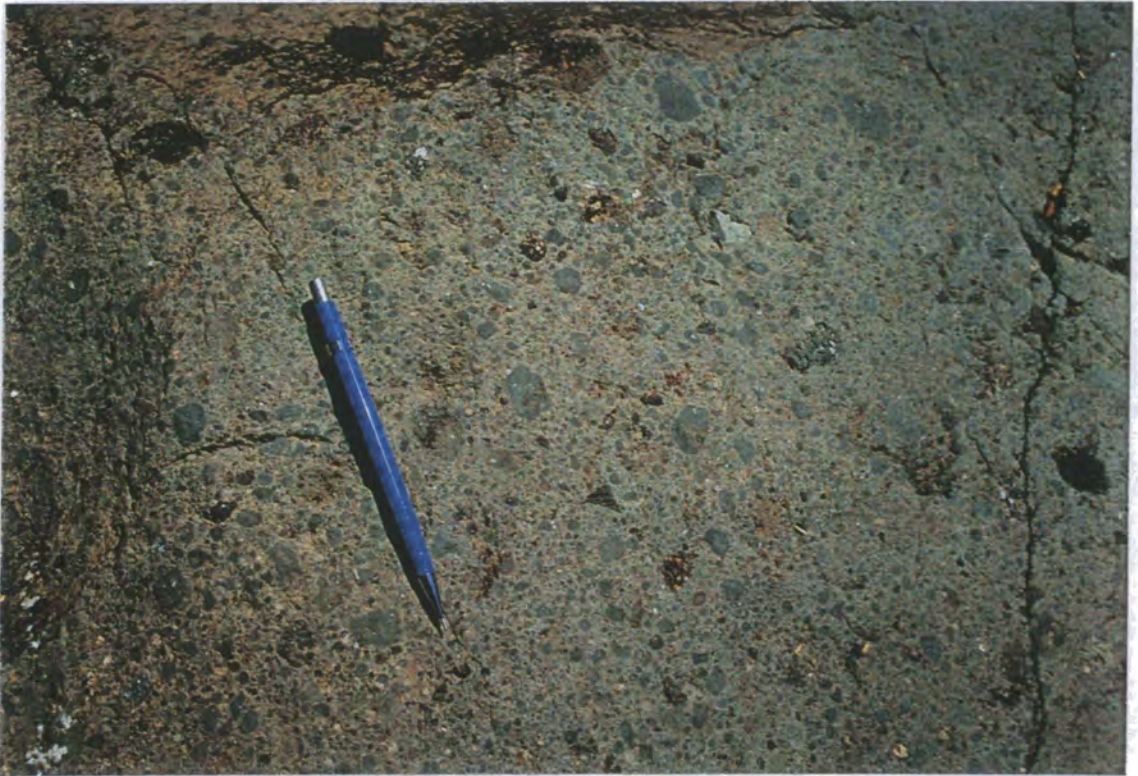


Figure IV.1.10 - Águas Emendadas. Appearance of the breccia matrix. The average grainsize is lapilli. Matrix composed of fragments with average lapilli-size. Note the abundance of juvenile and cognate fragments (dark-coloured rounded patches).

grained material is highest in Águas Emendadas while the Marimbondo breccia has a more coarse-grained and matrix-poor fabric (Fig. IV.1.11). Neuzinha is intermediate between these two extremes.

Through most of the Águas Emendadas outcrop the breccia matrix is entirely fragmental, but locally it grades over distances of 1-2m into homogeneous, vesicular, very fine-grained, mafic igneous rock (Fig. IV.1.12). This rock-type occurs over areas of up to 3x5m. This grading was not observed in the other two localities.

The fragments are mainly juvenile. They are irregular to rounded and locally vesiculated, with sizes varying from ash to block (<1m). Bombs are also present (Fig. IV.1.13). The freshest fragments have a dark grey colour, changing into green when altered. Compositionally, they consist of an aphanitic groundmass with clinopyroxene and olivine phenocrysts (Fig. IV.1.14). Crystals of clinopyroxene and megacrysts of phlogopite are common in the matrix of all three breccias.

Cognate fragments are very similar to the juvenile clasts, except that they reach up to 3m in size, are less rounded, and can be very rich in clinopyroxene phenocrysts (~70%). Some fragments show features of magma mixing, such as the presence of two compositional domains in the same fragment (usually with similar mineralogy but different modal proportions and grainsize), with crenulated contact between them (Fig. IV.1.15). Locally, broken cognate fragments are slightly separated by breccia matrix, but still retain their original orientation relatively to each other, suggesting that very little or no reworking occurred (Fig. IV.1.16).



Figure IV.1.11 - Marimbondo. Appearance of the breccia matrix. Fragments with lapilli-size in average but with irregular size distribution. Accessory fragments of sandstone reach up to 7cm (orange-coloured).



Figure IV.1.12 - Águas Emendadas. Homogeneous mafic igneous rock. The rock is dark grey, aphanitic, rich in vesicles filled with carbonate (up to 1cm).

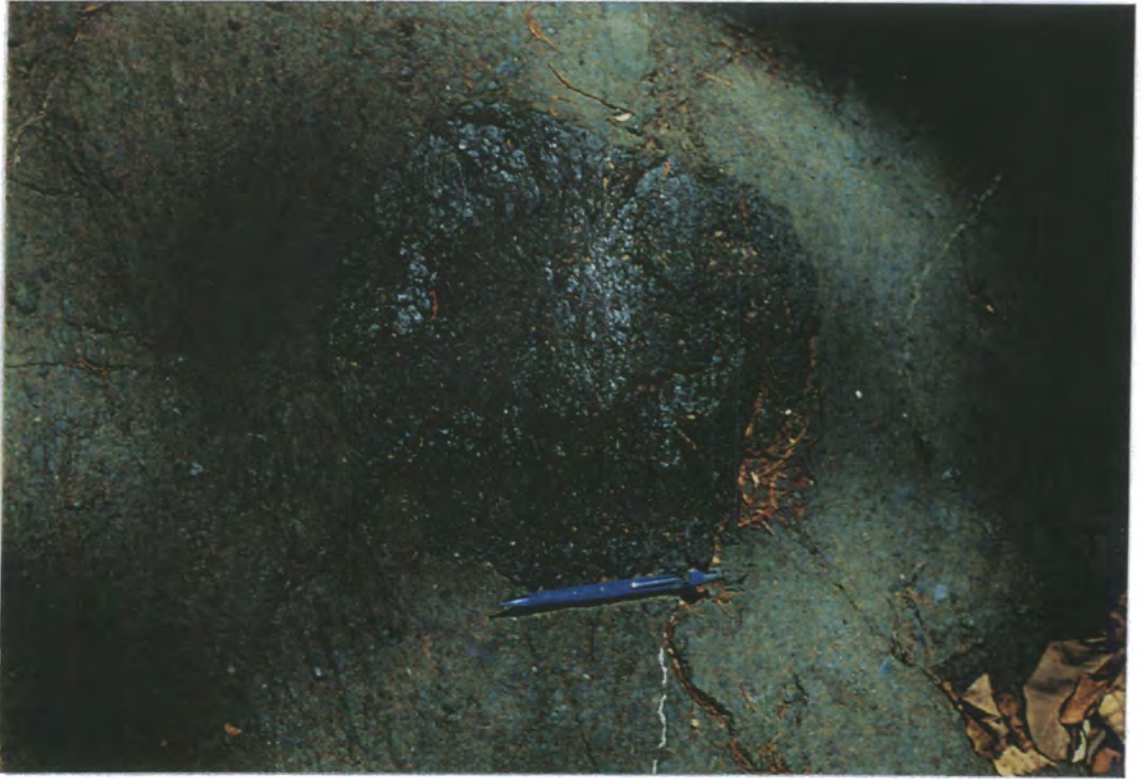


Figure IV.1.13 - Águas Emendadas. Bomb, approximately 35cm in diameter (juvenile fragment), surrounded by a more light-coloured breccia matrix.

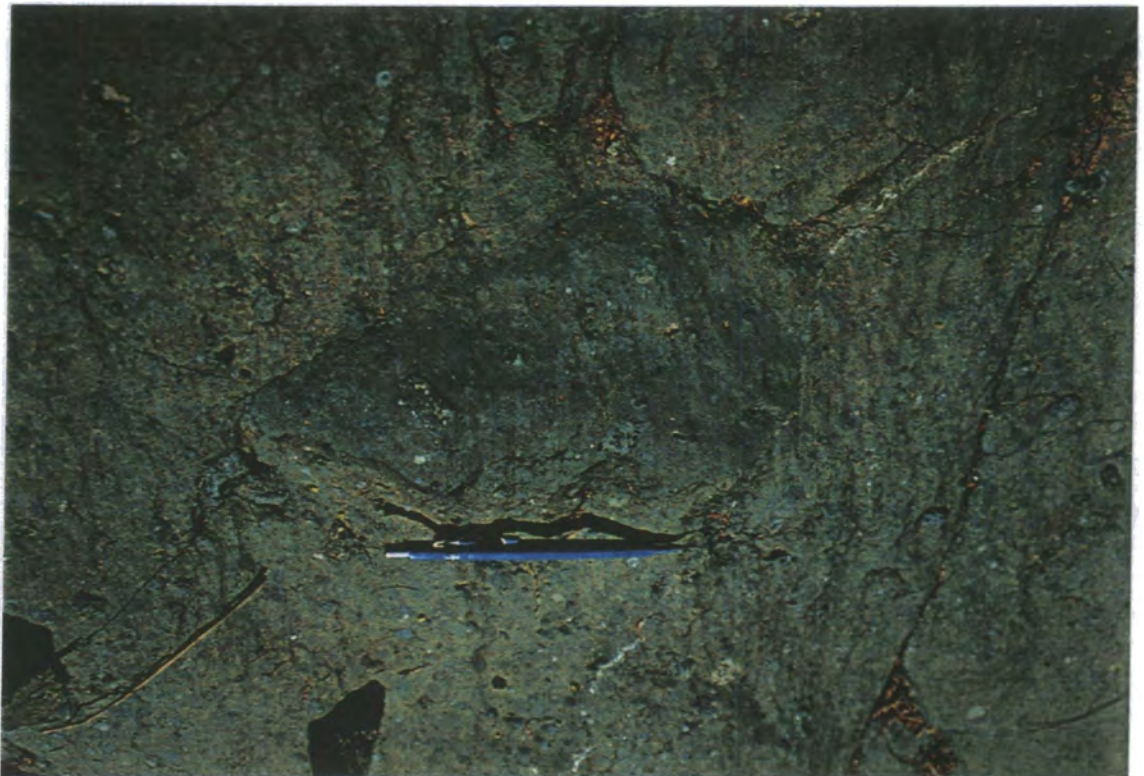


Figure IV.1.14 - Águas Emendadas. Juvenile fragment with irregular shape. The fragment is very rich in xenoliths.



Figure IV.1.15 - Águas Emendadas. Cognate fragment (centre). The fragment has irregular shape and is composed of two domains with different compositions. The contact between these two domains is irregular, suggesting magma mixing.

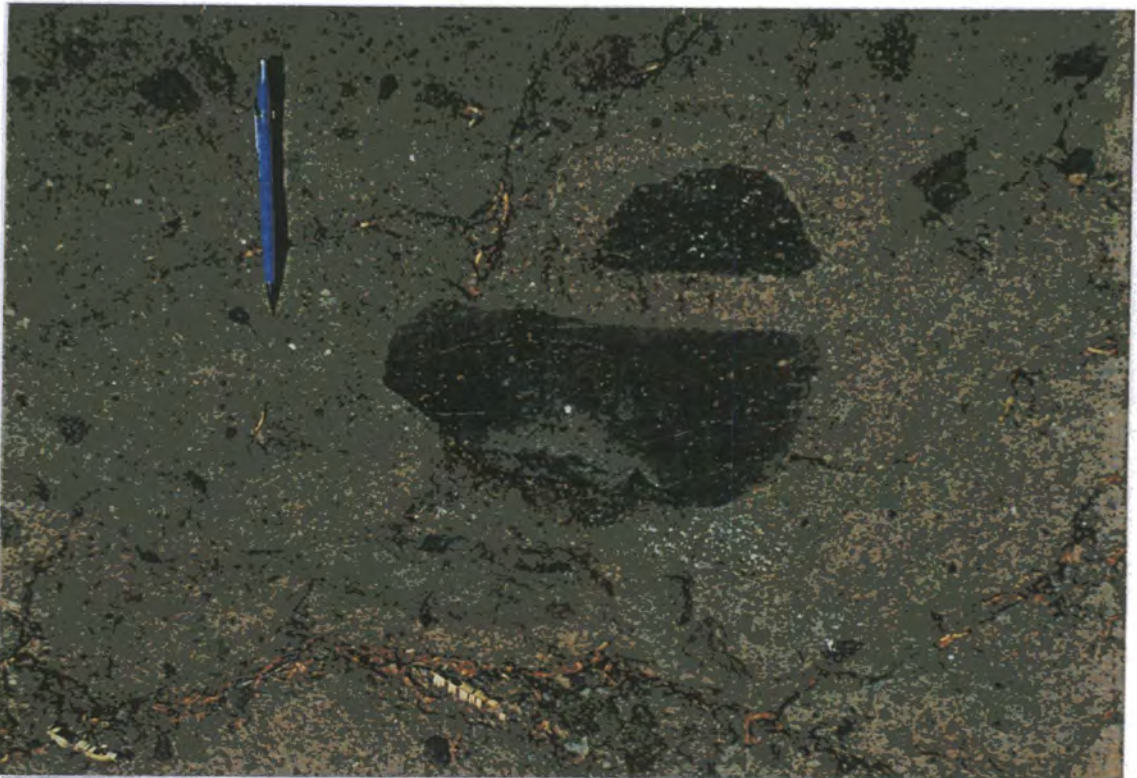


Figure IV.1.16 - Águas Emendadas. Cognate fragment. Although the fragment is broken up, the two halves are only slightly displaced, indicating that very little transport occurred

Accessory fragments comprise Pre-Cambrian igneous and metamorphic rocks, Palaeozoic sedimentary rocks, and Cretaceous alkaline rocks. They are usually angular, with an average that is lapilli size and rarely submetric. The margins of sandstones are often recrystallised. Except for the alkaline rocks, the accessory fragments are easily identified by their lighter colour (Fig. IV.1.17), relative to the juvenile and cognate ones. As is often the case in other pyroclastic deposits, accessory and accidental fragments are very difficult to distinguish from each other. Nevertheless, the outcrop style suggests that the accessory type is dominant. Marimbondo is the breccia with the highest variety and proportion of accessory fragments, followed by Neuzinha. Accessory and accidental fragments seem to be evenly distributed among the three breccias; no preferential concentration zone was observed. Xenocrysts are also present, K-feldspar is extremely common in Neuzinha. No depositional structure such as grading or bedding has been recognised in the breccias.

IV.1.3 Dykes

A small number of sinuous, poorly-vesicular dykes, ~2 to 100 cm wide, intrude these breccias (Fig. IV.1.18). They are mostly aphanitic but can vary locally to porphyritic facies, with clinopyroxene (up to 2,5cm) and olivine (up to 1cm) phenocrysts set in an aphanitic groundmass. Megacrysts of phlogopite are often found at the margins of these dykes (Fig. IV.1.19). When present, vesicles are concentrated in central parts of the dykes. The only chilling feature present is the development of columnar joints in one of the dykes (Fig. IV.1.20).



Figure IV.1.17 - Águas Emendadas. Accessory fragments (amphibolite). Usually this type of fragment has lighter colour and angular shape.



Figure IV.1.18 - Águas Emendadas. Dyke emplaced in breccia. The dyke is a light-green, aphanitic rock, poorly vesiculated and melanephelinitic (?) in composition. The irregular contact between them suggests that the breccia was still "soft" at the time of emplacement of the dyke.



Figure IV.1.19 - Águas Emendadas. Megacrysts of phlogopite (indicated by an arrow) on the margin of dyke. The phlogopites are oriented parallel to the dyke wall.



Figure IV.1.20 - Águas Emendadas. Columnar jointing at the margin of dyke. The rock is melanephelinitic in composition, poorly vesiculated, with abundant aphanitic groundmass and rare megacrysts of phlogopite.

The dykes were formed probably by a single injection of magma. When present, textural and compositional differences across the dyke appear to be related to flow and in-situ differentiation.

IV.1.4 Lavas

Samples of lava were collected from Neuzinha, Águas Emendadas, Marimbondo and Cacimba. The lavas occur as blocks on small hills around the breccias (Fig. IV.1.1) and seem to be located topographically above them. At Águas Emendadas it is possible to observe the lava covering the breccia. Contact between lavas and sandstones was not observed. The size of the outcropping blocks is variable, from a few cm to places where relatively fresh rock covers areas up to 20m². Lavas are mostly altered into a dark red soil but, when fresh, they are dark grey in colour (Fig. IV.1.21). Flow banding can be locally recognised by the alignment of clinopyroxene phenocrysts. Structures such as lava tubes and auto brecciation were not found. Vesicles are rare and were only observed locally, at Águas Emendadas (Fig. IV.1.22).

The lavas are usually porphyritic with a variable phenocryst content and aphanitic, dark grey groundmass (Fig. IV.1.21). Phenocrysts of clinopyroxene are always present, olivine is very common. Other phenocryst phases comprise phlogopite, Fe-Ti oxides and rare leucite.

The presence of "amoeboid" inclusions of different sizes, normally containing bigger phenocrysts than their host lava, is noticeable at Águas Emendadas (Fig. IV.1.23). This suggests that at least one episode of magma mixing occurred previously to the eruption of the lavas. Cognate xenoliths in



Figure IV.1.21 - Águas Emendadas. Appearance of lava (basanite). Dark grey rock, very rich in phenocrysts of olivine, pyroxene and less frequent plagioclase.



Figure IV.1.22 - Águas Emendadas. Appearance of lava (melanephelinite (?)). The rock is highly vesiculated and mostly aphanitic, except for rare pyroxene phenocrysts.



Figure IV.1.23 - Águas Emendadas. Appearance of lava. Rock rich in amoeboid inclusions, which have a lighter colour and are more phenocryst-rich than the "host".



Figure IV.1.24 - Águas Emendadas. Cognate xenolith (approximately 2cm) of dunite in melaleucitite.

the lavas range in size from mm to a few cm. They are normally more rich in phenocrysts than the enclosing lava. Xenoliths of cumulate rocks such as pyroxenites and dunites are also present (Fig. IV.1.24).

IV.2 PETROGRAPHY

IV.2.1 Introduction

Petrographic studies have been carried out with the use of transmitted-light petrographic microscope. Selected samples were submitted to microprobe analyses but the results of this work will be discussed separately in Chapter V. The nomenclature and classification of the rocks follows, as closely as possible, the IUGS recommendations (Le Maitre, 1989; Woolley et al., 1996).

The first attempt to classify the studied rocks resulted in two main groups:

Group 1 - Volcanic Breccias and Associated Dykes

Group 2 - Lavas

Petrographic description of the Group 1 rocks is concerned with aspects of the breccias in general, such as provenience and morphology of their fragments, but not with details of the original mineralogy and textures of the alkaline volcanic fragments. These are petrographically described within Group 2, since it is assumed that they represent examples of the same

magmatism in the region. The dykes and breccias are included in Group 1, due to their related origin.

The classification of the Group 2 volcanic rocks was based on their present mineralogy in most cases. An exception was made for pseudo-leucite-bearing rocks. In cases where leucite was clearly the original phase present in the rock, all pseudo-leucite was treated as leucite for classification purposes. The studied rocks suffered different stages of post-eruption modification. They were initially subjected to hydrothermal alteration, and later suffered tropical weathering.

The key minerals used for classification are very sensitive to the presence of fluids. Elements such as K and Na are easily mobilised, which results in important mineralogical and chemical changes to the composition of the studied rocks.

There is a strong possibility that the magmatism in the area had a kamafugitic-carbonatitic affinity, but this can not be definitely proved on the basis of petrographic observations alone. For a precise identification it would be necessary to carry out extensive microprobe and stable isotope analyses. In particular, it is important to stress that some of the rocks classified as "nephelinite" could have originally contained kalsilite, later converted to nepheline. Moreover, fine-grained kalsilite is indistinguishable from nepheline under the ordinary petrographic microscope. If the presence of kalsilite could be proved, then some of the nephelinites would be more accurately classified as kamafugites. For these reasons, the terms nephelinite and melanephelinite are hereafter accompanied by a question mark (?). Most rocks have a cryptocrystalline groundmass. The vast majority of them have phenocrysts of

mafic minerals only. These two characteristics, together with the alteration, make the classification of the volcanic rocks from the Águas Emendadas region extremely imprecise.

IV.2.2 Volcanic Breccias and associated Dykes

Breccia Matrix

Although many thin sections of the breccia matrix were prepared, the large majority of these were sufficiently hydrothermally altered and carbonated to obscure the details of their textures. Therefore, the petrographic descriptions are concentrated on only those sections with minimal alteration. The breccia matrix contains fine and coarse ash, carbonate, glass fragments, rounded fragments of magma, crystal fragments and armoured lapilli, alongside fragments of older alkaline rocks, sandstones of the Paraná Basin and rock and crystal fragments from the Pre-Cambrian basement. The matrix is best described as a poly lithic lapilli tuff.

Fragments of the Pre-Cambrian basement consist mainly of amphibolites, granites and gneisses. They were probably transported by the magma as xenoliths, since Pre-Cambrian rocks do not crop out near the studied area. They represent the most common type of accessory fragment in the breccia matrix. Loose K-feldspar crystals from the granites occur as xenocrysts. The fragments are usually angular and the xenocrysts are often broken. Fragments of basement rocks do not show any particular evidence of contact metamorphism (Fig. IV.2.1). Fragments of the Paraná Basin sedimentary rocks are mainly sandstones. They are angular in shape (Fig.

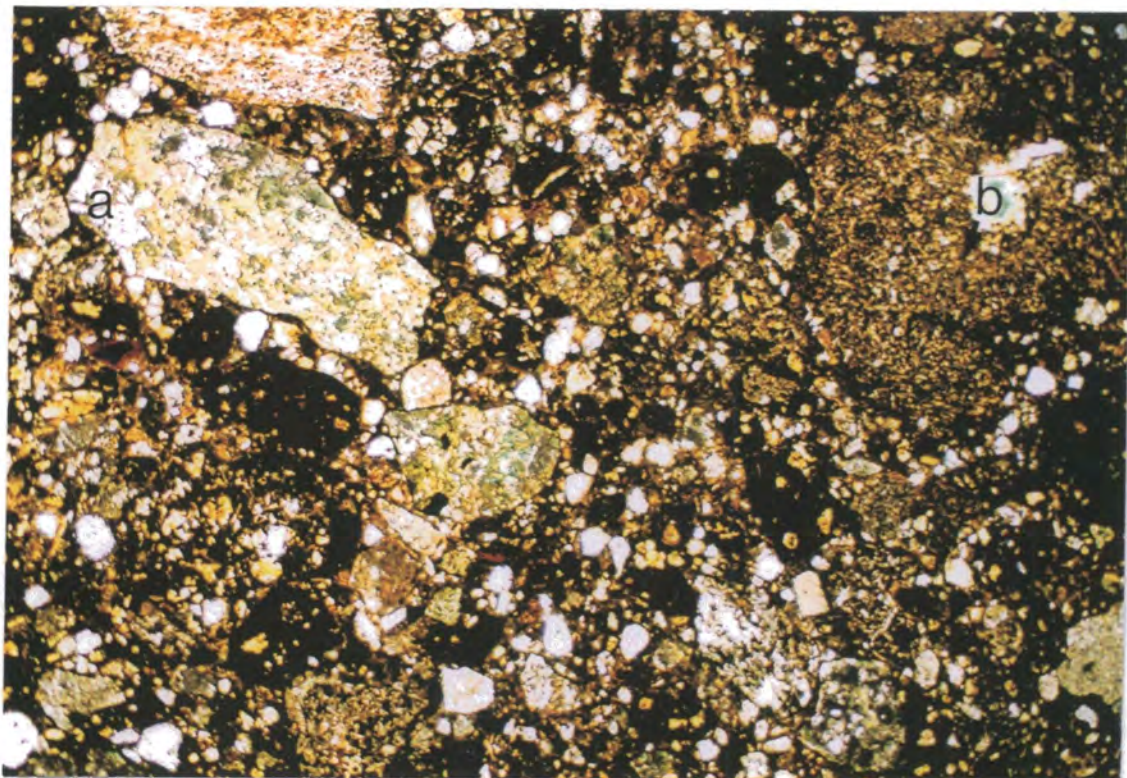


Figure IV.2.1 - Marimondo (96AE16). Breccia matrix composed of lapilli to ash size fragments. (a) angular accessory fragment of amphibolite. (b) Accessory fragment of melanephelinite (?). Field of view is 15x10mm. Plane-polarized light.

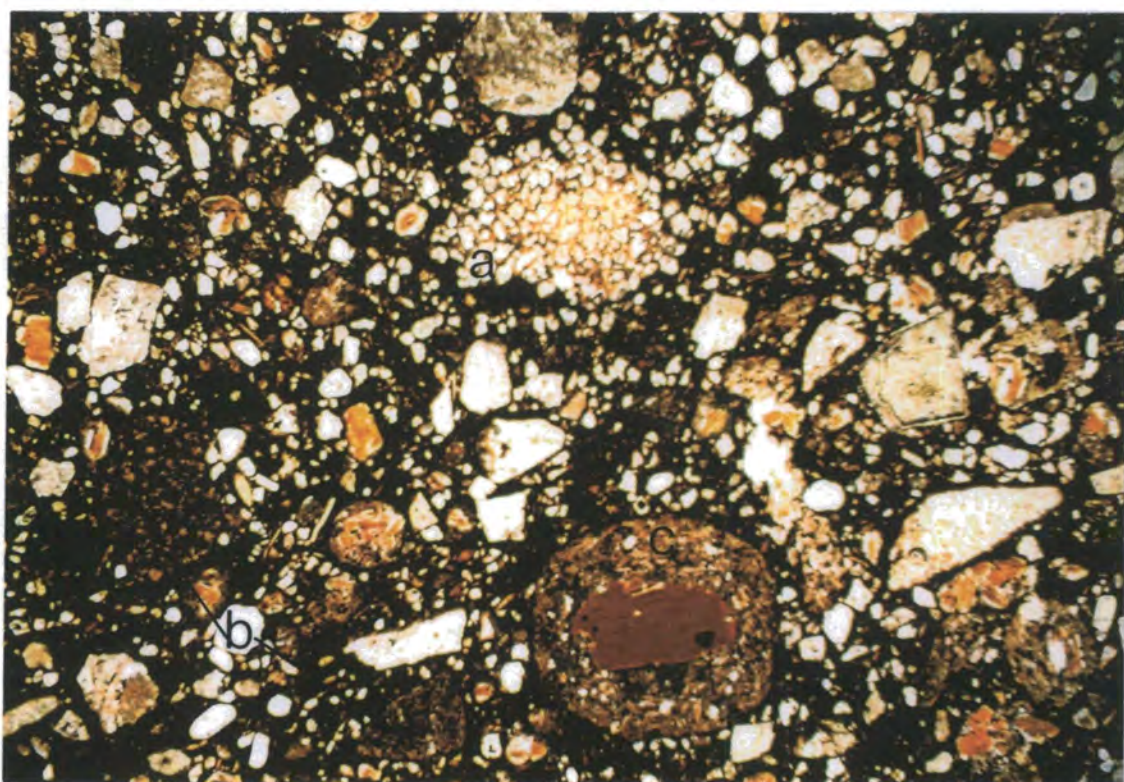


Figure IV.2.2 - Neuzinha (96AE09). Breccia matrix (a) accessory fragment of sandstone (Paraná Basin). (b) accessory fragment of alkaline rock. (c) Spinning droplet with phlogopite core. Field of view is 15x10mm. Plane-polarized light.

IV.2.2) but, unlike the Pre-Cambrian rocks, sandstone fragments locally show evidence of recrystallisation.

Some alkaline volcanic rocks from Iporá province are also present as accessory fragments (Fig. IV.2.2). The main rock types represented are, in order of abundance, leucitites, basanites, olivine basalts, melanephelinites (?), dunites and pyroxenites. Accessory fragments of melanephelinites (?) can be distinguished from juvenile and cognate fragments mainly by their angular shape.

Cognate fragments are compositionally classified as melanephelinites (?). Although on occasions they may be difficult to distinguish from the juvenile variety, cognate fragments are usually less rounded. Additionally, some cognate fragments show evidence of magma mixing, while others have larger and more abundant pyroxene phenocrysts than the juveniles (Fig. IV.2.3). Isolated crystal fragments of pyroxene, up to 3cm, also occur. These are interpreted as having originated in the magma chamber and become remobilised later by the ascending magma.

Juvenile fragments are dominant in the breccia matrix (Fig. IV.2.3). Compositionally they are probably melanephelinites (?). Texturally they range in size from ash to lapilli and have variable, usually rounded shapes. The occurrence of juvenile vesiculated fragments is uncommon. Three different types of spheroidal juvenile fragments are present, the important textural differences between them are shown in Fig. IV.2.5. The first type comprises "armoured lapilli", the second is best described as "frozen droplets" of a magma (glassy groundmass, microphenocrysts of pyroxene and olivine; Figs. IV.2.3

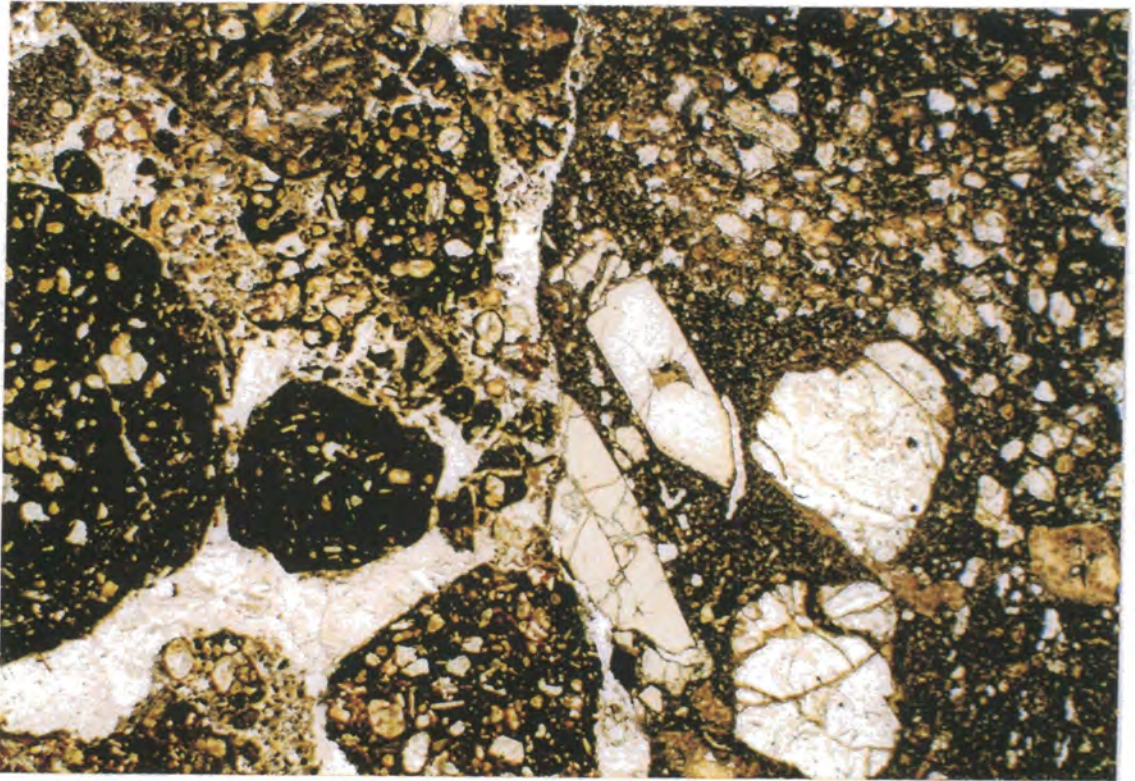


Figure IV.2.3 - Águas Emendadas (96SOB214). Breccia matrix. On the right-hand side, cognate fragment composed of two different rock types in irregular contact with each other. On the left-hand side, dark rounded juvenile fragment (frozen droplet), probably melanephelinitic in composition. Juvenile fragments are also present in the central portion of the photography (dark, rounded). Field of view is 7.5x5mm. Plane-polarized-light.

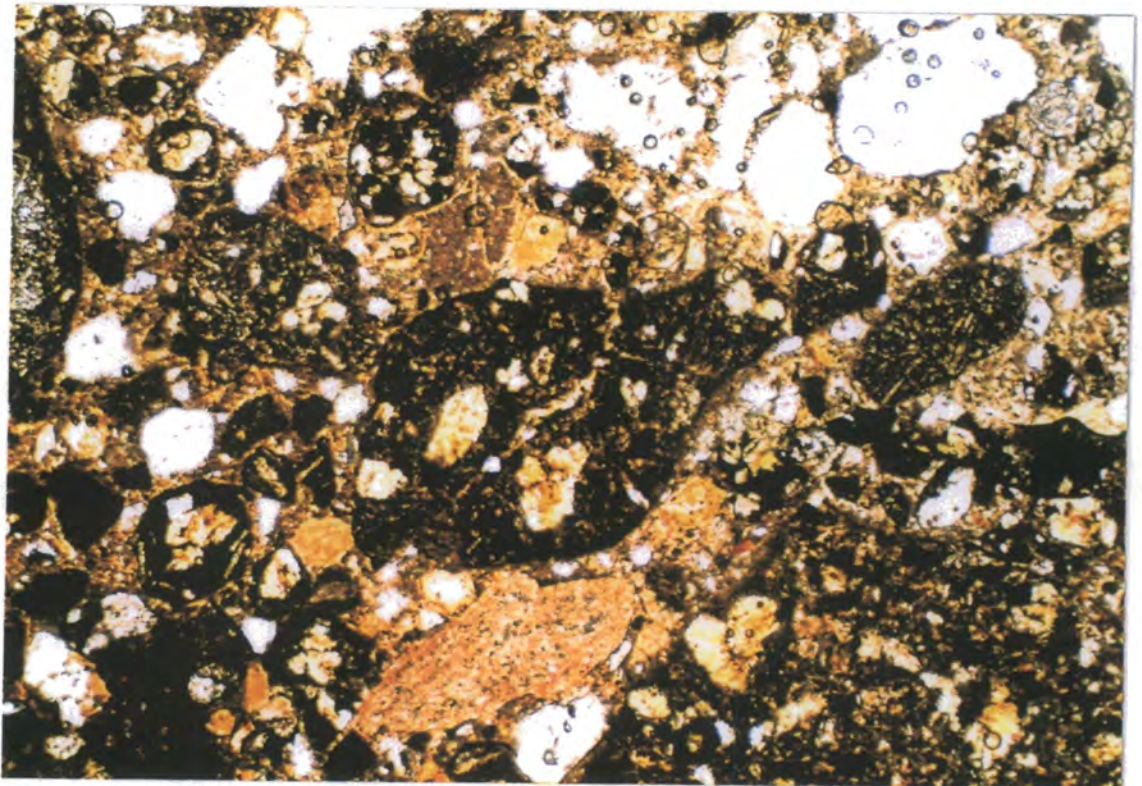


Figure IV.2.4 - Marimondo (96AE16). Breccia matrix. Dark, bottle-shaped, juvenile fragment (frozen droplet), at the centre of the picture. Field of view is 3.75x2.5mm. Plane-polarized light.




LAPILLI SIZE STRUCTURES				
structure	size	shape	description	model
armoured lapilli	lapilli	variable	They always have a core, which can be a lithic fragment (Pre-Cambrian rocks, sandstone, alkaline rocks) or crystal fragment. The rim is made of ash.	
"frozen droplets"	variable	variable	They have glassy groundmass, phenocrysts of olivine and pyroxene, small vesicles filled with carbonate. They do not have a core. The shape is variable but, usually, rounded.	
"spinning droplets"	lapilli	spherical	They have a core (usually phlogopite, pyroxene or olivine; sometimes lithic). The rim comprises a microcrystalline groundmass and a great number of microphenocrysts orientated concentrically around the core.	

Figure IV.2.5 - Summary of characteristics of different types of spheroidal juvenile fragments present in the breccia matrix.

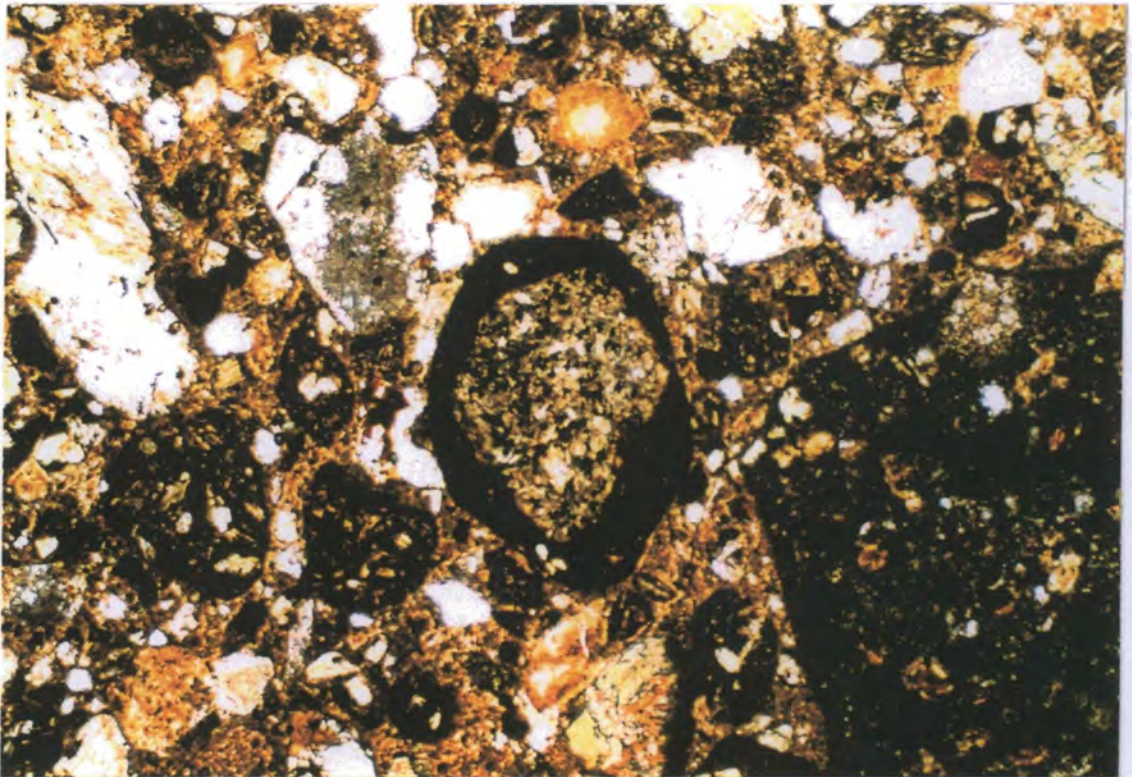


Figure IV.2.6 - Marimbondo (96AE16). Breccia matrix. Armoured lapillus with amphibolitic core, at the centre of the picture. Field of view is 3.75x2.5mm. Plane-polarized light.

and IV.2.4), and the third type consists of densely porphyritic, concentrically oriented, cored structures (called “spinning droplets” in this thesis).

Armoured lapilli are defined as lapilli-sized rock fragments coated with ash (e.g. Waters and Fisher, 1971; Lorenz, 1974; Schumacher and Schmincke, 1991; Gilbert and Lane, 1994). Armoured lapilli are very common in the matrix of the studied breccias. Such particles represent one of the types of rounded structure mentioned previously. They are smaller than 1cm, usually only identifiable under the microscope. The core has compositional range similar to the accessory fragments and xenocrysts. The ash rim varies from around 1/10 to 4/10 of the lapillus diameter (Fig. IV.2.6). Normally the lapilli are rounded but occasionally the ash rim follows the contours of the angular rock core (Fig. IV.2.7).

Frozen droplets of magma are often spherical, but they can also be tear- or irregularly-shaped. Despite being lapilli-size on average, some specimens can be smaller than 2mm. They have an abundant glassy groundmass and the microphenocrysts are randomly distributed in most cases, although concentric orientation is locally observed. The texture of the frozen droplets is very similar to those reported by Hay (1978), Keller (1981,1989), Hay and O’Neil (1983), Deans and Roberts (1984) and Riley *et. al.* (1996), for carbonatite-associated magmatism. Similar features are also described in kimberlites (e.g. Clement, 1973; Clement, 1975; Dawson, 1980; Clement and Skinner, 1985; Mitchell, 1995). The origin of such structures is controversial and will be discussed later, in section 3 of this chapter.

The third type of spherical structure is hereafter called “spinning droplets”. At first sight, they are very similar to armoured lapilli but can be

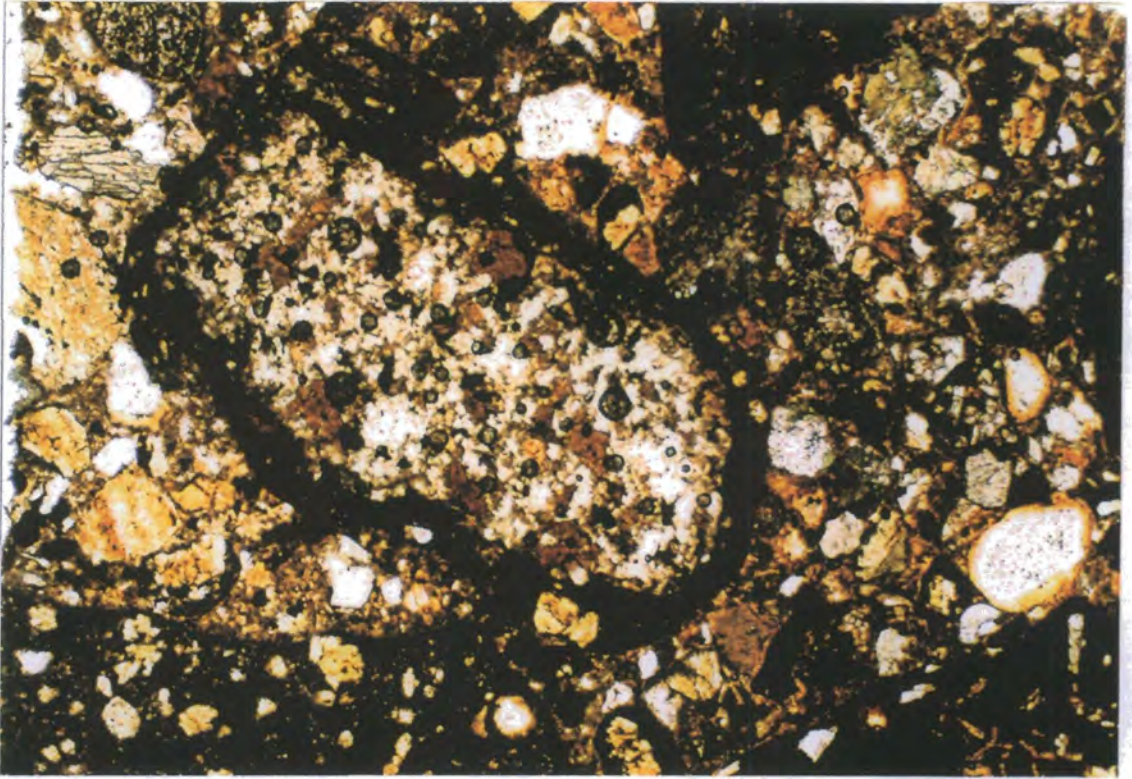


Figure IV.2.7 - Marimondo (96AE16). Breccia matrix. Armoured lapilli. Note that the ash rim follows the somewhat angular contours of the core. Field of view is 3.75x2.5mm. Plane-polarized light.

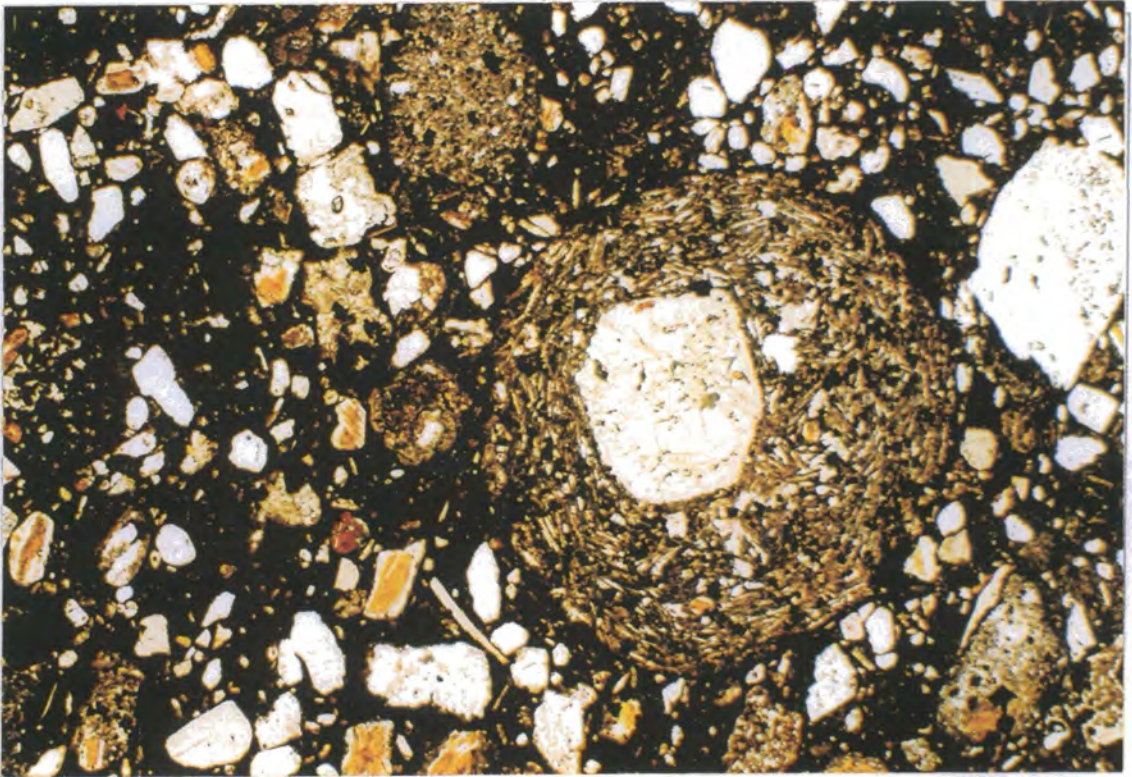


Figure IV.2.8 - Neuzinha (96AE09). Breccia matrix. In the centre-right portion, there is a spinning droplet with a pyroxene core and a concentric, microporphyritic rim. Field of view is 7.5x5mm. Plane-polarized light.

distinguished from the latter by the invariably present crystal nucleus and a rim composed of tangentially oriented microphenocrysts in a glassy groundmass (Fig. IV.2.2). These structures can reach up to 8mm in diameter. In Neuzinha, they are much more common than armoured lapilli. The core can be occupied by a crystal of phlogopite, pyroxene or olivine and, rarely, by rock fragments. Phlogopite is the most common core material, followed by pyroxene. The rim often represents more than half of the diameter of the structure. Although not always readily identifiable, most microphenocrysts are very likely to be pyroxenes. Other microphenocryst phases comprise oxides, carbonate, phlogopite and, perhaps, melilite. The microphenocrysts are concentrically orientated (Fig. IV.2.8). Spinning droplets differ from frozen droplets by the presence of a crystal nucleus, higher microphenocrysts/groundmass ratio and smaller, concentrically oriented microphenocrysts.

Very similar structures have been described in other alkaline rocks, such as carbonatites, kimberlites and melilitites, and called "pelletal lapilli", "spherical lapilli", "tuffisitic lapilli", "concentric shelled lapilli" or simply "concentric lapilli" (e.g. Clement, 1973; Dawson, 1980; Clement and Skinner, 1985; Mitchell, 1986; Keller, 1989; Dawson *et al.*, 1992; Stoppa and Lavecchia, 1992; Stoppa and Lupini, 1993; Mitchell, 1995; Stachel *et al.*, 1995; Stoppa, 1996; Stoppa and Principe, 1997; Stoppa and Woolley, 1997; Kurszlaukis and Lorenz, 1997; Lorenz and Kurszlaukis, 1997).

Homogeneous Mafic Igneous Rocks

Mineralogically, these rocks are composed of pyroxene, olivine, and perovskite microphenocrysts set in a very fine grained groundmass (Fig.

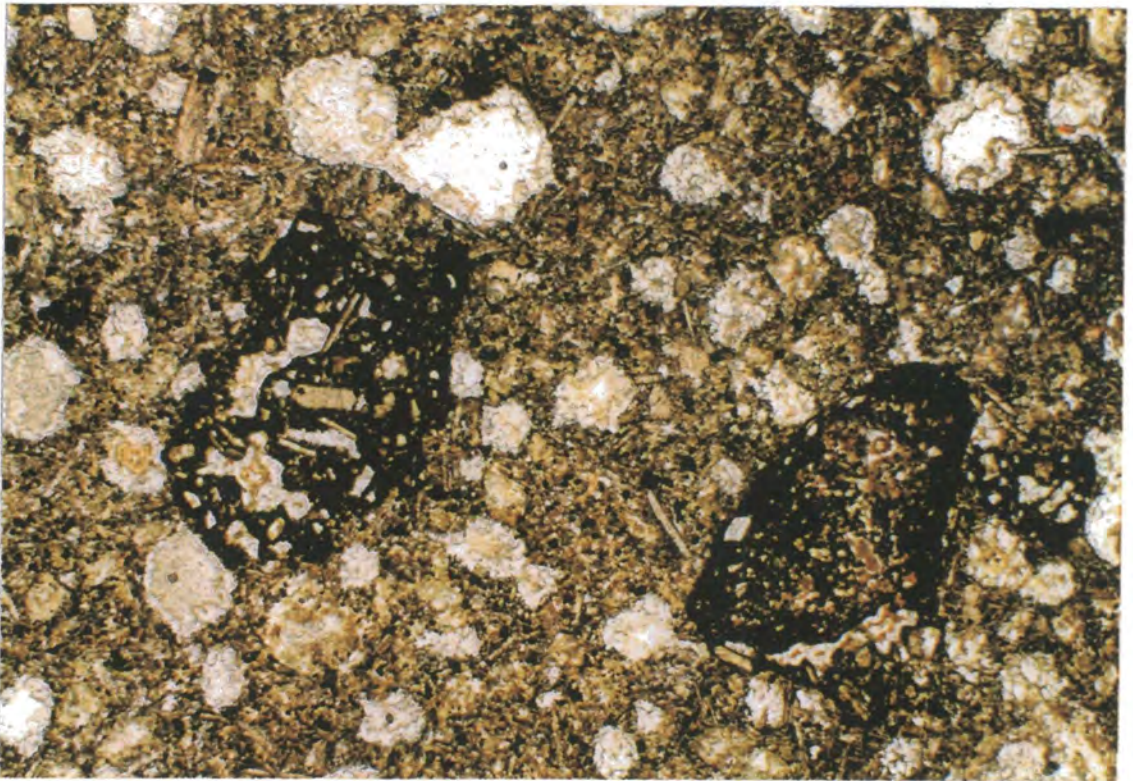


Figure IV.2.9 - Águas Emendadas (96AE35). Homogeneous mafic igneous rock. This is a highly vesicular rock, composed of pyroxene, olivine (mostly altered) and perovskite microphenocrysts in a cryptocrystalline groundmass. The two dark patches are irregularly-shaped inclusions of, probably, melanephelinitic (?) composition. Field of view is 7.5x5mm. Plane-polarized light.

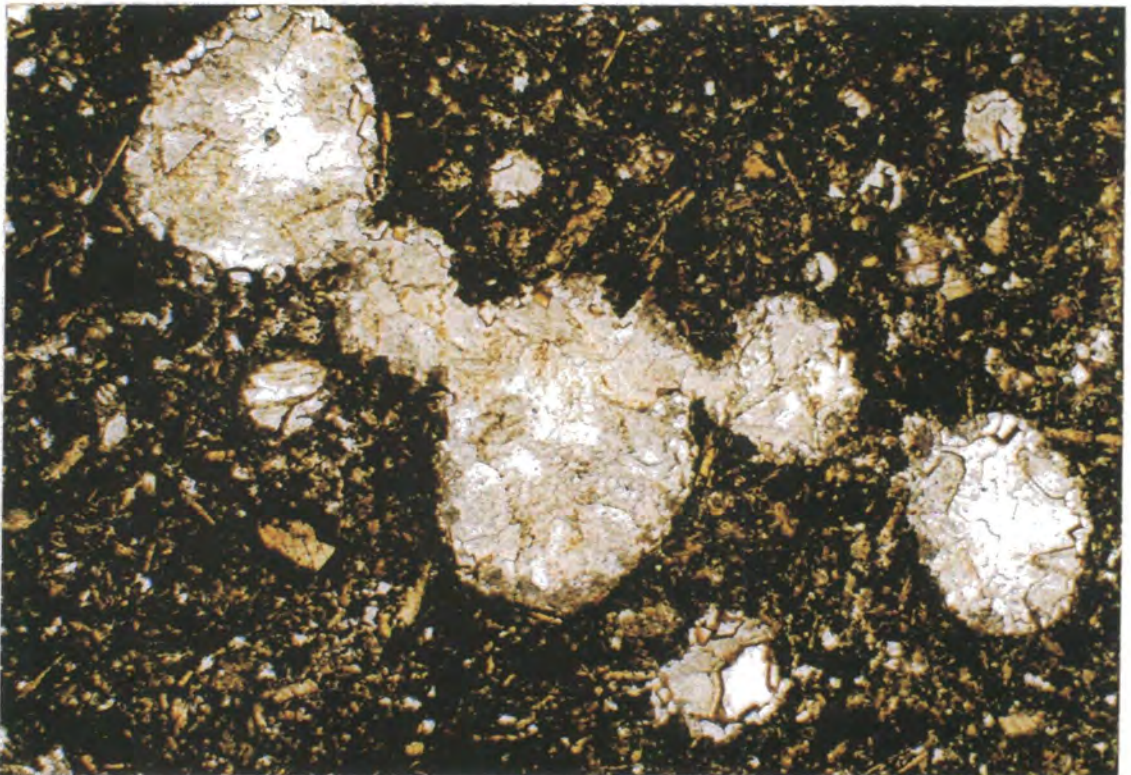


Figure IV.2.10 - Águas Emendadas (96AE35). Homogeneous mafic igneous rock. Joined vesicles, filled with carbonate, zeolites and some clay minerals. Field of view is 7.5x5mm. Plane-polarized light.

IV.2.9). Feldspathoids were not found. Petrographically these rocks are very similar to the dykes associated with the breccias, except that they are extremely vesicular and more rich in "inclusions". The vesicles are filled with carbonate and locally zeolite or clay minerals. The size of the vesicles varies from <1mm to 10mm. In some portions the vesicles are joined (Fig. IV.2.10).

Inclusions of an even more mafic rock-type can be often observed in both hand-samples and thin sections (Fig. IV.2.9). They have the same minerals as the host rock, but are more fine grained and appear to have higher modal abundances of pyroxene, olivine and perovskite microphenocrysts (Fig. IV.2.11). The inclusions have irregular, usually "amoeboid" shape (Fig. IV.2.12). Angular xenoliths of another mafic alkaline rock are also present and can have diameters up to 2cm (Fig. IV.2.13). They have phenocrysts of pyroxene up to 1cm and rare olivine.

Dykes

In thin section all of the sampled dykes are very similar, although variable in grain size. They are extremely mafic, comprising euhedral olivine (up to 6mm) and clinopyroxene (up to 1.5cm) phenocrysts set in a groundmass of these phases, opaques and perovskite. The largest euhedral perovskites may best be described as microphenocrysts. The olivine is entirely altered to carbonate and clay minerals, and these phases are also widespread in the groundmass. No recognisable groundmass feldspathoids were observed, but the presence of perovskite leaves no doubt that these dykes are strongly silica undersaturated (i.e. melanephelinites?) (Fig. IV.2.14).

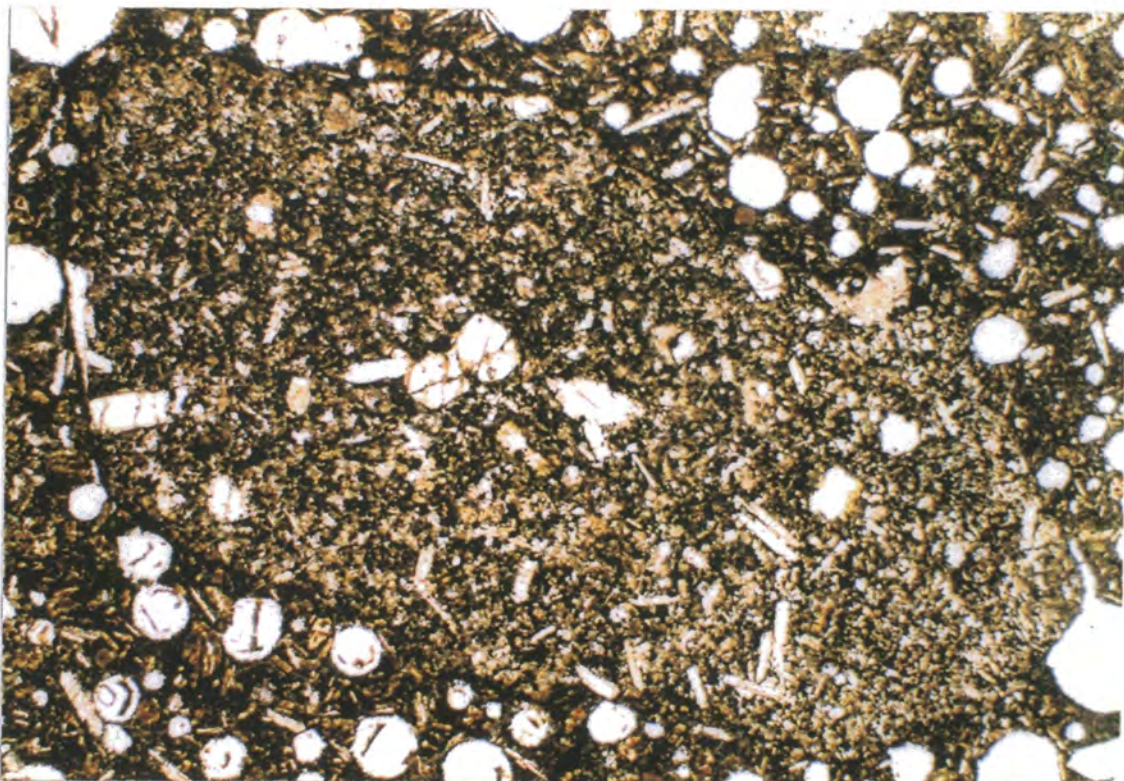


Figure IV.2.11 - Águas Emendadas (96AE33). Homogeneous mafic igneous rock. Irregularly-shaped, microphenocryst-rich inclusion, in a highly vesicular rock. The composition of the inclusion and the host rock are similar but the former is more fine-grained than the host rock. Field of view is 7.5x5mm. Plane-polarized light.

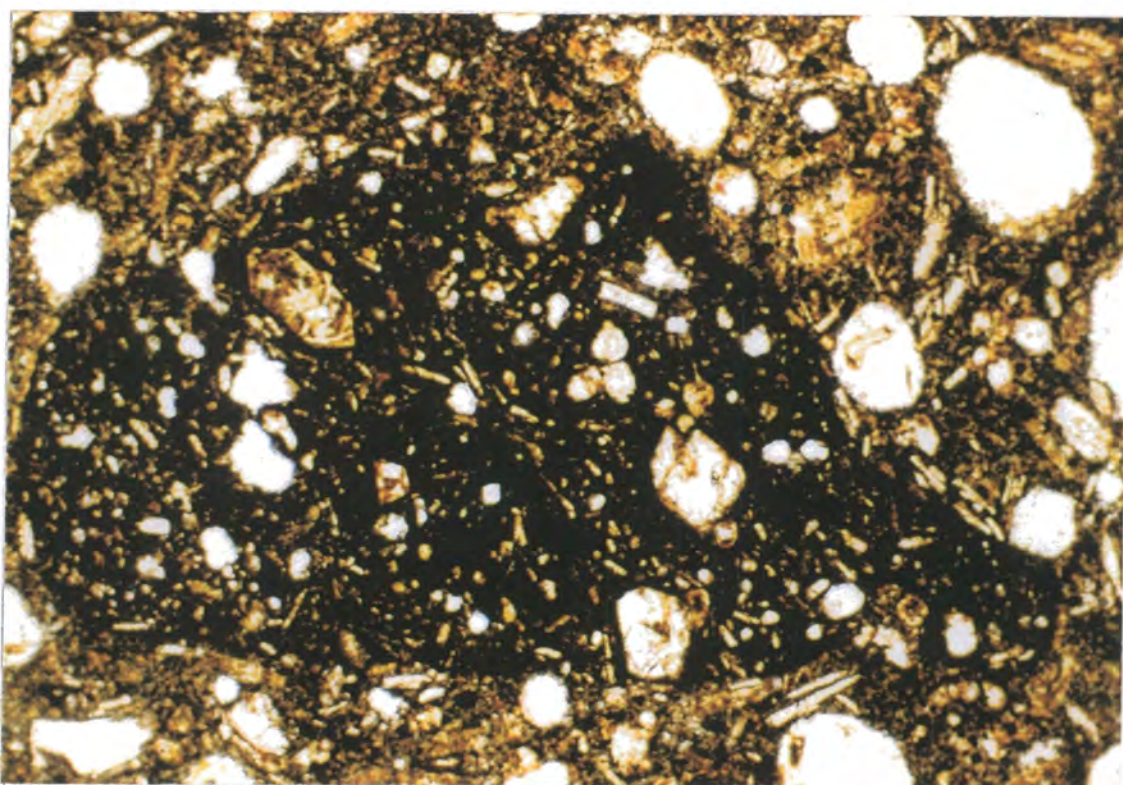


Figure IV.2.12 - Águas Emendadas (96AE33). Homogeneous mafic igneous rock. Dark-coloured inclusion with amoeboid shape. Field of view is 3.75x2.5mm. Plane-polarized light.

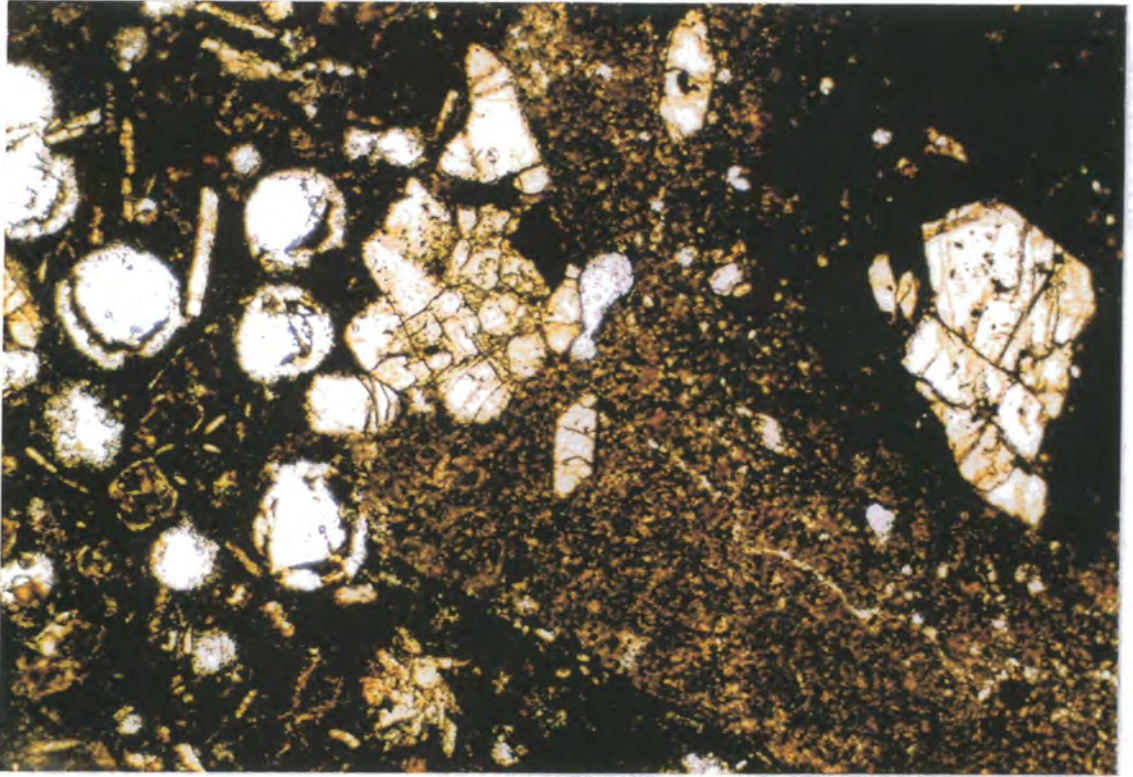


Figure IV.2.13 - Águas Emendadas (96AE33). Homogeneous mafic igneous rock. On the right-hand side, xenolith of porphyritic alkaline rock. Field of view is 3.75x2.5mm. Plane-polarized light.

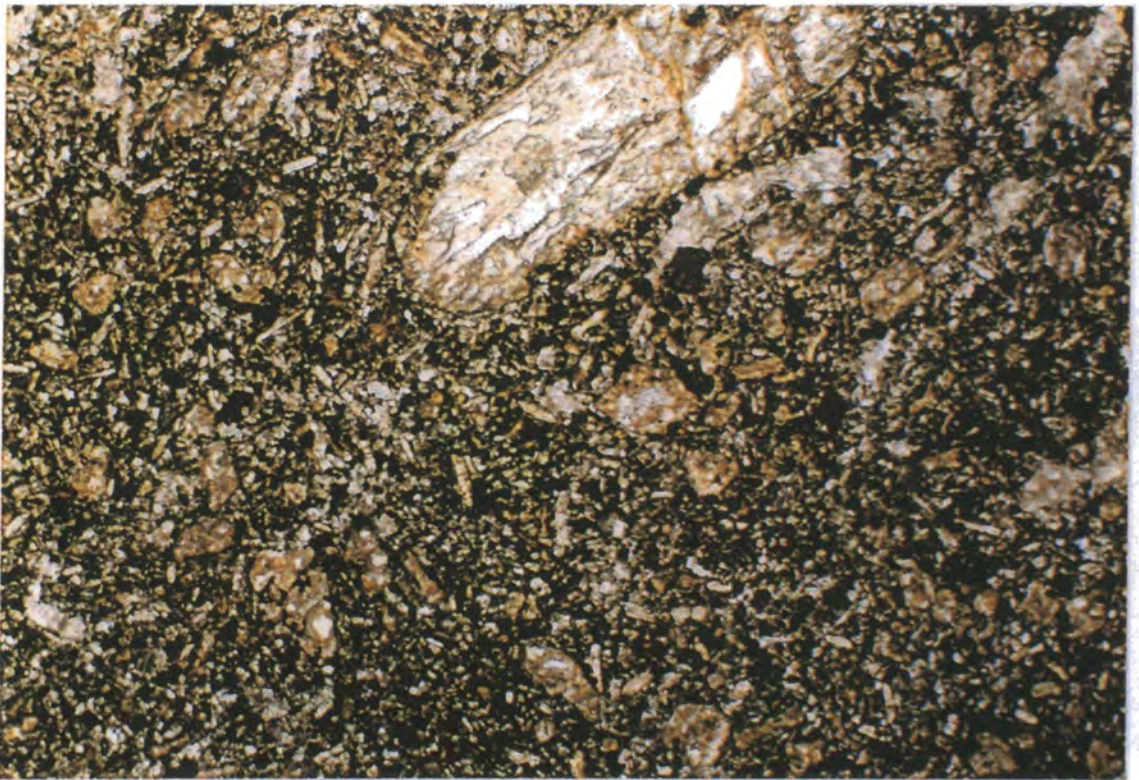


Figure IV.2.14 - Águas Emendadas (96AE42). Melanephelinite (?). Altered olivine phenocryst (on the top of the picture) set in a groundmass rich in olivine, pyroxene and perovskite. Field of view is 3.75x2.5mm. Plane-polarized light.

Locally the dykes are vesicular (infilled by carbonate and zeolites). Samples 96AE42 and 96AE46 (especially) contain scattered inclusions (up to 7mm) of extremely fine-grained melanephelinite(?), with rounded "amoeboid" margins (Fig. IV.2.15). These may be related to magma-mixing episodes shortly before emplacement.

IV.2.3 Lavas

As a general rule most of the volcanic rocks are ultramafic and porphyritic. The main mafic minerals are clinopyroxene (diopside) and olivine. Melilite was found in one sample, and the occurrence of kalsilite was observed during the microprobe work (Chapter V). The common accessories are phlogopite, perovskite, Fe-Ti oxides, carbonate and apatite. The main products of hydrothermal alteration and/or weathering are zeolites, serpentine, clay minerals, carbonate and Fe-hydroxides.

The volcanic rocks are divided into four groups according to their main felsic mineral:

Group 1 - melaleucitites

Group 2 - melanephelinites (?)

Group 3 - leucitites

Group 4 - basanites and basalts

Group 1 is formed by rocks which have frequent pseudoleucite in the groundmass. Group 2 comprises rocks with nepheline (?) in the groundmass. Group 3 rocks are characterised by phenocrysts of pseudoleucite. Group 4 is formed by feldspar-bearing rocks.

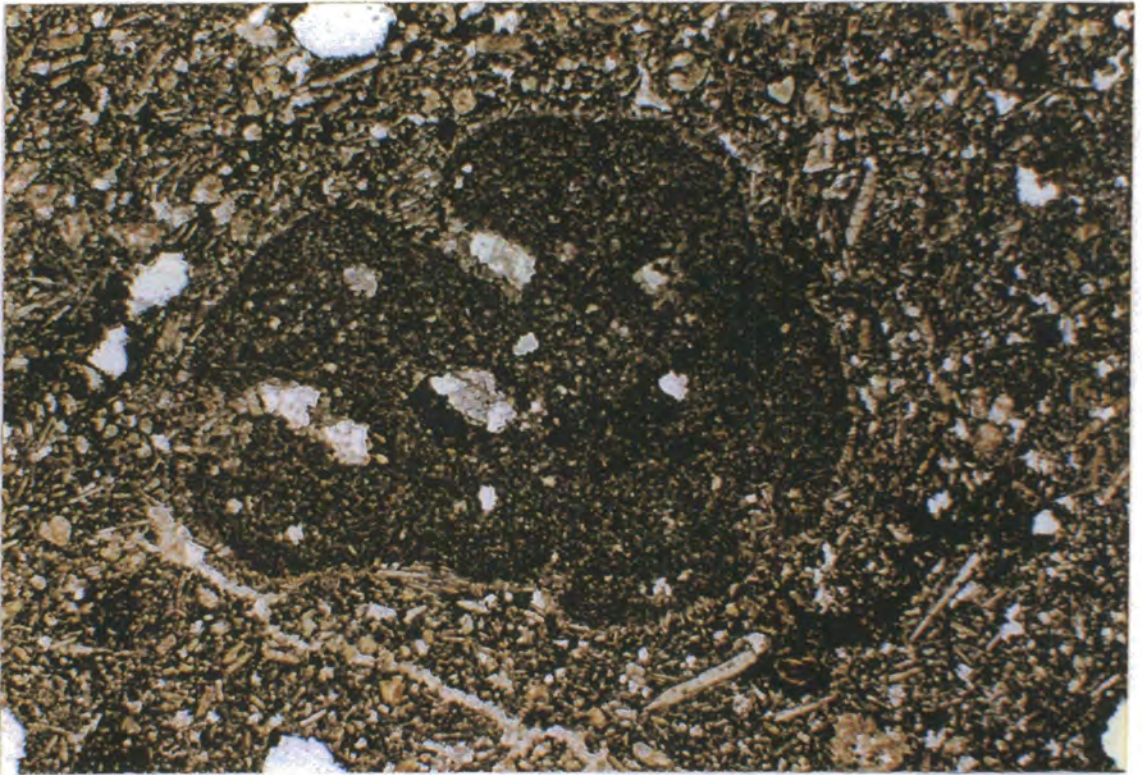


Figure IV.2.15 - Águas Emendadas (96AE46). Melanephelinite (?). Amoeboid inclusion of a cryptocrystalline, dark-coloured rock. Field of view is 7.5x5mm. Plane-polarized light.

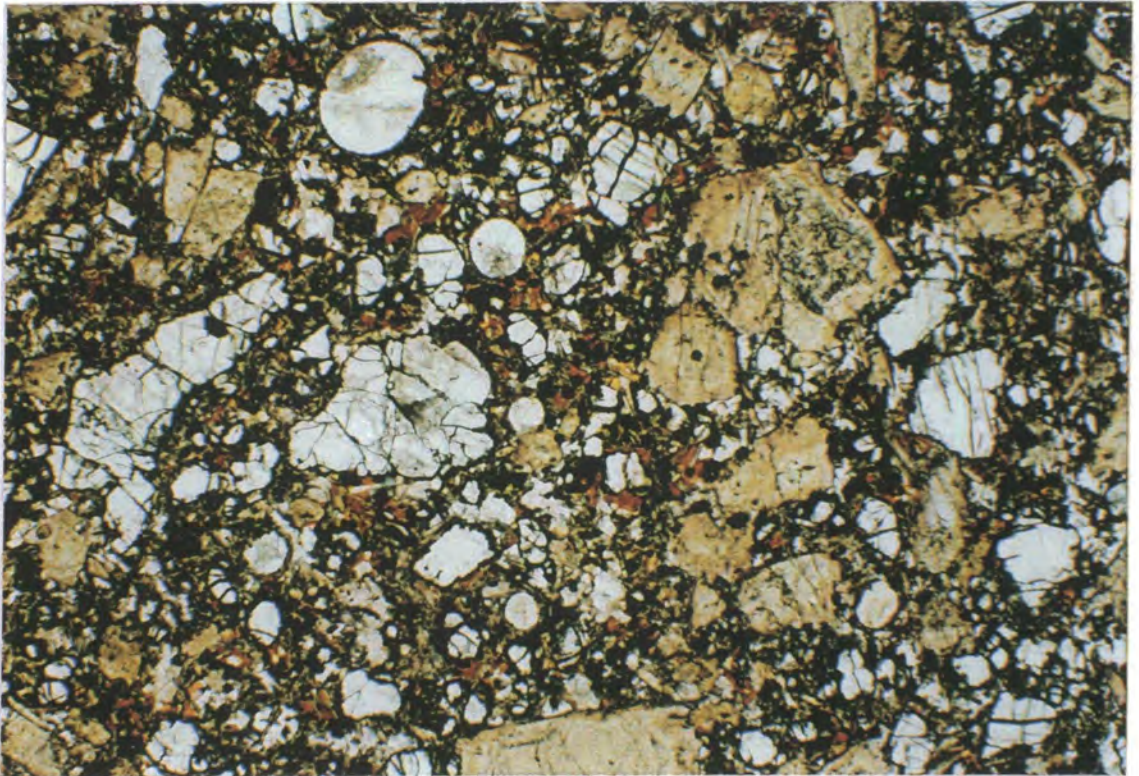


Figure IV.2.16 - Águas Emendadas (96AE22). Melaleucitite. This rock is rich in pyroxene and olivine phenocrysts, set in a groundmass of pyroxene, pseudo-leucite, phlogopite, perovskite, olivine, nepheline (?), apatite and oxide. The olivine phenocrysts are usually anhedral. Rounded vesicles filled with carbonate are common. Field of view is 7.5x5mm. Plane-polarized light.

Melaleucitites

The melaleucitites are very rich in phenocrysts. All rocks in this group have olivine and pyroxene as main constituents. Pseudo-leucite is present as a groundmass phase. The most common accessories are phlogopite, perovskite, Fe-Ti oxides, apatite and nepheline (?) (Fig. IV.2.16).

Olivine occurs mainly as phenocrysts. In some samples it is also found in the groundmass, although only in accessory amounts. Two generations of olivine phenocrysts are recognisable. One is euhedral to subhedral, usually less than 3mm in size (Fig. IV.2.17). The second is normally anhedral and up to 1cm in diameter, showing features of resorption (Figs. IV.2.16, IV.2.17 and IV.2.18). In the groundmass, olivine is usually euhedral. The olivines are often partially or totally altered to serpentine and/or a mixture of clay minerals and carbonate.

The pyroxene is normally fresh and diopsidic in composition. In thin section it can be strongly coloured from light brown to green. It occurs as phenocrysts (up to 6mm) and as the main constituent of the groundmass (Fig. IV.2.16). As a rule, phenocrysts are euhedral (Fig. IV.2.19), but some crystals may show evidence of instability within the magma (Fig. IV.2.20). In the groundmass the pyroxene occurs as euhedral microcrysts (Fig. IV.2.17).

Small crystals of pseudoleucite are the next main component of the groundmass. They are found as anhedral to rounded "cloudy" small masses (Figs. IV.2.16 and IV.2.17).

Phlogopite occurs both as phenocrysts and in the groundmass. The phenocrysts are often partially or totally transformed into a microcrystalline

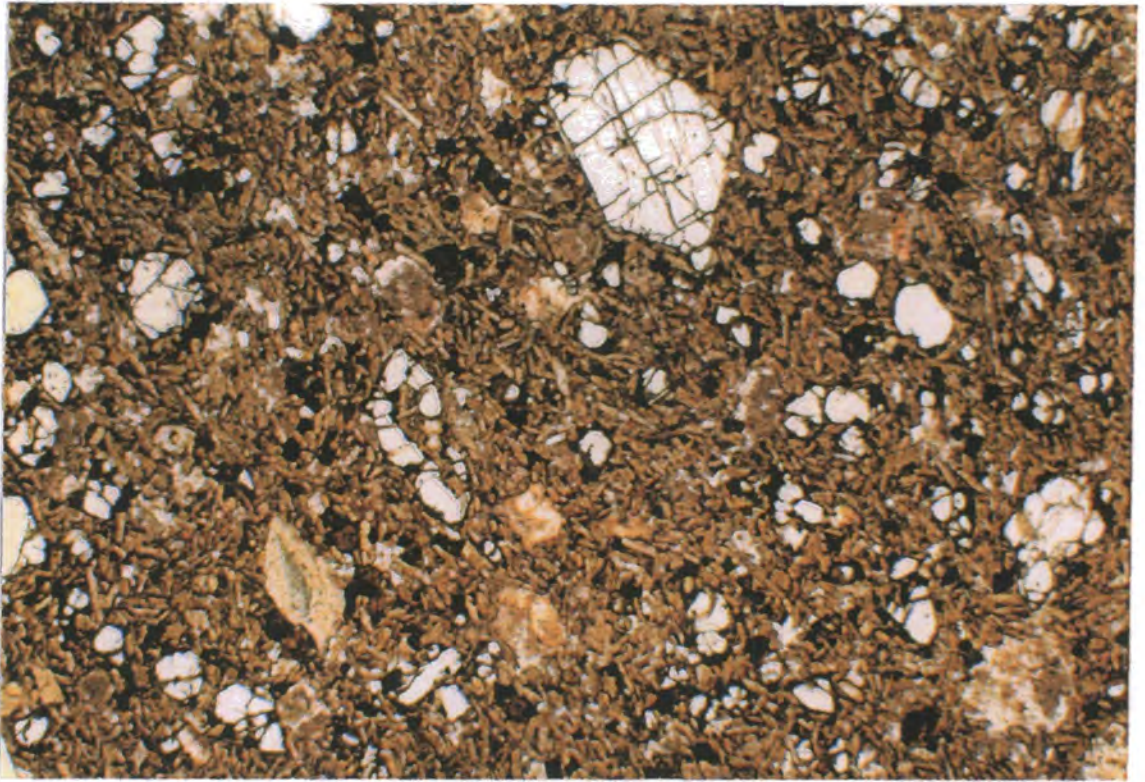


Figure IV.2.17 - Marimbondo (96AE13). Melaleucitite. Two generations of olivine phenocrysts are present, in the first variety of phenocrysts are euhedral to subhedral, and in the second, they are smaller and anhedral. The groundmass is composed mainly of pyroxene, pseudoleucite and perovskite. Field of view is 7.5x5mm. Plane-polarized light.

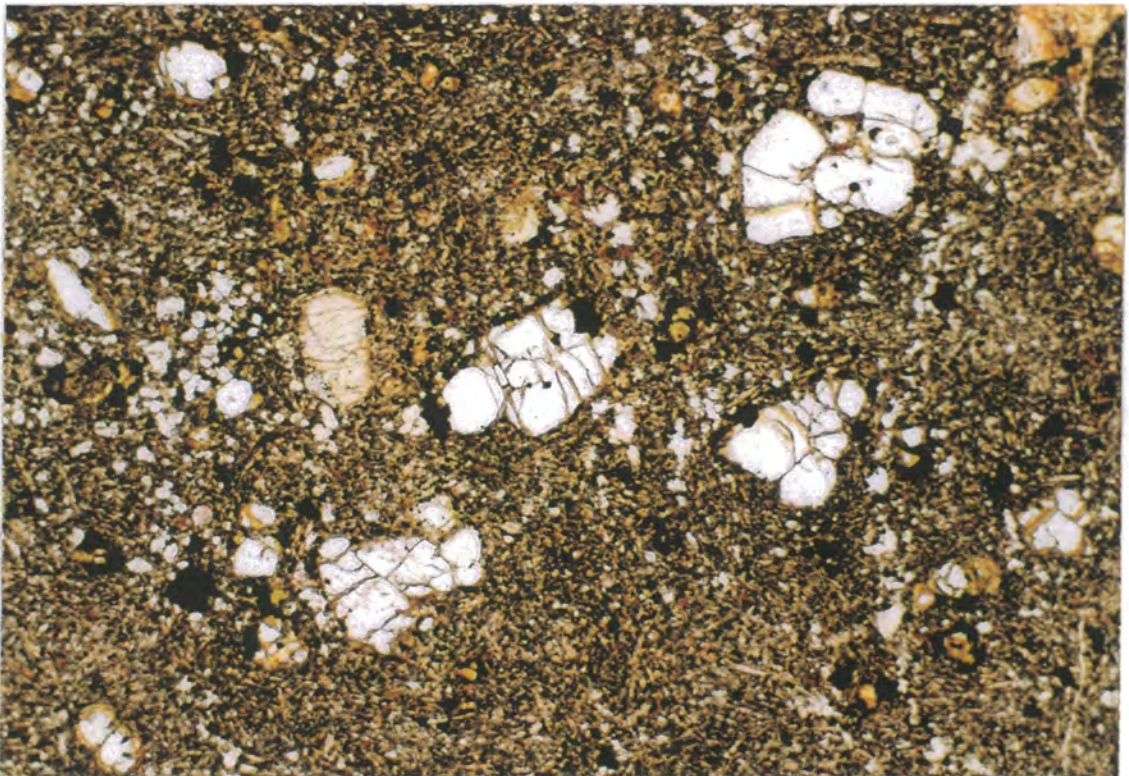


Figure IV.2.18 - Marimbondo (96AE12). Melaleucitite. Phenocrysts of olivine and pyroxene in a cryptocrystalline groundmass. Phlogopite is present as a late phase in the groundmass. Field of view is 3.75x2.5mm. Plane-polarized light.



Figure IV.2.19 - Neuzinha (96AE01). Melaleucitite. Rock rich in phenocrysts of olivine and pyroxene (euhedral to subhedral), in a microcrystalline groundmass. Field of view is 7.5x5mm. Plane-polarized light.



Figure IV.2.20 - Neuzinha (96AE06). Melaleucitite. Olivine and pyroxene phenocrysts set in a groundmass rich in microphenocrysts of pyroxene. Note that the pyroxene phenocrysts are subhedral to anhedral, showing evidence of disequilibrium. On the bottom right-hand side is a cognate xenolith of pyroxene-rich coarser-grained rock. Field of view is 7.5x5mm. Plane-polarized light.

mixture of Fe-Ti oxides, pyroxene, nepheline?, and olivine (Fig. IV.2.21). In the groundmass, phlogopite is a late phase (Figs. IV.2.16 and IV.2.18).

Euhedral perovskite is an important accessory mineral in most rocks of this group. It is found as microphenocrysts or as small crystals in the groundmass.

Fe-Ti oxides are very common and occur as euhedral microcrysts in the groundmass or as inclusions in pyroxene and phlogopite phenocrysts.

Small amounts of nepheline (?) are present in the groundmass of most melaleucitites. It seems to be a late phase. Rarely, nepheline (?) is found as phenocrysts, invariably associated with phlogopite (Fig. IV.2.22).

Some of the melaleucitites contain small vesicles filled with carbonate (Fig. IV.2.16). Cognate xenoliths of pyroxenite (Fig. IV.2.20) and dunite are very common.

Melanephelinites (?)

Compared with the melaleucitites, the melanephelinites (?) are much poorer in phenocrysts (Fig. IV.2.23). They have a dominant, microcrystalline, dark grey groundmass. Another major difference is that pyroxene is very rare in these rocks. When present it is mostly restricted to an accessory phase in the groundmass. The main phenocryst types are olivine and phlogopite, both often smaller than 2mm. The groundmass is mostly microcrystalline, with recognisable nepheline (?), olivine, Fe-Ti oxides, perovskite and carbonate (Fig. IV.2.24). Kalsilite was found in the groundmass of sample 96AE08 (Chapter V).

Phenocrysts of olivine range in shape from perfectly euhedral to anhedral (Figs. IV.2.23 and IV.2.25). The latter often show evidence of



Figure IV.2.21 - Neuzinha (96AE02). Melaleucitite. Phlogopite phenocryst pseudomorphically replaced by an assemblage of phlogopite, oxide, pyroxene, olivine and nepheline. Field of view is 3.75x2.5mm. Plane-polarized light.

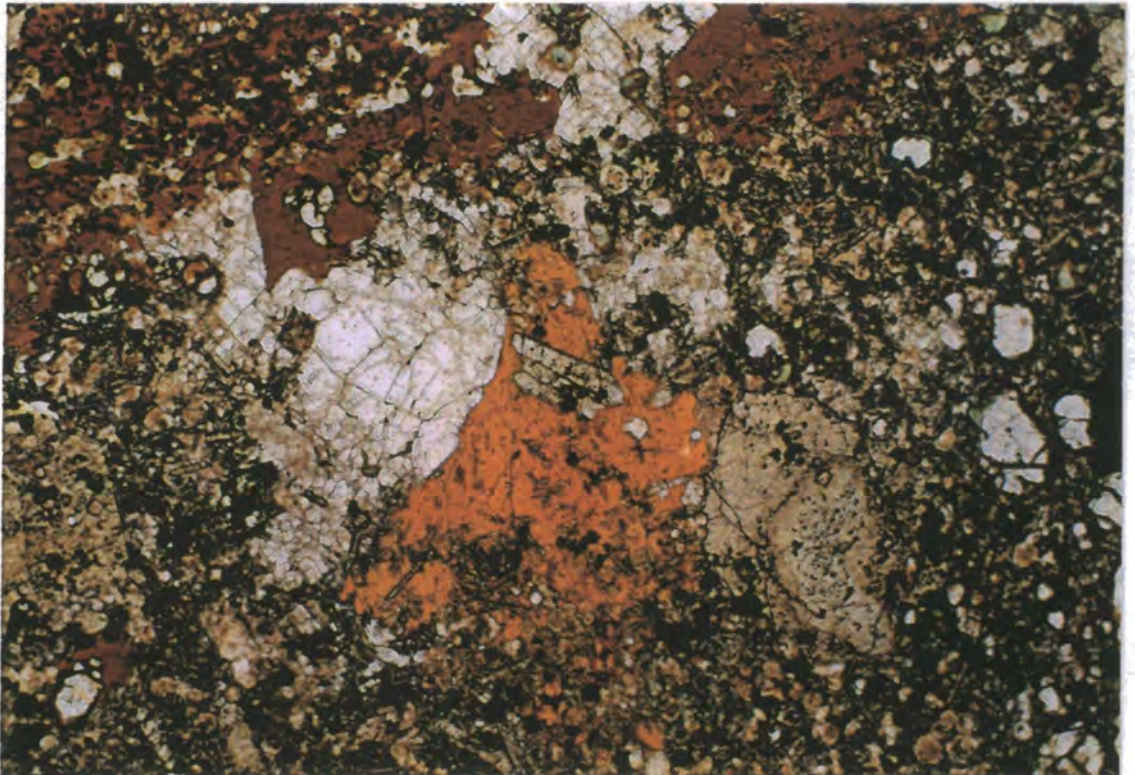


Figure IV.2.22 - Neuzinha (96AE04). Melaleucitite. Glomeroporphyritic "aggregate" of phlogopite, nepheline and pyroxene. Field of view is 3.75x2.5mm. Plane-polarized light.

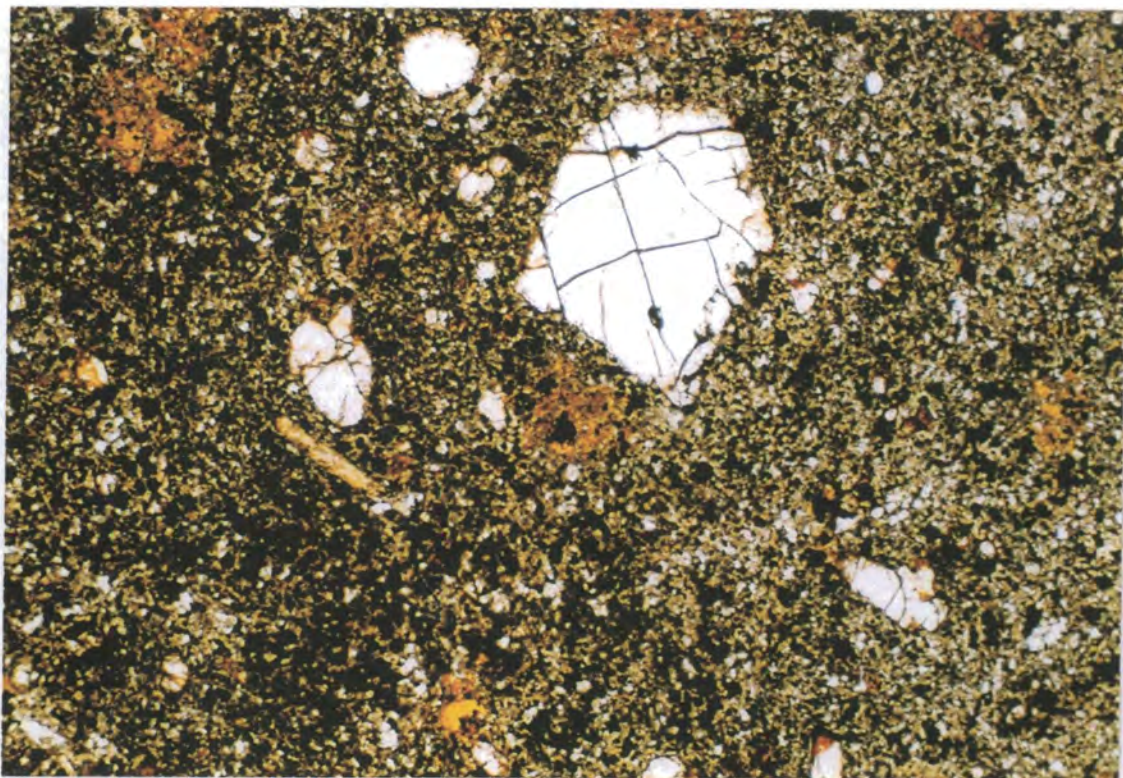


Figure IV.2.23 - Neuzinha (96AE05). Melanephelinite (?). Rock composed of a microcrystalline groundmass, with phenocrysts of olivine and rare pyroxene. Poikilitic phlogopite phenocrysts occur as a late phase. Field of view is 3.75x2.5mm. Plane-polarized light.



Figure IV.2.24 - Neuzinha (96AE08). Melanephelinite (?). Microcrystalline groundmass composed of nepheline (?), olivine, Fe-Ti oxides, perovskite and carbonate. Phlogopite phenocrysts are present as a late phase. Field of view is 7.5x5mm. Plane-polarized light.

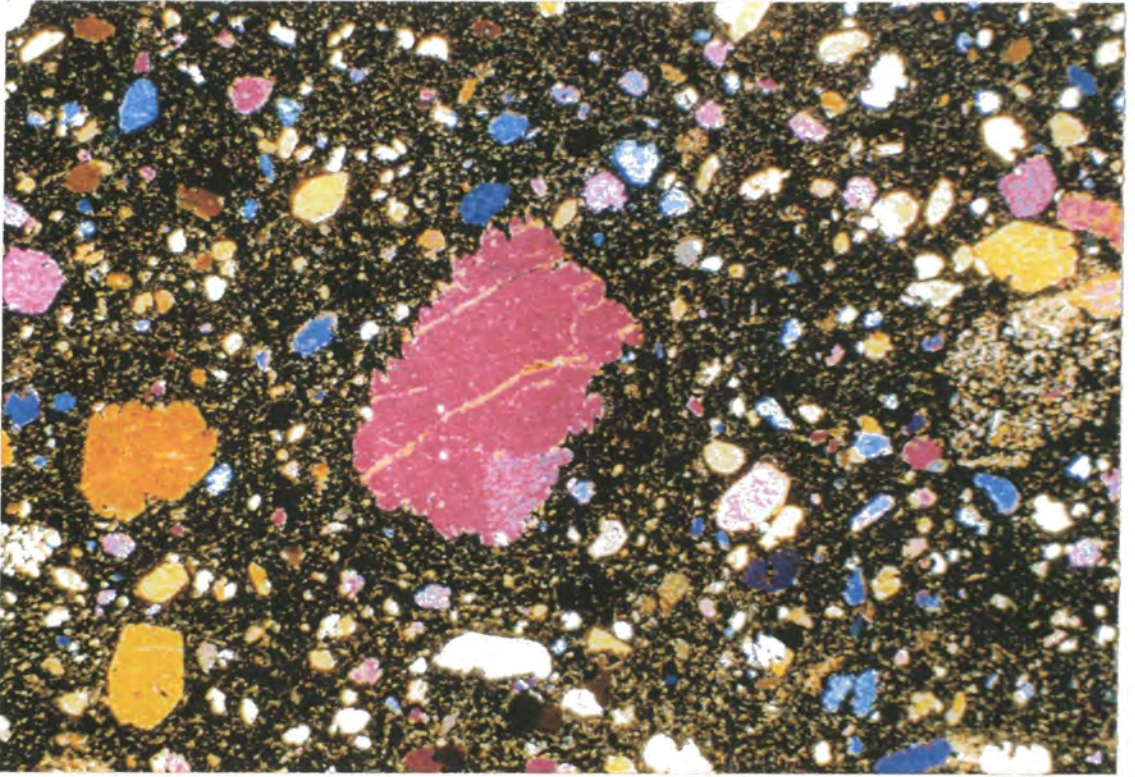


Figure IV.2.25 - Amorinópolis (96AE62). Melanephelinite (?). Rock rich in subhedral to anhedral olivine phenocrysts in a cryptocrystalline groundmass. Field of view is 7.5x5mm. Cross-polarized light.

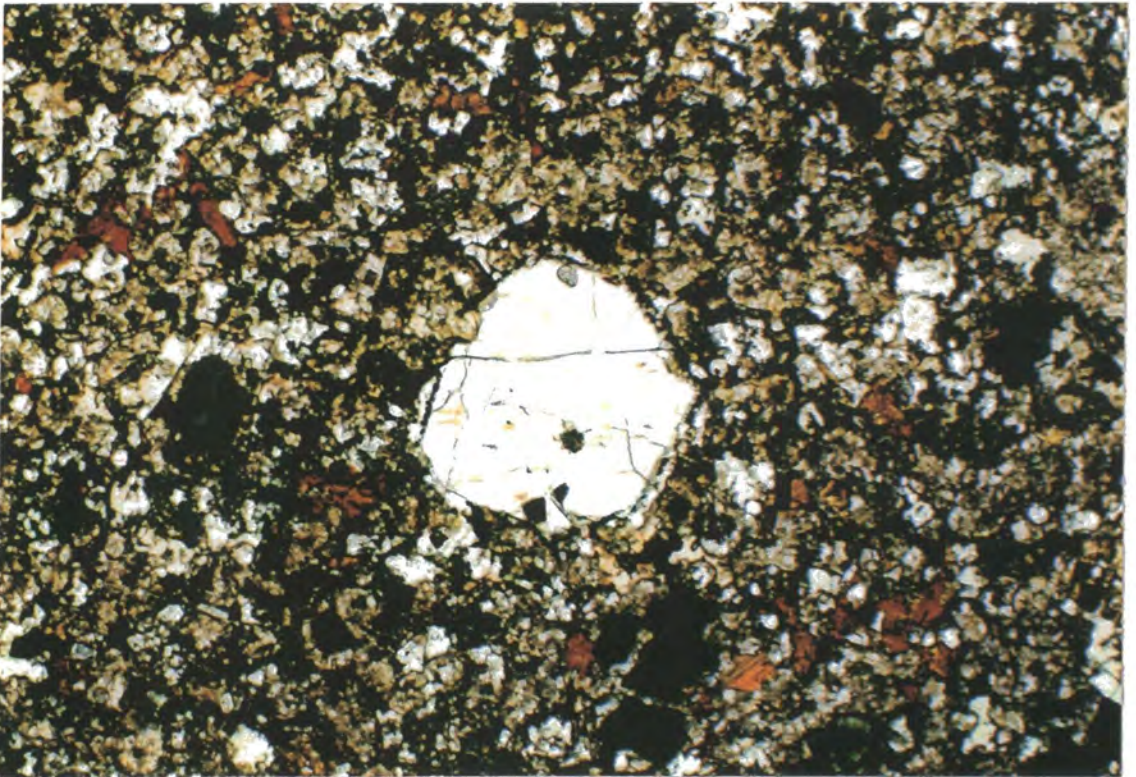


Figure IV.2.26 - Águas Emendadas (96AE20). Leucitite. Groundmass composed of leucite pyroxene, leucite, olivine, phlogopite, nepheline, oxides and apatite with leucite phenocrysts. Field of view is 3.75x2.5mm. Plane-polarized light.

disequilibrium and may represent a separate variety of olivine. In the groundmass, olivine is usually euhedral. All olivine varieties can be partially or entirely altered to a mixture of clay minerals and carbonate.

Poikilitic phenocrysts of phlogopite occur as a late phase, surrounding other minerals of the groundmass (Figs. IV.2.23 and IV.2.24). Nepheline (?) occurs only in the groundmass, as small crystals showing evidence of exsolution. Their shape varies from subhedral to anhedral.

Leucitites

This group is similar to the melaleucitites. The main difference is that rocks of this group either have phenocrysts of leucite or abundant leucite in the groundmass (Fig. IV.2.26). The main phenocrysts are leucite, pyroxene, olivine and phlogopite, in this order. All these phases are also present in the groundmass; pyroxene followed by leucite being the main ones (Fig. IV.2.27). Accessories are olivine, phlogopite, perovskite, Fe-Ti oxides, nepheline (?), apatite and carbonate. Cognate xenoliths of pyroxenite were also found in this group of rocks.

Basalts and basanites

This group comprises the only feldspar-bearing volcanic rocks found in the area. They range from aphanitic to porphyritic varieties very rich in phenocrysts. The main phenocryst phases are pyroxene (diopside, up to 1 cm, Fig. IV.2.28), olivine (usually euhedral, up to 5 mm) and plagioclase (up to 1 cm). The identifiable components of the groundmass are plagioclase, pyroxene, olivine and rare nepheline in some rocks.

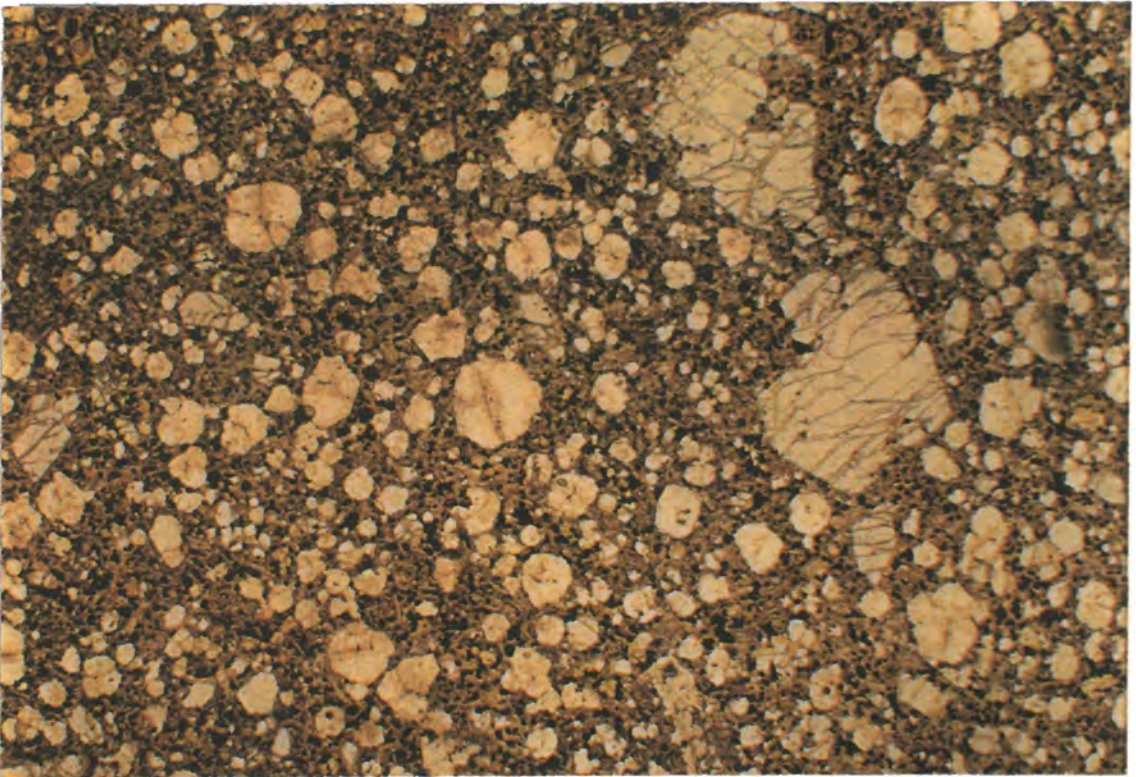


Figure IV.2.27 - Cacimba (96AE57). Leucitite. Phenocrysts of subhedral to anhedral olivine and leucite. The groundmass is very rich in pyroxene and leucite. Field of view is 7.5x5mm. Plane-polarized light.

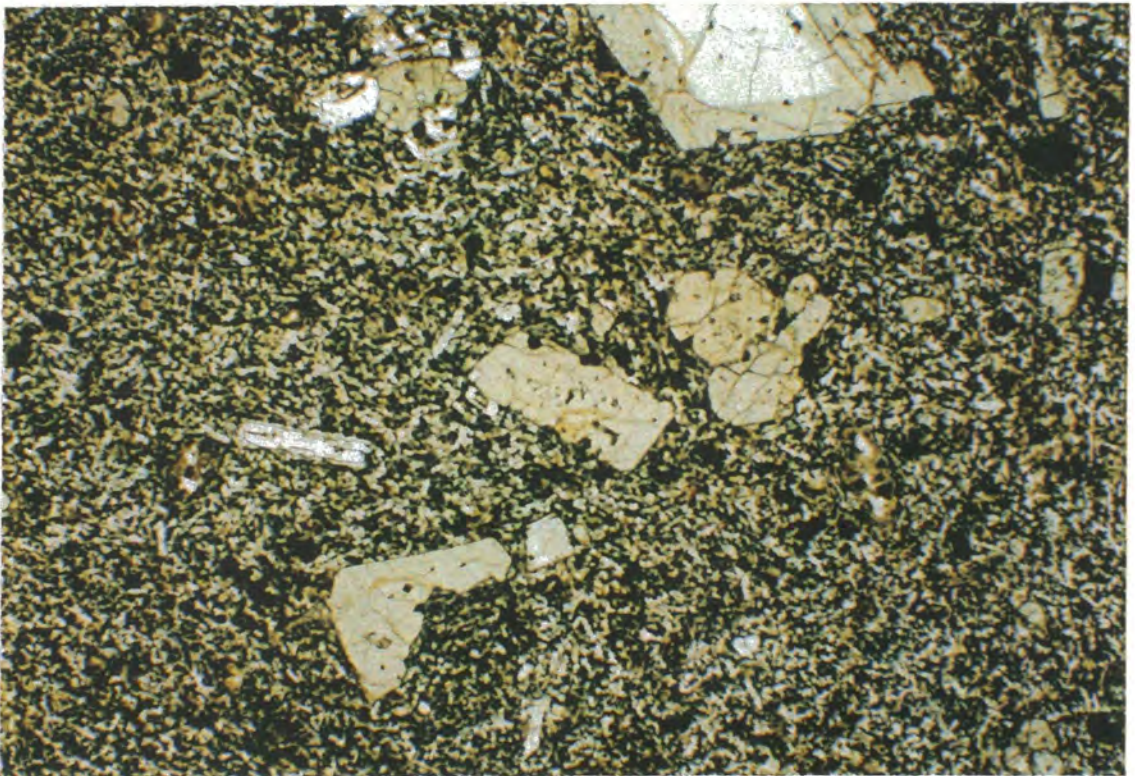


Figure IV.2.28 - Águas Emendadas (96AE18). Basanite. This rock is rich in pyroxene phenocrysts. Olivine and plagioclase phenocrysts are also present, although in subordinate amounts. The main minerals in the groundmass are plagioclase, pyroxene and olivine. Field of view 7.5x5mm. (20x) Plane-polarized light.

IV.3 INTERPRETATION

This section aims to present a tentative model to explain the morphology and formation of the volcanic deposits found in Águas Emendadas, Marimbondo and Neuzinha. It is based on data obtained in field work and petrographic observations, compared with descriptions from the literature. The following points are relevant to the interpretation of the field and petrographic characteristics observed:

1 “Diatreme” is defined by Cas and Wright (1987) as “a *pipe-like conduit filled with volcanoclastic debris*”. Alternatively, Mitchell (1986) gives a more complete definition: Diatremes are “*cone-shaped, downward-tapering, inclined or vertical structural units composed, wholly or partly, of angular or rounded clasts of cognate or xenolithic origin, with or without a matrix. Xenolithic clasts may be derived from the walls or the roof of the body. They are commonly well-mixed and some xenoliths have apparently sunk within the diatreme. Diatremes are volcanic features associated with volatile-rich magmatism, commonly of ultrabasic composition*”. The field relationships in all three localities indicate that they fit these definitions and therefore may be described as diatremes. The presence of sediments of the Paraná Basin topographically above the breccias in all three localities also supports this interpretation. The breccias have been exposed after emplacement by a combination of tectonic events and erosion (Figs. IV.1.1, IV.1.3 and IV.1.4).

2 The absence of structures such as cross-bedding, together with the distribution of the fragments (Fig. IV.1.16), angularity of the accessory

fragments (Fig. IV.1.17) and preserved rims of the armoured lapilli (Fig. IV.2.6) indicate little or no epiclastic transport.

3 The presence of contact metamorphism in the sandstone (Fig. IV.1.6) proves that the breccias were hot during emplacement. This, together with evidence of little or no post-emplacement transport, rules out an epiclastic origin (e.g. mud flow). Therefore the breccias represent pyroclastic deposits.

4 The presence of cognate fragments with different degrees of crystallinity and locally preserved characteristics of magma mixing (Figs. IV.1.15 and IV.2.3) both suggest the existence of a magma chamber prior to the eruption.

5 Cognate fragments can be compared with "autoliths", sensu Mitchell (1995), since they are interpreted as fragmented solid to semi-solid material from the magma-chamber.

6 The formation of armoured lapilli requires presence of water at some stage. Models for generation of accretionary lapilli are presented by various authors (e.g. Woods, 1993; Gilbert and Lane, 1994; Shumacher and Schimincke, 1995); they all consider water as the aggregating agent of ash. It is assumed here that armoured lapilli are a variant of accretionary lapilli.

7 Spinning droplets are genetically linked with diatreme facies (e.g. Clement and Skinner, 1985; Mitchell, 1995; Lorenz and Kurszlaukis, 1997; Kurszlaukis and Lorenz, 1997). These authors, among others, consider two possible alternative processes associated with the formation of diatremes: a magmatic and a phreatomagmatic model (Lorenz and Kurszlaukis, 1997). Mitchell (1995) gives a summary of the ideas involved in each model for

diatremes associated with kimberlitic magmatism, while Lorenz and Kurszlaukis (1997) extend the studies for carbonatite related volcanism.

The **magmatic** model involves the rapid exsolution of a juvenile volatile phase, where the particles are transported in a gas-liquid fluidized system, resulting in a "cold" emplacement. McCallum (1985) studied fluidization experimentally and suggests that it is an important process in the formation of breccia pipes. In this case the previously described "spinning droplets" would be formed inside the conduit, as proposed by Clement (1973) and later by Dawson (1980). The main problem in this model, regarding the formation of spinning droplets, is that in order to have a well-mixed system, as is the case in diatreme facies, a turbulent movement is required. Such movement would either prevent the formation of the spinning droplets or destroy their texture and shape before the eruption.

Phreatomagmatic eruptions are the result of hot magma interacting explosively with a body of water, also known as fuel-coolant interaction (e.g. Sheridan and Wohletz, 1983; Cas and Wright, 1987). Authors who adopt this model to explain the formation of diatremes and associated facies include Lorenz (1979), Zimanowski et al. (1997), Kurszlaukis and Lorenz (1997), Lorenz and Kurszlaukis (1997). In this model prior fragmentation of the magma is not taken into consideration. The spherical shape and texture (concentric orientation) of the spinning droplets is explained by magma adhering to a previously crystallised nucleus, due to surface tension and rotation of the droplets during transport (Mitchell, 1995).

"Spinning droplets" (Figs. IV.2.2 and IV.2.8) are interpreted here as the product of the rotation of magma droplets during ascent in a fluidized

system, and their subsequent solidification in the subaerial stage of a phreatomagmatic explosion. This mechanism requires fragmentation and high velocity of the rising "magma", in order to form and spin the droplets. The fragmentation, inside the magma chamber, could be associated with magma mixing, exsolution of a volatile phase (high vesiculation), liquid immiscibility or even a combination of two or more of these factors. The low density contrast between the hot magma and a second phase (probably volatile) permits a laminar transport at high velocity. When they reach the surface, the already-shaped droplets quench.

A model for the formation of spinning droplets is presented by Stoppa (1996) but it requires, by definition, a mantle xenolith/xenocryst as a core for each lapillus and a magma with carbonatitic-melilititic affinity (Stoppa, 1996; Stoppa and Woolley, 1997). The cores found in lapilli from the Águas Emendadas region seem to be crystals formed in the magma chamber and entrained by magma prior to the eruption. There is no evidence linking them with a mantle origin. Carbonatitic affinity of the magma, as well as liquid immiscibility, can neither be proved nor ruled out at the present stage.

The name "spinning droplet" is proposed here in order to avoid the size limitations implied by other definitions, and the misinterpretation of the processes involved in the formation of these structures. A detailed study of the spinning droplets, as well as experimental modelling and further comparison with similar spherical structures associated with ultrabasic alkaline volcanism elsewhere is required, in order to achieve a better understanding of their origin. Therefore, the term "spinning droplet" is used here in a textural sense.

8 Some of the frozen droplets (Figs. IV.2.3 and IV.2.4) are structureless, and were probably formed by fragmentation (like the spinning droplets), but erupted during a lower energy stage (e.g. fire fountain; Keller, 1981; Deans and Roberts, 1984). An alternative possibility is that frozen droplets are analogous to globular segregations (sensu Mitchell, 1995) present in hypabyssal facies of kimberlites. In this case the breccias from Águas Emendadas region would represent a transitional facies between hypabyssal and diatrema.

9 Pyroxene phenocrysts showing evidence of reabsorption by the magma and disequilibrium textures (Figs. IV.2.16 and IV.2.20) suggest magma mixing. The same applies to olivine phenocrysts (Fig. IV.2.17).

10 Another indication of magma mixing is the abundance of "amoeboid" inclusions in samples from Águas Emendadas region (Figs. IV.1.23, IV.2.3, IV.2.9, IV.2.11, IV.2.12 and IV.2.15).

11 The presence of vesicles in the igneous rocks implies exsolution of a volatile phase. However, the absence of amphiboles and the small amounts of phlogopite indicate that the original magma was relatively poor in water. This suggests that the juvenile volatile phase might have had a significant CO₂ component.

12 The dykes intruded the breccia while it was still "soft", as indicated by their contact relationships (Fig. IV.1.18). On the other hand, the breccia was cooler than the magma of the dykes, otherwise columnar jointing would not have developed in the margins of the dykes (Fig. IV.1.20).

13 The presence of accessory fragments of alkaline volcanic rocks within the breccias demonstrates that previous eruptions happened in the area.

14 Near the surface, the rising magma interacted with water, resulting in a phreatomagmatic explosion, when armoured lapilli were formed.

15 The absence of other deposits related to phreatomagmatic eruptions, such as ash beds, can be explained by erosion.

Based on the points discussed above, a model consisting of several stages is presented for the alkaline-rock formation in the Águas Emendadas region. This is summarised in Fig. IV.3.1.

Stage 1 - First episodes of magmatism in the region. These are preserved only as accessory fragments in the breccias.

Stage 2 - An alkaline magma (M1) fills a magma chamber. Formation of cumulates starts. Temperature in the magma chamber decreases.

Stage 3 - A second magma (M2) arrives at the magma chamber. The difference in temperature between M1 and M2 provokes exsolution of volatile phases in both magmas.

Stage 4 - The extra volume of M2, together with the exsolution of the volatile phases, increases the pressure inside the magma chamber, causing instability of the system followed by fragmentation of the liquid (mixture) and triggers a violent explosion. The mixture rises as a fluidized "body" at high velocity.

Stage 5 - At this stage the spinning droplets are formed. The rising mixture, near the surface, interacts with water, presumably from the surrounding country rocks.

Stage 6 - The magma arrives at the surface. An eruption column is formed (probably with a base surge). Products of this explosion include, for example, ash, armoured lapilli, spinning droplets and bombs.

Stage 7 - When the pressure is released, the rate of ascending magma decreases and the whole structure collapses.

Stage 8 - A pyroclastic deposit fills the crater.

Stage 9 - A vesiculated magma continues to ascend within the conduit and percolates the tephra, forming the small intrusive bodies of homogeneous mafic igneous rock. The first lava flow erupts.

Stage 10 - The content of volatile phase decreases, the magma becomes less vesiculated and with less energy. Dykes cut the breccia and feed further lava flows. The presence of "amoeboid" inclusions in rocks formed between stages 3 and 10 shows that M2 was still continuously filling the magma chamber.

Stage 11 - At a certain point M2 supply is interrupted, and magma differentiation restarts in the chamber, leading ultimately to the eruption of feldspar-bearing lava.

Stage 12 - Hydrothermal activity takes place. Volcanic products outside the crater are eroded.

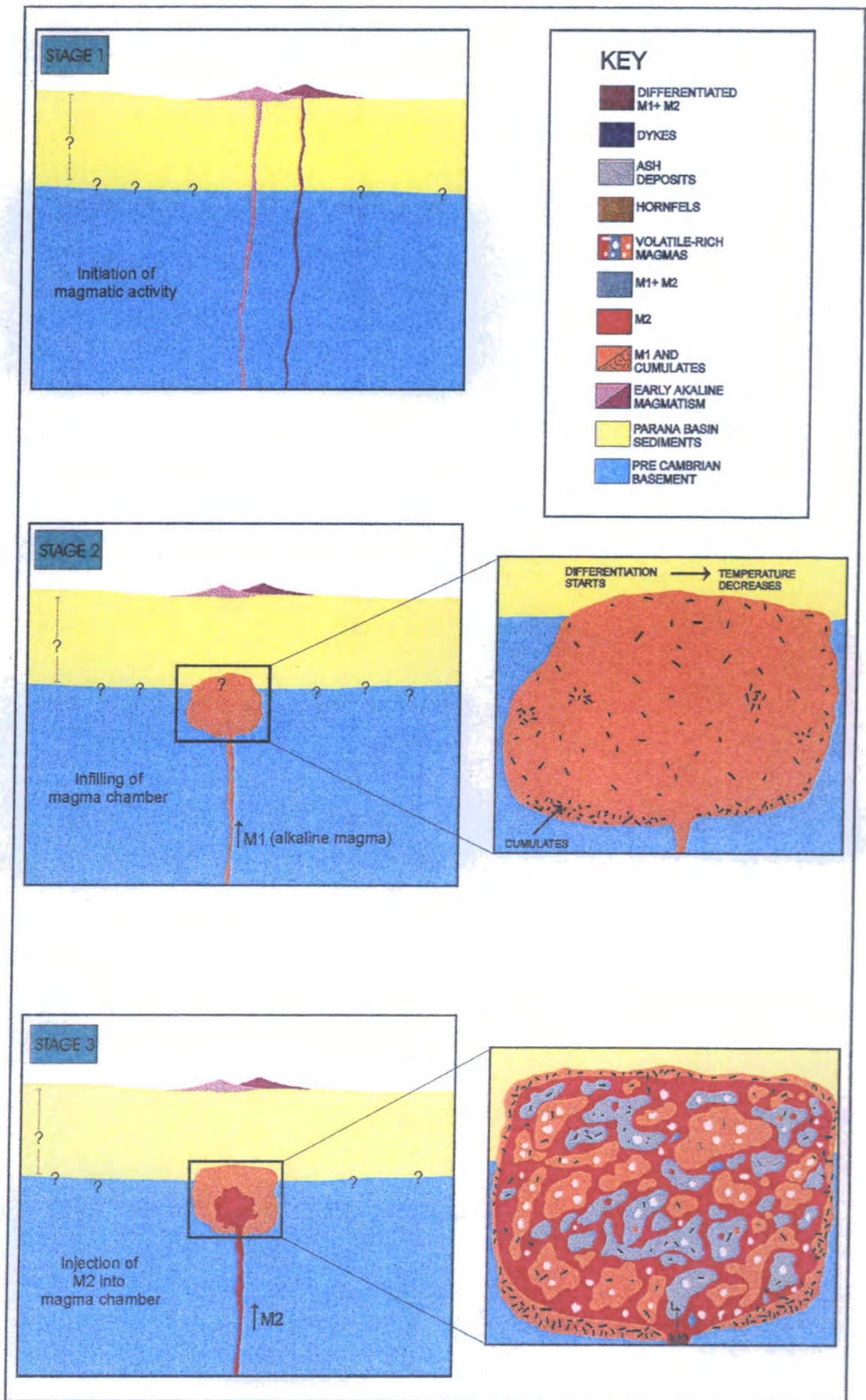
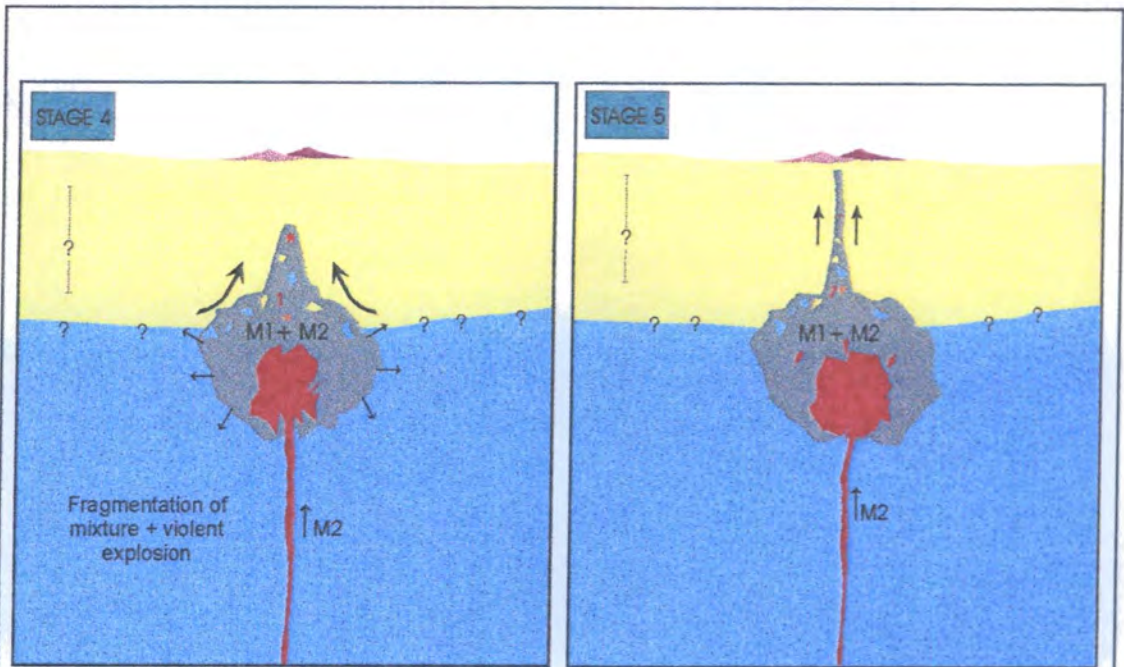


FIGURE IV.3.1 Model for the formation of Cretaceous alkaline rocks of Aguas Emendadas Region.



Model for the formation of spinning droplets in the conduct, during stage 5:

Detail of magma rising in the conduct during stage 5:

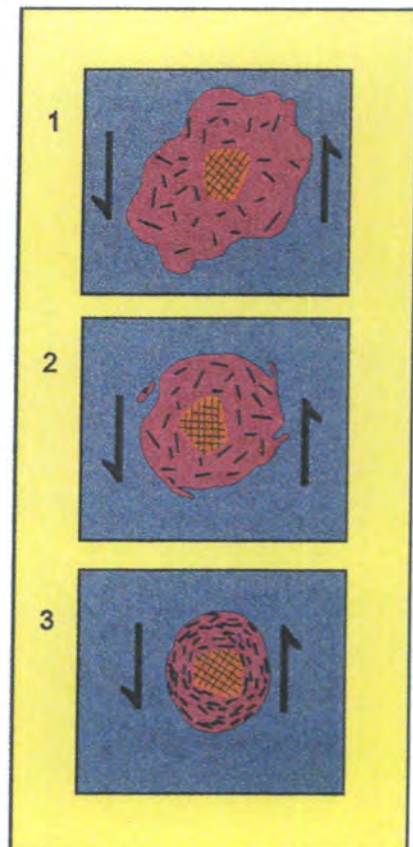
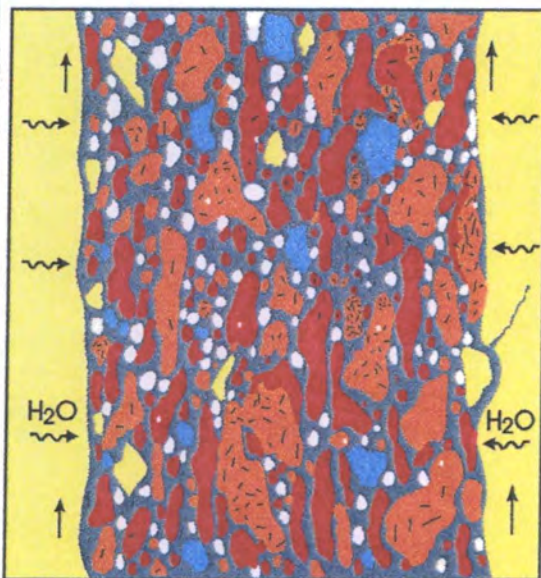


FIGURE IV.3.1 (cont.) Model for the formation of Cretaceous alkaline rocks of Aguas Emendadas Region.

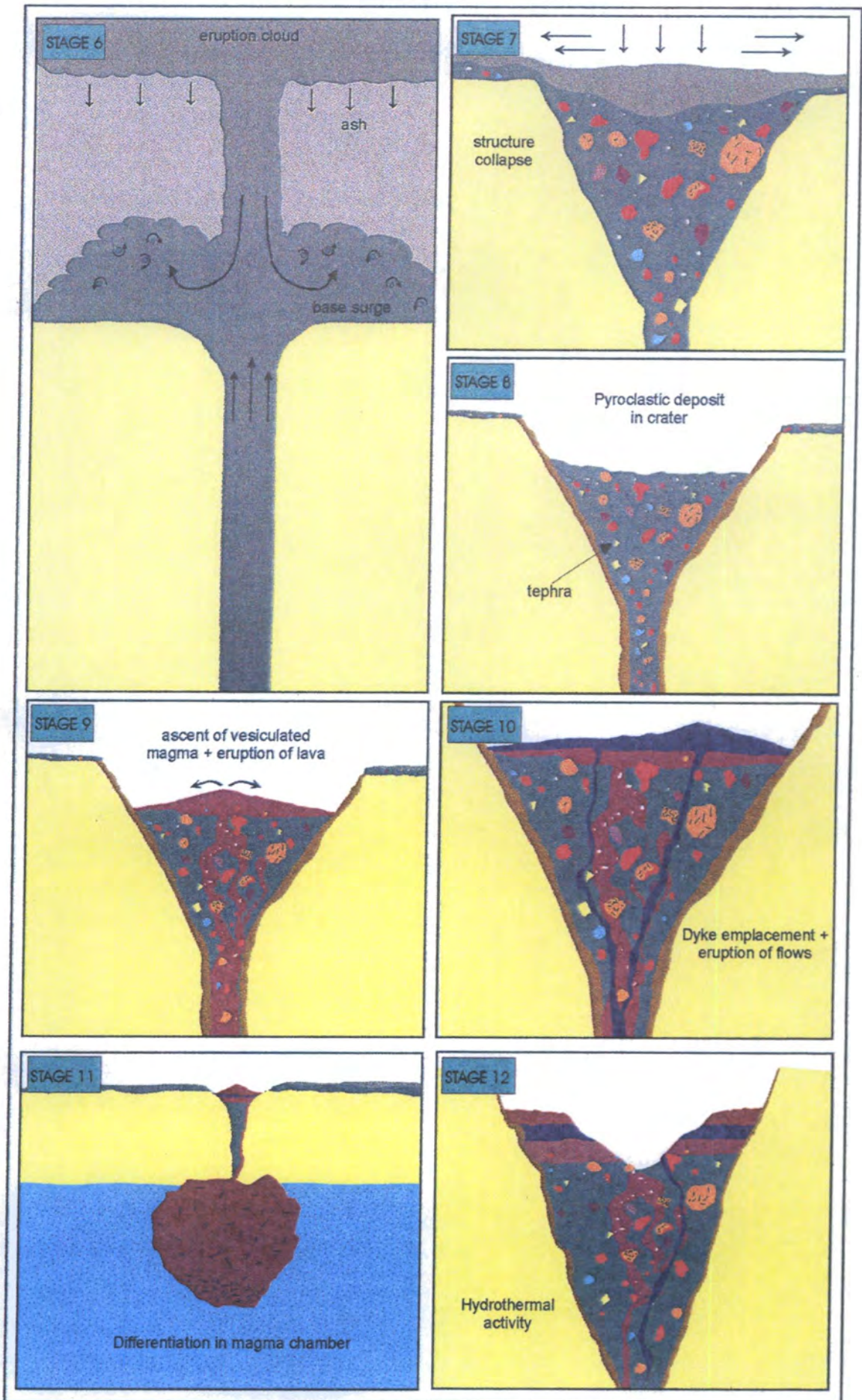


FIGURE IV.3.1 (cont.) Model for the formation of Cretaceous alkaline rocks of Aguas Emendadas Region.

V.1 INTRODUCTION

A preliminary study of the chemical composition of several minerals from the Águas Emendadas Region was carried out using an electron microprobe at the University of Cambridge. The minerals analysed comprise olivines, clinopyroxenes, feldspathoids, feldspars, opaques and perovskite. A description of the main characteristics of each of the studied minerals will be given below. Details of the analytical procedures are given in Appendix 2 and the microprobe data can be found in Appendix 4.

V.2 OLIVINE

The molecular proportions of forsterite in the studied olivines range from Fo₇₆ to Fo₈₈, which is consistent with the ultramafic character of the host rocks. Individual olivine crystals may be zoned, with the forsterite content decreasing from core to rim. Less frequently, a reverse zoning pattern is observed. Although no detailed microprobe traverses have been done in olivine, this may

suggest that reversely-zoned crystals are in fact a different generation of olivine that has been assimilated by a more high-magnesium magma. The existence of more than one generation of olivine phenocrysts is consistent with the petrographic observations (Chapter IV). Groundmass olivine has variable composition. The crystals are usually less magnesian than the cores of olivine phenocrysts, but may overlap the composition of the phenocryst rims. SiO₂, NiO (up to 0.37 wt.%) and Cr₂O₃ (up to 0.1 wt.%) have positive correlations with the forsterite content, while CaO (up to 1.21 wt.%) and MnO (0.73 wt.%) have the opposite behaviour.

V.3 CLINOPYROXENE

All samples studied by microprobe contain diopside, as phenocrysts and/or in the groundmass. The Na content of these pyroxenes is reflected in a low acmite component (up to 3.34 mol% of the acmite molecule). Therefore, they can be classified using the diagram for the four-component system CaMgSi₂O₆-CaFeSi₂O₆-Mg₂Si₂O₆-Fe₂Si₂O₆ (Morimoto *et al.*, 1988; Deer *et al.*, 1992). This is represented in Fig. V.1, where most of the pyroxenes plot within or very close to the diopside field. The composition of pyroxenes from melaleucitites, melanephelinites (?) and leucitites overlap. That of the pyroxenes from basanites is slightly more enriched in the hedenbergite molecule than the other three.

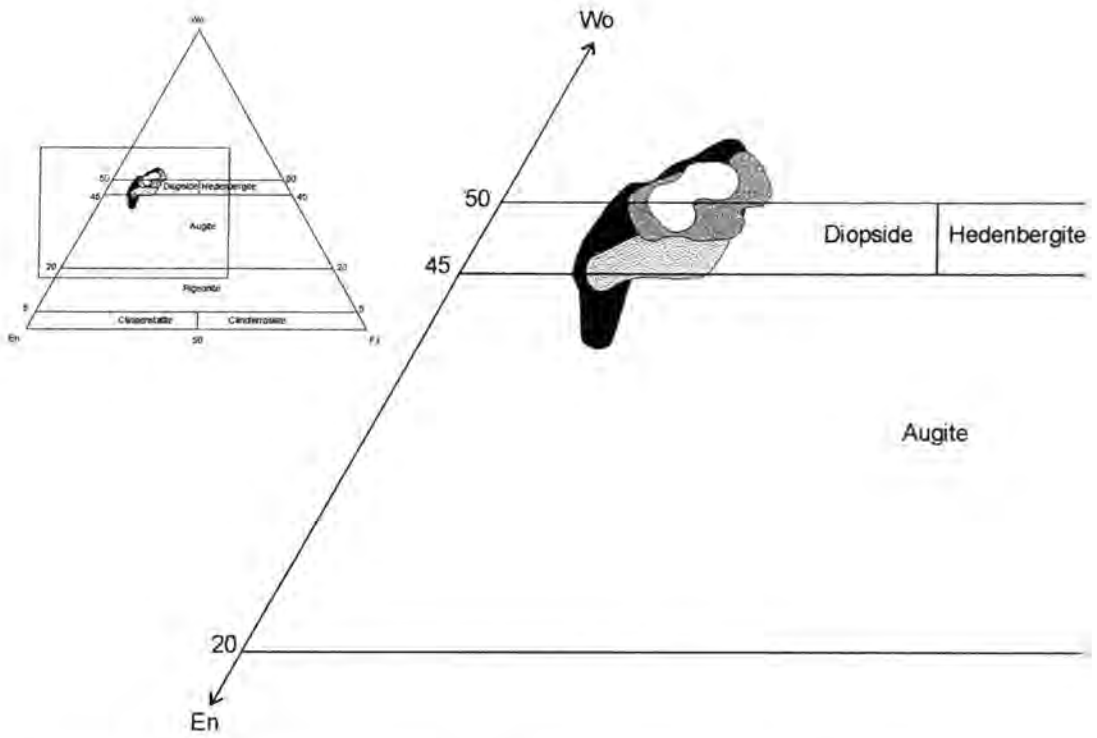


Figure V.1 - Classification of Aguas Emendadas clinopyroxenes (after Morimoto *et al.*, 1988). Fields are: melaleucitite - black, melanephelinite (?) - dark-grey, leucitite - white and basanite - light grey.

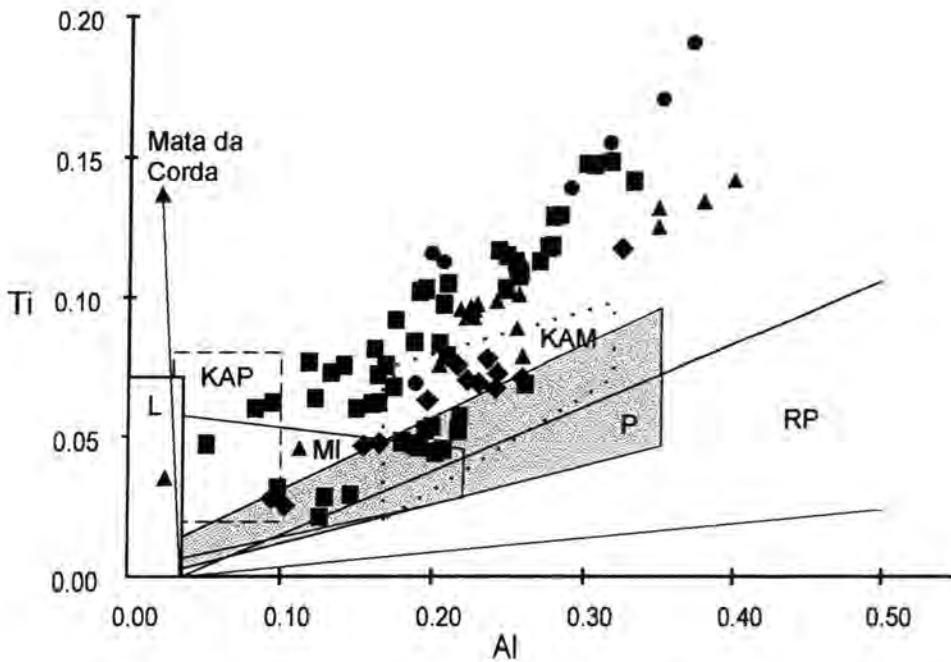


Figure V.2 - Al versus Ti variation of Aguas Emendadas clinopyroxenes compared with pyroxenes of alkaline rocks from other localities. Lamproite (L), Kapamba (KAP), Minette (MI), Kamafugite (KAM) and Roman Province (RP) fields are from Mitchell and Bergman (1991). Mata da Corda trend is indicated by an arrow; data from Sgarbi and Valenca (1994). Paraguay (P) data from Cundari and Comin-Chiaramonti (1996). All data from Aguas Amendadas Region, squares (melaleucitites), triangles (melanephelinites (?)), circles (leucitites) and diamonds (basanites).

One particular characteristic of the studied pyroxenes is that they have very high Ti contents (up to 5.97 wt.% TiO₂), with TiO₂ increasing from the core to the rim of the pyroxene. Similar high-Ti clinopyroxenes in Australian leucitites have been described by Cundari and Salviulo (1989), who suggested that Ti-enrichment is favoured by lower temperature and higher oxygen fugacity.

Figure V.2 shows the comparison between clinopyroxenes from the Águas Emendadas region and those from other alkaline rock-types and provinces. The Al content of most grains is higher than in lamproite pyroxenes. The Ti/Al ratio of the Águas Emendadas pyroxenes is higher than those from the Roman Province and alkaline rocks from Paraguay, although the Al contents are similar. The best fit is with pyroxenes from kamafugitic rocks (Uganda). However, the composition range is wider in Águas Emendadas pyroxenes.

V.4 FELDSPATHOIDS

Two types of feldspathoids were found in the studied rocks. Nepheline was identified in four samples of melanephelinite (?), melaleucitite and leucitite. All nephelines have an unusually high content of K₂O, ranging from 9.45 to 11.17 wt.%. This corresponds to an excess of K, in relation to the ideal nepheline formula (maximum of 2 potassium cations per 32 oxygen), for

all analysed grains. The proportion of the kalsilite molecule in these nephelines varies from 29.61 to 34.51 mol%.

Kalsilite ($K_{93.3}Ne_{6.6}$) was found in a melanephelinite (?) sample (96AE08). This was confirmed by XRD analyses of the sample, suggesting that kalsilite is a significant mineral in this rock, although only one grain was positively identified and analysed during the microprobe work.

V.5 FELDSPARS

Alkali feldspars occur as part of pseudoleucite aggregates, finely mixed with nepheline, zeolites (EDS qualitative analysis only) and carbonate in melaleucitites. Two analyses made of these feldspars gave compositions close to the orthoclase end-member ($Or_{96.4-98.8}$). Ba was not analysed, but the high totals of the analyses suggest that it is not present in significant amounts.

Plagioclase was only found in basanites. It varies from $An_{40.9}$ to $An_{53.6}$, corresponding to calcic andesine and sodic labradorite. It may contain up to 1.46 wt.% FeO, but this is probably related to the presence of impurities (Deer *et al.*, 1992).

V.6 PEROVSKITE

Perovskite composition is relatively restricted. During this work, only EDS analyses of perovskite from three samples were carried out. Therefore, it is not possible to do a direct evaluation of the concentration of trace-elements such as the REE, Nb and Sr. When these elements are dominant, they give origin to the end-members loparite, lueshite and tausonite, respectively (Mitchell, 1996). The high analytical totals indicate that these perovskites are relatively close to the ideal CaTiO_3 composition. Among the analysed elements, only Si, Al, Fe and Na occur as significant trace elements. If the analyses are recalculated on the basis of 3 oxygens, according to the general perovskite formula ABO_3 , calcium occupies 94 to 96% of the A site, and Ti occupies more than 99% of the B site. Thus, the end-members that involve substitution of Ti (such as the Nb-rich end member lueshite) are unlikely to be present in significant amounts. On the other hand, up to 4 to 6 mol % of end-members that require substitution of other cations for Ca (e.g. the Na+REE-rich end-member loparite or the Sr-rich end-member tausonite) may be expected.

V.7 OPAQUES

Opaque minerals generally occur as small groundmass grains that make the microprobe analysis difficult. Most of the analysed grains gave a

low analytical total, even after recalculation of the $\text{Fe}^{3+}/\text{Fe}^{2+}$ ratio to stoichiometry, according to the method of Droop (1987). This may be due to a) analytical error; b) the presence of non-analysed components or c) inaccuracy of the $\text{Fe}^{3+}/\text{Fe}^{2+}$ estimation method. Therefore, the analyses are given here a semi-quantitative status, and caution should be taken in the interpretation of the data.

Based on these semi-quantitative data, the opaque minerals are part of the ulvöspinel-magnetite series. They are represented in Fig. V.3, where most analyses plot near the titanomagnetite line, closer to the ulvöspinel than to the magnetite end-member. However, some other elements are also significant, although highly variable. Magnesium ranges from 0.33 to 10.23 wt.% MgO, chromium varies from 0.08 to 17.61 wt.% Cr_2O_3 and aluminium from 0.37 to 8.00 wt.% Al_2O_3 . The highest contents of Mg, Cr and Al are from opaques in the samples 96AE46 (melanephelinite (?)) and 96AE57 (leucitite). These represent some degree of solid solution towards Mg-Al-chromites.

V.8 CARBONATE

Carbonate minerals were not analysed by electron microprobe. However, since high trace-element contents of carbonates are considered an indication of their magmatic origin, two hand-picked separates of carbonate from veins were analysed by ICP-MS. Results are given in Appendix 3 and analytical procedures were the same as for whole-rock analysis (Appendix 2).

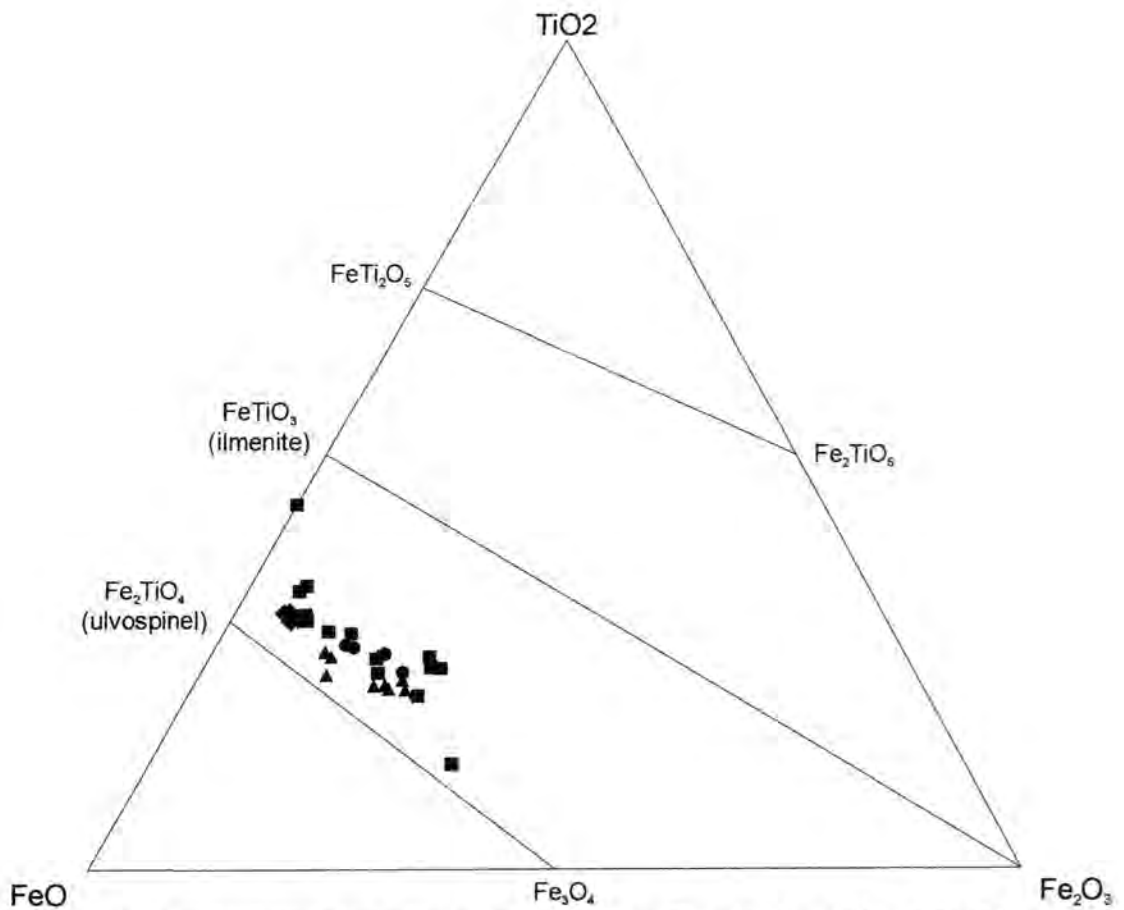


Figure V.3 - Compositional variation (mol%) of Aguas Emendadas oxides (after Deer *et al.*, 1992). Symbols as in Fig. VI.2.

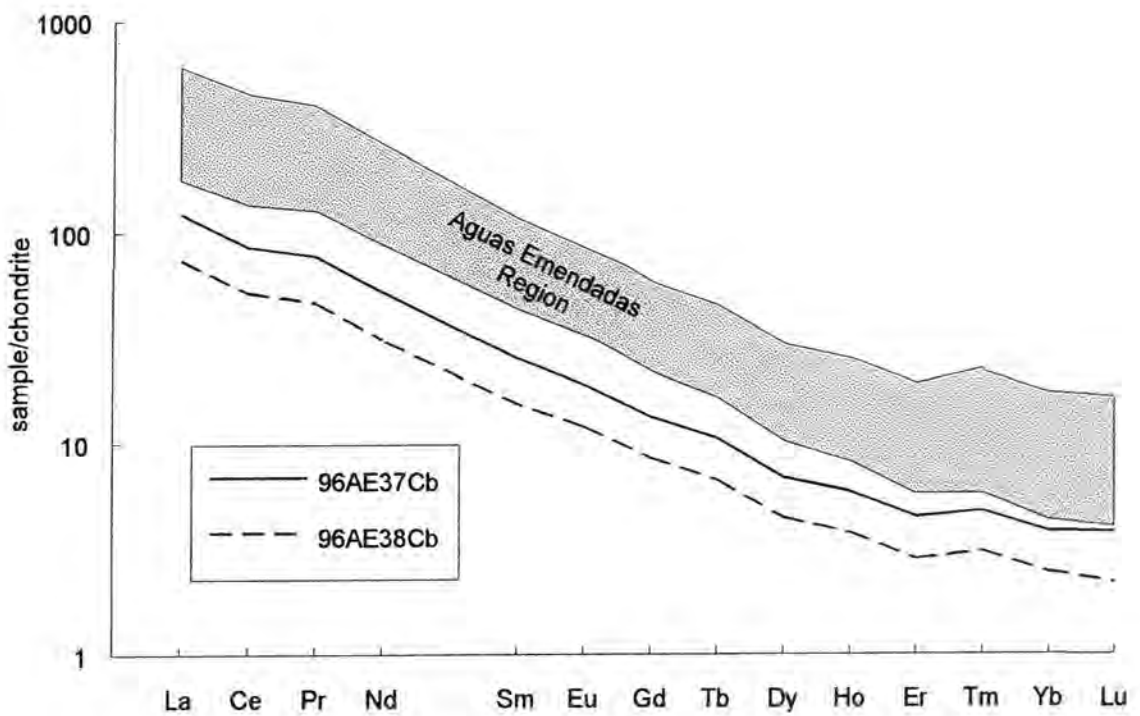


Figure V.4 - Chondrite-normalized REE diagram comparing carbonate REE-patterns with those from rocks of Aguas Emendadas Region. Normalization constants from Nakamura (1974), except Pr, Tb, Ho and Tm (Haskin *et al.*, 1968).

The Sr and Ba contents are in the ranges from 393 to 1596 ppm and from 391 to 722 ppm, respectively. These concentrations are low, if compared with carbonates from carbonatites, which usually have Ba and Sr at percentage levels. Based on the Ba and Sr concentrations, it is likely that the veins are a product of hydrothermal processes, rather than a direct manifestation of carbonatitic magmatism. On the other hand, the chondrite-normalized REE patterns of these carbonates (Fig. V.4) are parallel to the REE patterns of volcanic rocks from Águas Emendadas, although at a lower concentration level. To produce these parallel patterns, the partition coefficients for different REE would have to be the same in both the magmatic and the hydrothermal events. Möller and Morteani (1983) studied the REE distribution in calcites of different origins. They suggested that the REE patterns in chondrite-normalized diagrams can vary significantly between calcites of magmatic and hydrothermal origins. In the cases reported by them, the hydrothermal calcite shows a convex, middle-REE-enriched pattern, while the magmatic calcite has a steep, roughly linear LREE-enriched pattern. Although these results may not be necessarily applicable to this research, they illustrate the potential of hydrothermal systems to crystallise calcites with REE-patterns broadly different from those of magmatic carbonates. Short of a more detailed chemical and isotopic study, the problem is unlikely to be solved.

VI.1 INTRODUCTION

From the total of rocks collected during the field work, those with macroscopic pyroclastic textures, large amounts of xenoliths and pervasive weathering/hydrothermal alteration were avoided during the geochemical studies. A total of 45 samples from Águas Emendadas and Amorinópolis Regions were analysed for major and trace-elements by X-Ray Fluorescence (XRF) and 41 samples were analysed for trace and rare-earth elements (REE), by Inductively Coupled Plasma - Mass Spectrometry (ICP-MS). Appendix 2 describes the analytical procedures adopted. XRF and ICP-MS data are given in Appendix 3 (Table A3.1 and Table A3.2, respectively), Table A3.2 also includes the analyses of two samples of carbonate, collected from veins in the Águas Emendadas Complex (96AE37Cb and 96AE38Cb).

Among the analysed samples a second selection was made, based on petrography. Samples 96AE15 and 96AE64 were omitted, since they are metamorphic rocks and probably constitute part of the Pre-Cambrian basement. Sample 96AE65 is a gabbro and is excluded because it probably does not represent a liquid. Samples 96AE54 and 92SOB212 proved to be altered. The

final set of selected samples is intended to typify the various stages and/or the evolution of the magmatism in the region.

After these two selection steps, a data-base comprising 40 samples was studied in detail. The samples are divided into two regions and four groups, according to the field and petrographic information. The regions are Águas Emendadas and Amarinópolis. The former includes samples from the Águas Emendadas Complex, Neuzinha, Marimbondo and Cacimba, while the latter comprises samples from Amarinópolis and Morro do Macaco. The petrographic groups comprise: (i) melaleucitites, (ii) melanephelinites (?), (iii) leucitites and (iv) basalts and basanites. An exception in the petrographic classification was made for sample 96AE57. This is petrographically a leucitite, but behaves geochemically as part of the Melaleucitite Group and, therefore, has been moved to the latter for the purposes of this chapter.

The major elements (wt.%) were recalculated to a 100% total, on a volatile-free basis. Samples with high loss-on-ignition (LOI) proved to be rich in carbonate (e.g. 96AE42 - LOI=7.40 and 96AE46 - LOI=5.28). It is not clear whether the carbonate in these samples is of magmatic or hydrothermal origin; they were not excluded from the data set because their chemical behaviour is consistent with similar samples in their group.

Sample 96AE20 (leucitite) has some of its trace-element contents well above the average of the Leucitite Group (e.g. Nb, Zr, Y, Ba, Th, REE; see Fig. VI.3.1, section VI.3 - trace-elements). However, the sample appears to be fresh and no petrographically apparent reason, such as accumulation of one or more particular mineral phases, was found to justify this difference. This sample was therefore kept in the data base.

Tables A3.3 and A3.4 (Appendix 3) give, respectively, the norms calculated according to CIPW and to the method of Le Bas (1973) for selected samples. The norms were calculated using an arbitrary $\text{Fe}_2\text{O}_3/\text{FeO}$ ratio of 0.15.

The available information only allows limited inference about the magma sources. A more detailed investigation of this topic requires radiogenic isotope data.

The use of elements, such as potassium and rubidium, which are likely to have been mobile during hydrothermal alteration and/or weathering is avoided as much as possible. The discussion on the geochemistry of the rocks from Águas Emendadas will be focused, whenever possible, on those elements that are less susceptible to such changes.

Most of the analysed samples are porphyritic (up to 46 modal % phenocrysts), consequently the distinction between the effects of crystal accumulation and fractional crystallisation becomes very difficult.

Besides reporting the general chemical characteristics of the rocks from the Águas Emendadas Region, the discussion in this chapter will focus on the following points:

- 1 - It can be demonstrated that the grouping of samples on the basis of their chemical composition is in good agreement with the petrographic observations.

- 2 - Among the rocks with high magnesium contents (melaleucitites and melanephelinites (?)), it is possible to observe: (a) Small differences in composition which are possibly related to the effects of slight variation in the mantle sources or, alternatively, in the degrees of partial melting. (b) The

fractionation processes did not include significant amounts of clinopyroxene, despite the prominence of this mineral as a phenocryst.

3 - The way in which the mafic magmas evolved can be deduced from the chemical data.

4 - Inferences about the genesis of the Mg-poor rocks can be made, although these are limited by the small number of analyses available.

The diagrams of Figs. VI.1.1 and VI.1.2 establish a few themes to be explored in this chapter. The separation of the rocks in two main geochemical groups, one with high magnesium and the other low magnesium, is clear in from Fig. VI.1.1. Fig. VI.1.2 exemplifies the differences in the chondrite-normalized REE-patterns for two samples with similar MgO contents. It is obvious that the melanephelinite (?) and the melaleucitite have distinct levels of both REE-enrichment and LREE/HREE fractionation, which cannot be readily explained by magmatic differentiation (see below).

VI.2 MAJOR ELEMENTS

The rocks are ultrabasic to basic, with SiO₂ varying from 36.72 to 50.61 (wt.%). Their MgO content ranges from 3.58 to 18.46 (wt.%) and the magnesium-number ($Mg\# = \frac{wt.\% MgO}{wt.\% MgO + (wt.\% Fe_2O_3T * 0.899847)}$) varies from 23.52 to 60.50. The total alkalis content (Na₂O + K₂O) varies from 1.29 to 8.68 wt.%; the highest content of K₂O is 5.14 wt.% and the highest Na₂O is 5.48 wt.%. The range for Fe₂O₃T (total iron expressed as Fe₂O₃) is

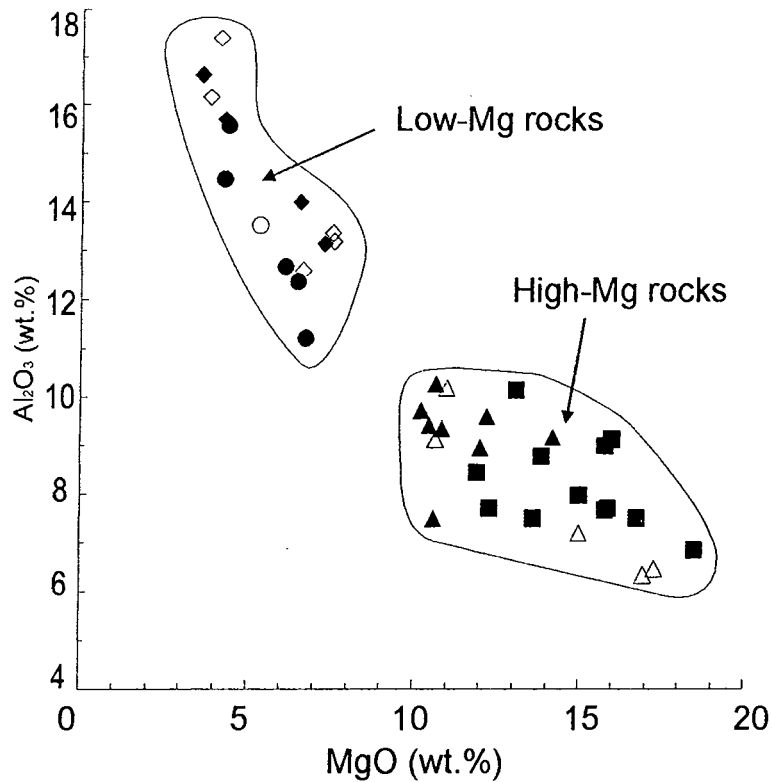


Figure VI.1.1 - Plot of Al_2O_3 against MgO , as a differentiation index. Solid and open symbols represent samples from the Aguas Emendadas Region and Amorinopolis Region, respectively. HMG = High-Magnesium Group, LMG = Low-Magnesium Group.

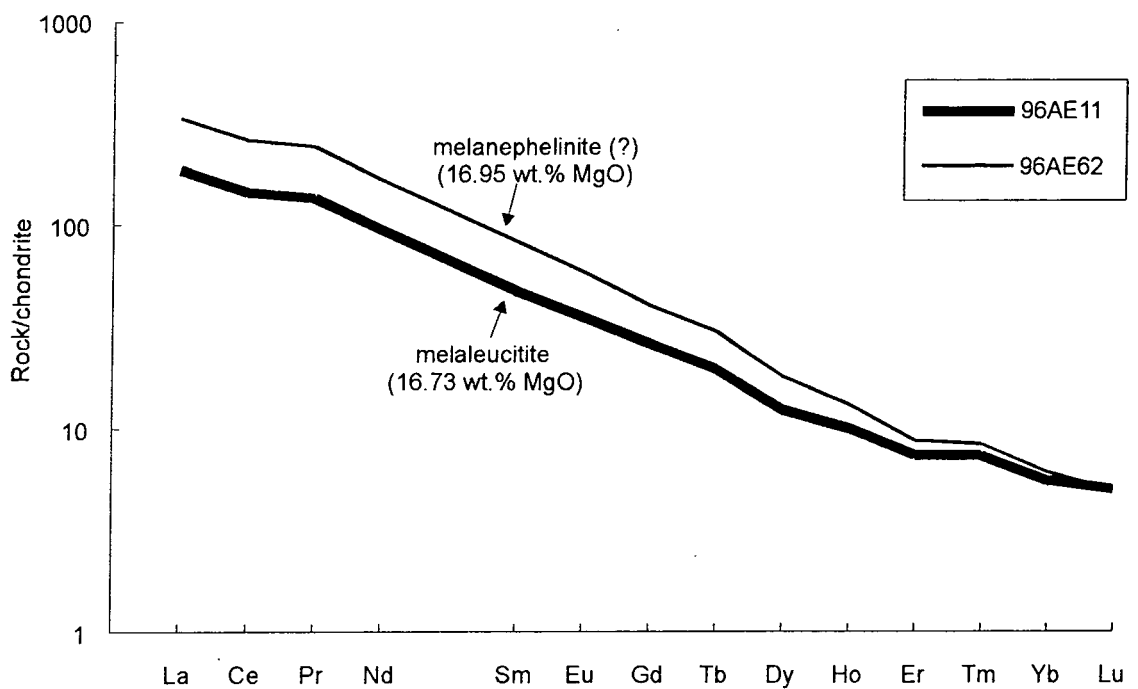
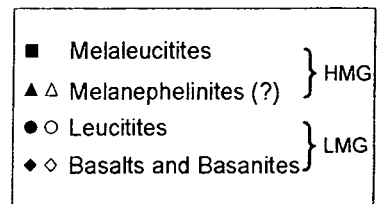


Figure VI.1.2 - Chondrite-normalized REE diagram. Normalization constants from Nakamura (1974), except Pr, Tb, Ho and Tm (Haskin *et al.*, 1968).

10.02 to 18.13 wt.% and for Al_2O_3 6.33 to 17.38 wt.%. The studied rocks can have up to 17.79 wt.% CaO, 6.00 wt.% TiO_2 and 1.56 wt.% P_2O_5 . In Fig. VI.2.1 some of the major element oxides are plotted against MgO (wt.%) to illustrate these variations.

It is apparent from Fig. VI.2.1 that the melaleucitites and melanephelinites (?) form a High-Magnesium Group (HMG), while the leucitites, basalts and basanites plot in a Low-Magnesium Group (LMG). The samples of HMG have lower SiO_2 and Al_2O_3 contents and tend to have higher CaO, compared with the LMG.

The high contents of SiO_2 and Al_2O_3 in the LMG correspond with the higher modal abundances of felsic minerals, such as leucite and feldspar, and lower modal olivine. The inflection of the trend in the CaO vs. MgO plot can be explained by the onset of crystal fractionation of pyroxene in the less Mg-rich magmas. This inflection occurs at approximately 11 wt.% MgO (LMG).

Within the HMG group, it is noticeable that there are two separate trends of differentiation, at the same level of MgO (Fig. VI.2.1). The melanephelinites (?) are substantially enriched in $\text{Fe}_2\text{O}_3\text{T}$ and poorer in SiO_2 (trend B), relative to melaleucitites (trend A). In both rock types the $\text{Fe}_2\text{O}_3\text{T}$ variation with MgO is consistent with removal of olivine, but not with the removal of pyroxene, which only seems to be effective in the LMG.

To test this point, a diagram of $\text{Fe}_2\text{O}_3\text{T}$ versus CaO (Fig. VI.2.2) was constructed, using only samples with more than 11 wt.% MgO (HMG). The shaded fields outline the composition range of analysed olivines (cores only) and clinopyroxenes from some of these rocks (data from Appendix 4, tables A4.1 and A4.2). The pyroxenes in the two rock-types are similar in composition,

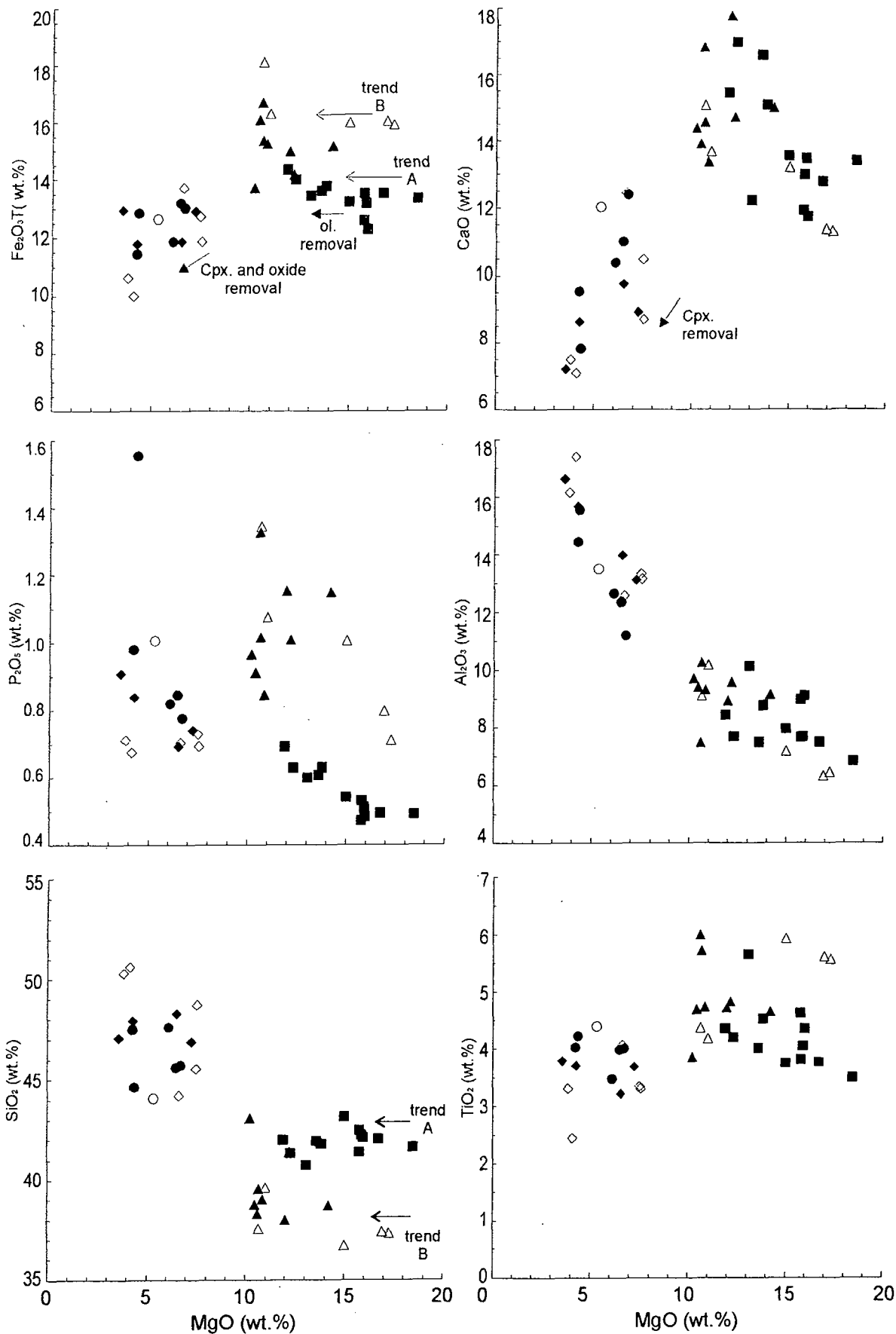
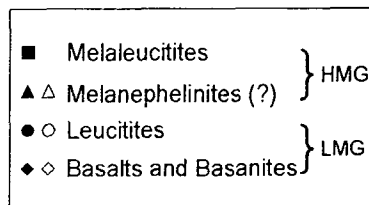


Figure VI.2.1 - Plots of selected major elements against MgO, as a differentiation index. Fe₂O₃T = total iron expressed as Fe₂O₃. Solid and open symbols represent samples from the Aguas Emendadas Region and Amorinopolis Region, respectively. HMG = High-Magnesium Group, LMG = Low-Magnesium Group.



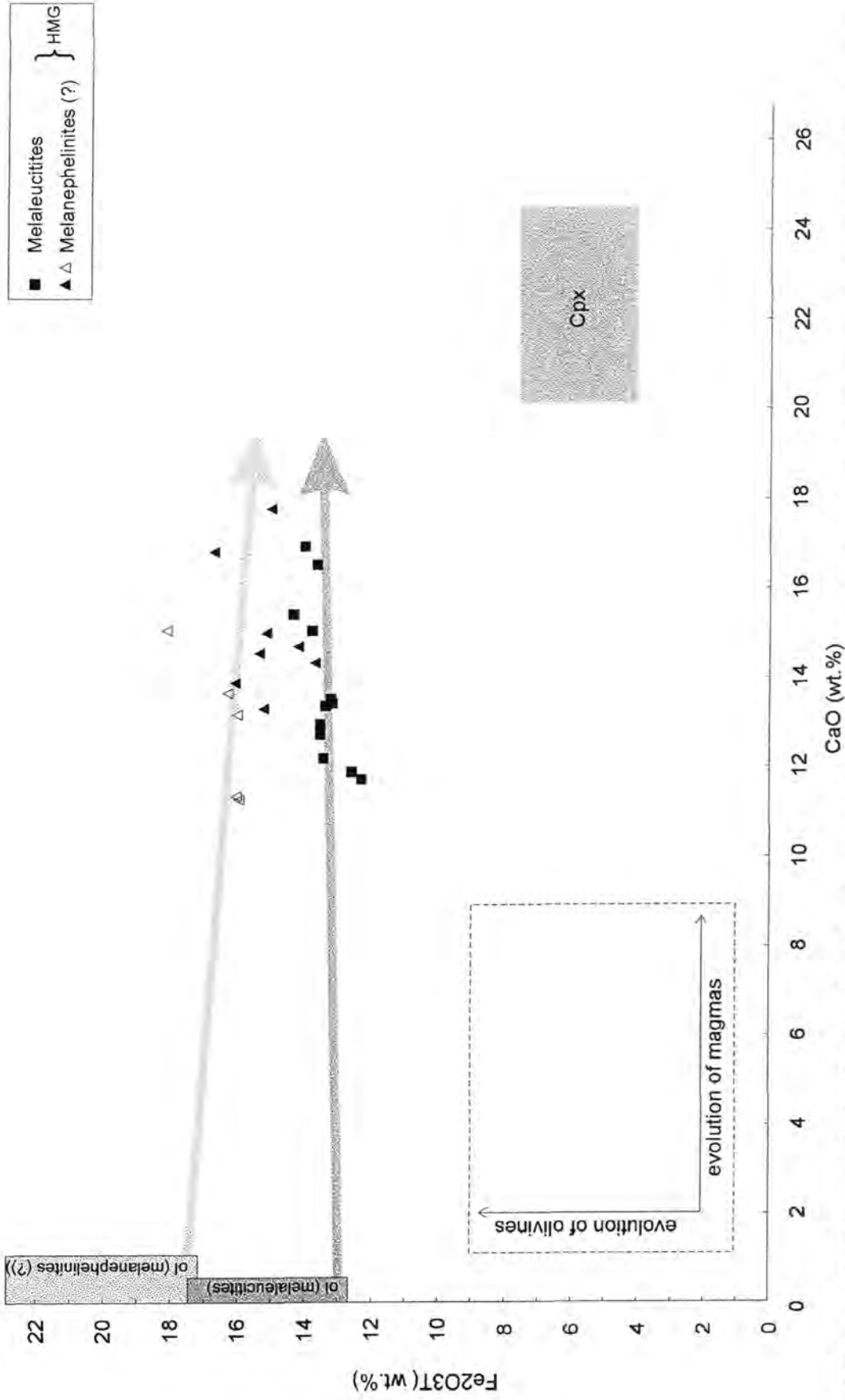


Figure VI.2.2 - Fe_2O_3T versus CaO diagram for HMG rocks. Closed and open symbols represent samples from Aguas Emendadas Region and Amorinópolis Region respectively. Shaded fields represent ranges in compositions for olivines and clinopyroxenes. Arrow indicates trends of olivine removal.

and for this reason they are represented by a single field. The same is not true of olivines, because olivine from the melanephelinites (?) are richer in Fe than those of the melaleucitites. The arrows in the figure represent the trends resulting of the removal of the most magnesian olivine from each type of rock. There is a good agreement between the trends defined by the whole-rock analyses and the predicted fractionation of the respective olivines. On the other hand, there is no trend indicating removal of clinopyroxene. In fact, as was deduced from Fig. VI.2.1, CaO increases with decreasing MgO in the HMG suite, which is contrary to the variation that would be expected if clinopyroxene was being removed. These results pose an interesting problem to the interpretation of the magmatic processes occurring in these rocks. The presence of clinopyroxene phenocrysts is an indication that crystallisation of this mineral from HMG magmas is possible and has occurred. On the other hand, the chemical data suggest that clinopyroxene was not extensively fractionated out of the HMG liquids. These two lines of evidence would be in good agreement, however, if the pyroxene phenocrysts were not separated from the magma after they formed. It is suggested here that clinopyroxene crystallised and largely remained suspended in the HMG magmas during their ascent, rather than being formed in a magma chamber, where they could have been fractionated. On the other hand, in the case of LMG magmas, the fractionation of clinopyroxene in a magma chamber is likely to have occurred.

If both the HMG and the LMG are considered together, the behaviour of $\text{Fe}_2\text{O}_3\text{T}$ and TiO_2 seems to be controlled by the crystallisation of more than one phase. $\text{Fe}_2\text{O}_3\text{T}$ is probably associated with the crystallisation of olivine, pyroxene and an oxide phase, while TiO_2 behaviour is probably

governed by the same phases as $\text{Fe}_2\text{O}_3\text{T}$ (except olivine) and perovskite. The high TiO_2 concentration in some samples can be linked with the presence of either an oxide phase or perovskite in the groundmass. According to the mineral chemistry data (Chapter V) the oxide phase involved is part of the ulvöspinel-magnetite series, with up to 39 wt.% TiO_2 .

Despite the occurrence of small amounts of phlogopite phenocrysts, the removal of this phase is not evident from the behaviour of major elements. This is probably due to a much stronger effect of the removal of olivine, clinopyroxene and oxides on the abundances of elements such as Mg, Fe and Ti. Al_2O_3 is not strongly affected by any of these phases. Furthermore, since plagioclase and perovskite do not crystallise simultaneously (Veksler and Tepteleev, 1990), Al_2O_3 will not be affected by the early fractionation of plagioclase. Therefore, the behaviour of this oxide could mark the removal of phlogopite phenocrysts in the perovskite-bearing rocks (HMG). The absence of significant inflections in the aluminium trend (Fig. VI.2.1), suggests that phlogopite phenocrysts were not extensively removed from these liquids.

Some of studied samples have low contents of alkalis, compared with similar petrographic types, indicating that there was a loss in these elements during weathering and/or hydrothermal alteration. The $\text{K}_2\text{O}/\text{Na}_2\text{O}$ ratio ranges from 0.07 to 3.11 for the whole of 40 samples and this ratio is highly variable within the groups. The alkali content is likely to have been affected by hydrothermal alteration more than the other major oxides. This may be especially the case for samples from the Águas Emendadas Complex, where some of the leucitites have higher contents of Na_2O than of K_2O , suggesting that minerals such as leucite were transformed into a sodic phase. Giampaolo

et al. (1997) studied similar transformation in leucite-bearing rocks, suggesting that a progressive Na increase occurs during alteration, while K, Ca and Mg decrease in the bulk-rock chemical composition.

The total alkalis versus silica diagram (TAS) of Fig. VI.2.3 shows the unreliability of alkalis as a means of classifying these rocks. Woolley *et al.* (1996) pointed out that this diagram is unsuitable for leucititic and nephelinitic rocks, and therefore recommended a classification based on modal criteria which was adopted during this research (Chapter IV). Thus, the petrographic classification is maintained here, regardless of the inconsistencies of whole-rock chemistry in the TAS diagram. The data for the foidites are still plotted for comparison in Fig. VI.2.3, where it is noticeable that the HMG and the LMG occupy different sectors of the diagram. Most of the melanephelinites (?) plot in the foidite field, except for samples 96AE24 (basanite) and 96AE53 (picro-basalt), while the basalt and basanites are distributed over the basanite/tephrite, trachy-basalt and basaltic trachy-andesite fields.

Foley *et al.* 1987 proposed the division of mafic ultrapotassic rocks into four groups. Group I, II, III correspond to Lamproitic, Kamafugitic, Roman Province-type rocks, respectively. Group IV is transitional, mostly between groups I and III. Before the classification scheme can be applied, the analysis must meet three criteria to confirm the ultrapotassic character of the rock: (a) $K_2O/Na_2O > 2$; (b) $K_2O > 3\text{wt.}\%$ and (c) $MgO > 3\text{wt.}\%$. The MgO content of the analysed rocks is always higher than 3 wt.% and therefore meets the first condition. On the other hand, as shown in Fig. VI.2.4, many samples have $K_2O < 3\text{wt.}\%$ and $K_2O/Na_2O < 2$. Only one sample, from the leucitites group, satisfies both the second and third conditions. However, when the 'chemical criteria' division of Foley *et al.* (1987) is applied, the samples still fit consistently in most

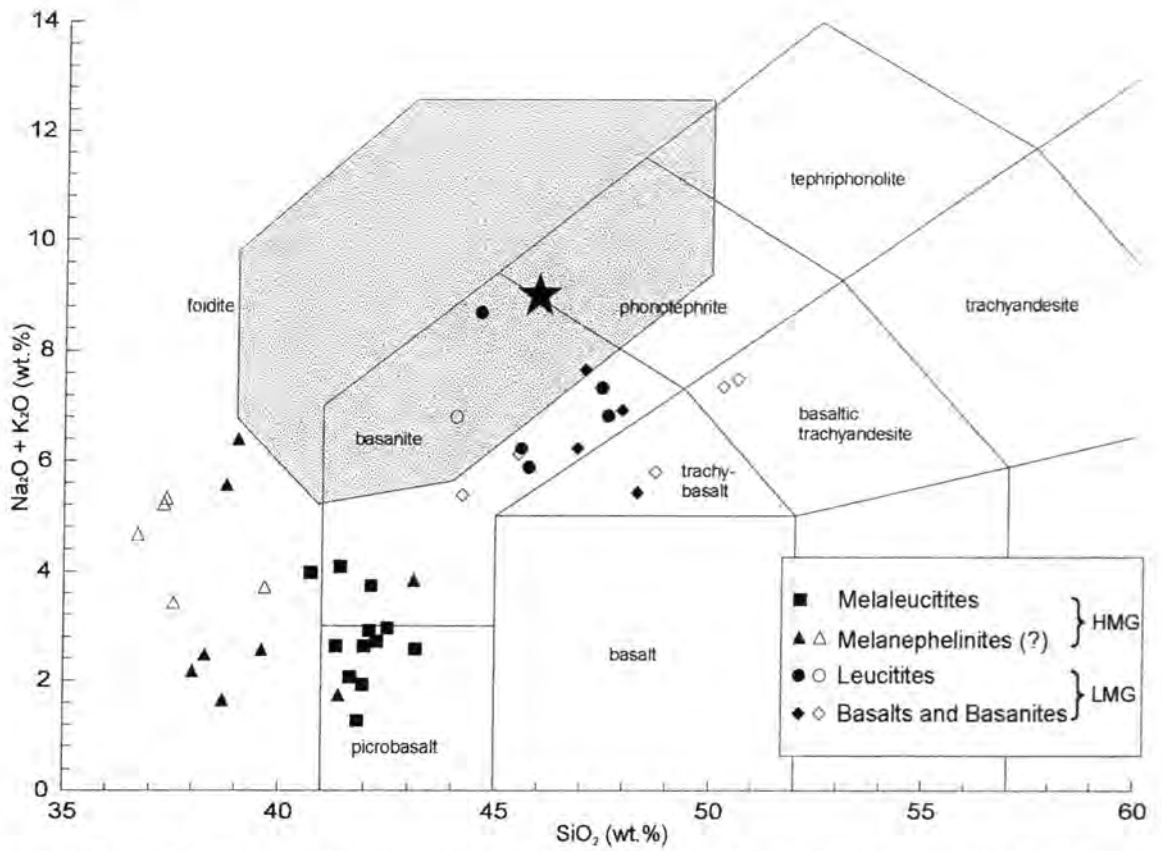


Figure VI.2.3 - Total alkali versus silica (TAS) diagram (Le Maitre, 1989). Solid and open symbols represent samples from Aguas Emendadas Region and Amarinopolis Region, respectively. Shaded field from Woolley *et al.* (1996) indicates frequency distribution of leucite samples (90%); star represents the peak of frequency distribution.

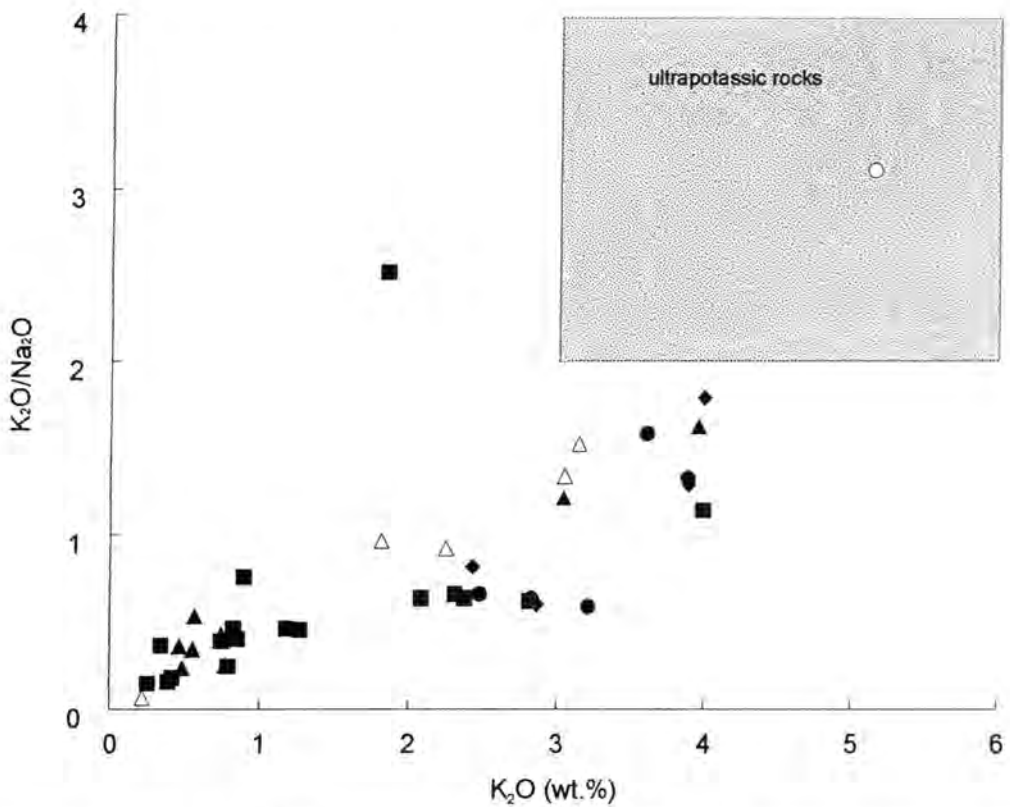


Figure VI.2.4 - Plot of K₂O/Na₂O ratio against K₂O. Shaded rectangle indicates the limits attributed to ultrapotassic rocks by Foley *et al.* (1987). Symbols as in Figure V.2.3.

of their diagrams (Fig. VI.2.5). The HMG can be classified as part of the Kamafugite group, while the LMG plots mostly in the Roman Province group. Although the alkali contents of these rocks are not reliable, it appears that most of the other oxides have a consistent behaviour.

As expected, none of the selected samples has normative (CIPW) quartz, demonstrating their degree of silica undersaturation. Normative nepheline is present in all of the samples, while normative leucite occurs mainly in the Melanephelinite (?) and Melaleucitite groups. Diopside and olivine are often the predominant minerals in the CIPW norm, confirming the mafic character of the rocks.

A norm calculation specific for alkaline rocks was developed by Le Bas (1973), to be applied when calcium orthosilicate and/or acmite appear in the CIPW norm. Most of the melanephelinites (?) and some of the melaleucitites satisfied this condition. When the norms are recalculated according to the method of Le Bas (1973), they are characterised by the presence of normative gehlenite or akermanite in rocks containing CIPW-normative acmite. Kalsilite is present in the norm of four rocks of the Melanephelinite (?) Group. Two of them also contain normative acmite, baddeleyite, akermanite, Fe-akermanite and perovskite, as the only Ti mineral. As in the CIPW norms, the calculated compositions also confirm the mafic character of these rocks.

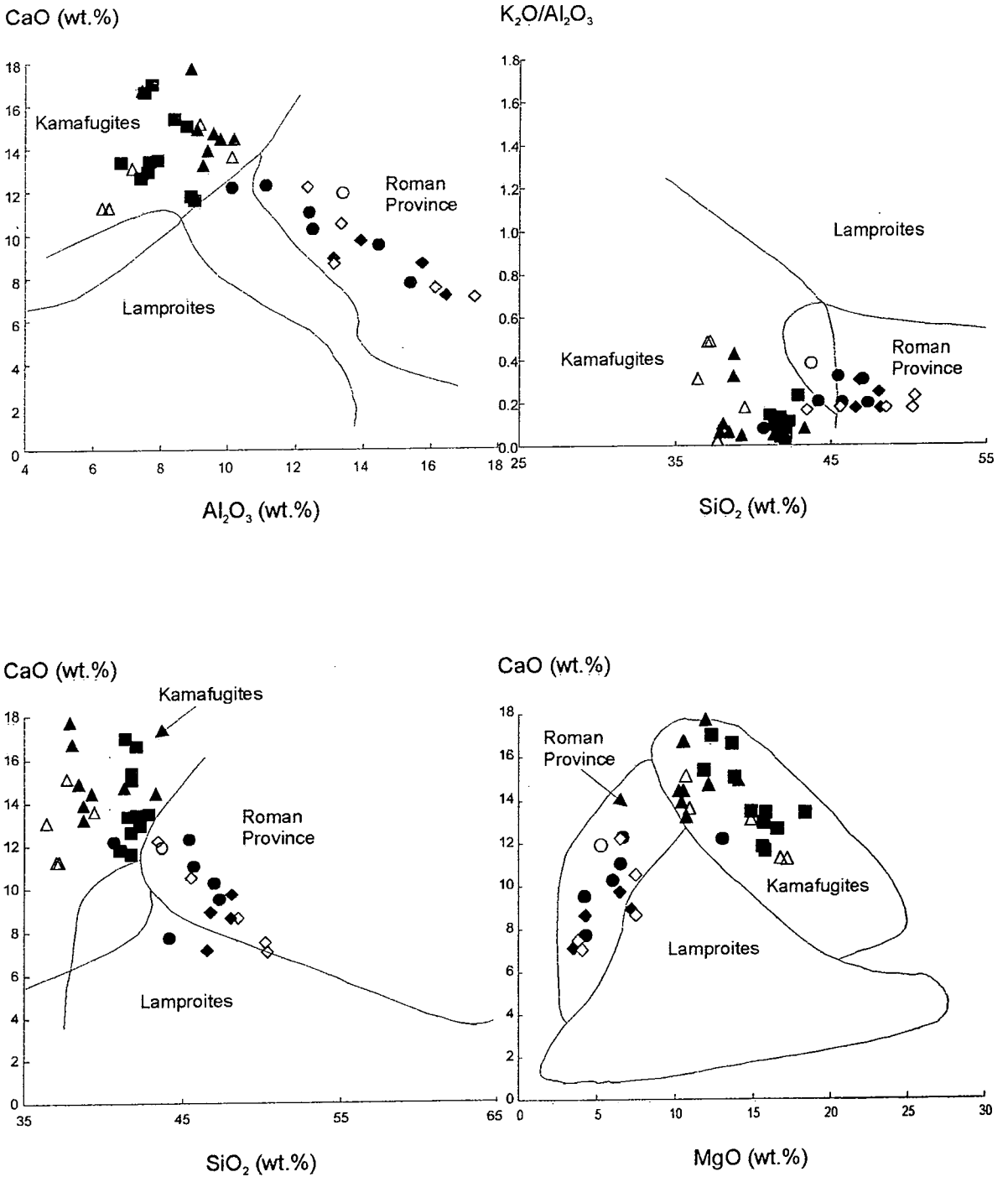
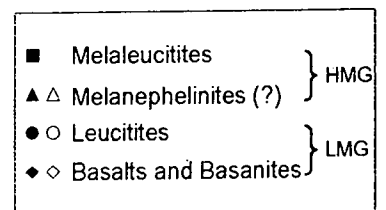


Figure VI.2.5 - Classification of ultrapotassic igneous rocks according to Foley *et al.* (1987), Groups I, II and III are represented by Lamproites, Kamafugites and Roman Province fields, respectively. Solid and open symbols are samples from the Aguas Emendadas Region and Amorinopolis Region, respectively.



VI.3 TRACE-ELEMENTS

VI.3.1 Compatible trace-elements

The Cr content of the analysed samples varies almost continuously, from 2 to 1952 p.p.m., as Ni ranges from 6 to 504 p.p.m. (Fig. VI.3.1). According to Wilson (1989), Cr values of 500-600 p.p.m. and Ni of 250-300 p.p.m. are considered high and suggest "derivation of parental magmas from a peridotite mantle source". Normally, the HMG rocks have higher Cr and Ni contents than the LMG. The behaviour of Ni is readily explained by the fractionation of olivine (Fig. VI.3.1). Cr is probably controlled by the fractionation of spinel-group minerals. Although microphenocrysts of chromite (*sensu strictu*) were not petrographically identified, the chromium content of some analysed spinels can reach up to 17 wt.% Cr₂O₃ (Chapter V), indicating that spinels are a major control in chromium distribution.

Scandium mimics the CaO when plotted against MgO. The concentration of this element initially increases with differentiation (in the HMG), inflecting later towards progressive depletion, caused by clinopyroxene removal from the LMG-type liquids. Sc contents vary from 10 to 43 p.p.m. (Fig. VI.3.1).

VI.3.2 Incompatible trace-elements

Nb (59-220 p.p.m.), Zr (206-789 p.p.m.), Hf (6-16 p.p.m.) and Th (1-24 p.p.m.) behave in a very similar way (Fig. VI.3.1) indicating that their concentrations are controlled by the same phases and/or melting processes. Barium behaves as an incompatible trace-element and tends to be present in

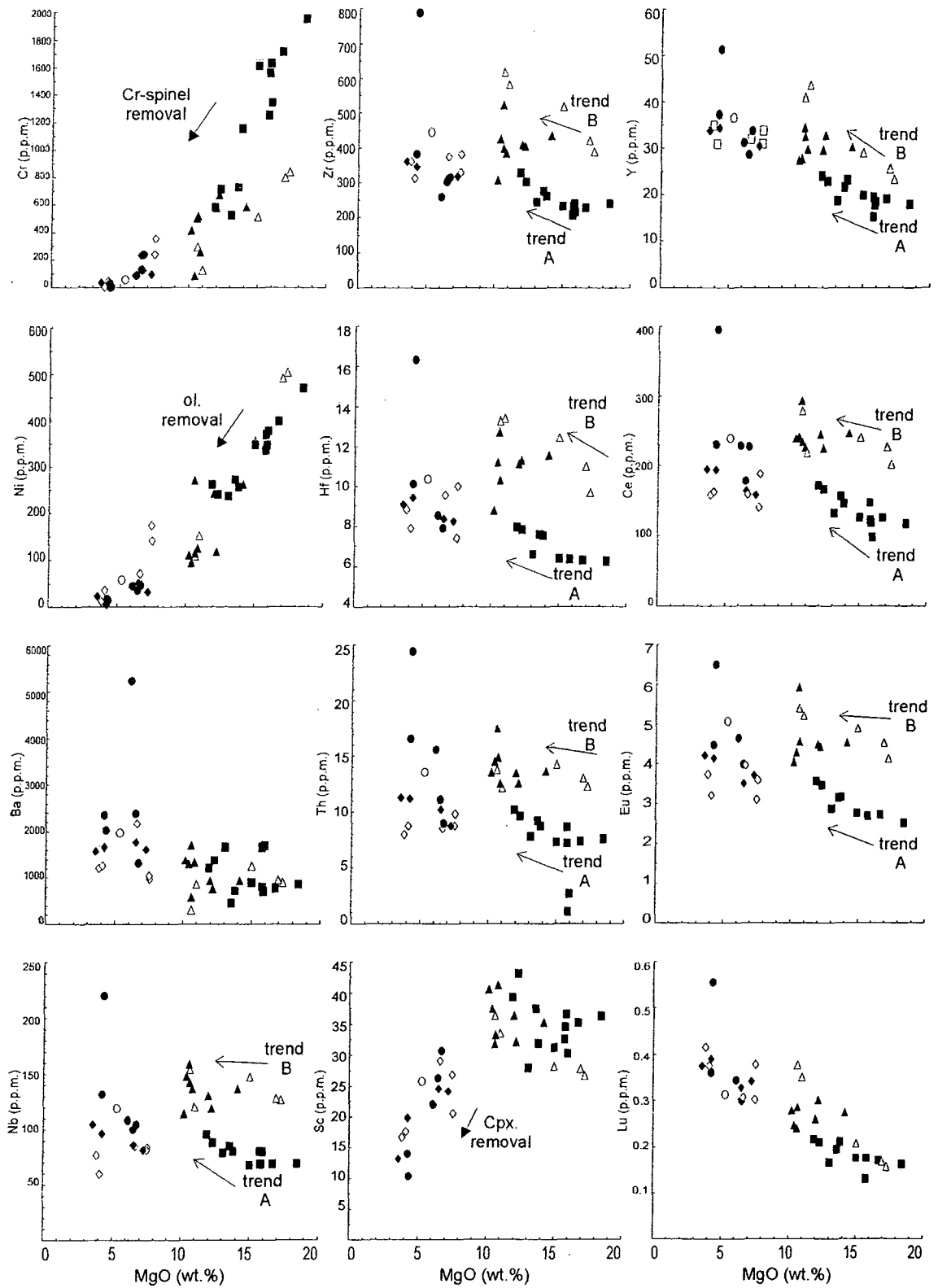
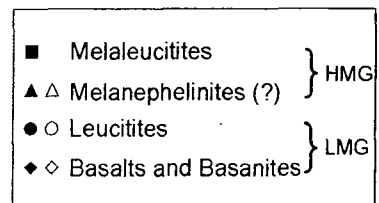


Figure VI.3.1 - Plots of selected Trace Elements against MgO as a differentiation index. Solid and open symbols represent samples from the Aguas Emendadas Region and Amorinópolis Region, respectively.



slightly higher in the LMG (Fig. VI.3.1), with an overall variation from 305 to 5240 p.p.m..

Yttrium ranges from 15 to 51 p.p.m and tends to increase from the HMG towards the LMG (Fig. VI.3.1). Yttrium behaviour resembles that of the HREE and this element does not appear to be removed in any important early-crystallising phase.

The Rare-Earth Element (REE) content increases from the HMG to the LMG, but this increment is much more conspicuous for the Heavy Rare-Earth Elements (HREE). From La to Lu the plots of REE against MgO become more linear, suggesting that the higher the atomic number of the element the more incompatible it behaves in the studied systems (Fig. VI.3.1).

As observed for the major elements, some of the trace-elements behave in a distinct way between melaleucitites and melanephelinites (?). These differences are most apparent in Zr, Hf, Th, Nb and LREE, which are enriched in the melanephelinites (?), relatively to melaleucitites for the same MgO contents.

On chondrite-normalized REE diagrams the melaleucitites display the lowest enrichment in light and heavy REE (Fig. VI.3.2). The highest normalised REE contents are observed in samples of leucitites. Nevertheless, as a group the leucitites span the widest range in abundances, partially or entirely overlapping the patterns of the other rock groups (Fig. VI.3.2); La_n values vary from 179 to 608 times chondrite, while Lu_n ranges from 4 to 16 times chondrite in the analysed rocks.

All of the analysed samples are strongly enriched in Light Rare-Earth elements (LREE) relative to HREE. Surprisingly, the LMG rocks have

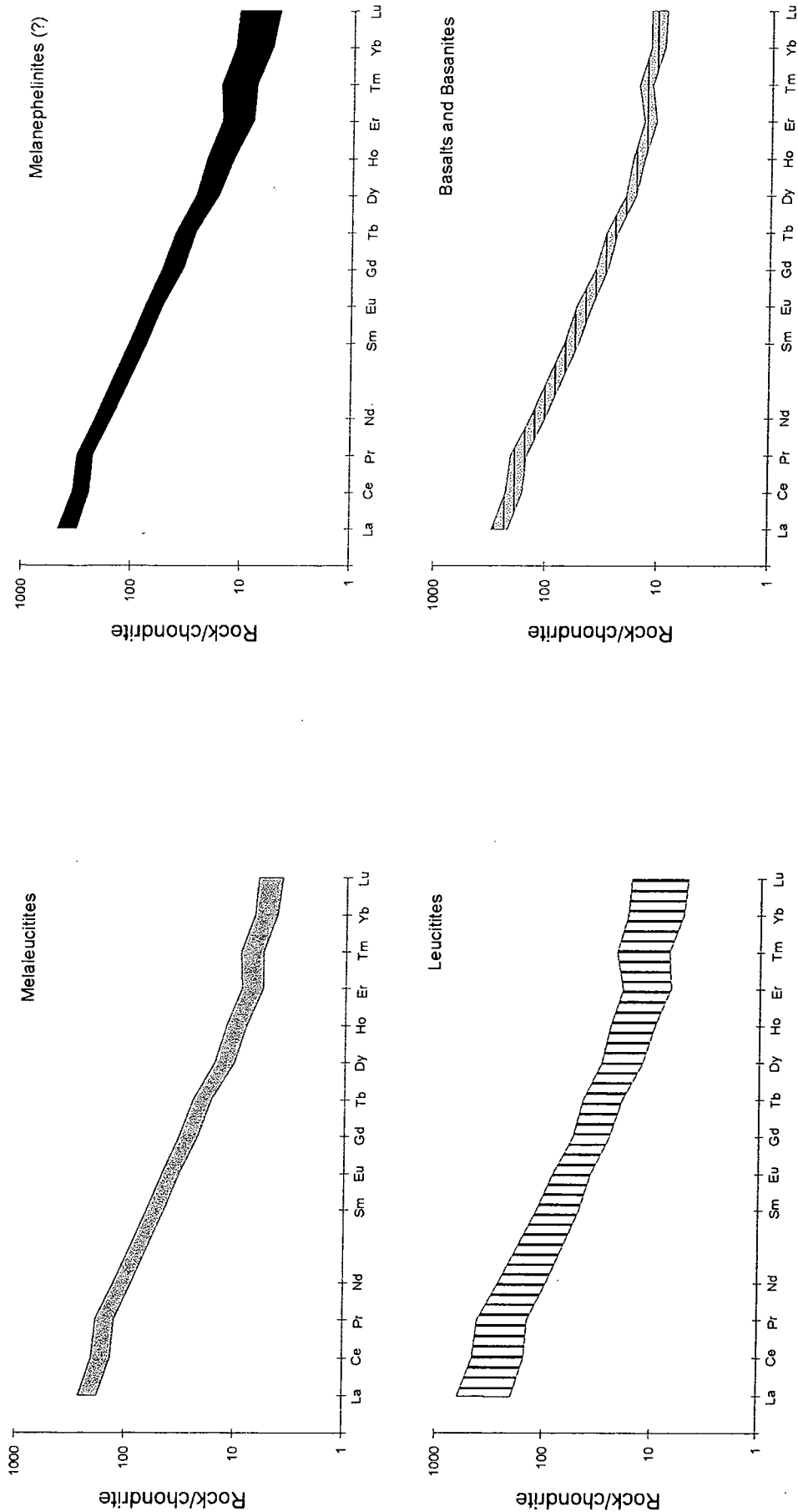
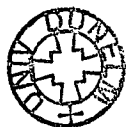


Figure VI.3.2 - Chondrite-normalized REE diagrams for Melaleucitites, Melanepheinites (?), Leucitites and Basalts/Basanites groups. Normalization constants from Nakamura (1974), except Pr, Tb, Ho and Tm (Haskin *et al.*, 1968).

lower La_n/Yb_n ratios than the HMG (Fig. VI.3.3). This indicates that during crystal fractionation a LREE-rich phase was removed from the liquid, controlling the REE distribution. When plotted against TiO_2 , the La_n/Yb_n ratio shows a positive correlation with this oxide (Fig. VI.3.3), indicating that perovskite is probably the most important phase affecting the behaviour of the REE in these rocks. The available perovskite microprobe analyses for these rocks do not include trace elements such as REE, Nb and Sr, but the estimation of site occupancies suggests that 4-6 mol % of end-members other than $CaTiO_3$ occur in solid solution. Among these a likely candidate is the Na+REE-rich end-member loparite (see discussion in Chapter V). Mitchell (1996) points out that perovskite is one of the most important REE-host in alkaline rocks and that it is particularly enriched in LREE, with La/Yb ratios exceeding 2000.

On chondrite-normalized multi-element diagrams (spiderdiagrams) the four groups of rocks have very similar patterns, although those of the Basalts/ Basanites Group plots are smoother than the other rocks (Fig. VI.3.4). Negative anomalies of Rb and K are probably associated with alteration, more than any other factor, such as residual phlogopite in the mantle source. Most of the samples are depleted in Sr, relative to Nd, and the HMG samples often show a small trough in P. The HMG also have a discrete positive anomaly in Ti, which is not apparent in most LMG rocks.

The behaviour of the trace-elements demonstrates the resemblance of these rocks to kamafugitic rocks. In a plot of the Th/Yb ratio versus Ta/Yb, the rocks from Águas Emendadas and Amorinópolis regions plot in a trend that is mostly contained in the Kamafugite field (Fig. VI.3.5). In this case the LMG



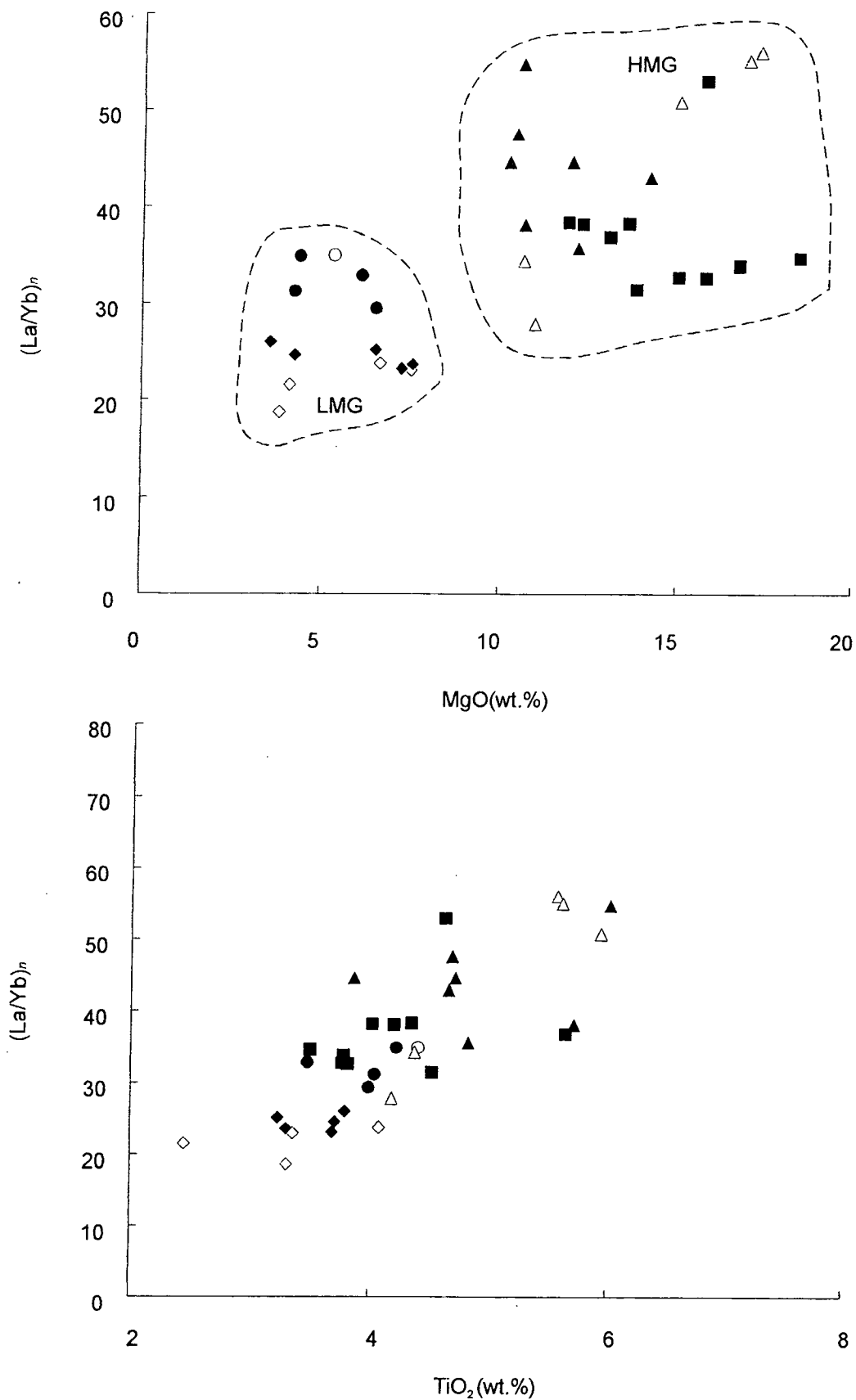
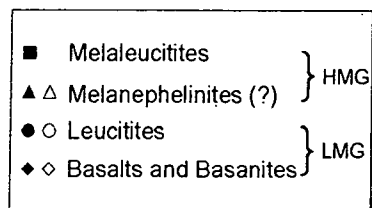


Figure VI.3.3 - Plots of chondrite-normalized La/Yb ratio against MgO and TiO_2 . Normalization constants from Nakamura (1974). Solid and open symbols represent samples from the Aguas Emendadas Region and Amornopolis Region, respectively.



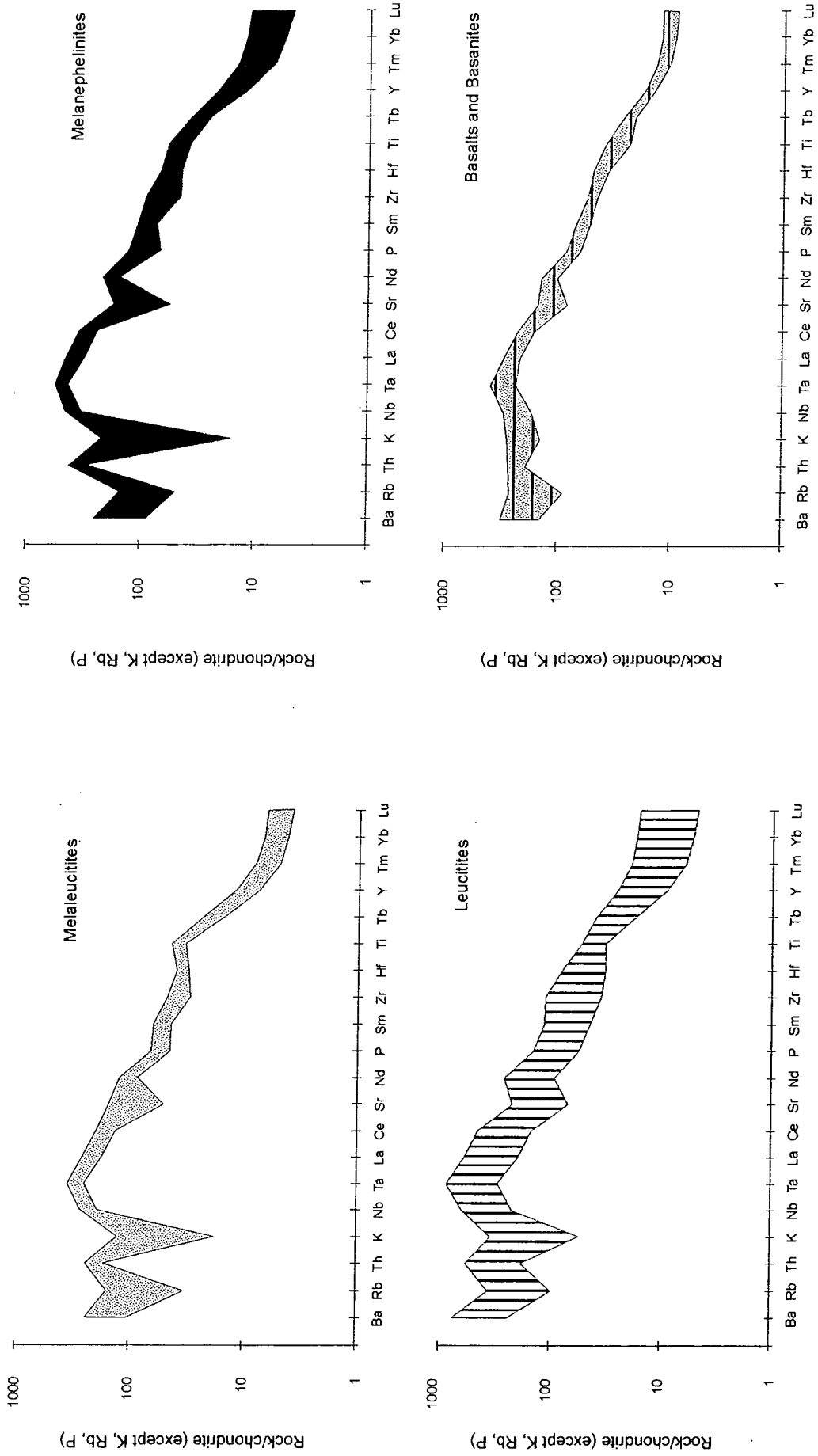


Figure VI.3.4 - Chondrite-normalized multi-element diagrams (spidergrams) for Melaleucitites, Melanephelinites (?), Leucitites and Basalts/Basanites groups. Normalization constants from Thompson *et al.* 1984, except Lu (Nakamura, 1974).

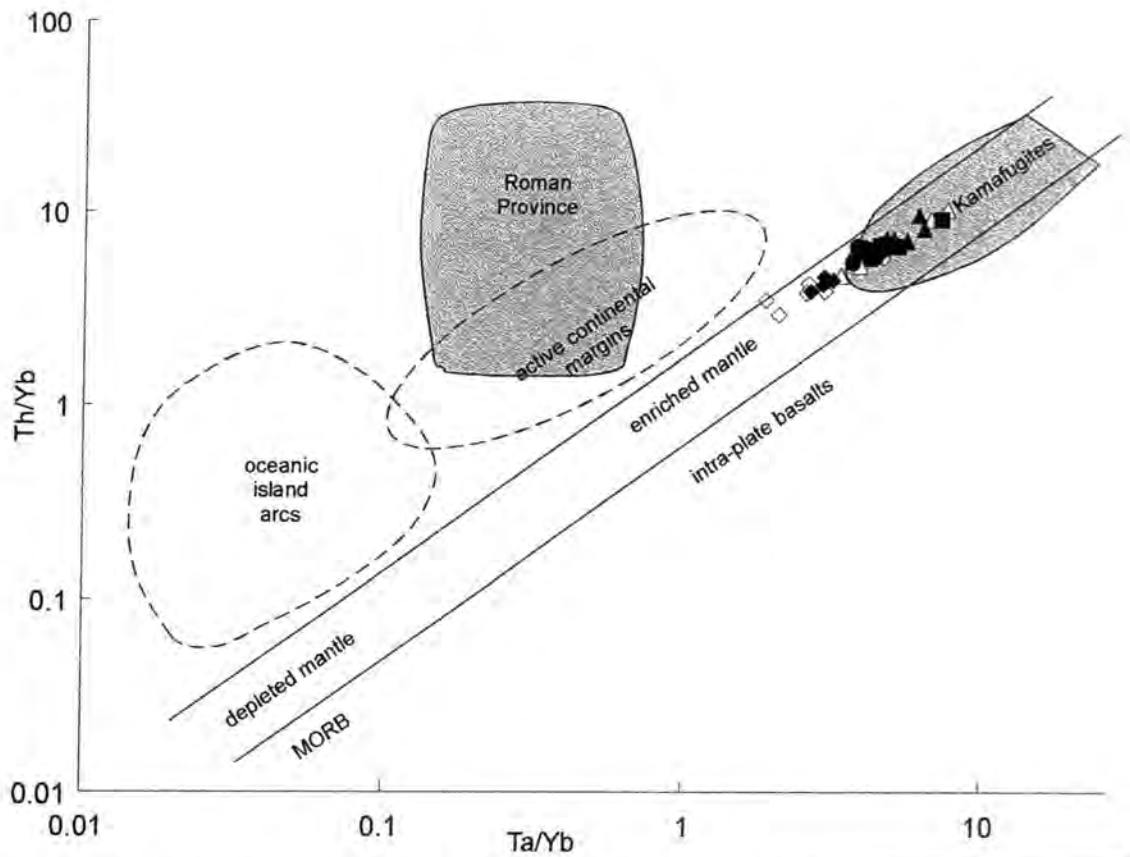


Figure VI.3.5 - Th/Yb against Ta/Yb showing the similarity of the analysed samples with kamafugitic rocks (fields after Wilson, 1989). Solid and open symbols represent samples from Aguas Emendadas Region and Amornopolis Region, respectively.

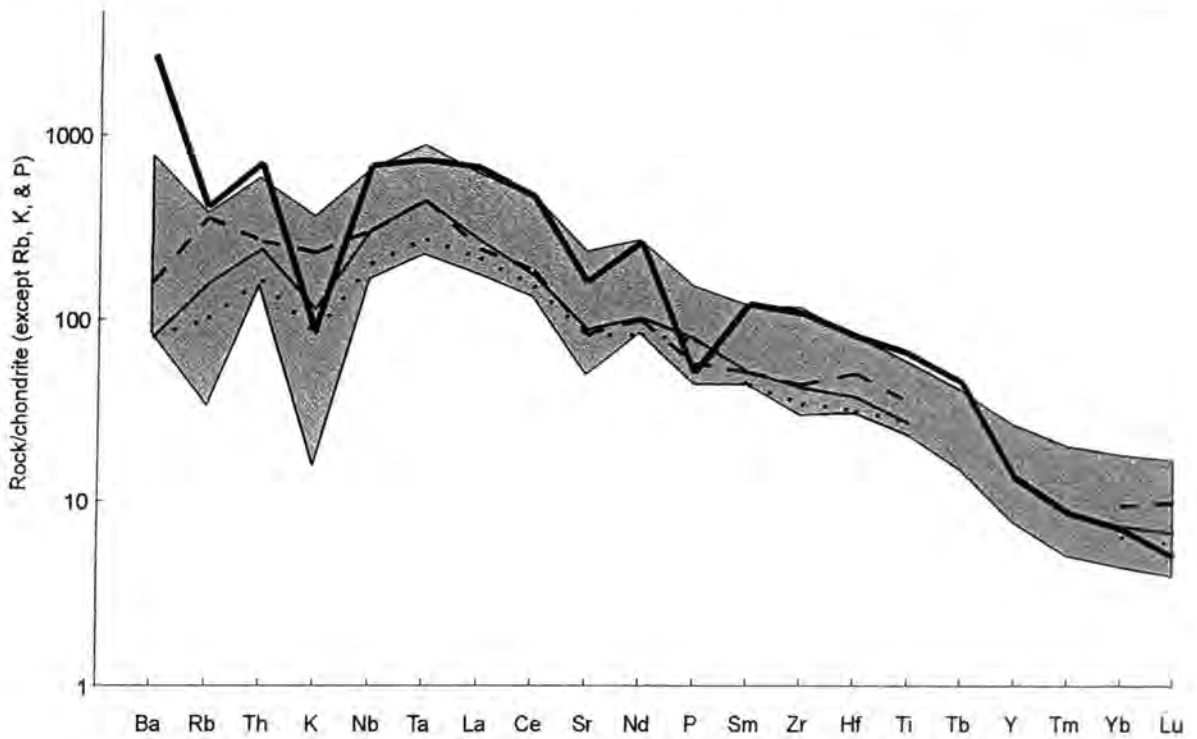
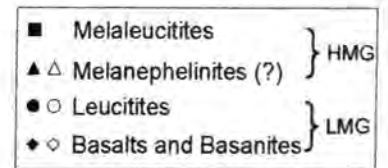
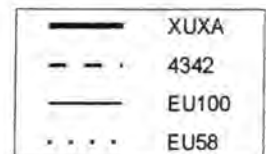


Figure VI.3.6 - Normalized multi-element diagram, comparing rocks from the Aguas Emendadas and Amornopolis regions (shaded field) with alkaline rocks from other provinces. Data sources are Thompson *et al.* (1984), for samples 4342, EU58 and EU100, and Gibson *et al.* (1995), for XUXA. Normalization constants are the same as in figure V.3.4.



group follows the same trend of the HMG and does not confirm the chemical affinity with the Roman Province previously suggested by the diagrams of Foley *et al.* (1987) (Fig. VI.2.4).

Fig. VI.3.6 shows a comparison between the studied rocks and mafic alkaline rocks from Alto Paranaíba Igneous Province (XUXA), Uganda (4342), Hegau, Germany (EU100) and Kaiserstuhl, Germany (EU58). They have equivalent degrees of enrichment, relative to chondrite, and the patterns are similar, with persistent negative K and Sr anomalies.

Nb/Ta ratios (Fig. VI.3.7) vary from 11.3 to 15.4. The fitting of a least-square regression line yields a Nb/Ta ratio of 13.5, which can be taken as an average value for these rocks. Zr/Hf ratios range from 30.5 to 48.4 with average of 38.7. Ho and Y show extremely good correlation, with Y/Ho ratios varying from 27.1 to 31.7 and averaging 28.2. The good linear correlation between these elements, in the samples from the four groups (except for three samples in the Zr-Hf diagram, Fig. VI.3.7), demonstrates the coherent behaviour of the trace-elements and general lack of analytical error. The apparent non-linearity of the Zr/Hf ratio in Fig. VI.3.7 is caused only by the three samples with the highest abundances. In this case, some analytical bias may be present at the higher end of the calibration range.

The diagram of Ni versus Lu (Fig. VI.3.8) shows that some samples from Águas Emendadas and Amarinópolis plot outside the trend of crystal fractionation for these rocks, indicating the presence of magma mixing during the magmatism. This supports field and petrographic evidence which also point to the presence of magma mixing (Chapter IV). The use of Lu in a diagram to illustrate magma mixing is unusual, but reference to Figs. VI.2.2 and

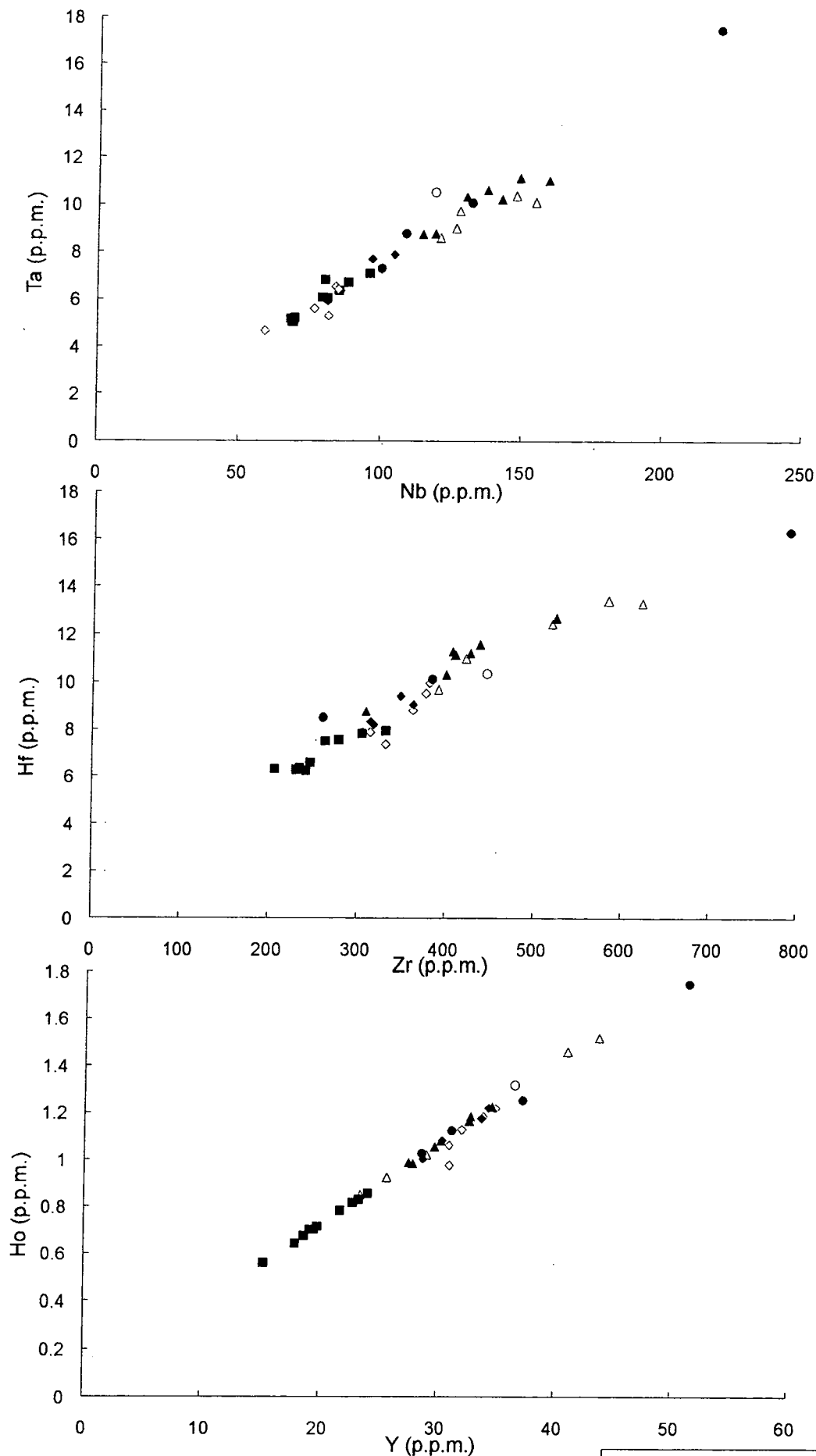
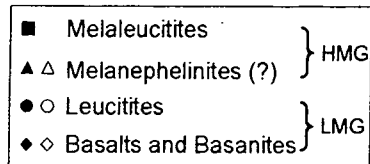


Figure VI.3.7 - Plots of Ta versus Nb, Hf versus Zr and Ho versus Y. Solid and open symbols represent samples from the Aguas Emendadas Region and Amorinopolis Region, respectively.



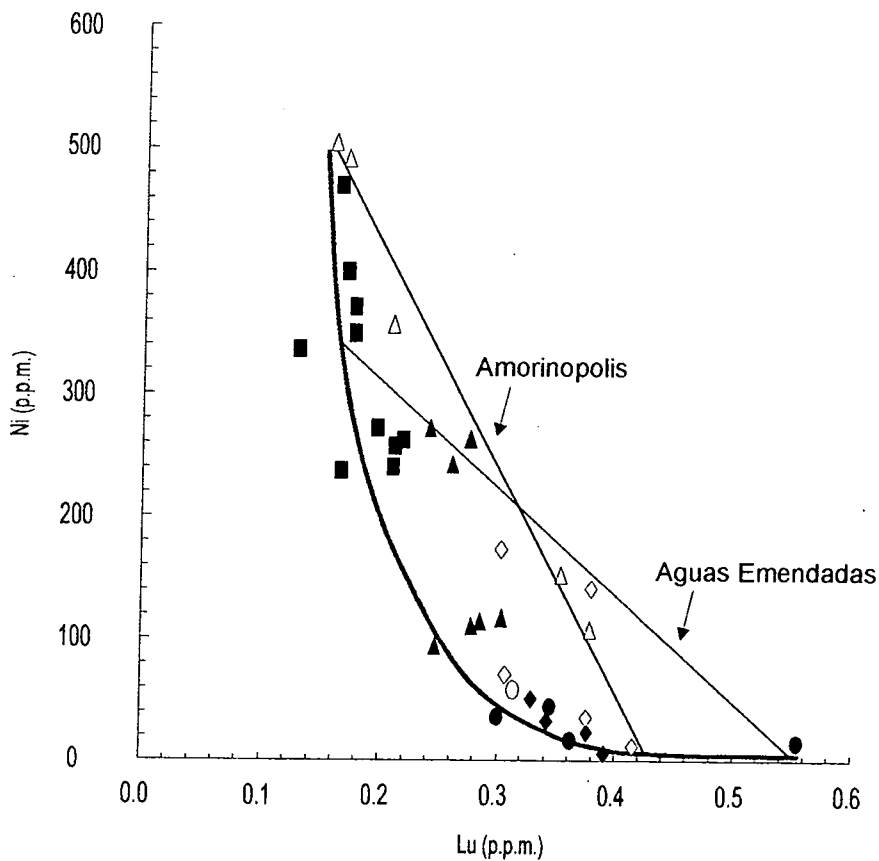
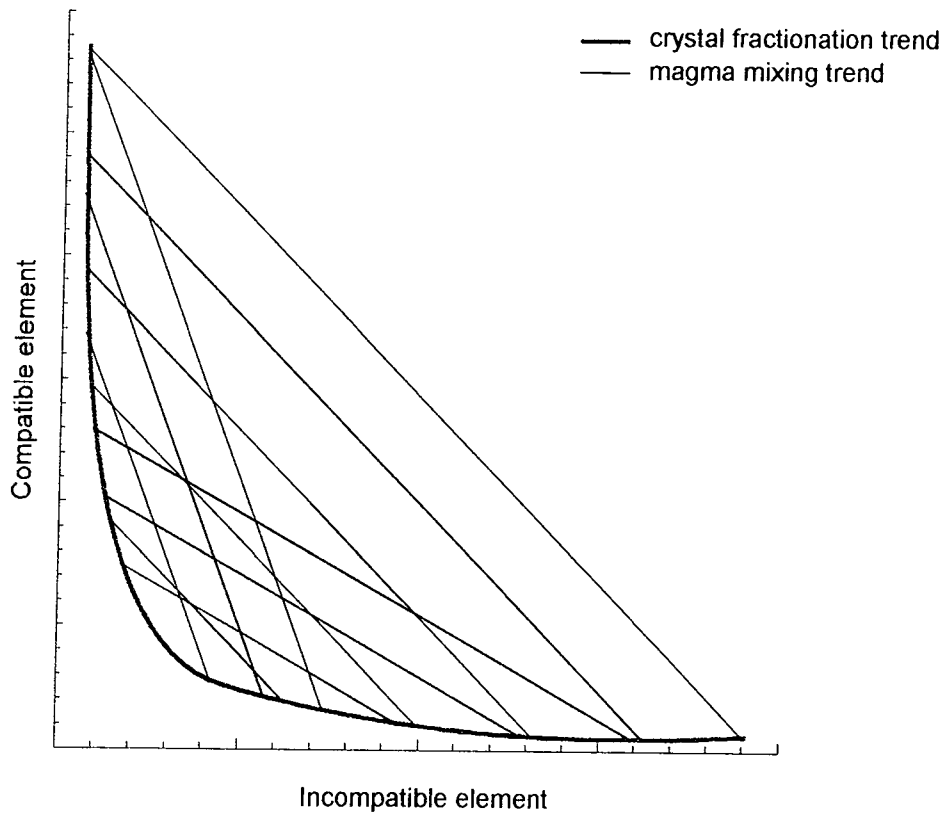
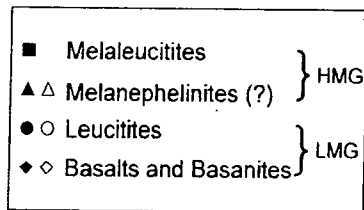


Figure VI.3.8 - Top: plot of a hypothetical compatible element against a hypothetical incompatible element showing expected trends for crystal fractionation and magma mixing. Bottom: plot of Ni against Lu, showing the trend of crystal fractionation for the analysed rocks and estimated trends of magma mixing for the Aguas Emendadas rocks and Amorinopolis rocks. Solid and open symbols represent samples from the Aguas Emendadas Region and Amorinopolis Region, respectively.



VI.3.1 shows that it behaves more like a theoretical incompatible element than any others analysed in this research.

VI.4 MELALEUCITITES AND MELANEPHELINITES (?)

Melaleucitites and melanephelinites (?) together constitute the High Magnesium Group. Although these rocks have similar bulk-rock compositions, there are some differences between them. Melaleucitites normally have higher MgO than melanephelinites (?), despite having higher SiO₂ contents. On the other hand, the melanephelinites (?) usually have higher Fe₂O_{3T} and P₂O₅ contents (Fig. VI.2.1).

The melaleucitites have higher Cr concentrations than the melanephelinites (?), but their Ni values widely overlap (Fig. VI.3.1). The two groups also have similar contents of HREE and Ba. Melanephelinites (?) are more enriched in LREE, Nb, Zr, Hf and Th. The differences in incompatible trace-elements between the two groups are more noticeable in chondrite-normalized REE diagrams (Fig. VI.3.2), and spiderdiagrams (Fig. VI.3.4); these clearly demonstrate the more enriched character of the melanephelinites (?).

The higher modal amounts of olivine and pyroxene phenocrysts in the melaleucitites could influence the chemical behaviour of this group. Where microprobe analyses of the phenocrysts are available, the chemical composition of the sample was recalculated to remove the modal amounts of phenocrysts. The results are shown graphically in Fig. VI.4.1. It is noticeable

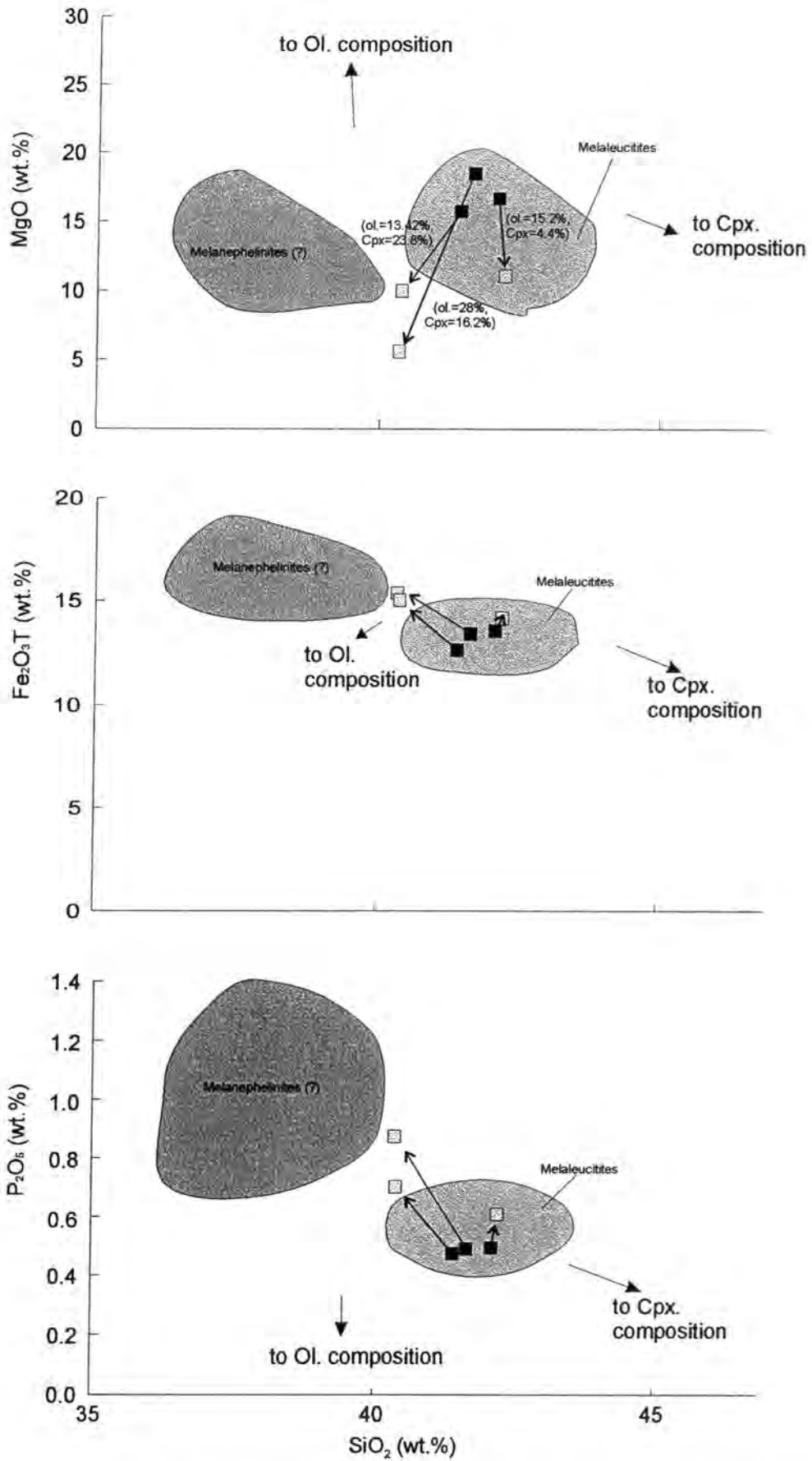


Figure VI.4.1 - Plots of selected Major Elements against SiO_2 for samples of Melaleucites and Melanephelinites (?). The dark squares represent original whole-rock chemical data, light shaded squares represent new compositions obtained by subtracting an amount of oxide equivalent to the modal percentage of olivine and pyroxene phenocrysts from the original data.

that, once the phenocrysts are removed, the recalculated analysis shifts towards, but does not quite reach the field of melanephelinites (?). This shows that the chemical differences may partially reflect mineralogical characteristics of the groups, but can not be entirely explained by them.

VI.5 INTERPRETATION

The rocks from Águas Emendadas and Amarinópolis regions have been chemically altered by a combination of weathering and hydrothermal processes. This has mainly affected the contents of K, Na and probably Rb as well; most of the other major and trace elements behave coherently.

The parental magma(s) was probably low in silica, high in magnesium, calcium, titanium and strongly alkaline. The contents of aluminium, calcium, magnesium and trace-elements suggest a strong kamafugitic affinity.

The compatible trace-element and MgO contents testify to the highly unevolved character of some of the HMG rocks (melaleucitites and melanephelinites (?)). These can be considered a good approximation of the primitive magmas in the studied rocks. Some other HMG rocks were produced from these primitive liquids by variable amounts of olivine fractionation.

Although clinopyroxene is a modal constituent in melaleucitites and melanephelinites (?), the chemical data indicate that it was not fractionated from these magmas.

The higher amounts of silica of the melaleucitites, compared to the melanephelinites (?), for a given MgO could perhaps be explained by a small amount of crustal contamination in the Melaleucitite Group.

The other chemical differences between melaleucitites and melanephelinites, such as the enrichment in REE of the latter, are unrelated to crystal fractionation and suggest that the two groups represent distinct parental magmas that either originated from different mantle sources or from the same source but with different degrees of melting. Since both groups have similar chondrite-normalized multi-element (spiderdiagrams) patterns (Fig. VI.3.4) the source for this magmas must have common characteristics.

The petrographic groups behave chemically in a coherent way, except for sample 96AE57. There is chemical evidence to support the inference, based on field and petrographic observations (Chapter IV), that some extent of magma mixing occurred. This most probably involved two high-Mg primitive magmas (melaleucitic and melanephelinitic (?)), and it is not easily recognisable. The rocks of the LMG may have evolved from each HMG rock-type or from the mixture, but a higher number of LMG samples would be required, together with isotope data, to clarify this.

Chapter VII - CONCLUSIONS AND SUGGESTIONS

FOR FURTHER STUDY

Field features and petrographic evidence indicate that magma mixing was important in the formation of the Cretaceous alkaline rocks from the Águas Emendadas Region. At the present this seems to have involved two unevolved magmas (melaleucitic and melanephelinitic (?)), but future work is necessary to identify precisely the components involved in the mixing, in order to understand the real importance of this process. Probably a more complete data base and a larger number of samples of the more evolved rocks, together with isotope geochemistry, would help elucidate this point.

At the moment, it is believed that the explosive volcanism started with an important fluidization component, related to escaping magmatic gas, and that subsequently phreatomagmatic processes became important throughout the top of the magma column, resulting in violent explosions and various pyroclastic deposits. The magma was strongly fragmented during uprise. In the most highly explosive eruption phases, "spinning droplets" were produced by the rotation of magma droplets, during their ascent. The rotation oriented the microphenocrysts around a solid crystal core and, at the time of eruption, the chilled structures were preserved. In a less-explosive eruption phase, when the magma was still fragmented but the energy was not high

enough to rotate the droplets, "frozen droplets" were produced. The latter structures lack the concentric orientation of microcrysts that is present in the "spinning droplets". The outpouring of lava flows was related to non-explosive phases of eruption.

The analysed rocks have TiO₂ contents compatible with those of the high-Ti group of Gibson et al. (1995b), as expected from their location in the northern margin of the Paraná Basin.

On the basis of the present evidence, it is believed that the rocks from the Águas Emendadas Region are the result of kamafugitic magmatism, perhaps associated with carbonatites. The presence of kalsilite in one of the melanephelinites reinforces this suggestion.

The primary magmas were silica-poor and rich in MgO, alkalis, CaO and incompatible trace-elements such as Sr and REE. A crustal contamination component was probably involved in the magmatic evolution, affecting the melaleucitites chemically and petrographically.

Weathering and hydrothermal alteration were responsible for mineralogical and whole-rock chemical changes in the studied rocks. The most noticeable results are the transformation of leucite into pseudo-leucite, serpentinization of olivines and extensive carbonatization of the groundmass. The main effect on the whole-rock chemistry is represented by a loss in alkalis.

A more extensive study of rocks from the region, with more detailed sampling and investigation of additional occurrences of alkaline rocks in the area would help to solve most of the problems summarised above.

A more complete mineral chemistry study is needed, in order to obtain more information on the composition of olivine and pyroxene

phenocrysts and to clarify the crystallisation history of the rocks from the Águas Emendadas Region. An extensive microprobe investigation of the feldspathoids would establish the importance of kalsilite as a rock-forming mineral in these samples. Determination of trace-elements such as Sr, Nb, Th and REE in the perovskites would help to constrain their origin and to evaluate the bearing of perovskite fractionation on the trace-elements contents of the evolving magmas.

A study of xenoliths is required to elucidate some of the magma chamber processes, as well as to constrain the origin of the magma.

A combined study of stable and radiogenic isotopes could help in understanding the relative roles of magmatic differentiation, crustal assimilation and post-magmatic alteration involved in the genesis of these rocks.

References cited

- Almeida, F.F.M., 1967. Origem e Evolução da Plataforma Brasileira. Boletim da Divisão de Geologia e Mineralogia, DNPM, Rio De Janeiro **241**.
- Almeida, F.F.M., 1983. Relações Tectônicas das Rochas Alcalinas Mesozóicas da Região Meridional da Plataforma Sul-Americana. Revista Brasileira de Geociências **13(3)**, 139-158.
- Almeida, F.F.M., 1986. Distribuição Regional e Relações Tectônicas do Magmatismo Pós-Paleozóico no Brasil. Revista Brasileira de Geociências **16(4)**, 325-349.
- Amaro, V.E, 1989. Geologia e petrologia da sequência metavulcânica de Jaupaci-GO e lineamentos associados. Dissertação de mestrado, UnB.
- Andrade, S.M. & Camarço, P.E.N., 1980. Estratigrafia dos sedimentos devonianos do flanco nordeste da Bacia do Paraná. In: Anais do XXXI Congresso Brasileiro de Geologia, Balneário de Camboriú, Santa Catarina, vol. **5**, 2828-2836.
- Andrade, S.M. & Camarço, P.E.N., 1982. Sequências sedimentares pré-Carboníferas dos flancos nordeste da Bacia do Paraná e sudoeste da Bacia do Parnaíba e suas possibilidades uraníferas. In: Anais do XXXII Congresso Brasileiro de Geologia, Salvador, vol. **5**, 2132-2144.
- Barbour, A.P., Girardi, V.A.V., Kawashita, K. & Soares De Souza, A.M., 1979. Geocronologia do Complexo Máfico-Ultramáfico Alcalino de Santa Fé, Goiás. Boletim do Instituto de Geociências, Instituto de Geociências, Usp, **10**, 11-18.
- Bez, L., Guimarães, J. E & Guimarães, D., 1971. Distrito Vulcânico de Rio Verde. In: Anais do XXV Congresso Brasileiro de Geologia, São Paulo, Santa Catarina, vol. **2**, 121-128.
- Burjack, M.I.A & Popp, M.T.B, 1981. A ocorrência do icnogênero *Arthropycus* no Paleozóico da Bacia do Paraná. Pesquisas, Porto Alegre, vol. **14**, 163-168.

- Camarço, P.E.N. & Souza Jr., J., 1986. Geologia da Bacia do Paraná no Sul de Goiás. In: Anais do XXXIV Congresso Brasileiro de Geologia, Goiânia, vol. 2, 27-241.
- Cas, R. & Wright, J.V., 1987. Volcanic Successions: Modern and Ancient. Allen & Unwin, London.
- Cerqueira, M.R.S. & Danni, J.M.C., 1994. Aspectos petrográficos e químicos do Complexo da Fazenda Buriti, Ipora, GO. Boletim de Geociências do Centro-Oeste 17(1/2), 29-33.
- Clement, C.R., 1973. Kimberlites from the Kao Pipe, Lesotho. In: Nixon, P.H. (Ed.), Lesotho Kimberlites. Lesotho National Development Corporation, Maseru, Lesotho 110-121.
- Clement, C.R. & Skinner, M.W., 1985. A textural-genetic classification of kimberlites. Transactions of the Geological Society of South Africa 88, 403-409.
- Cundari, A. & Comin-Chiaramonti, P., 1996. Mineral chemistry of alkaline rocks from the Asuncion-Sapucai graben (Central-Eastern Paraguay). In: Comin-Chiaramonti, P. and Gomes, C. B., (Eds.), Alkaline magmatism in Central-Eastern Paraguay. Relationships with coeval magmatism in Brazil. São Paulo, Edusp/Fapesp, 181-193.
- Cundari, A. & Salviulo, G., 1989. Ti solubility in diopsidic pyroxene from a suite of New South Wales leucitites (Australia). Lithos 22, 191-198.
- Danni, J.C.M., 1978. Magmatic differentiation of the alkaline ultrabasic intrusions of the Iporá region, southwest Goiás, Brazil. In: I International Symposium on Carbonatites, Proceedings. Poços de Caldas, 149-167.
- Danni, J.C.M., 1985. Rochas da série kamafugítica na região de Amarinópolis, Goiás. Contribuições à geologia e à petrografia -Núcleo de Minas Gerais- SBGM, Belo Horizonte, 5-13.
- Danni, J.C.M., 1994. Os picritos alcalinos da região de Ipora: implicações na gênese dos complexos do tipo central do Sul de Goiás. Revista Brasileira de Geociências 24, 112-119.
- Danni, J.C.M. & Gaspar, J.C., 1992. Mineralogia e química do katungito de Amarinópolis, Goiás. In: Boletim de Resumos do XXXVII Congresso Brasileiro de Geologia, SBG/SP, São Paulo vol. 2, 85-86.

- Danni, J.C.M. & Gaspar, J.C., 1994. Química do katungito de Amorinópolis - Goiás: Contribuição ao estudo do magmatismo kamafugítico. *Geochimica Brasiliense* **8**, 119-134.
- Danni, J.C.M., Silva, A.J.G.C. & Cerqueira, M.R., 1990. Petrografia e petroquímica das rochas alcalinas cretácicas da Serra do Caipó, sudoeste de Goiás. In: *Anais do XXXVI Congresso Brasileiro de Geologia*, Natal, vol. **4**, 1872-1882.
- Danni, J.C.M., Silva, A.J.G.C., Campos, J.E.G. & Cerqueira, M.R., 1992. Picritos Alcalinos do Sul de Goiás: Características Mineralógicas e Geoquímicas. In: *Boletim de Resumos do XXXVII Congresso Brasileiro de Geologia, SBG/SP*, São Paulo vol. **2**, 89.
- Dawson, J.B., 1980. *Kimberlites and Their Xenoliths*. Springer-Verlag, New York.
- Dawson, J.B., Smith, J.V. & Steele, I.M., 1992. 1966 ash eruption of the carbonatite volcano Oldoinyo Lengai: mineralogy of lapilli and mixing of silicate and carbonatite magmas. *Mineralogical Magazine* **56**, 1-16.
- Deans, T. & Roberts, B., 1984. Carbonatite tuffs and lava clasts of Tinderet foothills, western Kenya: a study of calcified natrocarbonatites. *Journal of the Geological Society, London* **141**, 563-580.
- Deer, W. A., Howie, R. A. & Zussman, J., 1992. *An introduction to rock-forming minerals*. Longman., 2nd ed., Essex.
- Droop, G. T. R., 1987. A general equation for estimating Fe³⁺ concentrations in ferromagnesian silicates and oxides from microprobe analyses, using stoichiometric criteria. *Mineralogical Magazine* **51**, 431-435.
- Faria, A., 1982. A Formação Vila Maria - Nova unidade litoestratigráfica siluriana da Bacia do Paraná. *Ciências da Terra* **3**, 12-15.
- Faria, A., Fuck, R.A., Veloso, J.A.V., Hirson, J.R., Marini, O.J., Andrade, G.F. & Fonseca, M.R.C.B., 1975. *Projeto Piranhas*. DNPM/FUB. Brasília.
- Foley, S.F., Venturelli, G., Green, D.H. & Toscani, L., 1987. The Ultrapotassic Rocks: Characteristics, Classification, and Constrains of Petrogenetic models. *Earth-Science Reviews* **24**, 81-134.
- Giampaolo, C., Godano, R.F., DiSabatino, B. & Barrese, E., (1997). The alteration of leucite-bearing rocks: A possible mechanism. *European Journal of Mineralogy* **9**, 1277-1291.

- Gaspar, J.C. & Danni, J.C.M., 1981. Aspectos petrográficos e vulcanológicos da província alcalina-carbonatítica de Santo Antônio da Barra, sudoeste de Goiás. *Revista Brasileira de Geociências* **11**, 74-83.
- Gibson, S.A., Thompson, R.N., Leonardos, O.H., Dickin, A.P. & Mitchell, J.G., 1995. The Late Cretaceous Impact of the Trindade Mantle Plume: Evidence from Large-volume, Mafic, Potassic Magmatism in SE Brazil. *Journal of Petrology* **36**, 189-229.
- Gibson, S.A., Thompson, R.N., Dickin, A.P. & Leonardos, O.H., 1995b. High-Ti and low-Ti mafic potassic magmas: Key to plume-lithosphere interactions and continental flood-basalt genesis. *Earth and Planetary Science Letters* **136**, 149-165.
- Gibson, S.A., Thompson, R.N., Weska, R.K., Dickin, A.P. & Leonardos, O.H., 1997. Late Cretaceous rift-related upwelling and melting of the Trindade starting mantle plume head beneath western Brazil. *Contributions to Mineralogy and Petrology* **126**, 303-314.
- Gilbert, J.S. & Lane, S.J., 1994. The origin of accretionary lapilli. *Bulletin of Volcanology* **56**, 498-411.
- Govindaraju, K., 1989. Compilation of working values and sample description for 272 geostandards. *Geostandards Newsletter*, XII, Special Issue.
- Haskin, L.A., Haskin, M.A., Frey, F.A. & Wildman, T.R., 1968. Relative and absolute terrestrial abundances of the rare earths. In: Ahrens, L.H. (Ed.), *Origin and distribution of the elements*, vol. 1. Pergamon, Oxford, 889-911.
- Hasui, Y., Cartner-Dyer, R. E. & Iwanuch, W., 1971. Geocronologia das Rochas Alcalinas de Santo Antônio da Barra, Go. In: *Anais do XXV Congresso Brasileiro de Geologia*, São Paulo vol. 1, 253-258.
- Hay, R.L., 1978. Melilitite-Carbonatite Tuffs in the Laetolil Beds of Tanzania. *Contributions to Mineralogy and Petrology* **67**, 357-367.
- Hay, R.L. & O'Neil, J.R., 1983. Carbonatite Tuffs in the Laetolil Beds of Tanzania and the Kaiserstuhl in Germany. *Contributions to Mineralogy and Petrology* **82**, 403-406.
- Ianhes, A.C., Pitthan, J.H.L., Simões, M.A.; Del'arco, J.O., Trindade, C.A.H., Luz, D.S., Fernandes, C.A.C. & Tassinari, C.C.G., 1983. Projeto RADAMBRASIL, MME-SBG, Rio de Janeiro **31**, 283-289.

- Keller, J., 1981. Carbonatitic volcanism in the Kaiserstuhl alkaline complex: evidence for highly fluid carbonatitic melts at the Earth's surface. *Journal of Volcanology and Geothermal Research* **9**, 423-431.
- Keller, J., 1989. Extrusive carbonatites and their significance. In: Bell, K. (Ed.), *Carbonatites: genesis and evolution*. Unwin Hyman, London, 70-88.
- Kurszlaukis, S. & Lorenz, V., 1997. Volcanological features of low-viscosity melt: carbonatitic Gross Brukkaros Volcanic Field, Namibia. *Bulletin of Volcanology* **58**, 421-431.
- Le Bas, M.J., 1973. A norm for feldspathoidal and melilitic igneous rocks. *Journal of Geology* **81**, 89-96.
- Le Maitre, R.W. (Ed.), 1989. *A Classification of Igneous Rocks and Glossary of Terms: Recommendations of the International Union of Geological Sciences Subcommittee on the Systematics of Igneous Rocks*. Blackwell Scientific Publications, Oxford, U.K..
- Lorenz, V., 1974. Vesiculated tuffs and associated features. *Sedimentology* **21**, 273-291.
- Lorenz, V. 1979. Phreatomagmatic origin of olivine melilite diatremes in Swabian Alb, Germany. In: Boyd, F.R. & Meyer, H.O.A. (Eds.). *Proceedings of the 2nd Second International Kimberlite Conference Vol. 1. Kimberlites, Diatremes and Diamonds: Their Geology, Petrology and Geochemistry*. American Geophysical Union, Washington, D.C., 354-363.
- Lorenz, V. & Kurszlaukis, S., 1997. On the last explosions of carbonatite pipe G3b, Gross Brukkaros, Namibia. *Bulletin of Volcanology* **59**, 1-9.
- Mamede, L., Ross, J.L.S., Santos, L.M. & Nascimento, M.A.L.S., 1983. Projeto RADAMBRASIL, MME-SBG, Rio de Janeiro, **31**, 373-376.
- McCallum, M.E., 1985. Experimental Evidence for Fluidization Processes in Breccia Pipe Formation. *Economic Geology* **80**, 1523-1543.
- Mitchell, R.H., 1986. *Kimberlites: Mineralogy, Geochemistry and Petrology*. Plenum Press. New York, NY.
- Mitchell, R.H., 1995. *Kimberlites, Orangeites and Related Rocks*. Plenum Press. New York, NY.

- Mitchell, R. H., 1996. Perovskites: a revised classification scheme for an important rare earth element host in alkaline rocks. In A. P. Jones, F. Wall and C. T. Williams (Eds.). Rare earth minerals: chemistry, origin and ore deposits. Chapman & Hall, London vol. 7, 372.
- Mitchell, R.H. & Bergman, S.C., 1991. Petrology of Lamproites. Plenum Press. New York, NY.
- Möller, P. & Morteani, G., 1983. On the geochemical fractionation of rare earth elements during the formation of Ca-minerals and its application to problems of the genesis of the ore deposits. In: Augustithis, S.S. (Ed.). The significance of trace elements in solving petrogenetic problems and controversies. Theophrastus Publications, Athens, 747-790.
- Morimoto, N., Fabries, J., Ferguson, A. K., Ginzburg, I. V., Ross, M., Seifert, F. A., Zussmann, J., Aoki, K. & Gotardi, G., 1988. Nomenclature of pyroxenes. American Mineralogist **73**, 1123-1133.
- Nakamura, N., 1974. Determination of REE, Ba, Fe, Mg, Na and K in carbonaceous and ordinary chondrites. Geochimica et Cosmochimica Acta **38**, 757-775.
- Pena, G.S. & Figueiredo, A.J.A., 1972. Projeto Alcalinas. DNPM/CPRM, Goiânia.
- Pereira, A.D.C., Takahashi, A.T., Pena, G.S., Oguino, K., Neto, M.H.F. & Araújo, V.A., 1980. Geologia da Região Sul-Sudoeste de Goiás e Partes do Leste Mato-Grossense e do Triângulo Mineiro. Projeto Goiânia II. DNPM/CPRM, Brasília.
- Pimentel, M.M., 1985. A sequência vulcano-sedimentar de Arenópolis - GO: Petrologia ígnea e metamórfica, contexto geotectônico e considerações metalogenéticas preliminares. Dissertação de mestrado, UnB. Brasília.
- Pimentel, M.M., 1992. Reajuste do sistema isotópico Sm-Nd durante o Neoproterozóico em gnaisses do oeste de Goiás. Revista Brasileira de Geociências **20**, 262-268.
- Pimentel, M.M. & Fuck, R.A., 1986. Geologia da sequência vulcano-sedimentar de Arenópolis (GO). Revista Brasileira de Geociências **16**, 217- 223.
- Pimentel, M.M. & Fuck, R.A., 1987(a). Origem e evolução das rochas metavulcânicas e metaplutônicas da região de Arenópolis (GO). Revista Brasileira de Geociências **17**(1), 2-14.
- Pimentel, M.M. & Fuck, R.A., 1987(b). Late Proterozoic granitic magmatism in southwestern Goiás, Brazil. Revista Brasileira de Geociências., **17**(4): 415-425.

- Pimentel, M.M. & Fuck, R.A., 1992. Características geoquímicas e isotópicas de unidades metavulcânicas e ortognáissicas neoproterozóicas do oeste de Goiás. SBG, Núcleo Centro-Oeste, Boletim n.15.
- Pimentel, M.M. & Fuck, R.A., 1992. Neoproterozoic crustal accretion in central Brazil. *Geology* **20**, 375-379.
- Pimentel, M.M., Fuck, R.A. & Alvarenga, C.J.S., 1996. Post-Brasiliano (Pan-African) high-K granitic magmatism in Central Brazil: the role of Late Precambrian-early Palaeozoic extension. *Precambrian Research* **80**, 217-238.
- Pimentel, M.M., Heman, L. & Fuck, R.A., 1991. Zircon and sphene U-Pb geochronology of Upper Proterozoic volcanic-arc rock units from southwestern Goiás, central Brazil. *Journal of South American Earth Sciences* **4**, 295-305.
- Reed, S. B. J., 1996. *Electron microprobe analysis and scanning electron microscopy in geology*. Cambridge University Press, Cambridge
- Riley, T.R., Bailey, D.K. & Lloyd, F.E., 1996. Extrusive Carbonatite from the Quaternary Rockeskyll Complex, West Eifel, Germany. *The Canadian Mineralogist* **34**, 389-401.
- Rosito, J.; Figueiredo, A.J. De A. & Pena, G.S., 1971. Nota preliminar sobre uma nova formação pré-devoniana no sudoeste de Goiás. In: Resumos das Comunicações do XXV Congresso Brasileiro de Geologia, São Paulo, 169-170.
- Schobbenhaus Filho, C., Ribeiro, C.L., Oliva, L.A., Takanohashi, J.T., Lindenmayer, Z.G., Vasconcelos, J.B. & Orlandi, V., 1975. Carta geológica do Brasil ao milionésimo; Folha Goiás (SD.22), DNPM/MME. Brasília. relatório + mapa.
- Schobbenhaus Filho, C., Campos, D.A.; Derze, G.R. & Asmus, H.E., 1984. *Geologia Do Brasil - Texto Explicativo do Mapa Geológico do Brasil e da Área Oceânica Adjacente, Incluindo Depósitos Minerais, Escala 1:2.500.000*. DNPM/MME. relatório. + mapa.
- Schumacher, R. & Schincke, H.-U., 1991. Internal structure and occurrence of accretionary lapilli - a case study at Laacher See Volcano. *Bulletin of Volcanology* **53**, 612-634.
- Schumacher, R. & Schincke, H.-U., 1995. Models for the origin of accretionary lapilli. *Bulletin of Volcanology* **56**, 626-639.
- Seer, H.J., 1985, *Geologia, deformação e mineralogia de cobre no Complexo Vulcano-Sedimentar de Bom Jardim de Goiás - Dissertação de Mestrado, UnB, Brasília.*

- Sgarbi, P. B. A. & Valença, J. G., 1994. Mineral and rock chemistry of the Mata da Corda kamafugitic rocks (MG State, Brazil). In: International Symposium on the Physics and Chemistry of the Upper Mantle (Extended Abstracts). São Paulo, Brazil, CPRM/FAPESP, 27-29.
- Sgarbi, P.B.A., Clayton, R.N., Toshiko, K.M. & Gaspar, J.C., 1998. Oxygen isotope thermometry of Brazilian potassic volcanic rocks of kamafugitic affinities. *Chemical Geology* **146**, 115-126.
- Stachel, T., Brey, G. & Lorenz, V., 1995. Carbonatite magmatism and fenitization of the epiclastic caldera-fill at Gross-Brukkaros (Namibia). *Bulletin of Volcanology* **57**, 185-196.
- Stoppa, F., 1996. The San Venanzo maar and tuff ring, Umbria, Italy: eruptive behaviour of a carbonatite-melilitite volcano. *Bulletin of Volcanology* **57**, 563-577.
- Stoppa, F. & Lavecchia, G., 1992. Late Pleistocene ultra-alkaline magmatic activity in the Umbria-Latium region (Italy): An overview. *Journal of Volcanology and Geothermal Research* **52**, 277-293.
- Stoppa, F. & Lupini, L., 1993. Mineralogy and Petrology of the Polino Monticellite Calcicarbonatite (Central Italy). *Mineralogy and Petrology* **49**, 213-231.
- Stoppa, F. & Principe, C., 1997. Eruption style and petrology of a new carbonatitic suite from the Mt. Vulture Southern Italy: The Monticchio Lakes Formation. *Journal of Volcanology and Geothermal Research* **78**, 251-265.
- Stoppa, F. & Woolley, A.R., 1997. The Italian carbonatites: field occurrence, petrology and regional significance. *Mineralogy and Petrology* **59**, 43-67.
- Tompkins, L.A., 1987. Exploration for kimberlites in southwest Goiás region, Brazil: Mineral chemistry of stream sediment samples. *Journal of Geochemical Exploration* **27**, 1-28.
- Thompson, R N., Morrison, M.A., Hendry, G.L & Parry, S.J., 1984. An assessment of the relative roles of crust and mantle in magma genesis: an elemental approach. *Philosophical Transactions Royal of the Society, London*, **A310**, 549-590.
- VanDecar, J.C., James, D.E. & Assumpção, M., 1995. Seismic evidence for a fossil mantle plume beneath South America and implications for plate driving forces. *Nature* **378**, 25-31.

- Veksler, I. M. & Tepteleev, M. P., 1990. Conditions for the crystallisation and concentration of perovskite-type minerals in alkaline magmas. *Lithos*, **26** 177-189.
- Waters, A.C. & Fisher, R.V., 1971. Base Surges and Their Deposits: Capelinhos and Taal Volcanoes. *Journal of Geophysical Research* **76**, 5596-5614.
- Wilson, M., 1989. *Igneous Petrogenesis - A Global Tectonic Approach*. Harper Collins. London.
- Woods, A.W., 1993. Moist Convection and the Injection of Volcanic Ash Into the Atmosphere. *Journal of Geophysical Research-Solid Earth* **98**(B10), 17627-17636.
- Woolley, A.R., Bergman, S.C., Edgar, A.D., Le Bas, M.J., Mitchell, R.H., Rock, N.M.S. & Scott Smith, B.H., 1996. Classification of lamprophyres, lamproites, kimberlites, and the kalsilitic, melilitic, and leucitic rocks. *The Canadian Mineralogist* **34**, 175-186.
- Zalán, P.V., Wolff, S., Conceição, J.C.J., Vieira, I.S., Astolfi, M.A.M.; Appi, V.T. & Zanotto, O.A., 1987. A divisão tripartite do Siluriano da Bacia do Paraná. *Revista Brasileira de Geociências* **17**, 242- 252.
- Zalán, P.V., Wolff, S., Conceição, J.C.J., Marques, A., Astolfi, M.A.M., Vieira, I.S., Appi, V.T. & Zanotto, O.A., 1990. Bacia do Paraná. In: De Raja Gabaglia, G.P. and Milani, E.J. (coords.), 1990. *Origem e Evolução de Bacias Sedimentares*. PETROBRÁS.
- Zimanowski B., Buttner, R. & Lorenz, V., 1997. Premixing of magma and water in MFCI experiments. *Bulletin of Volcanology* **58**, 491-495.

Appendix 1 - SAMPLE DESCRIPTIONS

Sample	Classification	Occurrence	Description
<u>NEUZINHA</u>		17°01'S 51°08'W	
96AE01	Melaleucitite	Lava	Dark grey rock, aphanitic groundmass, phenocrysts of pyroxene (8mm) and olivine (1cm).
96AE02	Melaleucitite	Block	Dark grey rock, aphanitic groundmass, phenocrysts of olivine (5mm), pyroxene (7mm) and phlogopite (6mm).
96AE03	Leucitite	Lava	Grey rock, aphanitic groundmass, phenocrysts of pyroxene (1cm) and olivine(rare, 5mm).
96AE04	Melaleucitite	Lava	Dark grey rock, aphanitic groundmass, phenocrysts of phlogopite (9mm), pyroxene (7mm) and olivine (4mm).
96AE05	Melanephelinite (?)	Block	Grey rock, aphanitic groundmass, phenocrysts of olivine (2mm), phlogopite (2mm) and rare pyroxene.
96AE06	Melaleucitite	Block	Dark grey rock, aphanitic groundmass, phenocrysts of pyroxene (7mm) and olivine (1cm).
96AE07	Melaleucitite	Block	Same as 96AE06 with flow banding.
96AE08	Melanephelinite(?)	Block	Grey rock, aphanitic groundmass, very small phenocrysts of olivine and phlogopite.
96AE09	Breccia	Matrix	Greenish rock, fragmental matrix (ash-lapilli size), fragments up to 1.5m, usually <20cm. Fragments include gneiss, granite, amphibolite, sandstone, alkaline rocks, crystals of k-feldspar, pyroxene and phlogopite.

MONTIVIDIU

17°18'S 51°13'W

96AE10	Lamprophyre	Dyke	Green rock, very altered, with megacrysts of phlogopite.
--------	-------------	------	--

MARIMBONDO

17°09'S 51°22'W

96AE11	Melaleucitite	Lava	Dark grey rock. Aphanitic groundmass. Phenocrysts of olivine up to 6mm.
96AE12	Melaleucitite	Lava	Grey rock with aphanitic groundmass. Phenocrysts of olivine up to 1cm and rare pyroxene.
96AE13	Melaleucitite	Block	Dark grey rock. Aphanitic groundmass. Phenocrysts of olivine up to 6 mm and small leucite.
96AE14	Melaleucitite	Block	Dark green rock. Aphanitic groundmass. Phenocrysts of olivine (1.2cm), rare leucite (3mm) and rare pyroxene (2mm).
96AE15	Amphibolite	Fragment	Grey rock. Fine-grained. Fragment in breccia 96AE16.
96AE16	Breccia	Matrix	Brown greenish rock. Very similar to 96AE09, but with less ash-size material.

CACIMBA

96AE57	Leucitite	Lava	Aphanitic grey rock with small phenocrysts of leucite and olivine.
--------	-----------	------	--

ÁGUAS EMENDADAS

17°02'S 51°02'W

96AE17	Leucitite	Lava	Dark grey rock. Aphanitic groundmass. Phenocrysts of pyroxene up to 4mm, rare leucite and olivine.
96AE18	Basanite	Lava	Grey rock. Aphanitic groundmass. Rich in phenocrysts of pyroxene (7mm) and olivine. Rare plagioclase.
96AE19	??	Lava	Dark grey rock, very rich in irregular inclusions of a porphyritic rock. Probably an example of

			magma mixing.
96AE20	Leucitite	Block	Grey rock with aphanitic groundmass and phenocrysts of leucite. Some vesicles, filled with carbonate.
96AE21	Melanephelinite (?)	Lava	Magma mixing? Phenocrysts of olivine and pyroxene. Texture similar to 96AE19.
96AE22	Melaleucitite	Lava	Dark grey rock. Rich in phenocrysts of pyroxene, olivine and phlogopite. Peridotite xenoliths (up to 3 cm).
96AE23	Melaleucitite	Lava	Dark grey rock, aphanitic groundmass, rich in phenocrysts of pyroxene (5mm) and olivine (3mm).
96AE24	Breccia	Block	Hydrothermal breccia. All fragments are of melanephelinite (?), cemented by carbonate and zeolites. Phenocrysts of olivine and pyroxene.
96AE25	Basanite	Block	Dark green rock. Aphanitic.
96AE26	Breccia	Matrix	Green rock. Altered. Fragmental matrix (ash-to lapilli-size), fragments up to 3m, usually <20cm. Fragments include gneiss, granite, amphibolite, sandstone, alkaline rocks, crystals of k-feldspar, pyroxene and phlogopite.
96AE27	Breccia	Matrix	Same as 96AE26.
96AE28	Breccia	Matrix	Same as 96AE26.
96AE29F	Melanephelinite (?)	Fragment	Dark green rock. Aphanitic groundmass, phenocrysts of olivine (1.2cm). Rare vesicles filled with calcite.
96AE30F	Melanephelinite (?)	Fragment	Cognate fragment. Green rock. Altered, very rich in vesicles and olivine phenocrysts (3mm).
96AE31F	Melaleucitite	Fragment	Grey rock. Altered. Rich in phenocrysts of olivine (5mm) and pyroxene (7mm). Some vesicles (filled with calcite).
96AE32F	Melanephelinite (?)	Fragment	Light green rock. Altered. very similar to 96AE30F. Rich in "xenoliths" of a fine grained rock.
96AE33	Melanephelinite (?)	Breccia	Part of the breccia matrix. Grey rock. Altered. Rich in vesicles, up to 5mm, filled with carbonate and zeolite. "Xenoliths" of a dark aphanitic volcanic rock.
96AE34F	Leucitite	Fragment	Dark grey rock. Aphanitic groundmass. Phenocrysts of leucite (4mm) and pyroxene (3mm). Vesicles.

96AE35	Melanephelinite (?)	Breccia	Part of the breccia matrix. Very similar to 96AE33, more rich in "xenoliths".
96AE36	Basanite	Block	Dark grey rock. Rich in phenocrysts of plagioclase (1.5cm), pyroxene (5mm) and altered olivine (3mm).
96AE37Cb	Carbonate	Vein	
96AE38Cb	Carbonate	Vein	
96AE39Cb	Carbonate	Fragment	
96AE40Cb	Carbonate	Vein	
96AE41Cb	Carbonate	Vein	
96AE42	Melanephelinite (?)	Dyke	Dark grey rock. Altered. Aphanitic groundmass. Scattered phenocrysts of olivine and pyroxene.
96AE43	Melanephelinite (?)	Dyke	Margin of the dyke. Dark grey rock. Aphanitic groundmass with megacrysts of phlogopite and small phenocrysts of olivine.
96AE44	Melaleucitite	Dyke	Central portion of the same dyke as 96AE43. Dark grey rock. Very rich in pyroxene (1cm), olivine (5mm) and phlogopite phenocrysts. Rare vesicles.
96AE45	Melanephelinite (?)	Dyke	Intermediate portion of the same dyke as 96AE43. Similar to 96AE43 but rich in vesicles.
96AE46	Melanephelinite (?)	Dyke	Dark grey rock. Aphanitic groundmass. Phenocrysts of pyroxene and olivine.
96AE47FI	Phlogopite	Dyke	
96AE48F	Leucitite	Fragment	Grey rock. Aphanitic groundmass. Phenocrysts of pyroxene (7mm) and rare olivine (4mm).
96AE49F	Melaleucitite	Fragment	Grey rock. Aphanitic groundmass. Small phenocrysts of olivine and pyroxene.
96AE50F	Melanephelinite (?)	Fragment	Dark grey rock. Aphanitic groundmass. Phenocrysts of olivine and pyroxene up to 5mm.
96AE51	Breccia	Matrix	same as 96AE26.
96AE52F	Basanite	Fragment	Grey rock. Aphanitic groundmass. Phenocrysts of pyroxene (2.5cm), olivine (5mm), plagioclase (5mm) and possibly leucite.
96AE53	Melanephelinite (?)	Dyke	Grey rock. Small phenocrysts of pyroxene and olivine. Central portion rich in vesicles.
92SOB212	Basanite	Block	Dark grey rock. Aphanitic with rare small phenocrysts of olivine.
92SOB214	Breccia	Matrix	Grey rock. Fragmental matrix (ash-to lapilli-size), Similar to 96AE26 but less altered.

AMORINÓPOLIS REGION

96AE54		Plug	Light green rock. Altered. 16°33'S 51°00'W.
96AE55	Olivine basalt?	Plug	Same locality as 96AE54. Dark grey rock. Aphanitic groundmass. Phenocrysts of pyroxene, plagioclase and olivine.
96AE56		Plug	Approximately 800m south of 96AE54. Grey rock. very altered. Phenocrysts of K-feldspar.
96AE58	Melanephelinite (?)	Block	Dark grey rock. Aphanitic groundmass. Small phenocrysts of olivine.
96AE64	Amphibolite	Block	Grey rock. Block of Pre Cambrian basement.
96AE65	Gabbro	Outcrop	Grey rock. Plagioclase, clinopyroxene and some olivine.
96AE66	Olivine basalt?	Block	Dark grey rock. Aphanitic groundmass. Phenocrysts of plagioclase (5mm), small olivine and rare pyroxene.
96AE69	Basanite	Block	North of 96AE54. Green rock Aphanitic groundmass with small and rare phenocrysts of olivine and plagioclase.

AMORINÓPOLIS

16°41'S 51°03'W

96AE59	Nephelinite (?)	Dyke	Dark grey rock. Aphanitic groundmass. Rare phenocrysts of olivine and pyroxene.
96AE60	Breccia	Outcrop	Hydrothermal. Grey rock. All fragments of melanephelinite (?). Carbonate cement.
96AE61	Melanephelinite (?)	Lava	Dark green rock. Aphanitic groundmass. Phenocrysts of olivine (4mm)
96AE62	Melanephelinite (?)	Lava	Same as 96AE61.
92SOB154	Basanite	Block	Grey rock. Aphanitic groundmass. Small phenocrysts of plagioclase and rare pyroxene.
92SOB156	Melanephelinite (?)	Lava	Dark grey rock. Rock rich in small phenocrysts of olivine and pyroxene.
96AE63	Melanephelinite (?)	Block	Dark grey rock. Aphanitic groundmass. Rich in phenocrysts of olivine.

MORRO DO MACACO

16°25'S 51°07'W

96AE68	Leucitite	Dyke	Dark grey rock. Aphanitic groundmass with phenocrysts of pseudoleucite up to 1cm.
--------	-----------	------	---

Appendix 2 - SAMPLE PREPARATION AND ANALYTICAL TECHNIQUES

A2.1 INTRODUCTION

During the field work, rock samples were collected trying to avoid weathered portions as much as possible. The samples were cut using a clipper saw at the Universidade de Brasília. Two pieces from the freshest centre were separated, washed and dried. One piece was separated to be crushed and powdered for later geochemical analysis and the other to produce thin sections for petrography and microprobe analyses.

At the University of Durham, the samples selected for geochemistry were crushed using a Fritsh Pulverisette jaw crusher (type 01-704). Before each sample the jaw crusher was cleaned using a wire brush and absolute alcohol in order to minimise contamination. The jaw crusher reduced the samples to ~ 5 mm grain size. After that, the samples were ground using an agate ball mill until a fine powder was obtained (~ 30 minutes). The powder was stored in a previously labelled bag and kept in a dry place.

Five samples of calcite were collected in the field, mostly from veins. These samples were washed, dried and pure mineral concentrates were

obtained using a binocular microscope. Two samples were ground using an agate ball mill and used for trace-element determinations by ICP-MS.

A single megacryst of phlogopite was extracted from a breccia collected in the area by Prof. R.N. Thompson and Dr. S.A. Gibson. Visible impurities were carefully removed from this crystal using a binocular microscope and the ground material was sent to the University of Newcastle for age determination.

All thin sections were made at the University of Durham.

A2.2 LOSS ON IGNITION (LOI)

Loss on ignition was determined by the following procedure. First a porcelain crucible was weighed. Subsequently, 2g of dry sample (dried overnight at 110°C) were weighed in the crucible and heated in a furnace at 900°C for 2 hours. After that, the crucible was put into a desiccator, allowed to cool and then re-weighed. The ignited powder was stored in a labelled glass bottle for future use in the production of fusion discs.

A2.3 FUSION DISC PREPARATION

Aliquots of 0.6 ± 0.001 g of ignited powder plus 3 ± 0.001 g of dry lithium tetraborate flux ("Spectrum 100B") were weighed together, then mixed in an agate ball mill that had been carefully cleaned. The mixture was transferred into a Pt crucible. This was heated in a furnace at 1050°C for 20 minutes. The fusion was poured into a graphite mould on a hot plate at 250°C and pressed

with a stainless steel plunger. Once the disc had cooled it was labelled, stored in a plastic bag and kept in a desiccator until analysis.

A2.4 POWDER PELLET PREPARATION

Approximately 10g of dry rock powder was mixed with 12-15 drops of Mowiol binding agent. The mixture was put into a mould and compressed at 10 tons in a hydraulic press for approximately 1 minute. The pellet was removed from the press, labelled and dried out for at least 30 minutes in an oven at 100°C.

A2.5 X-RAY FLUORESCENCE (XRF) ANALYSIS

The fusion discs were used to analyse 10 major elements. The powder pellets were used to analyse 20 trace elements. Results for 45 samples are presented in appendix 3 table A3.1, major elements are expressed as oxide wt.% and trace elements as parts per million (p.p.m.).

All XRF work was carried out at the University of Durham using a Philips PW1400 X-ray spectrometer, fitted with a PW1500/1072 sample changer, with a 3kW rhodium anode tube as the X-ray source. International standards (Govindaraju 1989) were used for calibration and analysed as unknowns in the same run as the samples, to monitor the accuracy of the calibration as well as the equipment performance. The readings were processed using Philips X40 software.

The 45 samples were analysed as a single batch in two runs, one for trace elements, the other for major elements. An example of the results obtained for international standards, as well as their recommended (rec) values (Govindaraju 1989) is showed in table A2.1a for major elements and table A2.1b for trace elements.

	BHVO-1 rec	BHVO-1
SiO ₂	49.94	50.21
TiO ₂	2.71	2.72
Al ₂ O ₃	13.80	13.69
Fe ₂ O ₃	12.23	12.30
MnO	0.17	0.17
MgO	7.23	7.04
CaO	11.40	11.54
Na ₂ O	2.26	2.23
K ₂ O	0.52	0.54
P ₂ O ₅	0.27	0.29

Table A2.1a

	BE-N rec	BE-N
Nb	100.0	100.3
Zr	265.0	261.5
Y	30.0	31.2
Sr	1370.0	1362.1
U	2.4	2.8
Th	11.0	11.3
Pb	4.0	6.2
Ga	17.0	16.2
Zn	120.0	123.5
Cu	72.0	71.1
Ni	267.0	269.4
Co	81.0	59.1
Cr	360.0	370.8
Rb	47.0	47.0
Ba	1025.0	1016.1
Ce	152.0	154.5
Nd	70.0	70.4
La	82.0	85.6
Sc	22.0	24.7
V	235.0	236.7

Table A2.1b

A2.6 INDUCTIVELY COUPLED PLASMA MASS SPECTROMETRY (ICP-MS)

The ICP-MS work was carried out at the University of Durham, using an Elan 6000 ICP Mass Spectrometer. Values for 36 trace elements were determined for 39 rocks and 2 carbonate concentrates. They were analysed in 3 different runs, all following the same procedure. Each run consisted of:

sample powders, a set of international standards and 3 blanks, making up to about 30 samples.

An aliquot of 0.1 ± 0.001 g of powder (previously dried overnight at 100°C) was digested in 1ml of Aristar HNO_3 and 4ml of Aristar HF, in closed Teflon vials on a hot plate at $130\text{-}150^\circ\text{C}$ for at least 48 hours. The mixture was then evaporated to a moist residue. 1ml of Aristar HNO_3 was added and the mixture was evaporated again. The last step was repeated. This procedure aims to remove all remaining traces of HF and silicon as SiF_4 formed during the digestion. The final residuum was re-dissolved in 2.5ml of Aristar HNO_3 and 10-15ml of MQ water, and heated for 30 minutes on a hot plate at $130\text{-}150^\circ\text{C}$. After cooling, the sample was spiked with 1.25ml of internal standard solution (2p.p.m. of Bi, Re and Rh) and the volume was completed to 50ml using MQ water. The analysed solution had a dilution factor of 1/5000.

The internal standard solution was used to allow compensation for signal fluctuation. The blanks controlled sample contamination during the digestion procedures and were used for processing the data. The international standards monitored the accuracy of the method. Calibration was based on the readings of international standards and blanks.

Blank concentrations were typically below 0.01 p.p.m. for Ti, Mn, Y, Nb, Cs, and all elements with atomic masses above 139 (except Pb). For V, Gd, Rb, Sr, Zr they were below 0.03 p.p.m.. The blank concentrations for Sc, Cr, Co, Ni, Cu, Zn, Ba, and Pb were extremely variable, indicating some kind of contamination or interference during the sample digestion and/or analysis. Relative standard deviations of replicate measurements of the same solution were typically below 0.025 (except for Sc, Cr, Co, Ni, Cu, Zn, Ba and Pb -

below 0.06). Table A2.2 shows the average values obtained for international standards and the respective recommended values (Govindaraju 1989).

The method proved to be very precise and accurate for those elements with atomic mass above 139 (except Pb). For some elements with lower masses it is necessary to be very cautious. Even taking great care during sample preparation, some contamination and/or analytical interference seems to affect the results for Sc, Cr, Co, Ni, Cu, Zn, Ba and Pb. When available, the XRF data for these elements were preferred.

	BCR-1-rec	BCR-1-av	BHVO-1-rec	BHVO-1-av	X-108-rec	X-108-av	AGV1-rec	AGV1-av
Sc	32.60	31.358	31.80	30.268	33.86	33.203	12.10	10.413
TiO ₂	2.24	2.197	2.71	2.743	0.14	0.122	1.06	1.012
V	407.00	403.531	317.00	315.097	218.34	212.313	123.00	116.570
Cr	16.00	68.612	289.00	293.936	466.83	456.559	12.00	47.575
MnO	0.18	0.182	0.17	0.169	0.16	0.140	0.10	0.094
Co	37.00	36.599	45.00	44.634	38.32	37.246	15.10	15.227
Ni	13.00	1838.301	121.00	126.747	116.67	115.180	17.00	608.264
Cu	19.00	21.490	136.00	135.123	85.63	190.291	60.00	56.353
Zn	129.50	110.273	105.00	103.392	66.12	99.552	88.00	73.580
Ga	22.00	21.544	21.00	21.056	9.33	9.173	20.00	19.827
Rb	47.20	47.554	9.60	9.457	13.03	12.512	67.00	66.581
Sr	330.00	332.061	403.00	404.011	85.47	87.506	662.00	655.034
Y	38.00	37.432	27.60	27.623	4.26	4.312	21.00	20.089
Zr	195.00	189.925	179.00	176.115	25.13	23.687	225.00	230.673
Nb	13.50	12.768	19.50	19.547	0.58	0.630	14.40	14.746
Cs	0.96	0.948	0.01	0.094	0.65	0.704	1.26	1.230
Ba	681.00	686.490	139.00	132.731	35.44	34.778	1221.00	1219.672
La	24.90	24.970	15.80	15.451	0.93	0.901	38.00	37.941
Ce	53.70	52.626	39.00	37.556	1.73	1.701	66.00	67.149
Pr	6.80	6.884	5.70	5.450	0.25	0.276	6.50	8.481
Nd	28.80	29.539	25.20	25.665	1.14	1.265	34.00	32.814
Sm	6.59	6.597	6.20	6.242	0.38	0.348	5.90	5.837
Eu	1.95	1.959	2.06	2.009	0.12	0.115	1.66	1.731
Gd	6.68	6.764	6.40	6.096	0.44	0.417	5.20	5.483
Tb	1.05	1.069	0.96	0.959	0.08	0.084	0.71	0.671
Dy	6.34	6.313	5.20	5.312	0.59	0.587	3.80	3.561
Ho	1.26	1.271	0.99	0.976	0.12	0.138	0.73	0.667
Er	3.63	3.529	2.40	2.484	0.48	0.458	1.61	1.789
Tm	0.56	0.559	0.33	0.362	0.09	0.088	0.32	0.279
Yb	3.38	3.365	2.02	2.041	0.68	0.625	1.67	1.675
Lu	0.51	0.522	0.29	0.295	0.11	0.113	0.28	0.258
Hf	4.95	4.927	4.38	4.477	0.69	0.658	5.10	5.118
Ta	0.81	0.820	1.23	1.258	0.05	0.043	0.92	0.902
Pb	13.60	13.807	2.80	2.467	1.62	7.949	36.00	35.824
Th	5.98	6.003	1.16	1.259	0.13	0.132	6.50	6.359
U	1.75	1.696	0.42	0.438	0.16	0.131	1.89	1.903

Table A2.2 Comparison between recommended values (rec) for international standards (Govindaraju 1989) and average (av) of results obtained in 3 runs (n=5).

A2.7 ELECTRON PROBE MICROANALYSIS

Microprobe work was carried out at the University of Cambridge. The samples selected were made into polished thin sections at the University of Durham and carbon-coated under vacuum at the University of Cambridge, following the method of Reed (1996).

After coating, regions of interest were marked on the thin section with use of a petrographic microscope. The samples were transferred to the microprobe (model CAMECA SX-50, equipped with a Link ED System).

Points of interest were marked and stored in the system for later batch analysis. Qualitative EDS analyses were also done when necessary to identify unknown mineral phases.

All elements were determined by EDS quantitative analysis. The calibration was set up with the use of a combination of minerals and synthetic standards. Operating conditions were 20 nA and 20 kV. Detection limits are typically 0.1%.

Microprobe results are given in Appendix 4.

Appendix 3 - WHOLE-ROCK CHEMICAL DATA*

Table A3.1 - XRF data**, loss on ignition (LOI) and magnesium number (Mg#). Major element oxides and LOI are expressed in weight percent (wt.%). Trace-elements are expressed in parts per million (p.p.m.). Data were recalculated on volatile-free basis. Magnesium number was calculated using the following equation:

$$\text{Mg-number (Mg\#)} = (\text{MgO}/(\text{MgO}+\text{FeOT}))\cdot 100, \text{FeOT} = 0.899847\cdot \text{Fe}_2\text{O}_3\text{T}.$$

Table A3.2 - ICP-MS data**. TiO₂ and MnO are given in weight percent (wt.%), the remaining elements are given in parts per million (p.p.m.).

Table A3.3 - CIPW norm results obtained with the computer program "IGPET 3". An arbitrary Fe₂O₃/FeO ratio of 0.15 were used to recalculate original Fe₂O₃T of the samples into Fe₂O₃ and FeO.

Table A3.4 - Normative composition of selected samples, calculated according to the method of Le Bas (1973). The same Fe₂O₃/FeO ratios of table A3.4 were used.

*For sample location and description see appendix 1

**For analytical techniques see appendix 2

Table A3.1

Sample	96AE01	96AE02	96AE03	96AE04	96AE05	96AE06	96AE08	96AE11	96AE12	96AE13	96AE14	96AE15	96AE17	96AE18	96AE20
SiO2	41.39	41.74	45.44	41.07	38.73	41.81	38.71	41.74	42.30	42.87	42.11	48.39	47.37	48.16	44.18
TiO2	4.20	4.32	3.99	4.58	4.69	4.33	4.68	3.74	3.79	3.74	4.04	3.01	4.03	3.22	4.17
Al2O3	7.73	9.02	11.12	8.90	9.26	8.41	9.40	7.42	7.62	7.91	7.67	13.33	14.44	13.93	15.41
Fe2O3T	14.03	12.20	12.97	12.52	15.13	14.31	16.07	13.45	13.49	13.16	13.15	14.74	11.43	11.85	12.74
MnO	0.21	0.18	0.22	0.18	0.24	0.22	0.25	0.20	0.20	0.20	0.19	0.28	0.46	0.23	0.28
MgO	12.33	15.82	6.68	15.63	10.76	11.85	10.42	16.59	15.71	14.91	15.83	5.66	4.24	6.51	4.33
CaO	16.99	11.62	12.30	11.81	13.23	15.37	13.89	12.64	12.91	13.45	13.40	9.37	9.52	9.73	7.74
Na2O	1.91	2.53	2.26	2.78	2.42	1.79	2.51	2.50	2.10	0.73	2.29	2.56	4.50	2.98	5.42
K2O	0.74	1.17	3.58	1.26	3.93	0.83	3.04	0.39	0.85	1.84	0.42	1.72	2.83	2.43	3.18
P2O5	0.63	0.48	0.77	0.47	0.84	0.69	0.91	0.49	0.53	0.54	0.51	0.34	0.98	0.69	1.54
TOTAL	100.16	99.07	99.33	99.20	99.23	99.60	99.88	99.16	99.50	99.34	99.61	99.40	99.80	99.73	98.99
L.O.I.	2.04	2.90	1.66	2.76	0.31	2.13	0.70	1.84	1.99	1.86	2.20	0.76	2.91	1.92	4.54
Mg-number	49.4	59.0	36.4	58.1	44.1	47.9	41.9	57.8	56.4	55.7	57.2	29.9	29.2	37.9	27.4
Ba	1371	1691	1320	1671	1332	1209	1308	775	611	897	703	1598	2346	1764	2035
Ce	118	97	227	107	226	168	245	136	132	139	118	71	289	208	547
Co	56	58	49	57	70	61	66	66	62	63	64	61	38	46	46
Cr	718	1344	241	1253	258	585	87	1718	1562	1618	1636	111	29	235	4
Cu	90	70	26	72	93	136	82	107	109	120	84	220	13	36	84
Ga	11	12	18	11	15	17	20	14	14	13	14	22	19	20	20
La	101	94	164	95	184	139	192	94	94	100	83	26	214	133	380
Nb	88	80	105	80	137	96	149	70	69	68	69	14	132	86	220
Nd	50	46	106	46	105	80	107	64	61	70	54	51	130	96	244
Ni	240	378	47	337	125	262	94	400	371	349	347	75	18	51	15
Pb	16	8	15	13	15	18	13	16	12	12	13	11	18	17	16
Rb	28	115	82	55	62	39	50	26	24	30	18	31	46	34	128
Sc	43	30	31	33	41	39	38	35	35	31	37	33	14	25	10
Sr	1499	776	1001	1000	1227	1842	1605	734	764	846	847	613	1366	1030	2655
Th	7	3	9	8	13	10	10	3	6	4	1	2	13	10	18
U	3	3	3	3	4	2	3	3	3	3	3	1	4	2	2
V	421	443	418	440	405	445	415	361	376	387	383	419	373	268	150
Y	20	19	34	11	30	23	29	19	18	19	18	23	29	23	62
Zn	77	60	95	59	91	88	103	75	79	73	73	109	94	94	105
Zr	304	216	315	207	386	331	426	230	235	234	242	212	383	314	789

Table A3.1

Sample	96AE22	96AE23	96AE24	96AE25	96AE29F	96AE34F	96AE36	96AE42	96AE43	96AE44	96AE46	96AE48F	96AE52F	96AE53	96AE54
SiO2	41.54	42.07	43.31	48.07	38.02	47.03	46.61	37.86	39.23	41.78	38.43	45.73	46.83	41.32	60.02
TiO2	3.48	4.03	3.88	3.72	5.96	3.43	3.75	4.69	5.66	4.52	4.62	4.00	3.88	4.81	1.72
Al2O3	6.83	7.51	9.77	15.75	7.43	12.51	16.46	8.90	10.17	8.78	9.09	12.39	13.12	9.56	15.74
Fe2O3T	13.36	13.69	13.78	11.84	16.61	11.75	12.83	14.97	15.23	13.80	15.06	13.26	12.88	14.19	6.78
MnO	0.20	0.21	0.24	0.19	0.26	0.22	0.21	0.24	0.24	0.25	0.37	0.23	0.23	0.35	0.15
MgO	18.41	13.63	10.26	4.28	10.54	6.04	3.55	11.96	10.56	13.80	14.08	6.53	7.26	12.18	1.71
CaO	13.36	16.60	14.43	8.66	16.72	10.26	7.14	17.73	14.44	15.05	14.90	11.05	8.93	14.70	3.36
Na2O	1.18	1.67	3.08	3.03	1.73	2.89	4.75	1.61	2.06	0.94	1.06	3.77	2.23	1.28	4.40
K2O	0.89	0.26	0.78	3.91	0.74	3.84	2.84	0.56	0.48	0.35	0.57	2.49	4.00	0.48	5.09
P2O5	0.49	0.61	0.97	0.84	1.32	0.81	0.90	1.15	1.01	0.63	1.14	0.85	0.74	1.01	0.55
TOTAL	99.74	100.27	100.49	100.28	99.33	98.79	99.04	99.67	99.08	99.89	99.31	100.30	99.90	99.87	99.51
L.O.I.	1.47	2.63	3.40	1.67	4.84	2.37	2.72	7.40	3.80	3.35	5.28	2.80	3.07	3.58	1.44
Mg-number	60.5	52.5	45.3	28.7	41.4	36.4	23.5	47.0	43.5	52.6	51.0	35.4	38.5	48.8	21.9
Ba	872	446	1374	1655	1701	5240	1570	936	583	727	943	2394	1617	765	1388
Ce	102	139	262	235	181	244	269	146	182	161	177	239	241	255	216
Co	69	56	51	43	61	51	46	45	53	57	58	52	53	46	15
Cr	1952	731	414	2	508	92	34	579	520	1158	585	130	98	675	2
Cu	121	101	77	4	83	80	36	57	112	124	72	16	16	57	3
Ga	17	15	14	22	18	14	22	15	16	15	17	13	17	16	25
La	69	98	190	161	189	166	175	127	193	132	149	168	144	221	128
Nb	69	85	115	97	159	109	105	130	142	81	138	100	81	119	83
Nd	55	60	112	108	85	99	133	63	75	82	82	115	114	108	104
Ni	470	272	111	6	272	45	23	243	114	258	283	36	33	117	4
Pb	8	12	15	17	15	27	14	11	15	14	14	19	11	16	18
Rb	27	21	26	79	27	54	38	27	17	12	32	34	46	17	102
Sc	36	37	41	20	32	22	13	36	33	32	35	26	24	32	8
Sr	1110	1185	1104	1286	1581	826	1767	990	975	605	1280	1272	1489	640	487
Th	3	4	11	11	13	16	8	8	7	6	9	10	7	10	13
U	3	3	4	3	3	4	3	2	3	3	4	3	2	3	4
V	335	428	308	284	485	335	272	440	552	465	430	393	304	431	93
Y	17	24	24	34	31	2	28	31	35	21	32	19	26	33	50
Zn	76	77	81	109	101	83	101	90	91	77	85	93	93	91	92
Zr	241	278	309	348	523	260	362	409	400	263	437	304	317	406	412

Table A3.1

Sample	96AE55	96AE57	96AE58	96AE59	96AE61	96AE62	96AE63	96AE64	96AE65	96AE66	96AE68	96AE69	92SOB154	92SOB156	92SOB212
SiO2	48.55	40.67	39.42	45.58	37.21	37.04	36.41	51.80	49.18	50.40	43.69	43.45	50.32	37.74	47.88
TiO2	3.29	5.63	4.16	3.36	5.55	5.56	5.88	0.95	2.66	2.44	4.37	4.01	3.32	4.36	3.67
Al2O3	13.13	10.11	10.11	13.34	6.47	6.27	7.16	14.04	14.27	17.31	13.38	12.35	16.28	9.17	16.02
Fe2O3T	11.87	13.43	16.21	12.75	15.92	15.91	15.89	9.69	11.16	9.98	12.55	13.50	10.66	18.27	11.12
MnO	0.19	0.19	0.24	0.20	0.21	0.21	0.22	0.17	0.16	0.16	0.20	0.25	0.19	0.30	0.50
MgO	7.54	13.05	10.93	7.53	17.25	16.80	14.86	10.30	5.66	4.10	5.28	6.53	3.48	10.05	4.53
CaO	8.66	12.19	13.60	10.51	11.26	11.27	13.08	7.89	9.13	7.06	11.93	12.22	7.56	15.24	8.37
Na2O	3.49	3.18	1.88	3.75	2.06	2.26	2.41	2.83	2.43	3.48	1.64	3.23	4.24	2.86	3.61
K2O	2.30	0.79	1.81	2.39	3.14	3.02	2.23	1.66	4.95	3.98	5.10	2.05	2.86	0.23	2.05
P2O5	0.69	0.60	1.07	0.73	0.71	0.79	1.00	0.20	0.55	0.67	1.00	0.69	0.69	1.35	0.84
TOTAL	99.70	99.85	99.43	100.14	99.78	99.13	99.16	99.53	100.16	99.58	99.14	98.27	99.60	99.59	98.59
L.O.I.	2.26	2.93	3.29	1.33	0.24	0.24	1.83	2.03	0.85	1.33	2.63	2.31	1.37	2.25	3.17
Mg-number	41.4	51.9	42.8	39.6	54.6	54.0	51.0	54.2	36.0	31.3	31.9	35.0	26.6	37.9	31.2
Ba	984	1665	863	1046	898	963	1257	703	1251	1258	1962	2166	1206	306	8669
Ce	244	102	274	204	208	214	172	63	168	202	236	209	210	356	200
Co	47	63	69	54	82	88	78	45	53	33	61	59	33	68	36
Cr	357	528	127	244	847	803	512	947	106	49	60	127	4	293	2
Cu	56	73	38	152	86	90	74	73	38	44	158	54	5	74	5
Ga	19	14	24	19	18	16	20	22	18	19	22	17	23	19	19
La	143	96	157	125	172	174	155	23	85	109	177	141	137	224	179
Nb	84	79	121	82	126	128	148	8	51	59	119	85	76	155	86
Nd	121	50	136	99	96	96	79	36	83	97	112	99	111	171	87
Ni	141	237	153	174	504	491	357	238	36	36	59	71	12	108	2
Pb	13	15	16	10	12	12	14	15	9	13	15	13	11	16	30
Rb	32	37	41	31	43	42	52	39	126	93	107	43	38	20	374
Sc	21	28	34	27	27	28	28	28	25	18	26	29	17	36	18
Sr	977	1172	1890	1083	1221	1253	1630	330	802	1150	1654	1395	1349	2040	1156
Th	6	5	6	3	8	4	9	6	7	6	6	5	6	9	11
U	3	3	1	3	4	4	2	1	2	3	3	3	3	3	2
V	235	547	275	309	397	406	447	170	288	223	364	431	235	411	337
Y	33	14	49	30	29	29	35	20	30	31	40	24	35	49	6
Zn	93	69	136	91	109	99	108	97	74	84	90	86	91	121	95
Zr	380	247	583	331	390	421	519	131	262	314	445	376	361	621	288

Table A3.2

Sample	96AE01	96AE04	96AE06	96AE08	96AE11	96AE12	96AE13	96AE15	96AE17	96AE18	96AE20	96AE22	96AE23	96AE24
Sc	47	37	40	41	34	34	33	38	10	23	12	33	48	36
TiO2	4.30	4.82	4.42	4.96	3.88	3.86	3.81	3.29	4.10	3.27	4.23	3.56	4.14	3.89
V	383	413	402	421	357	360	367	495	345	286	177	328	385	287
Cr	735	1341	623	85	1697	1673	1651	137	31	259	-	1998	807	437
MnO	0.20	0.18	0.21	0.25	0.20	0.19	0.19	0.31	0.44	0.23	0.28	0.19	0.20	0.23
Co	66	73	67	62	79	76	72	50	33	38	35	83	68	55
Ni	288	453	302	98	495	460	436	83	18	105	-	566	319	129
Cu	114	81	139	92	110	111	128	221	26	44	88	114	105	106
Zn	123	112	242	148	113	115	117	149	134	122	170	110	110	146
Ga	14.3	15.8	17.1	21.2	15.7	15.6	15.5	22.9	21.8	21.0	18.4	14.3	14.4	14.4
Rb	30.8	102.7	51.8	85.7	36.1	33.1	41.8	44.4	73.5	42.6	235.1	28.4	22.1	30.9
Sr	1611	1098	1953	1689	807	840	914	675	1434	1066	2823	1185	1301	1199
Y	22.8	15.2	24.1	27.9	19.2	19.5	19.8	35.3	37.2	28.7	51.3	17.9	21.7	27.5
Zr	317.3	258.9	332.7	475.0	265.6	265.7	263.1	228.9	483.2	364.4	921.7	260.4	301.2	366.6
Nb	112.4	106.4	118.1	178.2	85.6	83.9	84.2	19.2	171.6	107.2	286.1	84.8	105.2	150.0
Cs	1.32	5.92	3.21	1.47	1.19	1.21	0.39	2.16	32.00	7.91	144.34	0.50	0.40	33.63
Ba	1341	1654	1263	1463	879	848	894	1890	2648	1849	2317	847	427	1409
La	83.5	74.7	86.2	125.3	61.8	60.6	61.6	25.1	118.4	82.8	200.2	58.8	77.4	123.8
Ce	166.9	146.7	173.0	242.2	125.4	123.2	125.1	56.5	231.5	164.1	395.6	117.3	157.0	240.5
Pr	20.2	17.1	20.7	28.4	15.2	15.0	15.3	7.9	27.2	19.5	45.7	14.2	19.1	27.9
Nd	76.9	63.6	80.2	106.3	59.6	58.3	59.8	35.9	102.5	74.4	166.6	55.1	73.3	102.0
Sm	12.3	9.4	12.9	15.8	9.6	9.5	9.9	8.3	16.1	12.0	23.9	9.0	11.8	14.6
Eu	3.46	2.68	3.57	4.29	2.72	2.70	2.77	2.84	4.48	3.50	6.49	2.52	3.15	4.05
Gd	8.7	6.0	9.1	10.5	7.2	6.9	7.1	8.2	11.3	8.5	15.2	6.7	8.3	9.5
Tb	1.10	0.79	1.16	1.35	0.92	0.90	0.92	1.19	1.53	1.15	2.10	0.85	1.05	1.28
Dy	5.07	3.52	5.33	6.23	4.26	4.31	4.41	6.65	7.43	5.72	10.16	4.03	4.83	5.98
Ho	0.82	0.56	0.86	0.98	0.70	0.70	0.72	1.24	1.26	1.00	1.75	0.84	0.79	0.99
Er	1.87	1.29	1.99	2.39	1.66	1.64	1.67	3.25	3.18	2.53	4.36	1.52	1.79	2.36
Tm	0.26	0.17	0.28	0.31	0.22	0.22	0.23	0.48	0.45	0.37	0.68	0.21	0.24	0.32
Yb	1.46	0.94	1.50	1.76	1.22	1.24	1.26	2.79	2.53	2.20	3.84	1.13	1.35	1.86
Lu	0.21	0.13	0.22	0.25	0.17	0.18	0.18	0.40	0.36	0.33	0.55	0.16	0.20	0.28
Hf	7.85	6.33	7.95	11.22	6.29	6.33	6.37	5.68	10.12	8.35	16.32	6.25	7.57	8.77
Ta	6.71	6.83	7.10	11.13	5.22	5.07	5.18	1.21	10.06	6.37	17.43	5.04	6.36	8.75
Pb	5.1	2.9	13.7	4.4	4.8	4.7	5.0	3.4	8.8	8.7	8.5	4.2	4.5	7.8
Th	9.65	8.64	10.24	14.52	7.35	7.21	7.25	2.27	16.55	10.20	24.38	7.63	9.21	13.56
U	2.39	1.87	2.39	3.37	1.47	1.72	1.63	0.47	3.59	2.16	1.16	1.79	2.09	2.36

Table A3.2

Sample	96AE25	96AE 29F	96AE34F	96AE36	96AE37Cb	96AE38Cb	96AE 42	96AE 43	96AE 44	96AE46	96AE48F	96AE52F	96AE53	96AE54
Sc	17	26	24	12	11	8	33	30	37	33	19	23	32	8
TiO2	3.91	5.86	3.60	3.78	1.30	0.81	4.50	5.80	4.51	4.50	3.92	3.52	4.63	1.81
V	300	448	368	280	370	193	389	486	404	386	370	319	380	98
Cr	-	523	86	33	146	81	570	575	1053	604	132	104	758	-
MnO	0.20	0.24	0.24	0.21	0.11	0.06	0.22	0.23	0.24	0.34	0.21	0.21	0.33	0.15
Co	32	71	44	34	18	13	58	57	70	63	41	37	56	9
Ni	-	303	41	2	39	37	261	126	298	314	34	49	130	-
Cu	20	98	95	42	27	13	79	131	135	89	30	25	78	9
Zn	80	166	89	106	-	-	129	150	124	369	128	121	136	91
Ga	24.7	17.3	17.7	24.0	6.1	5.0	17.9	20.5	17.4	17.6	14.8	17.5	18.2	23.9
Rb	136.3	37.0	84.1	46.7	57.6	12.8	32.8	25.8	12.0	42.2	47.6	59.6	27.2	128.8
Sr	1405	1695	923	1819	393	1596	1100	1066	673	1358	1275	1458	699	528
Y	34.3	34.6	31.2	33.7	12.0	7.8	29.7	32.6	23.3	30.2	28.6	30.4	32.8	49.1
Zr	417.9	579.4	382.9	426.0	155.0	137.0	479.3	469.8	311.5	496.5	343.3	341.3	483.3	532.8
Nb	128.4	194.4	156.0	134.6	49.4	39.0	160.1	169.3	97.8	164.9	123.9	97.7	139.8	114.5
Cs	14.74	9.49	12.30	31.78	1.52	0.99	12.24	10.77	4.68	5.42	29.50	20.36	17.54	1.64
Ba	1979	1781	5899	1840	722	391	930	627	715	976	2574	1731	814	1536
La	98.0	148.7	115.3	98.8	40.5	24.4	125.1	117.3	71.0	123.9	89.4	78.1	115.2	100.8
Ce	193.6	294.1	228.9	195.5	74.5	45.2	246.2	235.2	146.2	247.5	178.8	157.4	226.1	201.5
Pr	23.0	34.9	26.6	23.1	8.7	5.2	29.3	28.3	17.9	29.5	21.4	19.2	27.1	24.4
Nd	87.5	135.6	97.8	87.6	33.1	19.7	111.4	107.1	70.9	111.4	82.2	75.0	103.2	92.8
Sm	14.2	21.7	14.6	13.9	5.2	3.1	16.9	16.9	11.7	16.9	13.2	12.5	16.5	15.3
Eu	4.13	5.94	4.64	4.20	1.47	0.93	4.49	4.56	3.16	4.53	3.99	3.72	4.44	3.98
Gd	10.3	15.0	10.1	10.1	3.7	2.4	11.5	11.8	8.2	11.6	9.7	9.5	11.8	11.5
Tb	1.39	1.84	1.38	1.36	0.50	0.31	1.44	1.56	1.08	1.47	1.28	1.26	1.55	1.70
Dy	6.96	8.03	6.50	6.66	2.36	1.51	6.58	7.18	5.08	6.78	6.08	6.25	7.25	8.79
Ho	1.22	1.23	1.12	1.17	0.41	0.26	1.06	1.17	0.83	1.08	1.03	1.08	1.18	1.62
Er	3.10	2.69	2.75	2.97	1.00	0.63	2.46	2.70	1.95	2.56	2.51	2.72	2.84	4.32
Tm	0.46	0.35	0.40	0.44	0.14	0.09	0.33	0.37	0.27	0.34	0.36	0.39	0.39	0.68
Yb	2.66	1.82	2.34	2.54	0.83	0.53	1.88	2.06	1.51	1.93	2.03	2.25	2.16	4.11
Lu	0.39	0.24	0.34	0.38	0.13	0.07	0.26	0.29	0.21	0.28	0.30	0.34	0.30	0.60
Hf	9.41	12.68	8.51	9.06	3.47	2.92	11.13	10.31	7.53	11.56	7.88	8.22	11.29	11.85
Ta	7.68	11.00	8.78	7.87	3.03	50.43	10.32	10.23	6.06	10.60	7.31	5.91	8.78	6.81
Pb	8.1	4.2	9.0	6.3	3.2	26.8	2.0	8.2	5.4	24.7	6.0	5.8	7.7	14.4
Th	11.20	17.52	15.54	11.28	4.16	2.20	13.47	14.88	8.73	13.65	11.09	8.73	12.62	15.22
U	2.75	4.26	3.21	2.54	3.17	0.86	3.29	3.65	2.07	3.50	2.33	1.42	2.82	3.83

Table A3.2

Sample	96AE55	96AE57	96AE58	96AE59C	96AE61	96AE62	96AE63	96AE66	96AE68	96AE69	92SOB154	92SOB156	92SOB212
Sc	24	29	24	24	21	25	23	17	15	28	15	35	27
TiO2	3.47	5.60	4.03	3.28	5.61	6.16	5.70	2.63	4.41	3.94	3.14	4.22	3.52
V	265	474	277	306	377	421	410	253	405	401	221	400	320
Cr	409	537	152	242	890	965	514	70	46	166	6	325	1548
MnO	0.20	0.18	0.22	0.19	0.20	0.23	0.20	0.17	0.20	0.24	0.18	0.29	0.46
Co	47	65	57	49	86	94	73	32	45	47	26	62	39
Ni	168	301	155	202	611	885	410	98	51	104	8	102	931
Cu	67	86	45	139	79	93	76	50	165	77	16	81	42
Zn	90	126	158	121	157	141	156	96	91	622	114	155	133
Ga	22.3	18.9	22.0	20.5	18.3	19.7	20.0	23.5	22.1	21.0	22.2	20.9	21.4
Rb	39.8	80.3	51.0	35.6	92.6	98.4	100.7	121.5	169.5	61.3	46.6	12.4	685.5
Sr	1066	1228	1901	1102	1250	1416	1643	1281	1752	1406	1377	2109	1198
Y	33.8	18.6	43.7	31.0	23.4	25.7	29.0	30.9	36.5	32.0	34.7	41.0	31.3
Zr	453.1	273.1	587.1	357.8	420.0	485.9	550.0	360.7	497.2	395.2	392.8	589.6	382.9
Nb	111.0	98.8	135.5	97.3	146.8	160.2	170.6	78.4	164.8	100.7	87.4	160.4	112.6
Cs	2.11	2.11	1.54	1.54	0.88	1.18	1.60	4.14	0.94	7.18	1.17	0.48	460.45
Ba	1087	1692	896	1108	1056	1232	1341	1474	2208	2214	1280	333	8698
La	90.5	65.2	108.6	70.8	100.2	111.1	118.9	80.7	120.9	77.6	76.9	135.5	89.1
Ce	188.0	131.1	219.8	139.8	203.0	227.5	240.9	162.4	239.9	159.3	159.5	279.2	178.7
Pr	22.7	15.8	27.1	16.7	24.6	27.4	28.9	19.2	28.9	19.7	19.2	33.8	20.7
Nd	87.4	60.0	108.4	64.6	95.4	105.9	111.4	72.0	111.3	77.5	76.1	129.6	79.5
Sm	13.9	9.7	18.6	10.6	15.3	16.9	18.0	11.1	17.6	13.3	12.6	20.2	12.5
Eu	3.60	2.87	5.22	3.09	4.13	4.55	4.89	3.21	5.07	3.96	3.76	5.39	4.76
Gd	9.6	6.9	14.3	8.0	10.6	11.2	12.3	8.0	12.8	10.2	9.6	14.2	9.9
Tb	1.36	0.91	1.93	1.12	1.27	1.41	1.53	1.11	1.68	1.36	1.31	1.85	1.24
Dy	6.73	4.22	9.25	5.60	5.62	6.19	6.76	5.71	8.01	6.67	6.69	8.67	6.05
Ho	1.18	0.68	1.52	0.98	0.85	0.92	1.02	1.06	1.32	1.13	1.23	1.46	1.08
Er	2.96	1.57	3.55	2.46	1.82	1.97	2.24	2.74	3.11	2.76	3.17	3.53	2.70
Tm	0.44	0.21	0.48	0.36	0.23	0.25	0.29	0.42	0.43	0.39	0.47	0.47	0.40
Yb	2.56	1.18	2.60	2.05	1.20	1.35	1.57	2.51	2.31	2.19	2.74	2.64	2.32
Lu	0.38	0.17	0.35	0.30	0.16	0.17	0.21	0.38	0.31	0.31	0.42	0.38	0.35
Hf	9.95	6.60	13.41	7.36	9.68	10.97	12.45	7.90	10.35	9.53	8.80	13.29	8.46
Ta	6.53	6.08	8.60	5.30	9.00	9.73	10.38	4.65	10.51	6.41	5.63	10.11	6.72
Pb	7.3	4.8	7.6	6.7	4.1	5.8	6.4	10.9	6.0	43.1	7.5	6.9	20.3
Th	9.82	7.83	12.21	8.73	12.28	13.04	14.30	8.75	13.54	8.51	7.97	13.83	10.56
U	2.40	1.88	2.82	2.02	2.90	3.07	3.45	1.91	3.10	1.95	2.04	3.58	2.54

Table A3.3

Sample	96AE01	96AE02	96AE03	96AE04	96AE05	96AE06	96AE08	96AE11	96AE12	96AE13	96AE14	96AE17	96AE18	96AE20	96AE22	96AE23	96AE24	96AE25	96AE29F	96AE34F
%AN	100.00	100.00	95.48	100.00	100.00	100.00	100.00	100.00	100.00	100.00	100.00	39.22	46.40	41.69	100.00	100.00	80.71	52.90	100.00	55.57
Q		3.50	21.33					0.79	2.46	2.99	1.43	16.72	14.42	18.97			4.55	23.05		22.99
or			0.46									16.86	20.21	11.76			2.51	15.84		7.92
ab		9.90	9.64	8.16	2.81	12.50	5.43	7.95	8.92	12.98	9.45	10.88	17.49	8.41	10.74	12.17	10.51	17.79	10.41	9.90
an	10.31	2.72		5.89	18.35	3.85	14.09	1.19	2.01	6.23	0.82				4.17	1.20			3.43	
lc	3.43			12.83	11.18	8.25	11.51	11.55	9.67	3.35	10.54	11.54	2.76	18.75	5.41	7.66	12.67	5.26	7.98	9.14
ne	8.76	11.69	10.20	35.81	19.46	46.27	22.63	41.79	41.76	40.71	43.24	24.91	21.69	16.80	35.91	46.03	44.20	16.26	38.17	29.82
di	42.33	36.07	38.33																	
hy																				
of	17.74	24.39	8.14	24.12	23.89	15.83	23.04	25.88	24.15	22.84	23.12	6.99	13.47	11.27	31.12	18.58	13.38	10.59	16.96	9.49
ac																				
mt	2.65	2.33	2.46	2.39	2.89	2.71	3.04	2.57	2.57	2.51	2.49	2.16	2.25	2.44	2.54	2.58	2.60	2.23	3.16	2.25
il	7.96	8.28	7.63	8.77	8.98	8.26	8.89	7.16	7.24	7.14	7.71	7.65	6.13	8.00	6.63	7.63	7.33	7.05	11.40	6.59
ap	1.46	1.11	1.81	1.09	1.97	1.60	2.11	1.14	1.23	1.25	1.18	2.27	1.60	3.61	1.14	1.41	2.25	1.95	3.08	1.90
COS	5.37			0.94	10.47	0.74	9.25								2.36	2.74			5.41	
Sample	96AE36	96AE42	96AE43	96AE44	96AE46	96AE48F	96AE52F	96AE53	96AE55	96AE57	96AE58	96AE59C	96AE61	96AE62	96AE63	96AE66	96AE68	96AE69	82SOB154	82SOB156
%AN	41.94	100.00	100.00	95.80	100.00	52.49	59.17	86.87	36.69	100.00	100.00	60.60	100.00	100.00	100.00	45.83	100.00	77.83	34.85	100.00
Q																				
or	16.86		0.35	2.07		14.66	23.84	2.72	13.85	3.43		14.07			23.58	10.76	12.29	16.67		
ab	21.22			0.82		8.60	9.66	2.87	23.13			8.15			23.61	28.71	3.81	28.71		
an	15.33	15.44	17.21	18.73	18.48	9.50	14.00	19.01	13.40	11.03	13.89	12.53			19.98	14.25	13.39	15.36	9.84	
lc		2.60	1.99		2.64					0.97	8.43		14.60	14.13	10.43	15.38				
ne	10.51	7.43	9.53	3.86	4.90	12.58	4.99	4.31	3.52	14.58	8.66	12.73	8.56	8.44	11.14	3.21	7.56	13.02	5.26	14.76
di	12.16	27.49	39.25	41.77	29.30	32.59	20.91	38.30	20.58	36.58	30.32	28.50	11.00	9.39	17.64	8.98	32.02	35.98	14.29	29.91
hy																				
ol	12.08	22.90	15.54	20.09	26.57	10.04	15.65	18.62	15.61	18.76	22.15	13.55	38.24	38.66	31.26	12.53	6.93	9.54	9.77	23.54
ac													1.44	3.27						
mt	2.45	2.84	2.90	2.61	2.87	2.49	2.44	2.68	2.25	2.54	3.09	2.41	2.29	1.39	3.03	1.90	2.39	2.60	2.02	3.42
il	7.20	8.95	10.84	8.58	8.83	7.58	6.99	9.15	6.27	10.71	7.94	6.38	10.58	10.65	11.26	4.65	8.36	7.75	6.29	8.30
ap	2.11	2.66	2.36	1.46	2.66	1.97	1.71	2.34	1.60	1.39	2.50	1.69	1.64	1.85	2.34	1.55	2.34	1.62	1.64	3.13
COS		9.71			3.75						3.02	11.64	12.23	10.78						6.10

Table A3.4

Sample	96AE01	96AE04	96AE05	96AE06	96AE08	96AE22	96AE23	96AE29F	96AE42	96AE46	96AE58	96AE61	96AE62	96AE63	92SOB156
qz										2.26					
co															
or	0.41	2.30		3.69		4.24	0.20	0.80	0.07	3.36	8.07				2.31
ab	4.87	9.01		11.76		7.08	10.36	4.60	4.53	9.00	8.49				
lc					0.23										
kal			9.11		5.75							7.35	7.07	3.39	
neph	8.31	10.83	15.27	2.51	15.73	2.14	2.74	7.48	6.75		5.53	11.71	11.52	15.20	2.73
car															11.45
ns												1.44	3.26		
ac															
th															
geh	10.11	7.99	2.77	12.28	5.31	10.52	11.99	10.20	15.19	18.16	13.63			2.12	9.65
akm												0.23	1.28		
Fe-ak												0.11	0.65		
wol															
wo	18.94	10.07	16.29	13.59	15.25	12.52	16.74	14.11	14.10	5.96	8.02	13.24	11.82	14.40	13.24
en	10.65	6.35	8.52	7.53	7.68	8.10	9.87	7.05	7.71	3.43	4.11	7.98	7.02	8.33	6.39
fs	7.51	3.09	7.30	5.54	7.22	3.58	6.04	6.77	5.89	2.26	3.71	4.55	4.20	5.41	6.64
fo	13.92	22.91	12.88	15.39	12.75	26.36	16.73	13.49	15.46	22.24	16.23	24.39	24.20	20.23	14.02
fa	10.81	12.31	12.17	12.48	13.21	12.84	11.28	14.27	13.01	16.15	16.15	15.33	15.94	14.48	16.05
andr															
hm	0.44														
mt	2.00	2.37	2.87	2.70	3.03	2.52	2.57	3.15	2.83	2.86	3.07	2.29	1.39	3.02	3.42
sph	10.24	11.28	8.37	10.61	11.45	8.52	9.82	14.66	11.51	11.37	10.22			2.28	10.68
perv			2.21									9.43	9.50	8.46	
ru															
ap	1.48	1.12	2.00	1.63	2.15	1.16	1.44	3.13	2.72	2.71	2.54	1.68	1.88	2.38	3.17
zr	0.06	0.04	0.08	0.07	0.09	0.05	0.06	0.11	0.08	0.09	0.12	0.05	0.06	0.10	0.12
bad															
cr	0.10	0.18	0.04	0.09	0.01	0.28	0.11	0.07	0.08	0.09	0.02	0.12	0.12	0.08	0.04
total	99.86	99.85	99.88	99.85	99.87	99.91	99.94	99.86	99.94	99.93	99.89	99.91	99.91	99.88	99.94

Appendix 4 - ELECTRON MICROPROBE ANALYSES

Table A4.1 - Olivines

Table A4.2 - Clinopyroxenes

Table A4.3 - Feldspathoids

Table A4.4 - Feldspars

Table A4.5 - Perovskites

Table A4.6 - Opaques

Fe₂O₃ concentration were estimated using the method of Droop (1987).

Table A4.1

	Olivines															
	96AE04 Melaleuc.	96AE04 Melaleuc.	96AE04 core Melaleuc.	96AE04 rim Melaleuc.	96AE04 Melaleuc.	96AE04 rim Melaleuc.	96AE04 core Melaleuc.	96AE04 rim Melaleuc.	96AE04 Melaleuc.	96AE04 core Melaleuc.	96AE04 rim Melaleuc.	96AE04 phl. pseud. Melaleuc.	96AE04 phl. pseud. Melaleuc.	96AE04 Melaleuc.		
SiO2	38.87	38.77	39.17	38.52	39.53	38.84	40.07	39.71	39.67	40.04	38.83	38.67	38.91	38.92	38.39	39.42
TiO2	0.00	0.00	0.04	0.06	0.00	0.02	0.08	0.05	0.01	0.00	0.01	0.21	0.09	0.02	0.15	0.03
Al2O3	0.00	0.00	0.00	0.01	0.14	0.07	0.03	0.00	0.00	0.00	0.01	0.02	0.00	0.00	0.00	0.08
Cr2O3	0.00	0.00	0.00	0.00	0.03	0.01	0.05	0.03	0.09	0.03	0.04	0.02	0.03	0.01	0.04	0.04
FeO	15.99	16.84	15.73	17.36	14.27	17.00	12.69	13.63	12.54	11.62	18.32	18.45	17.30	16.36	18.50	14.47
MnO	0.47	0.47	0.42	0.61	0.30	0.37	0.15	0.34	0.35	0.19	0.56	0.53	0.44	0.49	0.53	0.33
NiO	0.18	0.04	0.10	0.12	0.07	0.11	0.27	0.24	0.29	0.29	0.13	0.02	0.17	0.10	0.04	0.15
MgO	43.65	42.99	43.60	41.40	44.94	42.20	46.90	46.38	47.18	47.93	41.09	41.01	42.30	42.84	41.12	45.46
CaO	0.53	1.18	0.45	0.94	0.30	0.67	0.15	0.25	0.20	0.14	1.07	1.21	0.92	0.85	1.16	0.27
Na2O	0.10	0.31	0.08	0.06	0.27	0.17	0.28	0.27	0.40	0.24	0.31	0.13	0.19	0.22	0.13	0.14
K2O	0.00	0.00	0.00	0.06	0.00	0.00	0.04	0.00	0.00	0.02	0.00	0.00	0.00	0.00	0.02	0.02
Cl	0.01	0.02	0.01	0.01	0.00	0.00	0.00	0.00	0.00	0.00	0.01	0.01	0.00	0.00	0.00	0.02
P2O5	0.00	0.00	0.00	0.00	0.01	0.00	0.00	0.05	0.00	0.01	0.07	0.13	0.00	0.00	0.01	0.00
Total	99.79	100.62	99.58	99.14	99.86	99.46	100.72	100.95	100.73	100.51	100.45	100.41	100.35	99.79	100.09	100.42
per 4 oxygens																
Si	0.99	0.98	1.00	0.99	0.99	1.00	0.99	0.99	0.98	0.99	0.99	0.99	0.99	0.99	0.99	0.99
Ti	0.00	0.00	0.00	0.00	0.00	0.00	0.00	0.00	0.00	0.00	0.00	0.00	0.00	0.00	0.00	0.00
Al	0.00	0.00	0.00	0.00	0.00	0.00	0.00	0.00	0.00	0.00	0.00	0.00	0.00	0.00	0.00	0.00
Cr	0.00	0.00	0.00	0.00	0.00	0.00	0.00	0.00	0.00	0.00	0.00	0.00	0.00	0.00	0.00	0.00
Fe	0.34	0.36	0.33	0.37	0.30	0.36	0.26	0.28	0.26	0.24	0.39	0.39	0.37	0.35	0.40	0.30
Mn	0.01	0.01	0.01	0.01	0.01	0.01	0.00	0.01	0.01	0.00	0.01	0.01	0.01	0.01	0.01	0.01
Ni	0.00	0.00	0.00	0.00	0.00	0.00	0.01	0.00	0.01	0.01	0.00	0.00	0.00	0.00	0.00	0.00
Mg	1.66	1.63	1.65	1.59	1.68	1.61	1.73	1.72	1.75	1.77	1.57	1.56	1.60	1.63	1.58	1.70
Ca	0.01	0.03	0.01	0.03	0.01	0.02	0.00	0.01	0.01	0.00	0.03	0.03	0.02	0.02	0.03	0.01
Na	0.00	0.02	0.00	0.00	0.01	0.01	0.01	0.01	0.02	0.01	0.02	0.01	0.01	0.01	0.01	0.01
K	0.00	0.00	0.00	0.00	0.00	0.00	0.00	0.00	0.00	0.00	0.00	0.00	0.00	0.00	0.00	0.00
P	0.00	0.00	0.00	0.00	0.00	0.00	0.00	0.00	0.00	0.00	0.00	0.00	0.00	0.00	0.00	0.00
Total	3.01	3.02	3.01	3.01	3.01	3.01	3.01	3.02	3.03	3.02	3.01	3.01	3.01	3.01	3.01	3.02
%Fo	82.53	81.57	82.80	80.41	84.61	81.24	86.68	85.55	86.71	87.85	79.50	79.38	80.96	81.92	79.38	84.56

Table A4.1

	96AE11		96AE11		96AE11		96AE13		96AE13		96AE13		96AE22		96AE22		96AE22		96AE22		96AE22	
	core Melaleuc.	rim Melaleuc.	core Melaleuc.	rim Melaleuc.	core Melaleuc.	rim Melaleuc.	core Melaleuc.	rim Melaleuc.	core Melaleuc.	rim Melaleuc.	core Melaleuc.	rim Melaleuc.	core Melaleuc.	rim Melaleuc.	core Melaleuc.	rim Melaleuc.	core Melaleuc.	rim Melaleuc.	core Melaleuc.	rim Melaleuc.	core Melaleuc.	rim Melaleuc.
Olivines																						
SiO2	39.66	39.89	39.30	38.99	39.44	39.66	39.78	39.69	39.78	39.66	39.78	39.69	39.78	39.65	39.36	40.05	39.36	40.02	39.36	40.02	39.36	39.80
TiO2	0.10	0.00	0.03	0.02	0.03	0.01	0.04	0.03	0.04	0.01	0.04	0.03	0.03	0.00	0.08	0.05	0.08	0.00	0.03	0.00	0.03	0.00
Al2O3	0.00	0.00	0.00	0.11	0.00	0.00	0.00	0.00	0.00	0.00	0.00	0.00	0.00	0.00	0.00	0.05	0.00	0.00	0.01	0.00	0.01	0.00
Cr2O3	0.00	0.04	0.07	0.02	0.00	0.10	0.05	0.03	0.05	0.10	0.05	0.03	0.01	0.03	0.00	0.07	0.00	0.09	0.02	0.10	0.02	0.10
FeO	14.62	12.27	14.49	16.99	14.09	13.75	12.62	12.94	12.62	13.75	12.62	12.94	14.49	12.33	16.14	13.10	16.14	13.77	14.96	13.77	14.96	12.19
MnO	0.25	0.32	0.26	0.34	0.24	0.23	0.12	0.20	0.12	0.23	0.12	0.20	0.24	0.16	0.34	0.17	0.34	0.24	0.28	0.19	0.28	0.19
NiO	0.17	0.29	0.35	0.12	0.20	0.21	0.18	0.18	0.18	0.21	0.18	0.18	0.07	0.17	0.21	0.21	0.21	0.20	0.25	0.27	0.25	0.27
MgO	45.43	47.23	45.42	43.05	45.66	45.68	46.58	46.93	46.58	45.68	46.58	46.93	45.64	47.22	43.81	46.70	43.81	46.19	45.33	46.19	45.33	47.51
CaO	0.29	0.32	0.18	0.62	0.21	0.32	0.25	0.27	0.25	0.32	0.25	0.27	0.18	0.34	0.77	0.41	0.77	0.23	0.19	0.29	0.19	0.29
Na2O	0.22	0.08	0.10	0.24	0.23	0.14	0.00	0.27	0.00	0.14	0.00	0.27	0.34	0.17	0.26	0.39	0.26	0.02	0.33	0.28	0.33	0.28
K2O	0.00	0.01	0.00	0.00	0.01	0.04	0.00	0.00	0.00	0.04	0.00	0.00	0.02	0.00	0.02	0.00	0.02	0.01	0.00	0.02	0.00	0.02
Cl	0.00	0.02	0.01	0.00	0.00	0.02	0.00	0.00	0.00	0.02	0.00	0.00	0.01	0.02	0.02	0.00	0.02	0.00	0.02	0.00	0.02	0.00
P2O5	0.00	0.00	0.00	0.00	0.00	0.00	0.00	0.01	0.00	0.00	0.00	0.01	0.03	0.00	0.00	0.07	0.00	0.03	0.00	0.00	0.00	0.00
Total	100.74	100.45	100.21	100.50	100.11	100.17	99.63	100.55	99.63	100.17	99.63	100.55	100.84	100.09	101.00	101.27	101.00	100.81	100.76	100.81	100.76	100.66
per 4 oxygens																						
Si	0.99	0.99	0.99	0.99	0.99	0.99	0.99	0.99	0.99	0.99	0.99	0.99	0.99	0.99	0.99	0.99	0.99	0.99	0.99	0.99	0.99	0.99
Ti	0.00	0.00	0.00	0.00	0.00	0.00	0.00	0.00	0.00	0.00	0.00	0.00	0.00	0.00	0.00	0.00	0.00	0.00	0.00	0.00	0.00	0.00
Al	0.00	0.00	0.00	0.00	0.00	0.00	0.00	0.00	0.00	0.00	0.00	0.00	0.00	0.00	0.00	0.00	0.00	0.00	0.00	0.00	0.00	0.00
Cr	0.00	0.00	0.00	0.00	0.00	0.00	0.00	0.00	0.00	0.00	0.00	0.00	0.00	0.00	0.00	0.00	0.00	0.00	0.00	0.00	0.00	0.00
Fe	0.31	0.25	0.30	0.36	0.30	0.29	0.26	0.27	0.26	0.29	0.26	0.27	0.30	0.26	0.34	0.27	0.34	0.29	0.31	0.25	0.31	0.25
Mn	0.01	0.01	0.01	0.01	0.01	0.00	0.00	0.00	0.00	0.00	0.00	0.00	0.01	0.00	0.01	0.00	0.01	0.01	0.01	0.00	0.01	0.00
Ni	0.00	0.01	0.01	0.00	0.00	0.00	0.00	0.00	0.00	0.00	0.00	0.00	0.00	0.00	0.00	0.00	0.00	0.00	0.00	0.01	0.00	0.01
Mg	1.69	1.75	1.70	1.63	1.71	1.70	1.74	1.74	1.74	1.70	1.74	1.74	1.70	1.76	1.65	1.72	1.65	1.71	1.69	1.76	1.69	1.76
Ca	0.01	0.01	0.00	0.02	0.01	0.01	0.01	0.01	0.01	0.01	0.01	0.01	0.00	0.01	0.02	0.01	0.02	0.01	0.01	0.01	0.01	0.01
Na	0.01	0.00	0.01	0.01	0.01	0.01	0.00	0.01	0.00	0.01	0.00	0.01	0.02	0.01	0.01	0.02	0.01	0.00	0.02	0.01	0.02	0.01
K	0.00	0.00	0.00	0.00	0.00	0.00	0.00	0.00	0.00	0.00	0.00	0.00	0.00	0.00	0.00	0.00	0.00	0.00	0.00	0.00	0.00	0.00
P	0.00	0.00	0.00	0.00	0.00	0.00	0.00	0.00	0.00	0.00	0.00	0.00	0.00	0.00	0.00	0.00	0.00	0.00	0.00	0.00	0.00	0.00
Total	3.01	3.02	3.02	3.02	3.02	3.01	3.01	3.02	3.01	3.01	3.01	3.02	3.02	3.03	3.02	3.02	3.02	3.01	3.02	3.01	3.02	3.02
%Fo	84.49	86.99	84.59	81.58	85.03	85.34	86.70	86.42	86.70	85.34	86.70	86.42	84.67	87.08	82.58	86.25	82.58	85.45	84.14	85.45	84.14	87.25

Table A4.2

Cinopyroxenes	96AE11		96AE11		96AE11		96AE11		96AE11		96AE11		96AE13		96AE13		96AE13		96AE13	
	groundm. Melaleuc.	groundm. Melaleuc.	groundm. Melaleuc.	groundm. Melaleuc.	rim Melaleuc.	rim Melaleuc.	rim Melaleuc.	rim Melaleuc.	rim Melaleuc.	rim Melaleuc.	core Melaleuc.	core Melaleuc.	groundm. Melaleuc.	groundm. Melaleuc.	rim Melaleuc.	rim Melaleuc.	rim Melaleuc.	rim Melaleuc.	rim Melaleuc.	rim Melaleuc.
SiO2	50.03	45.80	49.14	48.91	45.19	48.81	48.97	48.79	49.59	48.62	47.73	48.31	45.67	48.21	48.31	45.67	48.21	48.31	45.67	48.21
TiO2	2.31	4.07	1.93	2.60	3.97	2.21	1.87	1.90	1.65	2.56	2.97	2.67	3.90	2.88	2.67	3.90	2.88	2.67	3.90	2.88
Al2O3	2.80	5.61	4.54	3.00	5.71	3.63	4.94	4.93	4.36	3.71	4.64	3.82	5.75	3.64	3.82	5.75	3.64	3.82	5.75	3.64
Cr2O3	0.34	0.51	0.39	0.28	0.09	0.69	0.64	0.64	0.44	0.23	0.18	0.25	0.34	0.20	0.25	0.34	0.20	0.25	0.34	0.20
FeO	4.89	5.76	5.53	5.07	6.35	4.55	5.33	5.37	5.09	5.79	5.99	5.80	6.64	6.00	5.80	6.64	6.00	5.80	6.64	6.00
MnO	0.07	0.03	0.03	0.09	0.04	0.08	0.14	0.00	0.13	0.08	0.11	0.09	0.13	0.08	0.09	0.13	0.08	0.09	0.13	0.08
NiO	0.00	0.03	0.04	0.00	0.04	0.00	0.00	0.12	0.04	0.04	0.04	0.00	0.10	0.05	0.00	0.10	0.05	0.00	0.10	0.05
MgO	15.46	13.63	14.28	14.77	13.29	14.98	14.49	14.44	15.15	14.28	14.20	14.38	13.14	14.04	14.38	13.14	14.04	14.38	13.14	14.04
CaO	24.11	23.88	23.03	24.30	24.48	23.89	22.70	22.61	22.57	23.77	23.65	23.57	23.76	23.89	23.57	23.76	23.89	23.57	23.76	23.89
Na2O	0.42	0.42	0.63	0.29	0.44	0.31	0.53	0.55	0.79	0.51	0.58	0.42	0.46	0.34	0.42	0.46	0.34	0.42	0.46	0.34
K2O	0.00	0.01	0.04	0.03	0.02	0.05	0.01	0.01	0.00	0.00	0.00	0.00	0.04	0.00	0.03	0.04	0.00	0.03	0.04	0.00
Cl	0.03	0.01	0.00	0.01	0.00	0.03	0.04	0.02	0.00	0.00	0.04	0.00	0.00	0.01	0.00	0.00	0.01	0.00	0.00	0.01
P2O5	0.00	0.07	0.17	0.08	0.14	0.11	0.03	0.07	0.08	0.05	0.06	0.08	0.12	0.10	0.08	0.12	0.10	0.08	0.12	0.10
Total	100.46	99.83	99.74	99.45	99.77	99.33	99.69	99.44	99.90	99.64	100.18	99.44	100.05	99.41	99.44	100.05	99.41	99.44	100.05	99.41
per 6 oxygens																				
Si	1.85	1.72	1.83	1.83	1.71	1.82	1.82	1.82	1.84	1.82	1.78	1.81	1.72	1.81	1.81	1.72	1.81	1.81	1.72	1.81
Ti	0.06	0.12	0.05	0.07	0.11	0.06	0.05	0.05	0.05	0.07	0.08	0.08	0.11	0.08	0.08	0.11	0.08	0.08	0.11	0.08
Al	0.12	0.25	0.20	0.13	0.25	0.16	0.22	0.22	0.19	0.16	0.20	0.17	0.26	0.16	0.17	0.26	0.16	0.17	0.26	0.16
Cr	0.01	0.02	0.01	0.01	0.00	0.02	0.02	0.02	0.01	0.01	0.01	0.01	0.01	0.01	0.01	0.01	0.01	0.01	0.01	0.01
Fe	0.15	0.18	0.17	0.16	0.20	0.14	0.17	0.17	0.16	0.18	0.19	0.18	0.21	0.19	0.18	0.21	0.19	0.18	0.21	0.19
Mn	0.00	0.00	0.00	0.00	0.00	0.00	0.00	0.00	0.00	0.00	0.00	0.00	0.00	0.00	0.00	0.00	0.00	0.00	0.00	0.00
Ni	0.00	0.00	0.00	0.00	0.00	0.00	0.00	0.00	0.00	0.00	0.00	0.00	0.00	0.00	0.00	0.00	0.00	0.00	0.00	0.00
Mg	0.85	0.76	0.79	0.82	0.75	0.83	0.80	0.80	0.84	0.80	0.79	0.80	0.74	0.79	0.80	0.74	0.79	0.80	0.74	0.79
Ca	0.95	0.96	0.92	0.97	0.99	0.96	0.90	0.90	0.90	0.95	0.95	0.95	0.96	0.96	0.95	0.96	0.96	0.95	0.96	0.96
Na	0.03	0.03	0.05	0.02	0.03	0.02	0.04	0.04	0.06	0.04	0.04	0.03	0.03	0.02	0.03	0.03	0.02	0.03	0.03	0.02
K	0.00	0.00	0.00	0.00	0.00	0.00	0.00	0.00	0.00	0.00	0.00	0.00	0.00	0.00	0.00	0.00	0.00	0.00	0.00	0.00
P	0.00	0.00	0.01	0.00	0.00	0.00	0.00	0.00	0.00	0.00	0.00	0.00	0.00	0.00	0.00	0.00	0.00	0.00	0.00	0.00
Total	4.04	4.04	4.03	4.03	4.06	4.03	4.03	4.03	4.04	4.04	4.05	4.04	4.05	4.03	4.04	4.05	4.03	4.04	4.05	4.03
En	42.81	39.40	41.09	41.59	37.94	42.62	41.93	41.96	42.88	40.43	40.15	40.88	37.98	40.05	40.88	37.98	40.05	40.88	37.98	40.05
Fs	7.70	9.40	8.97	8.16	10.22	7.38	8.87	8.75	8.29	9.33	9.68	9.39	10.97	9.72	9.39	10.97	9.72	9.39	10.97	9.72
Wo	47.96	49.61	47.60	49.19	50.20	48.85	47.20	47.21	45.91	48.37	48.05	48.17	49.33	48.98	48.17	49.33	48.98	48.17	49.33	48.98
Ac	1.52	1.59	2.34	1.06	1.63	1.15	2.01	2.07	2.92	1.86	2.12	1.56	1.71	1.24	1.56	1.71	1.24	1.56	1.71	1.24

Table A4.2

Cinopyroxenes	96AE18		96AE18		96AE18		96AE18		96AE18		96AE18		96AE18		96AE22		96AE22		96AE22		96AE22	
	rim Basanite	core Basanite	rim Basanite	core Basanite	rim Basanite	core Basanite	rim Basanite	core Basanite	rim Basanite	core Basanite	rim Basanite	core Basanite	rim Basanite	core Basanite	rim Melaleuc.	core Melaleuc.	rim Melaleuc.	core Melaleuc.	rim Melaleuc.	core Melaleuc.	rim Melaleuc.	core Melaleuc.
SiO ₂	47.53	50.11	47.72	49.70	47.89	48.77	47.78	47.82	47.89	51.78	47.89	47.63	47.89	46.96	48.86	49.87	46.96	47.89	47.63	47.89	48.86	49.87
TiO ₂	2.59	1.68	2.77	1.70	2.45	2.24	2.55	2.40	2.50	1.02	2.50	3.64	2.50	3.71	2.22	1.73	3.71	2.50	3.64	2.50	2.22	1.73
Al ₂ O ₃	5.47	3.55	5.37	3.77	5.18	4.44	5.94	5.47	5.07	2.18	5.07	4.33	5.07	4.72	3.74	4.11	4.72	5.07	4.33	5.07	3.74	4.11
Cr ₂ O ₃	0.02	0.07	0.13	0.10	0.08	0.02	0.19	0.08	0.08	0.84	0.16	0.09	0.16	0.08	1.08	0.40	0.09	0.16	0.09	1.08	0.40	0.40
FeO	7.11	7.45	6.83	7.44	7.24	7.53	7.14	7.30	7.15	4.64	7.15	5.65	7.15	6.60	4.44	5.11	6.60	7.15	5.65	7.15	4.44	5.11
MnO	0.21	0.41	0.16	0.27	0.25	0.23	0.08	0.24	0.17	0.16	0.17	0.08	0.17	0.10	0.07	0.05	0.10	0.17	0.08	0.07	0.05	0.05
NiO	0.00	0.05	0.00	0.00	0.04	0.01	0.04	0.05	0.05	0.04	0.05	0.09	0.05	0.03	0.00	0.00	0.03	0.05	0.09	0.00	0.00	0.00
MgO	13.54	14.29	13.73	13.90	13.45	13.41	13.69	13.61	13.61	16.76	13.86	13.92	13.86	12.77	14.85	15.33	12.77	13.86	13.92	14.85	15.33	15.33
CaO	22.50	22.27	22.98	22.65	22.35	22.81	22.34	22.40	22.40	22.41	22.67	24.33	22.67	23.97	24.17	22.22	23.97	22.67	24.33	24.17	24.17	22.22
Na ₂ O	0.51	0.92	0.64	0.77	0.46	0.43	0.86	0.57	0.57	0.60	0.57	0.21	0.57	0.68	0.19	0.67	0.21	0.57	0.21	0.19	0.67	0.67
K ₂ O	0.05	0.03	0.03	0.00	0.01	0.00	0.00	0.01	0.01	0.00	0.00	0.00	0.01	0.02	0.01	0.01	0.00	0.01	0.03	0.02	0.01	0.01
Cl	0.02	0.04	0.00	0.01	0.02	0.01	0.00	0.00	0.00	0.00	0.02	0.01	0.00	0.00	0.00	0.03	0.00	0.02	0.00	0.00	0.00	0.03
P ₂ O ₅	0.08	0.05	0.04	0.14	0.00	0.10	0.17	0.00	0.00	0.10	0.00	0.05	0.00	0.04	0.02	0.02	0.05	0.00	0.05	0.02	0.02	0.02
Total	99.63	100.91	100.40	100.46	99.42	100.00	100.77	99.96	99.96	100.54	100.09	100.05	100.09	99.70	99.65	99.55	99.70	100.09	100.05	99.65	99.65	99.55
per 6 oxygens																						
Si	1.78	1.86	1.78	1.85	1.80	1.82	1.77	1.79	1.79	1.90	1.79	1.78	1.79	1.77	1.82	1.85	1.78	1.79	1.78	1.82	1.85	1.85
Ti	0.07	0.05	0.08	0.05	0.07	0.06	0.07	0.07	0.07	0.03	0.07	0.10	0.07	0.11	0.06	0.05	0.10	0.07	0.10	0.06	0.05	0.05
Al	0.24	0.15	0.24	0.17	0.23	0.20	0.26	0.24	0.24	0.09	0.22	0.19	0.22	0.21	0.16	0.18	0.19	0.22	0.19	0.16	0.16	0.18
Cr	0.00	0.00	0.00	0.00	0.00	0.00	0.01	0.00	0.00	0.02	0.00	0.00	0.00	0.00	0.03	0.01	0.00	0.00	0.00	0.03	0.01	0.01
Fe	0.22	0.23	0.21	0.23	0.23	0.24	0.22	0.23	0.23	0.14	0.22	0.18	0.22	0.21	0.14	0.16	0.18	0.22	0.18	0.14	0.14	0.16
Mn	0.01	0.01	0.01	0.01	0.01	0.01	0.00	0.01	0.01	0.00	0.01	0.00	0.01	0.00	0.00	0.00	0.00	0.01	0.00	0.00	0.00	0.00
Ni	0.00	0.00	0.00	0.00	0.00	0.00	0.00	0.00	0.00	0.00	0.00	0.00	0.00	0.00	0.00	0.00	0.00	0.00	0.00	0.00	0.00	0.00
Mg	0.76	0.79	0.76	0.77	0.75	0.75	0.76	0.76	0.76	0.92	0.77	0.78	0.77	0.72	0.83	0.85	0.78	0.77	0.78	0.83	0.85	0.85
Ca	0.91	0.88	0.92	0.90	0.90	0.91	0.89	0.90	0.90	0.88	0.91	0.97	0.91	0.97	0.96	0.88	0.97	0.91	0.97	0.96	0.88	0.88
Na	0.04	0.07	0.05	0.06	0.03	0.03	0.06	0.04	0.04	0.04	0.04	0.02	0.04	0.05	0.01	0.05	0.02	0.04	0.02	0.01	0.05	0.05
K	0.00	0.00	0.00	0.00	0.00	0.00	0.00	0.00	0.00	0.00	0.00	0.00	0.00	0.00	0.00	0.00	0.00	0.00	0.00	0.00	0.00	0.00
P	0.00	0.00	0.00	0.00	0.00	0.00	0.01	0.00	0.00	0.00	0.00	0.00	0.00	0.00	0.00	0.00	0.00	0.00	0.00	0.00	0.00	0.00
Total	4.04	4.05	4.05	4.04	4.03	4.02	4.05	4.04	4.04	4.03	4.04	4.03	4.04	4.04	4.03	4.03	4.03	4.04	4.03	4.03	4.03	4.03
En	39.28	39.80	39.23	39.15	39.20	38.62	39.22	39.23	39.23	46.13	39.61	39.90	39.61	36.86	42.43	43.73	36.86	39.61	39.90	42.43	43.73	43.73
Fs	11.91	12.29	11.21	12.17	12.24	12.55	11.59	12.20	12.20	7.41	11.72	9.22	11.72	10.85	7.23	8.25	10.85	11.72	9.22	7.23	8.25	8.25
Wo	46.90	44.58	47.17	45.84	46.81	47.23	46.00	46.42	46.42	44.31	46.55	50.11	46.55	49.74	49.62	45.55	49.74	46.55	50.11	49.62	45.55	45.55
Ac	1.91	3.34	2.39	2.84	1.76	1.60	3.19	2.15	2.15	2.15	2.11	0.78	2.11	2.55	0.72	2.48	2.55	2.11	0.78	0.72	2.48	2.48

Table A4.2

Cinopyroxenes	96AE22		96AE22		96AE22		96AE22		96AE22		96AE22		96AE22		96AE22	
	core Melaleuc.	Melaleuc.	rim Melaleuc.	Melaleuc.	core Melaleuc.	Melaleuc.	rim Melaleuc.	Melaleuc.	core Melaleuc.	Melaleuc.	rim Melaleuc.	Melaleuc.	core Melaleuc.	Melaleuc.	rim Melaleuc.	Melaleuc.
SiO ₂	49.99	51.76	46.75	49.65	47.59	44.10	49.29	49.31	49.67	44.04	48.94	43.74	48.94	44.04	43.74	45.78
TiO ₂	1.71	1.15	3.42	2.73	3.49	5.23	2.15	1.62	1.60	4.96	1.87	5.16	1.87	4.96	5.16	4.12
Al ₂ O ₃	4.31	2.26	5.14	2.68	4.70	7.11	3.42	4.71	4.61	7.41	4.43	6.81	4.43	7.41	6.81	5.46
Cr ₂ O ₃	0.49	1.05	0.96	0.12	0.10	0.12	1.04	0.27	0.32	0.03	0.70	0.14	0.70	0.03	0.14	0.28
FeO	5.05	3.98	5.28	6.54	5.68	6.44	4.27	4.95	4.94	6.45	5.74	6.44	5.74	6.45	6.44	6.05
MnO	0.08	0.05	0.01	0.19	0.09	0.03	0.08	0.10	0.12	0.04	0.06	0.11	0.06	0.04	0.11	0.11
NiO	0.04	0.09	0.07	0.00	0.00	0.04	0.00	0.09	0.00	0.05	0.11	0.00	0.11	0.05	0.00	0.00
MgO	14.98	16.39	13.72	13.48	13.65	12.31	15.28	15.15	15.03	11.69	14.31	12.29	14.31	11.69	12.29	13.42
CaO	22.36	23.21	24.09	24.01	24.39	23.94	24.01	22.51	22.61	24.03	22.74	24.03	22.74	24.03	24.03	23.84
Na ₂ O	0.97	0.35	0.33	0.59	0.40	0.48	0.44	0.64	0.60	0.46	0.62	0.31	0.62	0.46	0.31	0.31
K ₂ O	0.06	0.05	0.00	0.05	0.01	0.05	0.05	0.01	0.02	0.01	0.00	0.03	0.00	0.01	0.03	0.02
Cl	0.02	0.00	0.00	0.00	0.03	0.03	0.01	0.00	0.00	0.05	0.00	0.00	0.00	0.05	0.00	0.02
P ₂ O ₅	0.01	0.00	0.12	0.10	0.07	0.00	0.01	0.03	0.12	0.10	0.07	0.03	0.07	0.10	0.03	0.11
Total	100.06	100.34	99.89	100.16	100.20	99.89	100.07	99.40	99.63	99.32	99.59	99.09	99.59	99.32	99.09	99.53
per 6 oxygens																
Si	1.85	1.90	1.75	1.86	1.78	1.67	1.83	1.83	1.84	1.67	1.83	1.67	1.83	1.67	1.67	1.73
Ti	0.05	0.03	0.10	0.08	0.10	0.15	0.06	0.05	0.04	0.14	0.05	0.15	0.05	0.14	0.15	0.12
Al	0.19	0.10	0.23	0.12	0.21	0.32	0.15	0.21	0.20	0.33	0.20	0.31	0.20	0.33	0.31	0.24
Cr	0.01	0.03	0.03	0.00	0.00	0.00	0.03	0.01	0.01	0.00	0.02	0.00	0.02	0.00	0.00	0.01
Fe	0.16	0.12	0.17	0.20	0.18	0.20	0.13	0.15	0.15	0.20	0.18	0.21	0.18	0.20	0.21	0.19
Mn	0.00	0.00	0.00	0.01	0.00	0.00	0.00	0.00	0.00	0.00	0.00	0.00	0.00	0.00	0.00	0.00
Ni	0.00	0.00	0.00	0.00	0.00	0.00	0.00	0.00	0.00	0.00	0.00	0.00	0.00	0.00	0.00	0.00
Mg	0.83	0.90	0.77	0.75	0.76	0.69	0.85	0.84	0.83	0.66	0.80	0.70	0.80	0.66	0.70	0.75
Ca	0.89	0.91	0.97	0.96	0.98	0.97	0.95	0.90	0.90	0.98	0.91	0.98	0.91	0.98	0.98	0.96
Na	0.07	0.02	0.02	0.04	0.03	0.04	0.03	0.05	0.04	0.03	0.05	0.02	0.05	0.03	0.02	0.02
K	0.00	0.00	0.00	0.00	0.00	0.00	0.00	0.00	0.00	0.00	0.00	0.00	0.00	0.00	0.00	0.00
P	0.00	0.00	0.00	0.00	0.00	0.00	0.00	0.00	0.00	0.00	0.00	0.00	0.00	0.00	0.00	0.00
Total	4.04	4.02	4.03	4.03	4.03	4.04	4.04	4.04	4.03	4.03	4.03	4.04	4.03	4.03	4.04	4.04
En	42.57	45.81	39.85	38.20	39.07	36.46	42.98	43.30	43.08	35.20	41.21	36.55	41.21	35.20	36.55	38.99
Fs	8.18	6.32	8.62	10.71	9.27	10.75	6.87	8.10	8.13	10.96	9.38	10.92	9.38	10.96	10.92	10.04
Wo	45.65	46.61	50.27	48.91	50.17	50.94	48.53	46.24	46.57	52.02	47.07	51.33	47.07	52.02	51.33	49.78
Ac	3.60	1.26	1.26	2.17	1.48	1.85	1.61	2.37	2.22	1.82	2.34	1.20	2.34	1.82	1.20	1.19

Table A4.2

Cinopyroxenes	96AE22		96AE22		96AE22		96AE22		96AE22		96AE46		96AE46		96AE46		96AE46		96AE46		
	Melaleuc.	Melaleuc.	Melaleuc.	Melaleuc.	Melaleuc.	Melaleuc.	Melaleuc.	Melaleuc.	Melaleuc.	Melaleuc.	Melaleuc.	Melaleuc.	Melaleuc.	Melaleuc.	Melaleuc.	Melaleuc.	Melaleuc.	Melaleuc.	Melaleuc.	Melaleuc.	
SiO ₂	44.83	48.96	47.35	50.54	48.17	47.39	41.91	45.84	47.04	46.54	46.86	47.50	44.36	42.99	47.00						
TiO ₂	4.56	2.05	2.80	2.23	3.27	3.66	4.95	3.58	3.41	3.28	3.30	2.79	4.38	4.72	3.13						
Al ₂ O ₃	6.38	4.97	4.73	2.17	3.97	4.41	8.87	5.78	4.94	4.99	5.13	5.86	7.77	8.49	5.73						
Cr ₂ O ₃	0.38	0.94	1.03	0.10	0.09	0.00	0.06	0.07	0.12	0.14	0.08	0.07	0.11	0.01	0.03						
FeO	6.15	4.89	4.86	6.46	5.68	5.66	6.86	6.40	5.94	5.84	6.02	7.61	7.72	7.15	7.10						
MnO	0.05	0.13	0.14	0.14	0.14	0.08	0.10	0.08	0.03	0.08	0.03	0.15	0.15	0.15	0.19						
NiO	0.10	0.00	0.01	0.04	0.00	0.00	0.01	0.02	0.05	0.05	0.00	0.01	0.00	0.02	0.13						
MgO	12.89	14.64	14.20	14.05	13.74	13.84	12.99	13.25	14.00	13.79	13.69	12.81	11.37	11.83	12.34						
CaO	24.28	22.60	23.86	24.42	24.32	24.26	22.52	24.40	24.53	24.39	24.37	22.49	22.69	24.29	22.72						
Na ₂ O	0.30	0.54	0.26	0.51	0.36	0.38	0.49	0.38	0.26	0.41	0.55	0.82	0.52	0.42	0.82						
K ₂ O	0.01	0.00	0.00	0.04	0.00	0.03	0.13	0.00	0.02	0.00	0.02	0.01	0.02	0.00	0.03						
Cl	0.02	0.00	0.00	0.01	0.00	0.03	0.01	0.01	0.04	0.00	0.00	0.00	0.00	0.00	0.00						
P ₂ O ₅	0.00	0.01	0.05	0.03	0.12	0.01	0.15	0.18	0.07	0.04	0.09	0.03	0.03	0.08	0.01						
Total	99.96	99.75	99.29	100.74	99.88	99.73	99.06	99.99	100.45	99.53	100.14	100.16	99.12	100.14	99.24						
per 6 oxygens																					
Si	1.69	1.82	1.78	1.88	1.80	1.78	1.60	1.73	1.76	1.75	1.76	1.78	1.69	1.63	1.78						
Ti	0.13	0.06	0.08	0.06	0.09	0.10	0.14	0.10	0.10	0.09	0.09	0.08	0.13	0.13	0.09						
Al	0.28	0.22	0.21	0.09	0.18	0.19	0.40	0.26	0.22	0.22	0.23	0.26	0.35	0.38	0.26						
Cr	0.01	0.03	0.03	0.00	0.00	0.00	0.00	0.00	0.00	0.00	0.00	0.00	0.00	0.00	0.00						
Fe	0.19	0.15	0.15	0.20	0.18	0.18	0.22	0.20	0.19	0.18	0.19	0.24	0.25	0.23	0.22						
Mn	0.00	0.00	0.00	0.00	0.00	0.00	0.00	0.00	0.00	0.00	0.00	0.00	0.00	0.00	0.01						
Ni	0.00	0.00	0.00	0.00	0.00	0.00	0.00	0.00	0.00	0.00	0.00	0.00	0.00	0.00	0.00						
Mg	0.73	0.81	0.80	0.78	0.77	0.77	0.74	0.74	0.78	0.77	0.76	0.72	0.65	0.67	0.70						
Ca	0.98	0.90	0.96	0.97	0.97	0.98	0.92	0.98	0.98	0.99	0.98	0.90	0.93	0.99	0.92						
Na	0.02	0.04	0.02	0.04	0.03	0.03	0.04	0.03	0.02	0.03	0.04	0.06	0.04	0.03	0.06						
K	0.00	0.00	0.00	0.00	0.00	0.00	0.01	0.00	0.00	0.00	0.00	0.00	0.00	0.00	0.00						
P	0.00	0.00	0.00	0.00	0.00	0.00	0.00	0.01	0.00	0.00	0.00	0.00	0.00	0.00	0.00						
Total	4.04	4.02	4.03	4.03	4.02	4.04	4.07	4.05	4.04	4.05	4.05	4.04	4.03	4.06	4.04						
En	37.68	42.55	41.17	39.07	39.31	39.56	38.53	37.94	39.65	39.21	38.77	37.24	34.71	34.87	36.48						
Fs	10.17	8.19	8.14	10.29	9.34	9.20	11.58	10.40	9.48	9.44	9.61	12.67	13.48	12.07	12.10						
Wo	51.01	47.20	49.72	48.79	50.01	49.84	47.99	50.23	49.92	49.85	49.59	46.99	49.76	51.44	48.27						
Ac	1.14	2.06	0.97	1.85	1.34	1.40	1.90	1.43	0.94	1.50	2.03	3.11	2.05	1.62	3.14						

Table A4.2

Cinopyroxenes		96AE46	96AE46	96AE46	96AE46	96AE46	96AE46	96AE46	96AE46	96AE57	96AE57	96AE57	96AE57	96AE57	96AE57	96AE57
	Melaneph. (?)	Melaneph. (?)	Melaneph. (?)	Melaneph. (?)	Melaneph. (?)	Melaneph. (?)	Melaneph. (?)	Melaneph. (?)	Melaneph. (?)	Leucitite	Leucitite	Leucitite	Leucitite	Leucitite	Leucitite	Leucitite
SiO ₂	48.16	49.12	46.48	45.95	46.37	43.66	46.96	4.11	4.50	46.86	44.42	47.89	42.67	47.89	42.67	47.89
TiO ₂	2.70	2.48	3.46	3.67	3.52	5.46	4.11	4.00	4.00	4.00	4.89	2.46	5.97	2.46	5.97	2.46
Al ₂ O ₃	4.64	3.95	5.14	5.58	5.49	7.09	4.50	4.67	4.67	4.67	6.51	4.26	7.83	4.26	7.83	4.26
Cr ₂ O ₃	0.06	0.01	0.05	0.10	0.10	0.14	0.12	0.09	0.09	0.09	0.20	0.19	0.09	0.19	0.09	0.19
FeO	6.76	6.72	5.85	6.09	6.17	6.45	6.10	5.75	5.75	5.75	5.99	5.44	6.61	5.44	6.61	5.44
MnO	0.18	0.18	0.11	0.02	0.02	0.04	0.04	0.08	0.08	0.08	0.08	0.00	0.04	0.00	0.04	0.00
NiO	0.04	0.03	0.00	0.07	0.03	0.00	0.00	0.06	0.06	0.06	0.01	0.06	0.03	0.06	0.03	0.06
MgO	13.83	13.48	13.62	13.49	13.50	12.64	13.96	13.95	13.95	13.95	12.95	14.40	12.21	14.40	12.21	14.40
CaO	23.22	23.17	24.46	24.41	24.52	24.01	23.41	24.23	24.23	24.23	24.06	24.38	23.51	24.38	23.51	24.38
Na ₂ O	0.43	0.46	0.19	0.39	0.57	0.44	0.74	0.29	0.29	0.29	0.42	0.34	0.39	0.34	0.39	0.34
K ₂ O	0.04	0.00	0.01	0.00	0.04	0.03	0.04	0.00	0.00	0.00	0.00	0.00	0.05	0.00	0.05	0.00
Cl	0.01	0.01	0.01	0.00	0.00	0.00	0.00	0.01	0.01	0.01	0.00	0.02	0.00	0.02	0.00	0.02
P ₂ O ₅	0.09	0.05	0.04	0.02	0.19	0.00	0.07	0.08	0.08	0.08	0.00	0.11	0.14	0.11	0.14	0.11
Total	100.16	99.68	99.42	99.79	100.52	99.94	100.03	100.09	100.09	100.09	99.54	99.56	99.55	99.56	99.55	99.56
per 6 oxygens																
Si	1.80	1.84	1.75	1.73	1.73	1.65	1.76	1.75	1.75	1.75	1.68	1.80	1.62	1.80	1.62	1.80
Ti	0.08	0.07	0.10	0.10	0.10	0.16	0.12	0.11	0.11	0.11	0.14	0.07	0.17	0.07	0.17	0.07
Al	0.20	0.17	0.23	0.25	0.24	0.32	0.20	0.21	0.21	0.21	0.29	0.19	0.35	0.19	0.35	0.19
Cr	0.00	0.00	0.00	0.00	0.00	0.00	0.00	0.00	0.00	0.00	0.01	0.01	0.00	0.01	0.00	0.01
Fe	0.21	0.21	0.18	0.19	0.19	0.20	0.19	0.18	0.18	0.18	0.19	0.17	0.21	0.17	0.21	0.17
Mn	0.01	0.01	0.00	0.00	0.00	0.00	0.00	0.00	0.00	0.00	0.00	0.00	0.00	0.00	0.00	0.00
Ni	0.00	0.00	0.00	0.00	0.00	0.00	0.00	0.00	0.00	0.00	0.00	0.00	0.00	0.00	0.00	0.00
Mg	0.77	0.75	0.77	0.76	0.75	0.71	0.78	0.78	0.78	0.78	0.73	0.81	0.69	0.81	0.69	0.81
Ca	0.93	0.93	0.99	0.99	0.98	0.97	0.94	0.97	0.97	0.97	0.98	0.98	0.96	0.98	0.96	0.98
Na	0.03	0.03	0.01	0.03	0.04	0.03	0.05	0.02	0.02	0.02	0.03	0.02	0.03	0.02	0.03	0.02
K	0.00	0.00	0.00	0.00	0.00	0.00	0.00	0.00	0.00	0.00	0.00	0.00	0.00	0.00	0.00	0.00
P	0.00	0.00	0.00	0.00	0.01	0.00	0.00	0.00	0.00	0.00	0.00	0.00	0.00	0.00	0.00	0.00
Total	4.03	4.02	4.04	4.05	4.06	4.05	4.05	4.03	4.03	4.03	4.05	4.04	4.04	4.04	4.04	4.04
En	39.55	38.95	39.15	38.57	38.20	37.06	39.67	39.85	39.85	39.85	37.88	40.66	36.62	40.66	36.62	40.66
Fs	11.14	11.19	9.61	9.81	9.82	10.66	9.79	9.34	9.34	9.34	9.95	8.62	11.18	8.62	11.18	8.62
Wo	47.72	48.11	50.53	50.17	49.86	50.59	47.82	49.74	49.74	49.74	50.56	49.47	50.67	49.47	50.67	49.47
Ac	1.60	1.74	0.70	1.45	2.11	1.69	2.72	1.07	1.07	1.07	1.60	1.25	1.52	1.25	1.52	1.25

Table A4.3

Feldspathoids										
	96AE04	96AE04	96AE08	96AE08	96AE08	96AE08	96AE22	96AE22	96AE22	96AE57
	Meleleuc.	Meleleuc.	Melaneph. (?)	Melaneph. (?)	Melaneph. (?)	Melaneph. (?)	Meleleuc.	Meleleuc.	Meleleuc.	Leucitite
SiO2	40.43	40.33	40.21	40.88	37.77	40.74	40.84	40.62	40.94	40.67
TiO2	0.06	0.02	0.06	0.04	0.08	0.05	0.06	0.06	0.09	0.09
Al2O3	32.91	32.87	32.62	32.84	30.52	32.75	32.98	32.68	33.21	32.88
Cr2O3	0.01	0.03	0.05	0.00	0.06	0.00	0.04	0.08	0.03	0.03
FeO	1.03	0.87	1.44	1.09	1.23	0.78	0.63	0.79	0.69	0.66
MnO	0.00	0.00	0.00	0.08	0.06	0.02	0.00	0.00	0.00	0.05
NiO	0.00	0.00	0.01	0.05	0.04	0.01	0.01	0.02	0.00	0.00
MgO	0.00	0.02	0.16	0.21	0.22	0.09	0.00	0.48	0.12	0.15
CaO	0.30	0.11	0.06	0.08	0.02	0.13	0.07	0.41	0.47	0.06
Na2O	14.78	14.53	15.00	14.62	1.35	14.44	14.04	13.98	13.77	13.95
K2O	9.45	10.47	9.64	9.74	28.83	10.41	10.94	10.11	10.55	11.17
Cl	0.00	0.02	0.00	0.00	0.03	0.00	0.00	0.00	0.01	0.00
P2O5	0.06	0.03	0.00	0.00	0.00	0.00	0.00	0.00	0.00	0.00
Total	99.01	99.30	99.24	99.65	100.22	99.42	99.60	99.22	99.88	99.72
per 32 oxygens										
Si	8.05	8.04	8.02	8.09	8.01	8.10	8.10	8.07	8.08	8.08
Ti	0.01	0.00	0.01	0.01	0.01	0.01	0.01	0.01	0.01	0.01
Al	7.72	7.72	7.67	7.66	7.63	7.67	7.71	7.65	7.73	7.69
Cr	0.00	0.00	0.01	0.00	0.01	0.00	0.01	0.01	0.01	0.00
Fe	0.17	0.14	0.24	0.18	0.22	0.13	0.10	0.13	0.11	0.11
Mn	0.00	0.00	0.00	0.01	0.01	0.00	0.00	0.00	0.00	0.01
Ni	0.00	0.00	0.00	0.01	0.01	0.00	0.00	0.00	0.00	0.00
Mg	0.00	0.01	0.05	0.06	0.07	0.03	0.00	0.14	0.04	0.05
Ca	0.06	0.02	0.01	0.02	0.01	0.03	0.01	0.09	0.10	0.01
Na	5.70	5.61	5.80	5.61	0.56	5.56	5.40	5.38	5.27	5.37
K	2.40	2.66	2.45	2.46	7.80	2.64	2.77	2.56	2.66	2.83
P	0.01	0.01	0.00	0.00	0.00	0.00	0.00	0.00	0.00	0.00
Total	24.12	24.22	24.26	24.11	24.33	24.16	24.12	24.06	24.00	24.16
Ne	70.39	67.84	70.29	69.53	6.66	67.83	66.11	67.76	66.48	65.49
Ks	29.61	32.16	29.71	30.47	93.34	32.17	33.89	32.24	33.52	34.51

Table A4.4

Feldspars	96AE13	96AE18	96AE18	96AE18	96AE18	96AE18	96AE18	96AE22
	Melaleuc.	Basanite	Basanite	Basanite	Basanite	Basanite	Basanite	Melaleuc.
SiO2	62.38	56.03	52.79	54.01	55.72	55.85	62.47	
TiO2	0.14	0.34	0.35	0.27	0.59	0.44	0.15	
Al2O3	18.77	26.16	28.51	27.74	20.57	26.62	18.70	
Cr2O3	0.00	0.00	0.02	0.05	0.00	0.01	0.01	
FeO	0.32	0.79	0.77	0.72	1.46	0.74	0.25	
MnO	0.03	0.08	0.04	0.02	0.00	0.01	0.00	
NiO	0.08	0.04	0.00	0.03	0.00	0.00	0.06	
MgO	0.05	0.09	0.08	0.00	1.85	0.20	0.80	
CaO	0.06	8.92	11.37	10.20	9.37	8.85	0.00	
Na2O	0.38	6.20	5.18	5.62	6.23	6.29	0.13	
K2O	16.83	0.64	0.29	0.33	1.74	0.76	16.95	
Cl	0.00	0.02	0.01	0.00	0.02	0.00	0.02	
P2O5	0.00	0.00	0.00	0.00	1.57	0.00	0.00	
Total	99.03	99.31	99.40	99.00	99.13	99.79	99.56	
per 32 oxygens								
Si	11.76	10.21	9.68	9.90	10.30	10.14	11.71	
Ti	0.02	0.05	0.05	0.04	0.08	0.06	0.02	
Al	4.17	5.62	6.16	5.99	4.48	5.69	4.13	
Cr	0.00	0.00	0.00	0.01	0.00	0.00	0.00	
Fe	0.05	0.12	0.12	0.11	0.23	0.11	0.04	
Mn	0.00	0.01	0.01	0.00	0.00	0.00	0.00	
Ni	0.01	0.01	0.00	0.00	0.00	0.00	0.01	
Mg	0.01	0.02	0.02	0.00	0.51	0.05	0.22	
Ca	0.01	1.72	2.20	1.98	1.83	1.70	0.00	
Na	0.14	2.19	1.84	2.00	2.23	2.21	0.05	
K	4.05	0.15	0.07	0.08	0.41	0.18	4.05	
P	0.00	0.00	0.00	0.00	0.25	0.00	0.00	
soma	20.23	20.10	20.15	20.10	20.33	20.15	20.25	
An	0.28	42.38	53.61	48.80	40.93	41.56	0.00	
Ab	3.29	53.96	44.75	49.29	49.88	54.11	1.17	
Or	96.43	3.66	1.64	1.91	9.19	4.33	98.83	

Table A4.5

Perovskites												
	96AE22	96AE22	96AE46	96AE46	96AE46	96AE46	96AE46	96AE46	96AE46	96AE57	96AE57	96AE57
	Melaleuc.	Melaleuc.	Melaneph. (?)	Melaneph. (?)	Melaneph. (?)	Melaneph. (?)	Melaneph. (?)	Melaneph. (?)	Melaneph. (?)	Leucitite	Leucitite	Leucitite
SiO ₂	0.21	0.25	0.26	0.18	0.18	0.18	0.20	0.18	0.18	0.18	0.24	0.53
TiO ₂	58.89	59.29	58.54	58.15	58.43	58.38	58.38	58.15	59.48	59.47	59.47	58.37
Al ₂ O ₃	0.24	0.34	0.31	0.29	0.28	0.30	0.30	0.28	0.18	0.21	0.21	0.30
Cr ₂ O ₃	0.00	0.00	0.00	0.00	0.00	0.00	0.00	0.00	0.00	0.00	0.00	0.00
FeO	0.94	0.87	1.38	1.37	1.38	1.28	1.28	1.47	0.98	0.91	0.91	1.01
MnO	0.00	0.00	0.00	0.00	0.00	0.03	0.03	0.00	0.00	0.00	0.00	0.00
NiO	0.07	0.03	0.07	0.08	0.16	0.06	0.06	0.10	0.00	0.00	0.00	0.05
MgO	0.06	0.10	0.00	0.06	0.00	0.11	0.11	0.08	0.14	0.02	0.02	0.10
CaO	38.65	38.72	39.29	39.05	39.36	39.28	39.28	38.98	39.45	39.88	39.88	38.73
Na ₂ O	0.63	0.30	0.40	0.21	0.22	0.31	0.31	0.26	0.39	0.20	0.20	0.03
K ₂ O	0.04	0.04	0.03	0.03	0.06	0.08	0.08	0.05	0.05	0.07	0.07	0.28
Cl	0.01	0.00	0.01	0.00	0.03	0.00	0.00	0.00	0.01	0.00	0.00	0.01
P ₂ O ₅	0.00	0.00	0.00	0.00	0.00	0.00	0.00	0.00	0.00	0.00	0.00	0.00
Total	99.73	99.92	100.29	99.41	100.10	100.01	100.01	99.55	100.86	101.00	101.00	99.41
per 3 oxygens												
Si	0.00	0.01	0.01	0.00	0.00	0.00	0.00	0.00	0.00	0.00	0.01	0.01
Ti	1.00	1.01	0.99	1.00	1.00	0.99	0.99	1.00	1.00	1.00	1.00	1.00
Al	0.01	0.01	0.01	0.01	0.01	0.01	0.01	0.01	0.00	0.01	0.01	0.01
Cr	0.00	0.00	0.00	0.00	0.00	0.00	0.00	0.00	0.00	0.00	0.00	0.00
Fe	0.02	0.02	0.03	0.03	0.03	0.02	0.02	0.03	0.02	0.02	0.02	0.02
Mn	0.00	0.00	0.00	0.00	0.00	0.00	0.00	0.00	0.00	0.00	0.00	0.00
Ni	0.00	0.00	0.00	0.00	0.00	0.00	0.00	0.00	0.00	0.00	0.00	0.00
Mg	0.00	0.00	0.00	0.00	0.00	0.00	0.00	0.00	0.00	0.00	0.00	0.00
Ca	0.94	0.94	0.95	0.95	0.95	0.95	0.95	0.95	0.95	0.96	0.96	0.94
Na	0.03	0.01	0.02	0.01	0.01	0.01	0.01	0.01	0.02	0.01	0.01	0.00
K	0.00	0.00	0.00	0.00	0.00	0.00	0.00	0.00	0.00	0.00	0.00	0.01
Cl	0.00	0.00	0.00	0.00	0.00	0.00	0.00	0.00	0.00	0.00	0.00	0.00
P	0.00	0.00	0.00	0.00	0.00	0.00	0.00	0.00	0.00	0.00	0.00	0.00
Total	2.00	1.99	2.01	2.00	2.00	2.01	2.01	2.00	2.00	2.00	2.00	1.99

Table A4.6

Opaques	96AE04		96AE04		96AE04		96AE04		96AE04		96AE04		96AE08		96AE08		96AE11		96AE11		96AE11	
	Melaleuc.	Melaleuc.	Melaleuc.	Melaleuc.	Melaleuc.	Melaleuc.	Melaleuc.	Melaleuc.	Melaleuc.	Melaleuc.	Melaleuc.	Melaleuc.	Melaleuc.	Melaleuc. (?)	Melaleuc. (?)	Melaleuc. (?)	Melaleuc.	Melaleuc.	Melaleuc.	Melaleuc.	Melaleuc.	Melaleuc.
SiO ₂	0.10	0.11	0.19	0.17	0.21	3.18	0.05	2.56	0.24	0.43	0.14	0.13	0.43	0.14	0.13	0.14	0.13	0.14	0.13	0.13	0.38	0.38
TiO ₂	39.27	28.07	28.62	14.90	18.24	8.20	20.00	19.41	22.64	22.62	18.00	16.62	22.62	18.00	16.62	18.00	16.62	18.00	16.62	16.62	16.40	16.40
Al ₂ O ₃	0.76	1.12	1.04	0.96	1.30	1.39	0.78	1.26	0.28	0.37	3.18	3.36	0.37	3.18	3.36	3.18	3.36	3.18	3.36	3.53	3.53	3.53
Cr ₂ O ₃	1.66	1.58	1.77	2.03	1.77	1.43	1.33	0.05	0.18	0.18	2.12	1.95	0.18	2.12	1.95	2.12	1.95	2.12	1.95	2.93	2.93	2.93
Fe ₂ O ₃	0.00	9.55	10.30	35.37	29.05	41.93	28.19	22.35	22.66	21.85	33.09	34.59	21.85	33.09	34.59	33.09	34.59	33.09	34.59	33.25	33.25	33.25
FeO	45.27	45.49	45.32	35.04	39.59	32.06	40.39	46.93	48.81	48.75	32.31	31.20	48.75	32.31	31.20	32.31	31.20	32.31	31.20	31.45	31.45	31.45
MnO	1.10	0.76	0.90	0.60	0.80	0.71	0.72	0.95	1.46	1.61	0.91	0.92	1.61	0.91	0.92	0.91	0.92	0.91	0.92	0.78	0.78	0.78
NiO	0.06	0.21	0.06	0.10	0.13	0.13	0.13	0.00	0.00	0.00	0.04	0.13	0.00	0.04	0.13	0.04	0.13	0.04	0.13	0.05	0.05	0.05
MgO	6.85	5.58	6.02	4.22	4.16	4.76	3.67	1.21	0.07	0.33	8.33	8.65	0.33	8.33	8.65	8.33	8.65	8.33	8.65	8.71	8.71	8.71
CaO	0.28	0.53	0.16	0.30	0.01	0.39	0.19	0.14	0.20	0.08	0.15	0.21	0.08	0.15	0.21	0.15	0.21	0.15	0.21	0.25	0.25	0.25
Na ₂ O	0.07	0.07	0.16	0.16	0.06	0.09	0.31	0.09	0.20	0.12	0.43	0.18	0.12	0.43	0.18	0.43	0.18	0.43	0.18	0.20	0.20	0.20
K ₂ O	0.02	0.00	0.00	0.04	0.00	0.17	0.03	0.37	0.01	0.02	0.02	0.02	0.02	0.02	0.02	0.02	0.02	0.02	0.02	0.00	0.00	0.00
Cl	0.02	0.00	0.00	0.00	0.00	0.01	0.00	0.00	0.00	0.00	0.01	0.00	0.00	0.00	0.00	0.00	0.00	0.00	0.00	0.04	0.04	0.04
P ₂ O ₅	0.01	0.26	0.00	0.00	0.05	0.05	0.00	0.05	0.03	0.00	0.00	0.00	0.00	0.00	0.00	0.00	0.00	0.00	0.00	0.04	0.04	0.04
Total	95.48	93.34	94.55	93.90	95.37	94.48	95.80	95.37	96.78	96.39	98.71	97.96	96.39	98.71	97.96	98.71	97.96	98.71	97.96	98.02	98.02	98.02
per 32 oxygens																						
Si	0.03	0.03	0.06	0.05	0.06	0.96	0.02	0.79	0.07	0.13	0.04	0.04	0.13	0.04	0.04	0.04	0.04	0.04	0.04	0.11	0.11	0.11
Ti	8.43	6.41	6.44	3.47	4.17	1.87	4.57	4.48	5.27	5.27	3.81	3.54	5.27	3.81	3.54	3.81	3.54	3.81	3.54	3.49	3.49	3.49
Al	0.26	0.40	0.37	0.35	0.47	0.50	0.28	0.45	0.10	0.13	1.06	1.12	0.13	1.06	1.12	1.06	1.12	1.06	1.12	1.18	1.18	1.18
Cr	0.37	0.38	0.42	0.50	0.43	0.34	0.32	0.01	0.04	0.05	0.47	0.44	0.05	0.47	0.44	0.47	0.44	0.47	0.44	0.65	0.65	0.65
Fe ₃	2.18	2.18	2.32	8.23	6.64	9.57	6.44	5.16	5.27	5.09	7.01	7.38	5.09	7.01	7.38	7.01	7.38	7.01	7.38	7.07	7.07	7.07
Fe ₂	10.81	11.54	11.33	9.06	10.06	8.13	10.25	12.04	12.63	12.63	7.61	7.40	12.63	7.61	7.40	7.61	7.40	7.61	7.40	7.43	7.43	7.43
Mn	0.27	0.19	0.23	0.16	0.21	0.18	0.18	0.25	0.38	0.42	0.22	0.22	0.42	0.22	0.22	0.22	0.22	0.22	0.22	0.19	0.19	0.19
Ni	0.01	0.05	0.02	0.02	0.03	0.03	0.03	0.00	0.00	0.00	0.01	0.03	0.00	0.01	0.03	0.01	0.03	0.01	0.03	0.01	0.01	0.01
Mg	2.92	2.53	2.68	1.95	1.88	2.15	1.66	0.55	0.03	0.15	3.50	3.66	0.15	3.50	3.66	3.50	3.66	3.50	3.66	3.67	3.67	3.67
Ca	0.08	0.17	0.05	0.10	0.00	0.13	0.06	0.05	0.07	0.03	0.04	0.06	0.03	0.04	0.06	0.04	0.06	0.04	0.06	0.07	0.07	0.07
Na	0.04	0.04	0.09	0.10	0.04	0.05	0.18	0.05	0.12	0.07	0.23	0.10	0.07	0.23	0.10	0.23	0.10	0.23	0.10	0.11	0.11	0.11
K	0.01	0.00	0.00	0.02	0.00	0.06	0.01	0.15	0.00	0.01	0.01	0.01	0.00	0.01	0.01	0.01	0.01	0.01	0.01	0.00	0.00	0.00
Cl	0.01	0.00	0.00	0.00	0.00	0.00	0.00	0.00	0.00	0.01	0.00	0.00	0.00	0.00	0.00	0.00	0.00	0.00	0.00	0.00	0.00	0.00
P	0.00	0.07	0.00	0.00	0.01	0.01	0.00	0.01	0.01	0.00	0.00	0.00	0.00	0.01	0.01	0.00	0.00	0.00	0.00	0.00	0.00	0.00
Total	23.24	24.00	24.00	24.00	24.00	24.00	24.00	24.00	24.00	24.00	24.00	24.00	24.00	24.00	24.00	24.00	24.00	24.00	24.00	24.00	24.01	24.01

Table A4.6

Opaques	96AE13		96AE18		96AE18		96AE18		96AE22		96AE22		96AE46		96AE46		96AE46		96AE46	
	Melaleuc.	Melaleuc.	Basanite	Basanite	Basanite	Melaleuc.	Melaleuc.	Melaleuc.	Melaleuc.	Melaleuc.	Melaleuc.	Melaleuc.	Melaleuc.	Melaleuc.	Melaleuc.	Melaleuc.	Melaleuc.	Melaleuc.	Melaleuc.	Melaleuc.
SiO2	0.44	0.21	0.26	0.24	0.27	0.25	0.18	0.17	0.27	0.17	0.27	0.39	0.99	0.28	0.30					
TiO2	23.19	21.93	27.70	28.01	27.09	27.35	28.41	28.06	27.56	28.06	27.56	19.49	16.61	16.17	14.69					
Al2O3	4.31	4.53	1.73	2.67	1.64	1.52	0.79	0.80	2.32	0.80	2.32	3.05	2.27	4.94	5.71					
Cr2O3	2.16	1.43	0.37	0.40	0.36	0.24	0.09	0.08	0.15	0.08	0.15	0.11	1.11	2.07	4.00					
Fe2O3	18.23	21.30	10.74	10.11	12.73	14.59	13.71	14.16	14.01	14.16	14.01	26.96	29.00	29.69	30.78					
FeO	43.73	40.53	51.43	52.06	50.33	50.58	51.88	51.60	49.81	51.60	49.81	38.54	39.73	37.81	33.98					
MnO	0.83	0.71	1.11	0.86	1.64	0.91	1.04	0.91	0.90	0.91	0.90	1.10	1.87	1.39	1.20					
NiO	0.11	0.11	0.00	0.00	0.09	0.22	0.12	0.00	0.00	0.00	0.00	0.07	0.03	0.07	0.00					
MgO	5.41	6.32	2.03	2.45	1.51	2.75	2.23	2.32	3.71	2.32	3.71	4.98	2.29	3.63	5.81					
CaO	0.05	0.07	0.29	0.02	0.15	0.08	0.07	0.03	0.07	0.03	0.07	0.08	0.26	0.19	0.24					
Na2O	0.11	0.11	0.01	0.03	0.25	0.15	0.20	0.19	0.14	0.19	0.14	0.28	0.22	0.26	0.19					
K2O	0.02	0.01	0.04	0.03	0.02	0.00	0.00	0.02	0.00	0.02	0.00	0.00	0.00	0.04	0.01					
Cl	0.00	0.01	0.00	0.00	0.01	0.00	0.03	0.00	0.01	0.00	0.01	0.00	0.02	0.00	0.00					
P2O5	0.02	0.00	0.03	0.00	0.01	0.01	0.00	0.00	0.00	0.00	0.00	0.00	0.00	0.02	0.00					
Total	98.60	97.27	95.73	96.89	96.08	98.64	98.74	98.34	98.94	98.34	98.94	95.03	94.39	96.56	96.94					
per 32 oxygens																				
Si	0.13	0.06	0.08	0.07	0.08	0.07	0.05	0.05	0.08	0.05	0.08	0.12	0.30	0.08	0.09					
Ti	4.98	4.74	6.34	6.29	6.20	6.06	6.33	6.28	6.02	6.28	6.02	4.38	3.85	3.59	3.19					
Al	1.45	1.53	0.62	0.94	0.59	0.53	0.27	0.28	0.80	0.28	0.80	1.07	0.82	1.72	1.94					
Cr	0.49	0.32	0.09	0.09	0.09	0.06	0.02	0.02	0.03	0.02	0.03	0.27	0.27	0.48	0.91					
Fe3	3.91	4.60	2.46	2.27	2.91	3.23	3.05	3.17	3.06	3.17	3.06	6.07	6.73	6.60	6.68					
Fe2	10.43	9.74	13.09	12.99	12.80	12.45	12.85	12.83	12.09	12.83	12.09	9.64	10.24	9.33	8.20					
Mn	0.20	0.17	0.29	0.22	0.42	0.23	0.26	0.23	0.22	0.23	0.22	0.28	0.49	0.35	0.29					
Ni	0.02	0.03	0.00	0.00	0.02	0.05	0.03	0.00	0.00	0.00	0.00	0.02	0.01	0.02	0.00					
Mg	2.30	2.71	0.92	1.09	0.68	1.21	0.98	1.03	1.60	1.03	1.60	2.22	1.05	1.60	2.50					
Ca	0.02	0.02	0.09	0.01	0.05	0.02	0.02	0.01	0.02	0.01	0.02	0.03	0.09	0.06	0.07					
Na	0.06	0.06	0.01	0.02	0.15	0.08	0.11	0.11	0.08	0.11	0.08	0.16	0.13	0.15	0.11					
K	0.01	0.00	0.01	0.01	0.01	0.00	0.00	0.01	0.00	0.01	0.00	0.00	0.00	0.01	0.00					
Cl	0.00	0.00	0.00	0.00	0.01	0.00	0.01	0.00	0.01	0.00	0.01	0.00	0.01	0.00	0.00					
P	0.00	0.00	0.01	0.00	0.00	0.00	0.00	0.00	0.00	0.00	0.00	0.00	0.00	0.01	0.00					
Total	24.00	24.00	24.00	24.00	24.00	24.00	24.00	24.00	24.00	24.00	24.00	24.00	24.00	24.00	24.00					

Table A4.6

Opaques	96AE46	96AE46	96AE57	96AE57	96AE57	96AE57	96AE57	96AE57	96AE57	96AE57
	Melaneph. (?)	Melaneph. (?)	Leucitite	Leucitite	Leucitite	Leucitite	Leucitite	Leucitite	Leucitite	Leucitite
SiO2	0.19	0.26	0.18	0.98	0.41	0.18	0.38	0.18	0.18	0.38
TiO2	15.03	14.45	11.09	14.81	20.63	19.41	20.92	19.41	19.41	20.92
Al2O3	6.04	6.05	8.00	5.85	4.27	4.53	3.77	4.53	4.53	3.77
Cr2O3	5.41	6.91	17.61	8.62	1.03	1.00	0.67	1.00	1.00	0.67
Fe2O3	29.71	28.01	25.75	27.00	22.72	27.93	21.97	27.93	27.93	21.97
FeO	33.40	34.38	25.92	30.80	40.59	37.61	41.35	37.61	37.61	41.35
MnO	1.05	0.94	0.55	0.44	0.86	0.68	0.99	0.68	0.68	0.99
NiO	0.01	0.00	0.03	0.18	0.04	0.03	0.02	0.03	0.03	0.02
MgO	6.13	6.13	10.23	9.68	4.83	6.71	4.77	6.71	6.71	4.77
CaO	0.14	0.13	0.01	0.03	0.37	0.12	0.35	0.12	0.12	0.35
Na2O	0.35	0.02	0.20	0.11	0.20	0.22	0.02	0.22	0.22	0.02
K2O	0.00	0.05	0.00	0.00	0.00	0.01	0.00	0.01	0.01	0.00
Cl	0.01	0.00	0.00	0.00	0.04	0.03	0.00	0.03	0.03	0.00
P2O5	0.00	0.00	0.00	0.00	0.00	0.06	0.00	0.06	0.06	0.00
Total	97.47	97.31	99.58	98.48	95.99	98.51	95.22	98.51	98.51	95.22
per 32 oxygens										
Si	0.05	0.07	0.05	0.27	0.12	0.05	0.11	0.05	0.05	0.11
Ti	3.23	3.12	2.25	3.07	4.56	4.14	4.69	4.14	4.14	4.69
Al	2.03	2.04	2.54	1.90	1.48	1.51	1.32	1.51	1.51	1.32
Cr	1.22	1.57	3.75	1.88	0.24	0.22	0.16	0.22	0.22	0.16
Fe3	6.38	6.04	5.22	5.60	5.03	5.96	4.92	5.96	5.96	4.92
Fe2	7.97	8.24	5.84	7.10	9.98	8.92	10.30	8.92	8.92	10.30
Mn	0.25	0.23	0.13	0.10	0.22	0.16	0.25	0.16	0.16	0.25
Ni	0.00	0.00	0.01	0.04	0.01	0.01	0.00	0.01	0.01	0.00
Mg	2.61	2.62	4.11	3.98	2.12	2.84	2.12	2.84	2.84	2.12
Ca	0.04	0.04	0.00	0.01	0.12	0.04	0.11	0.04	0.04	0.11
Na	0.20	0.01	0.11	0.06	0.11	0.12	0.01	0.12	0.12	0.01
K	0.00	0.02	0.00	0.00	0.00	0.00	0.00	0.00	0.00	0.00
Cl	0.01	0.00	0.00	0.00	0.02	0.01	0.00	0.02	0.01	0.00
P	0.00	0.00	0.00	0.00	0.00	0.02	0.00	0.02	0.01	0.00
Total	24.00	24.00	24.00	24.00	24.00	24.00	24.00	24.00	24.00	24.00

